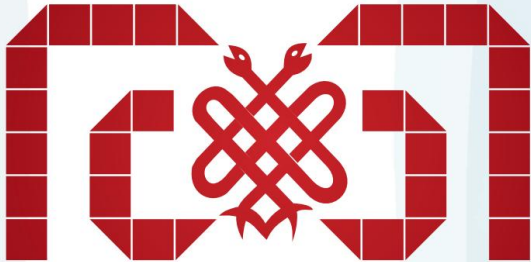


Year: 2025 March

Vol: 26

Issue: 1

E-ISSN: 2149-9063



MEANDROS

MEDICAL AND DENTAL JOURNAL



MEANDROS MEDICAL AND DENTAL JOURNAL

THE OFFICIAL JOURNAL OF ADNAN MENDERES UNIVERSITY
FACULTY OF MEDICINE AND DENTISTRY

Citation Abbreviation: *Meandros Med and Dental J*
(Formerly Adnan Menderes Üniversitesi Tıp Fakültesi Dergisi)



www.meandrosmedicaljournal.org

EDITORIAL BOARD

Editor in Chief

Seda ÖRENAY BOYACIOĞLU

Aydın Adnan Menderes University Faculty of Medicine, Department of Medical Genetics, Aydın, Türkiye
ORCID: 0000-0003-1651-1940

Associate Editors

Esra TALAY ÇEVİLİK

Aydın Adnan Menderes University Faculty of Dentistry, Department of Prosthodontics, Aydın, Türkiye
ORCID: 0000-0002-8898-6710

Mahmut Alp KILIÇ

Aydın Adnan Menderes University Faculty of Medicine, Department of Biophysics, Aydın, Türkiye
ORCID: 0000-0003-2645-1988

Secretary & Layout Editors

Umut Kerem KOLAÇ

Aydın Adnan Menderes University Faculty of Medicine, Department of Medical Biology, Aydın, Türkiye
ORCID: 0000-0003-0266-9069

Bakiye GÖKER BAĞÇA

Aydın Adnan Menderes University Faculty of Medicine, Department of Medical Biology, Aydın, Türkiye
ORCID: 0000-0002-5714-7455

İlkim Pınar SARAL

Aydın Adnan Menderes University Faculty of Dentistry, Department of Endodontics, Aydın, Türkiye
ORCID: 0000-0003-1278-7464

Hüseyin ŞEKER

Aydın Adnan Menderes University Faculty of Dentistry, Department of Prosthodontics, Aydın, Türkiye
ORCID: 0000-0002-6690-3267

Issue Editors

Seda ÖRENAY BOYACIOĞLU

Aydın Adnan Menderes University Faculty of Medicine, Department of Medical Genetics, Aydın, Türkiye
ORCID: 0000-0003-1651-1940

Beral AFACAN

Aydın Adnan Menderes University Faculty of Dentistry, Department of Periodontology, Aydın, Türkiye
ORCID: 0000-0003-2581-1400

Esra TALAY ÇEVİLİK

Aydın Adnan Menderes University Faculty of Dentistry, Department of Prosthodontics, Aydın, Türkiye
ORCID: 0000-0002-8898-6710

Yener OKUTAN

Aydın Adnan Menderes University Faculty of Dentistry, Department of Prosthodontics, Aydın, Türkiye
ORCID: 0000-0002-7188-4929

Kadriye ULU GÜZEL

Aydın Adnan Menderes University Faculty of Dentistry, Department of Pedodontics, Aydın, Türkiye
ORCID: 0000-0002-3129-8490

Mahmut Alp KILIÇ

Aydın Adnan Menderes University Faculty of Medicine, Department of Biophysics, Aydın, Türkiye
ORCID: 0000-0003-2645-1988

Bakiye GÖKER BAĞÇA

Aydın Adnan Menderes University Faculty of Medicine, Department of Medical Biology, Aydın, Türkiye
ORCID: 0000-0002-5714-7455

Özge ÇEVİK

Aydın Adnan Menderes University Faculty of Medicine, Department of Biochemistry, Aydın, Türkiye
ORCID: 0000-0002-9325-3757

CONTENT

- 1** **Protective Effects of Intermittent Fasting and Probiotics Usage on Oxidative Stress and Molecular Alterations in Aging Lung**
Burcu BABA, Dilek YONAR, Hikmet Taner TEKER, Taha CEYLANI
- 12** **Detection of Staphylococcus Aureus via Aptamer-Gated MCM-41 Nanoparticles**
Samet UÇAK
- 19** **Gene Expressions Associated with Neurotransmitter Metabolism in Children with Attention Deficit Hyperactivity Disorder**
Hilal AKALIN, Yakut ERDEM, Recep ERÖZ, İzel Olcay ŞAHİN, Nuriye GÖKÇE, Sevgi ÖZMEN, Muhammet Ensar DOĞAN, Munis DÜNDAR, Yusuf ÖZKUL
- 33** **Clinical Features, Genetic Spectrum, and Outcomes of Hereditary Tyrosinemia Type 1: A Multicenter Study from Southeastern Türkiye**
Emine GÖKSOY, Ayşe ERGÜL BOZACI, Berrak BİLGİNER GÜRBÜZ
- 42** **Mouse Model Study: Early Life Chronic Stress Effects on Sox2 and Bcl2 mRNA Expression in Gastrointestinal Tissues**
Keziban Korkmaz BAYRAM, Aida Nurul BAROKAH, Merve Hilal DÖNMEZ, Tuba Dilay KÖKENEK ÜNAL, Arslan BAYRAM
- 49** **Clinical Results of Diagnosis and Treatment of Penile Fracture: Our Experience of the Past 10 Years**
Tuncer BAHÇEÇİ, Burak GÜLER, Ozan AYDOĞAN
- 56** **Comparison of Chromosome Analysis, Factor V Leiden, And Prothrombin G20210a Mutation Results According to the Number of Pregnancy Losses in Recurrent Pregnancy Loss**
Hande ÖZKALAYCI, Mehmet KOCABEY
- 63** **Comparison of Radiofrequency Thermocoagulation at High Temperatures with Combined Radiofrequency Thermocoagulation and Pulsed Radiofrequency in Trigeminal Neuralgia**
Esra ERTİLAV, Öznur YILDIRIM, Osman Nuri AYDIN
- 69** **Factors Leading to Elevated Cardiac Biomarkers in Severe Community-Acquired Pneumonia**
Betül DUMANLI, Onur YAZICI, Fisun KARADAĞ
- 78** **Usability Of Saturation/Respiratory Rate As A Parameter In Pulmonary Thromboembolism Risk Scoring**
Maşide ARI, Fatma YILDIRIM, Eren USUL, Emrah ARI, Ömer Faruk TÜTEN, Ali Türker ÇİFTÇİ

CONTENT

- 86** **Decision making for optimal treatment for patients with periodontitis based on recent classification criteria**
Ceren KÜTÜK , Hanife Merva PARLAK , Ayhan PARMAKSIZ , Nermin TARHAN , H. Gencay KEÇELİ
- 94** **Impact of reuse of dental implant analogs on impression accuracy**
Sergen DENİZ, Mustafa ZORTUK, Taha Yaşar MANAV
- 101** **Factors Affecting Arterial Stiffness Level In Cancer Patients Receiving Immunotherapy**
Emine Esra Güner Yıldırım, Merve Bıyıklı Alemdar, Bilgin Demir, Merve Turan, Esin Oktay
- 108** **The Effect Of Different Fit-Indicating Materials And Preparation Designs on the Marginal and Internal Fit of 3D-Printed Permanent Endocrowns**
İzim TÜRKER KADER, Safa ÖZER, Burçin ARICAN
- 117** **Impact Of Different Substructure And Superstructure Materials On Bone Stress Distribution In All-On-4 Prosthetic Restorations**
Ege ÇOLAK, Muharrem Erhan ÇÖMLEKOĞLU, Mehmet SONUGELLEN, Makbule Heval ŞAHAN
- 129** **Investigation of Inflammation Rates (Neutrophil/Lymphocyte) and Hemogram Results in The Stages of Non-Alcoholic Fatty Liver Disease**
Mehmet Ali GÜL, Duygu TOZCU YILMAZ, Mustafa ÇAPRAZ

Research Article

PROTECTIVE EFFECTS OF INTERMITTENT FASTING AND PROBIOTICS USAGE ON OXIDATIVE STRESS AND MOLECULAR ALTERATIONS IN AGING LUNG

 Burcu BABA ^{1*},  Dilek YONAR ²,  Hikmet Taner TEKER ³,  Taha CEYLANI ⁴

¹Department of Medical Biochemistry, Faculty of Medicine, Yuksek Ihtisas University, Ankara, Türkiye

²Department of Biophysics, Faculty of Medicine, Yuksek Ihtisas University, Ankara, Türkiye

³Department of Medical Biology and Genetics, Ankara Medipol University Ankara, Türkiye

⁴Department of Molecular Biology and Genetics, Muş, Alparslan University Muş, Türkiye

*Correspondence: burcubaba@yiu.edu.tr

ABSTRACT

Objective: Aging is associated with increased oxidative stress and diminished cellular repair mechanisms, particularly in the lungs. This study investigates the protective effects of intermittent fasting (IF), SCD probiotics, and their combination on oxidative stress and molecular alterations in the lungs of aging rats.

Materials and Methods: Sprague-Dawley rats (24 months old) were divided into four groups: control, intermittent fasting, probiotics, and a combination of both treatments. Malondialdehyde (MDA), advanced oxidation protein products (AOPP), and myeloperoxidase (MPO) activity were measured as markers of oxidative stress. Attenuated Total Reflectance-Fourier Transform Infrared (ATR-FTIR) spectroscopy was employed to detect molecular changes in lung tissues.

Results: Our findings demonstrated that both IF and probiotics, individually and in combination, reduced the MDA and AOPP levels, as well as MPO activity, compared to the control group, indicating a reduction in oxidative stress. Spectral analyses revealed molecular changes in lipid composition, protein conformation and oxidation, as well as phosphodiester groups of nucleic acids. The highest classification accuracy (93.18%) was obtained in the 1300-800 cm⁻¹ region by LDA analysis.

Conclusion: Intermittent fasting and probiotics may ameliorate age-related oxidative damage in the lungs and offer promising therapeutic potential for maintaining lung health in aging populations.

Keywords: Aging, intermittent fasting, FTIR spectroscopy, lung, oxidative stress, probiotics.

Received: 13 November 2024
Revised: 16 January 2025
Accepted: 04 February 2025
Published: 20 March 2025



Copyright: © 2025 by the authors. Published by Aydın Adnan Menderes University, Faculty of Medicine and Faculty of Dentistry. This article is openly accessible under the Creative Commons Attribution-NonCommercial 4.0 International (CC BY-NC 4.0) License.

INTRODUCTION

Human lungs, which have the largest surface area of any organ in the body, serve as a unique interface with the external environment. They consist of various cell types and are continuously exposed to a range of stresses, including chemical, mechanical, biological, immunological, and xenobiotic factors, throughout a lifetime (1). Age-related alterations in the intrinsic mechanisms responsible for cell regeneration and repair, including the depletion of adult stem cell reserves, mitochondrial dysfunction, and increased oxidative stress, lead to a diminished capacity of lung cells to sustain normal homeostasis (2). Oxidative stress results from the imbalance between the reactive oxygen and nitrogen species (RONS) generation and the capacity of antioxidant defenses. Reactive species are produced by all aerobic cells and are crucial in the aging process and age-related diseases. While RONS production is involved in energy extraction from organic molecules, immune defense, and cellular signaling, it can also have harmful effects (3). Excessive production of oxidants can cause lipid peroxidation and protein oxidation, leading to damage in cells and tissues. Myeloperoxidase (MPO) is an essential enzyme found in neutrophils that generates powerful oxidants, including hypochlorous acid (HOCl), which serves as a defense mechanism against pathogens (4).

The reactive species oxidize amino acid side chains, leading to a conformational alteration, partial unfolding, and fragmentation of the protein backbone. Due to the accumulation of oxidized proteins, cross-linking processes such as the formation of dityrosine, disulphide, and other types of intermolecular bonds occur, generating protein aggregates that polymerize into non-degradable structures, evading proteolysis (5). Aromatic amino acid residues are primary targets for various reactive species, resulting in the generation of cross-links containing dityrosine, which are known as advanced oxidation protein products (AOPPs) (6). Free radicals, including ROS and RNS, also attack the double bonds in lipids by removing hydrogen atoms and adding oxygen, resulting in lipid peroxidation. This process results in primary products like lipid peroxyl radicals and hydroperoxides, along with secondary products including malondialdehyde (MDA) and 4-hydroxynonenal (7).

Intermittent fasting (IF) is associated with reduced oxidative damage and diminished inflammatory responses (8). Intermittent fasting is a dietary pattern that involves a period of food restriction and normal nutrition. It has recently become popular because of its potential health benefits, such as anti-aging and rejuvenation effects

(9, 10). IF improves health and combats disease processes through cellular and molecular mechanisms that activate adaptive stress response pathways. These pathways support mitochondrial function, DNA repair, and autophagy (11).

Various factors including diet, age, illnesses, stress, and lifestyle can affect the composition of the gut microbiota. The microbes in our gut are more numerous than the total number of body cells by over tenfold. They have important roles in maintaining health, such as aiding digestion, regulating the immune system, and even combating diseases (12). Given the crucial role of diet in shaping the gut microbiome, there has been considerable interest in using prebiotics and probiotics as nutritional strategies to enhance microbiome diversity and promote health (13). Due to the deterioration of physiological and biological systems in the elderly, probiotics present a promising option for mitigating the associated increased disease susceptibility (14).

There is a crosstalk between the respiratory tract and the gastrointestinal tract, defined as the gut-lung axis. Alterations in components of the gut microbiome by diet, disease, or medical interventions are associated with changes in immune responses and the maintenance of homeostasis in the respiratory tract (15, 16). With the rapid increase in the aging population, it is crucial to investigate how physiological and cellular alterations in aging lungs influence the onset and progression of respiratory diseases (2). It is hypothesized that the treatment with IF and SCD probiotics may alleviate increased oxidative damage in aged lung tissue and contribute to the restoration of lung tissue. Additionally, it is suggested that interventions such as IF could further improve lung health by complementing probiotic treatment. Therefore, we aimed to investigate the effects of IF and SCD probiotics, both individually and in combination, on aging lungs by evaluating oxidative stress indicators, including myeloperoxidase, AOPP, and MDA. Moreover, ATR-FTIR spectroscopy combined with multivariate analysis was used to specify the molecular differences in the lung tissue after intermittent fasting and probiotics intake.

MATERIALS AND METHODS

Animal studies

In this study, male Sprague-Dawley rats (24 months old) were used. The animals were divided into four groups: the control group (CNT), the intermittent fasting group (IF), the SCD Probiotics group (PRB), and the group receiving

SCD Probiotics supplementation during intermittent fasting (IFPRB), with 7 rats in each group. The rats in the IF groups were subjected to food restriction for 18 hours a day, with a 6-hour window (between 9 a.m. and 3 p.m.) for food intake. Water was available to them at all times. The animals were fed a typical rodent diet ad libitum (11), and their body weight was recorded throughout the study. The probiotic supplement was given orally at a daily dose of 3 mL (1×10^8 CFU) (17), using the product provided by SCD probiotics company (Essential Probiotics XI - 500 ml H.S. Code: 2206.00.7000), which contains 11 different probiotics, including *Bacillus subtilis*, *Bifidobacterium longum*, *Bifidobacterium bifidum*, *Lactobacillus bulgaricus*, *Lactobacillus acidophilus*, *Lactobacillus fermentum*, *Lactobacillus casei*, *Lactobacillus plantarum*, *Lactococcus lactis*, *Saccharomyces cerevisiae*, and *Streptococcus thermophilus* species during 30 days (18). At the end of the treatment period, rats in all groups were sacrificed, and then lung tissues were obtained. The lung tissues were immediately shocked on dry ice and stored in a -80°C deep freezer until analysis. The study was approved by the Ethics Committee of the Saki Yenilli Experimental Animal Production and Practice Laboratory (approval number: 2022/03) and conducted according to the standard animal care protocols.

Tissue Preparation

Lung tissues were homogenized to disrupt the tissue structure, leading to the release of cells and intracellular components for further analysis. The lung tissues were homogenized in 10 mM cold phosphate buffered saline (PBS; 1:5 w/v; pH 7.4) with protease inhibitor (PIC002, BioShop, Canada) and 0.5% Triton X-100 to determine the oxidative stress markers. The homogenate was centrifuged at $5,000 \times g$ for 10 minutes at 4°C , and the supernatant was collected. The obtained supernatant was stored in aliquots at -80°C until analysis. Protein concentrations in the samples were measured using the method described by Bradford (19) with bovine serum albumin used as a standard.

Malondialdehyde Measurement

Malondialdehyde, a lipid peroxidation marker, was assessed by measuring the formation of thiobarbituric acid reactive substances. Briefly, the samples were mixed with 20% trichloroacetic acid and 0.67% thiobarbituric acid, heated in a water bath at 100°C , and then cooled on ice. Absorbance was measured at 532 nm, and MDA levels were calculated as nanomoles per milligram of protein.

Advanced Oxidation Protein Products Measurement

AOPPs, which serve as indicators of oxidative protein damage, were assessed by measuring dihydroxy-

containing and cross-linked protein products. AOPP levels were quantified following the procedure established by Witko-Sarsat et al. (20). In this procedure, samples were first diluted to a concentration of 20 mM with PBS (pH 7.4), and then potassium iodide and acetic acid were added. Absorbance was then measured at 340 nm, and the values were presented as nanomoles per milligram of protein.

Determination of Myeloperoxidase Activity

The activity of myeloperoxidase was measured using a spectrophotometric method. The samples were mixed with 50 mM PBS (pH 6.0) containing o-dianisidine (0.167 mg/ml) and hydrogen peroxide (0.0005%). The change in absorbance was measured at 460 nm for 5 min. The activity of MPO was presented as units per milligram of protein, following the method as described by Bradley et al. (21).

Sampling for ATR-FTIR spectroscopy and data analysis

The ATR-FTIR spectra of lung tissues were obtained using Perkin Elmer Frontier FTIR spectrometer (Perkin Elmer Inc., USA) with a Quest single reflection ATR accessory (Specac Ltd., UK). The background spectrum was obtained by recording the spectrum of air and automatically subtracted using the Spectrum 10 software program. The spectra of lung tissues compressed on the diamond crystal of the ATR unit were collected at room temperature within the range of $4000\text{-}450\text{ cm}^{-1}$ region with 64 scans at 4 cm^{-1} resolution. Under the same conditions, each tissue was scanned from three randomly selected fractions, all of which produced the same spectra. Spectral analyses were performed using the average spectra of these three replicates. The spectra acquisition and data manipulation were obtained by the same software program (Spectrum 10).

Machine learning method in prediction studies

Linear Discriminant Analysis (LDA) as a machine learning tool was implemented on spectral data for differentiating the experimental groups from each other. The goal of LDA is to find the linear combination of original variables that maximizes the difference between classes. In the LDA technique, the best fit parameters for the sample classification are determined with a developed model, and then the model can be applied to classify unknown samples. The development of machine learning-based detection models requires independent training and test/validation data sets. In order to create a classification model and categorize samples, principal component analysis (PCA) has been frequently used to train data sets. Additionally, the detection performance of the classification model has been assessed by a validation data set using LDA. The PCA data of the second derivative and

normalized spectra in the whole spectral range (4000-450 cm^{-1}), lipid (3020-2800 cm^{-1}), protein (1700-1500 cm^{-1}), and nucleic acid (1300-800 cm^{-1}) regions were used as LDA model inputs using The Unscrambler X 10.3 (CAMO Software AS, Norway) software. Initially, the category variable column was added into the data matrix, and then a training set was created by using all the spectra of the different sample classes. The method used was quadratic, utilizing the projections of 7 principal components and the prior probabilities calculated from the training set for the prediction. LDA results are represented by a discrimination plot, the matrices of prediction and confusion. The prediction matrix exhibits the predicted class for each sample and the probability of membership for each class. However, the confusion matrix reports the predicted and actual classifications of samples (22).

Statistical Analysis

Statistical analyses of the data using one-way ANOVA and the graph plots were performed using GraphPad Prism 10 (GraphPad, USA). The values were reported as mean \pm standard error of the mean (SEM). The significance level was denoted as * $p < 0.05$, ** $p < 0.01$, *** $p < 0.001$, and **** $p < 0.0001$.

RESULTS

The body weight, water and food consumption of animals

The IF groups showed significant weight loss, whereas the IFPRB group exhibited less weight loss. The lower weight loss observed between the IF and PRB groups in comparison with the control demonstrates the role of the probiotic in stabilizing weight gain. Although the feed consumption of rats in the IF groups increased because of adaptation, no significant differences in water consumption were observed among the groups, as shown in our previous study (18).

Effects of Treatment with Probiotics and Intermittent Fasting on Oxidative Stress Markers

In the present study, MPO activities, MDA, and AOPP levels as indicators of oxidative stress were measured in lung homogenates from 24-month-old rats treated with intermittent fasting and probiotics, either individually or in combination. MDA levels statistically reduced in aged rats treated with probiotics alone and in those treated with both probiotics and IF compared to the control group. Although there was no statistically significant difference in MDA levels between the IF group and the control group, a notable reduction in MDA levels was observed in the IF group (Figure 1a). The levels of AOPP decreased significantly in all treated groups compared to the controls

(Figure 1b). MPO activity in the aging lung was found to be significantly reduced with treatment using probiotics and IF, either administered individually or in combination (Figure 1c). When comparing the groups treated with probiotics and IF, either individually or in combination, no significant difference was observed among them in terms of oxidative stress markers.

Lipid, protein and nucleic acid profiles of lung tissues altered by intermittent fasting and probiotics supplementation

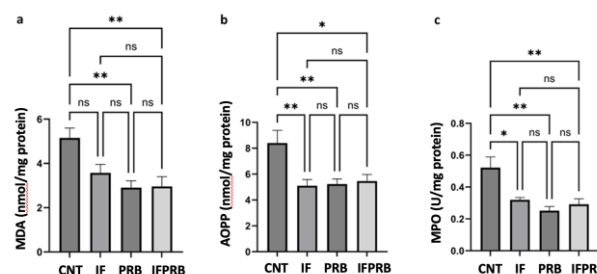


Figure 1 Effects of probiotics and intermittent fasting on MDA (a), AOPP (b) and MPO (c) activity of the lung tissue of aged rats. CNT (control), IF (intermittent fasting), PRB (SCD Probiotics) and IFPRB applications (in which IF and PRB were applied together). The significance levels were denoted as * $p < 0.05$, ** $p < 0.01$.

FTIR spectroscopy has arisen as a potent technique for simultaneously analyzing the structure, conformation, and function of all molecules in a biological system (23). ATR-FTIR spectroscopy was performed to elucidate the altered biomolecular changes in rat lung tissues after intermittent fasting (IF), probiotics supplementation (PRB), and in combination (IFPRB). For this purpose, quantitative measurements of spectral parameters such as shifts in the peak positions, alterations in bandwidths, band areas of spectral bands or the area ratios and machine learning approaches were carried out. Figure 2a-b exhibits the averaged IR spectra of all groups (CNT, IF, PRB and IFPRB) in the 3025-2800 and 1800-800 cm^{-1} regions where the absorption bands originate from the functional groups of lipids, proteins, nucleic acids, and carbohydrates. The below panels in Figure 2a-b show difference spectra obtained by subtracting the average spectrum of each group from the average spectrum of the control to explore the differences between the groups more plainly. The difference spectra showed notable changes in the functional groups of specific biomolecules between the control group and different treatment groups (Figure 2a-b). In order to determine the quantitative differences between the groups, spectral band areas and area ratios for individual bands were calculated. According to Beer-Lambert's law, the concentration of the functional groups in the relevant molecule is exactly proportional to the signal intensity/area under the spectral bands. To exclude potential artifacts from experimental conditions, the

integrated area ratios of a few selected bands were assessed for relative quantitative analysis (22, 23). Some prominent bands for lipids such as olefinic C=CH at 3011 cm^{-1} , CH_3 asymmetric stretching at 2960 cm^{-1} , CH_2 asymmetric stretching at 2923 cm^{-1} , CH_2 symmetric stretching at 2852 cm^{-1} and C=O stretching at 1740 cm^{-1}

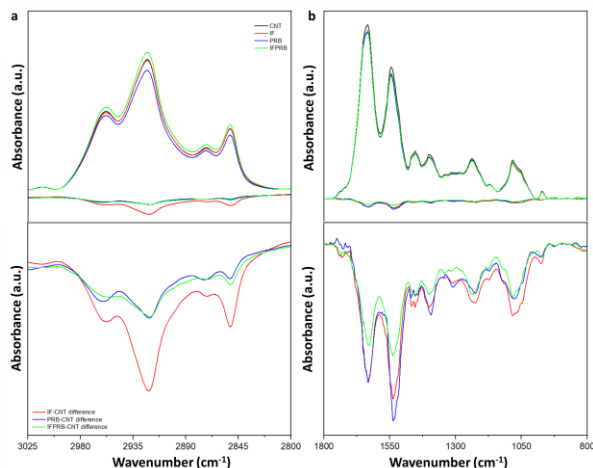


Figure 2. The normalized average IR spectra of the groups in the a) 3025–2800 and b) 1800–800 cm^{-1} regions. The normalization was performed according to the amide A band located at 3280 cm^{-1} . Difference IR spectra were acquired via subtracting the control spectrum from the spectra of the groups treated by intermittent fasting (IF), probiotics supplementation (PRB) and the combined administration of both (IFPRB) in the below panels for both regions.

were evaluated. The area of CH_3 antisymmetric ($p < 0.001$), CH_2 antisymmetric and symmetric stretching bands ($p < 0.05$) in all treatment groups decreased significantly compared to controls. Total saturated lipid content calculated from the sum of CH_2 symmetric and antisymmetric stretching bands decreased in treated groups compared to the control group (Figure 3a). Moreover, the CH_2/CH_3 antisymmetric stretching area ratio provides acyl chain length information. A higher value indicates the presence of relatively longer chain lipids, while a lower value implies the presence of shorter chain and/or more branched lipids. No remarkable changes in acyl chain length were observed among the groups. The bandwidth of CH_2 symmetric or antisymmetric stretching bands indicates membrane dynamics, as it is connected with the motional rates of the lipid molecule. An increase in membrane dynamics is indicated by the increase in the bandwidths of these bands. A nonsignificant decrease was observed in the bandwidth values of CH_2 antisymmetric stretching bands for treated groups when compared to the control group (Figure 3b). The olefinic band points out the content of double bonds in the lipid structure, which is utilized for monitoring the unsaturated lipid content. There was also a decrease in the area of the olefinic C=CH stretching band compared to the

control as seen from Figure 3c. C=O stretching band indicates the carbonyl ester concentration in lipids. Moreover, this band can be used to visualize protein oxidation due to resulting in the production of some additional carbonyls. A nonsignificant decrease in the C=O stretching band was observed in all groups.

The protein associated bands Amide I at 1635 cm^{-1} (mainly from the C=O stretching vibration), Amide II at 1545 cm^{-1} (arises from N-H bending vibration and from C-N stretching vibration) and some major nucleic acids related bands such as PO_2^- antisymmetric stretching at 1238 cm^{-1} , PO_2^- symmetric stretching at 1083 cm^{-1} and PO_4^- stretching at 971 cm^{-1} were also evaluated. Amide I and amide II bands are sensitive to conformational alterations in the proteins. The shifts in the band positions and the alterations in the bandwidth of amide I and amide II as well as the amide I/amide II band area ratio can provide the change in the protein conformation and structure. Our results show that no significant change in these parameters is observed. However, the area of amide I and amide II bands dropped significantly ($p < 0.05$) in all treatment groups. Figure 3d reveals an increase in the amide I/amide II ratio in all of the treated groups in comparison with the control. This increase is significant in fasting and SCD probiotics groups, which proposes the higher decrease in the content of N-H bending and C-N stretching relative to the content of C=O stretching in the proteins of IF and PRB treated groups. The broadening of the amide I band and area ratio of C=O stretching band to

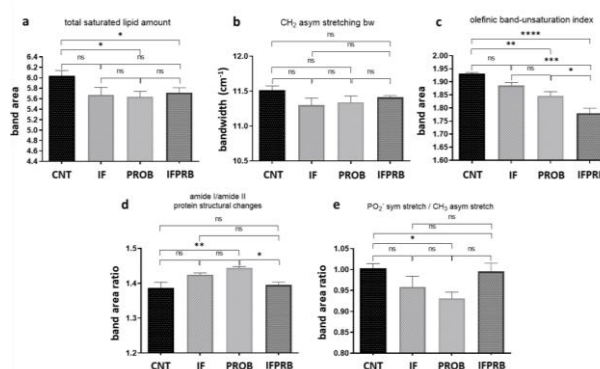


Figure 3. Quantitative changes in spectral parameters including band areas and band area ratios for: (a) total saturated lipid amount, (b) bandwidth of CH_2 antisymmetric stretching band, (c) olefinic band area, (d) protein conformation (A1653/A1545) and (e) protein phosphorylation (A1083/A2955). The significance levels were denoted as * $p < 0.05$, ** $p < 0.01$, *** $p < 0.001$, and **** $p < 0.0001$.

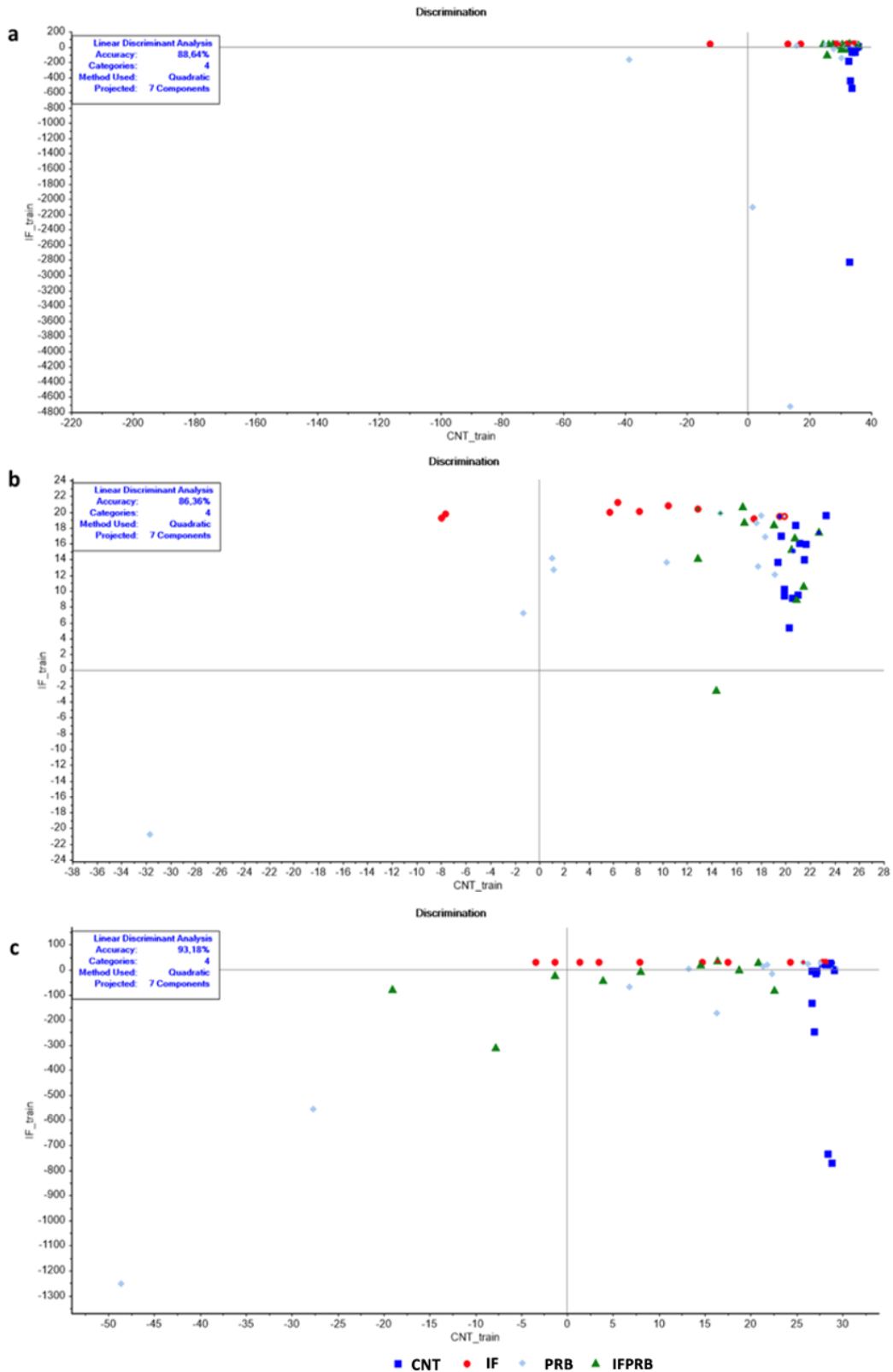


Figure 4. LDA discrimination plot for lung tissue samples in a) the lipid region ($3020\text{-}2800\text{ cm}^{-1}$), b) the protein region ($1700\text{-}1500\text{ cm}^{-1}$) and c) the nucleic acid region ($1300\text{-}800\text{ cm}^{-1}$). CNT (control), IF (intermittent fasting), PRB (SCD Probiotics) and IFPRB applications (in which the IF and PRB were applied together).

the amide I band (A1740/A1635) were measured to assess the relative level of protein carbonylation in the studied groups. No significant change in the broadening of amide I band was obtained and although there was a decreasing trend in A1740/A1635 ratio, no significant change was achieved.

The PO_2^- antisymmetric, symmetric stretching (antisymmetric phosphate and symmetric phosphate) bands are attributed to the phosphodiester groups of nucleic acids, whereas PO_4^- stretching band is attributed to the phosphate monoester groups of phosphorylated proteins and cellular nucleic acids. All of these bands decreased in all treated groups compared to controls. The band ratios of PO_2^- antisymmetric, symmetric stretching to the CH_3 antisymmetric stretching (A1238/A2955, A1083/A2955) are related to protein phosphorylation. A decrease in protein phosphorylation was observed in all treated groups, but was not significant in groups other than the PROB group (Figure 3e).

LDA analyses were performed in regions where functional groups related to lipids, proteins, and nucleic acids are predominant. LDA analysis indicated a clear distinction in the biomolecular content of lung tissue among the control groups, IF, SCD Probiotics, and the combined treated groups. The discrimination plots obtained as a result of LDA analyses are given in Figure 4. The prediction matrix and the confusion matrix are given in the supplementary document (Table S1-S6). LDA analysis revealed notable differentiation in the regions associated with functional groups related to lipids, proteins, and nucleic acids, achieving accuracy rates of 88.64%, 86.36%, and 93.18%, respectively (Figure 4). While all treatments caused similar differences in lipid (Figure 4a, Table S1, S2) and nucleic acid profiles, the intermittent fasting group had the most distinct protein profile (Figure 4b; Table S3, S4). A high level of accuracy with 93.18% in the nucleic acid region ($1300\text{-}800\text{ cm}^{-1}$) was obtained (Figure 4c, Table S5, S6).

DISCUSSION

In the present study, we assessed the effects of IF and probiotics, both individually and in combination, on markers related to oxidative damage in aging lungs. According to our findings, treatment with probiotics and IF has a beneficial effect on aging lungs by leading to a reduction in oxidative damage indicators, including AOPP, MDA, and myeloperoxidase. In addition, the efficacy of IF and PRB supplementation on the molecular content of lung tissues was investigated using FTIR. We detected prominent changes in the lipid, protein, and nucleic acid profiles in the lung tissue using spectral

analysis and machine learning techniques. According to spectral analyses, we observed decreases in all lipid-related bands, such as olefinic groups of unsaturated lipids, C-H stretching groups indicating total saturated lipids, and C=O stretching bands representing the triglyceride and cholesterol ester amounts by IF and SCD probiotics supplementation. These results support the reduced fat mass in old rats with treatment (24).

Aging is a process associated with a decline in the function and efficiency of tissues and organs. According to the oxidative stress theory of aging, these age-related functional declines are attributed to damage caused by reactive species (25). Luceri et al. observed that during aging, excessive ROS production results in oxidative damage at both the liver and systemic levels, which occurs as early as middle age (26). In a previous study, elevated levels of protein oxidation and lipid peroxidation in the liver tissue of aged female rats were demonstrated through AOPP and MDA measurements, which indicate the extent of oxidative damage to proteins and lipids (27). Higher MDA and AOPP levels were found in older rats compared to their younger counterparts (28–30). In addition, myeloperoxidase, a heme protein found in neutrophils and monocytes, plays a role in multiple stages of inflammation by generating various potent oxidants. MPO activity is significantly elevated with aging (4).

Intermittent fasting may enhance resistance to oxidative stress, reduce inflammation, and support longevity at the cellular level (24). A study in rats reported that both time-restricted feeding and alternate-day fasting improve metabolic profile and redox homeostasis by increasing the antioxidant defense system and decreasing oxidative stress markers such as MDA and AOPP, indicating their potential for aging intervention (31). A previous study demonstrated that alternate-day fasting reduced mitochondrial oxidative stress in aged mice, suggesting it may contribute to diminishing age-related cellular damage (32). According to our findings, a notable reduction in the MDA levels was observed in the IF group, but it was not statistically significant. This finding may be influenced by sample variability due to individual differences among rats. Therefore, further research with larger sample sizes is needed to confirm these findings. However, both AOPP levels and MPO activity were significantly reduced with IF treatment. The reductions in lipid peroxidation and protein oxidation markers as well as MPO activity may result from an increase in the antioxidant defense system, indicating a reduction in inflammation and oxidative stress.

As individuals age, their biological and physiological processes undergo changes, leading to alterations in

gastrointestinal and immune functions (14). The gut microbiota is crucial for various functions, including signaling pathways, homeostasis, nutrient and drug metabolism, intestinal barrier integrity, protection against pathogens, and immune system interaction. There's increasing interest in the link between microbiota dysbiosis and oxidative stress. Disruptions in gut microbiota can lead to excessive ROS production, increasing oxidative stress. It was suggested that the probiotics have antioxidant effects by modulating oxidative stress mechanisms in healthy individuals (33). Lactic acid bacteria are considered a promising source of antioxidants, with potential benefits in mitigating the detrimental effects of oxidative stress, a key factor in aging (34). Research shows that these bacteria produce various antioxidants that neutralize free radicals and alleviate oxidative stress, potentially improving cellular health and promoting healthy aging (35, 36). Administration of *Lactobacillus helveticus* led to a significant reduction in MDA and AOPP levels in a randomized double-blind study (37). Probiotics, prebiotics, and, when used together, synbiotics are widely recognized as immunomodulators and promoters of gut health. In addition to their proven effects in supporting a healthy microbiota composition and gut health, there is emerging evidence on how these components may improve lung health (15, 16). Our study demonstrated that probiotic treatment resulted in a decrease in MPO activity, lipid peroxidation, and protein oxidation, which suggests a reduction in oxidative stress in the aged lung. A decrease in short-chain lipid peroxidation product, MDA, was observed, while no change in total short-chain fatty acids was found between the groups according to the spectral analysis. It is suggested that this might be due to an increase in short-chain fatty acids (acetate, propionate, and butyrate), which are important bacterial fermentation metabolites that regulate many essential aspects of human physiology (15, 38). Protein carbonylation is commonly used to indicate oxidative stress and serve as a marker of oxidative damage. However, protein carbonyls are not only important as a biomarker for protein oxidation in aging and disease, but also they can disrupt protein structure and function by changing the conformation of the polypeptide chain and leading to partial or complete inactivation of proteins (39). No significant change was observed in the bandwidth of the amide I band and A1740/A1635 area ratio values, which are used to evaluate protein carbonylation, possibly due to sample variability. However, a decreasing trend was observed in the A1740/A1635 ratio of the treatment group compared to the control. This may indicate that treatments such as IF and probiotic supplementation applied in old age contribute to reducing carbonylation. It was suggested that IF and probiotic supplementation might promote the expression of antioxidant genes and

boost the activity of antioxidant enzymes in the development of age-related lung diseases, leading to lessening inflammation and oxidative stress. Exposure to oxidative stress triggers a series of lipid peroxidation and phosphorylation reactions in cells. Certain protein phosphorylation events take place during apoptosis and are crucial for controlling programmed cell death (40). Aging is largely caused by increased reactive oxygen species and enhanced apoptosis (41). In our study, decreases in the band ratios related to protein phosphorylation and the band area of phosphate monoester groups of phosphorylated proteins by treatments were observed, suggesting a potential modulation of the apoptotic pathway.

Oxidative stress is a key factor in the development of age-related lung diseases including chronic obstructive pulmonary disease (42), pulmonary hypertension (43, 44), and fibrotic lung disease (45). In many respiratory disorders, the gut-lung axis plays an essential role and provides the bidirectional communication between the respiratory system and the gut microbiota. The gut microbiota is affected by age, diet, and lifestyle, which may have an effect on lung health and the emergence of both acute and chronic lung diseases. Altering the gut microbiota using strategies such as probiotics and dietary interventions could serve as potential therapeutic approaches for lung diseases through microbial balance restoration and the growth of beneficial strains in the gut (15, 16). Probiotic supplementation during IF has been demonstrated to be more effective in restoring colon and ileum tissues in aged rats (18). Moreover, both IF and SCD probiotics supplementation may help mitigate age-associated liver alterations (46). The findings of our study suggest that lipid and protein oxidative damage in the aging lung was reduced with IF and probiotic supplementation, whether administered individually or in combination. Additionally, a reduction in MPO activity was observed, which may indicate a decrease in inflammation and oxidative stress. The reductions in MPO activity, lipid peroxidation, and protein oxidation indicators might result from an enhancement of the antioxidant defense system, supporting the notion that IF and probiotic supplementation exert antioxidant effects. All the results proposed that both IF and probiotic treatments, individually or combined, are promising strategies for reducing age-related oxidative damage in the lungs. However, little is known about the gut-lung axis, and the mechanisms by which the gut microbiota influences lung homeostasis and diseases are not yet fully understood and require further investigation (15, 16).

CONCLUSION

This study demonstrates that IF and probiotics, both individually and in combination, have significant protective effects against age-related oxidative damage and molecular alterations in the lungs of aged rats. The reduction in oxidative stress markers such as MDA, AOPP, and MPO activity suggests that these interventions can mitigate lipid and protein oxidation, key contributors to lung aging and dysfunction. Additionally, the application of ATR-FTIR spectroscopy, combined with machine learning, revealed distinct biomolecular changes further supporting the beneficial impact of these treatments on aging lung tissues. The findings emphasize the potential of intermittent fasting and probiotics as non-invasive, dietary-based strategies to enhance cellular resilience and reduce oxidative damage in the aging lung. However, further research is required to explore the long-term efficacy, underlying mechanisms, and potential clinical applications in aging-related lung diseases. These insights offer promising avenues for future interventions targeting age-related oxidative stress and respiratory decline. Besides, we acknowledge the challenges of applying IF regimens to elderly individuals. Therefore, a better understanding of the complex interactions between the gut microbiota, dietary interventions such as IF, and the host is essential for developing personalized medical treatments for a range of health conditions.

Acknowledgments

None to declare.

Authorship contributions

Concept and design: T.C., H.T.T.; Data Collection and Processing: B.B., D.Y.; Analysis or Interpretation: B.B., D.Y., H.T.T., T.C.; Literature Search: and Writing: B.B., D.Y., H.T.T., T.C.

Data availability statement

The data that support the findings of this study are available from the corresponding author upon reasonable request.

Declaration of competing interest

The authors declared no conflict of interest.

Ethics

The study was approved by the Ethics Committee of the Saki Yenilli Experimental Animal Production and Practice Laboratory (approval number: 2022/03)

Funding

No funding was used for the study

REFERENCES

1. Schneider JL, Rowe JH, Garcia-de-Alba C, Kim CF, Sharpe AH, Haigis MC. The aging lung: Physiology, disease, and immunity. *Cell* 2021; 184: 1990–2019.
2. Cho SJ, Stout-Delgado HW. Aging and Lung Disease. *Annu Rev Physiol* 2020; 82: 433–459.
3. Liguori I, Russo G, Curcio F, Bulli G, Aran L, Della-Morte D, et al. Oxidative stress, aging, and diseases. *Clin Interv Aging* 2018; 13: 757–772.
4. Son TG, Zou Y, Yu BP, Lee J, Chung HY. Aging effect on myeloperoxidase in rat kidney and its modulation by calorie restriction. *Free Radic Res* 2005; 39: 283–289.
5. Chaudhary MR, Chaudhary S, Sharma Y, Singh TA, Mishra AK, Sharma S, et al. Aging, oxidative stress and degenerative diseases: mechanisms, complications and emerging therapeutic strategies. *Biogerontology* 2023; 24: 609–662.
6. Kehm R, Baldensperger T, Raupbach J, Höhn A. Protein oxidation - Formation mechanisms, detection and relevance as biomarkers in human diseases. *Redox Biol* 2021; 42: 101901.
7. Aguilar Diaz De Leon J, Borges CR. Evaluation of Oxidative Stress in Biological Samples Using the Thiobarbituric Acid Reactive Substances Assay. *J Vis Exp* 2020; doi:10.3791/61122.
8. Zou Y-F, JiZe X-P, Li C-Y, Zhang C-W, Fu Y-P, Yin Z-Q, et al. Polysaccharide from aerial part of *Chuanminshen violaceum* alleviates oxidative stress and inflammatory response in aging mice through modulating intestinal microbiota. *Front Immunol* 2023; 14: 1159291.

9. Golbidi S, Daiber A, Korac B, Li H, Essop MF, Laher I. Health Benefits of Fasting and Caloric Restriction. *Curr Diab Rep* 2017; 17. doi:10.1007/s11892-017-0951-7.
10. Teker HT, Ceylani T. Intermittent fasting supports the balance of the gut microbiota composition. *Int Microbiol* 2022; doi: 10.1007/s10123-022-00272-7.
11. Mattson MP, Longo VD, Harvie M. Impact of intermittent fasting on health and disease processes. *Ageing Res Rev* 2017; 39: 46–58.
12. Wan MLY, Ling KH, El-Nezami H, Wang MF. Influence of functional food components on gut health. *Crit Rev Food Sci Nutr* 2019; 59: 1927–1936.
13. Bosco N, Noti M. The aging gut microbiome and its impact on host immunity. *Genes Immun* 2021; 22: 289–303.
14. Sivamaruthi BS, Fern LA, Rashidah Pg Hj Ismail DSN, Chaiyasut C. The influence of probiotics on bile acids in diseases and aging. *Biomed Pharmacother* 2020; 128: 110310.
15. Zhou A, Lei Y, Tang L, et al. Gut Microbiota: the Emerging Link to Lung Homeostasis and Disease. *J Bacteriol.* 2021;203(4):e00454-20. doi:10.1128/JB.00454-20.
16. Alswat AS. The Influence of the Gut Microbiota on Host Health: A Focus on the Gut-Lung Axis and Therapeutic Approaches. *Life (Basel).* 2024;14(10):1279. doi:10.3390/life14101279
17. Ceylani T. Effect of SCD probiotics supplemented with tauroursodeoxycholic acid (TUDCA) application on the aged rat gut microbiota composition. *J Appl Microbiol.* 2023 May 2;134(5):lxad092. doi: 10.1093/jambio/lxad092.
18. Teker HT, Ceylani T, Keskin S, Samgane G, Allahverdi H, Acikgoz E, et al. Supplementing probiotics during intermittent fasting proves more effective in restoring ileum and colon tissues in aged rats. *J Cell Mol Med* 2024; 28: 1–13.
19. Bradford MM. A rapid and sensitive method for the quantitation of microgram quantities of protein utilizing the principle of protein-dye binding. *Anal Biochem* 1976; 72: 248–254.
20. Witko-Sarsat V, Friedlander M, Capeillère-Blandin C, et al. Advanced oxidation protein products as a novel marker of oxidative stress in uremia. *Kidney Int* 1996; 49: 1304–1313.
21. Bradley PP, Priebe DA, Christensen RD, et al. Measurement of cutaneous inflammation: estimation of neutrophil content with an enzyme marker. *J Invest Dermatol* 1982; 78: 206–209
22. Ceylani T, Teker HT, Samgane G, Gurbanov R, Intermittent fasting-induced biomolecular modifications in rat tissues detected by ATR-FTIR spectroscopy and machine learning algorithms. *Anal Biochem* 2022; 654, 114825.
23. Yonar D, Severcan M, Gurbanov R, Sandal A, Yilmaz U, Emri S, Severcan F, Rapid diagnosis of malignant pleural mesothelioma and its discrimination from lung cancer and benign exudative effusions using blood serum. *Biochim Biophys Acta Mol Basis Dis* 2022; 1868(10), 166473.
24. Stockman MC, Thomas D, Burke J, Apovian CM. Intermittent Fasting: Is the Wait Worth the Weight? *Curr Obes Rep* 2018; 7: 172–185.
25. Hajam YA, Rani R, Ganie SY, Sheikh TA, Javaid D, Qadri SS, et al. Oxidative Stress in Human Pathology and Aging: Molecular Mechanisms and Perspectives. *Cells* 2022; 11. doi:10.3390/cells11030552.
26. Luceri C, Bigagli E, Femia AP, Caderni G, Giovannelli L, Lodovici M. Aging related changes in circulating reactive oxygen species (ROS) and protein carbonyls are indicative of liver oxidative injury. *Toxicol reports* 2018; 5: 141–145.
27. Aydin S, Atukeren P, Cakatay U, Uzun H, Altuğ T. Gender-dependent oxidative variations in liver of aged rats. *Biogerontology* 2010; 11: 335–346.
28. Kumar D, Rizvi SI. A critical period in lifespan of male rats coincides with increased oxidative stress. *Arch Gerontol Geriatr* 2014; 58: 427–433.
29. Tripathi SS, Kumar R, Arya JK, Rizvi SI. Plasma from Young Rats Injected into Old Rats Induce Antiaging Effects. *Rejuvenation Res* 2021; 24: 206–212.
30. Uzun D, Korkmaz GG, Sitar ME, Cebe T, Yanar K, Cakatay U, et al. Oxidative damage parameters in renal

- tissues of aged and young rats based on gender. *Clin Interv Aging* 2013; 8: 809–815.
31. Bhoumik S, Kumar R, Rizvi SI. Time restricted feeding provides a viable alternative to alternate day fasting when evaluated in terms of redox homeostasis in rats. *Arch Gerontol Geriatr.* 2020; 91: 104188. doi:10.1016/j.archger.2020.104188.
32. Descamps O, Riondel J, Ducros V, Roussel AM. Mitochondrial production of reactive oxygen species and incidence of age-associated lymphoma in OF1 mice: effect of alternate-day fasting. *Mech Ageing Dev.* 2005; 126(11): 1185-1191. doi:10.1016/j.mad.2005.06.007.
33. Sánchez Macarro M, Ávila-Gandía V, Pérez-Piñero S, Cánovas F, García-Muñoz AM, Abellán-Ruiz MS, et al. Antioxidant Effect of a Probiotic Product on a Model of Oxidative Stress Induced by High-Intensity and Duration Physical Exercise. *Antioxidants (Basel)* 2021; 10. doi:10.3390/antiox10020323.
34. Liu R, Sun B. Lactic Acid Bacteria and Aging: Unraveling the Interplay for Healthy Longevity. *Aging Dis* 2023; 15: 1487–1498.
35. Li W, Gao L, Huang W, Ma Y, Muhammad I, Hanif A, et al. Antioxidant properties of lactic acid bacteria isolated from traditional fermented yak milk and their probiotic effects on the oxidative senescence of *Caenorhabditis elegans*. *Food Funct* 2022; 13: 3690–3703.
36. Nakagawa H, Miyazaki T. Beneficial effects of antioxidative lactic acid bacteria. *AIMS Microbiol* 2017; 3: 1–7.
37. Michalickova D, Kotur-Stevuljevic J, Miljkovic M, Dikic N, Kostic-Vucicevic M, Andjelkovic M, et al. Effects of Probiotic Supplementation on Selected Parameters of Blood Prooxidant-Antioxidant Balance in Elite Athletes: A Double-Blind Randomized Placebo-Controlled Study. *J Hum Kinet* 2018; 64: 111–122.
38. Hays KE, Pfaffinger JM, Ryznar R. The interplay between gut microbiota, short-chain fatty acids, and implications for host health and disease. *Gut Microbes.* 2024; 16(1): 2393270. doi:10.1080/19490976.2024.2393270.
39. Gonos ES, Kapetanou M, Sereikaite J, Bartosz G, Napařo K, Grzesik M, et al. Origin and pathophysiology of protein carbonylation, nitration and chlorination in age-related brain diseases and aging. *Aging (Albany NY)* 2018; 10: 868–901.
40. Vileno B, Jeney S, Sienkiewicz A, Marcoux PR, Miller LM, Forró L. Evidence of lipid peroxidation and protein phosphorylation in cells upon oxidative stress photo-generated by fullerols. *Biophys Chem.* 2010; 152(1-3): 164-169. doi:10.1016/j.bpc.2010.09.004.
41. Schindowski K, Leutner S, Kressmann S, Eckert A, Müller WE. Age-related increase of oxidative stress-induced apoptosis in mice prevention by Ginkgo biloba extract (EGb761). *J Neural Transm (Vienna).* 2001; 108(8-9): 969-978. doi:10.1007/s007020170016.
42. Matera MG, Calzetta L, Cazzola M. Oxidation pathway and exacerbations in COPD: the role of NAC. *Expert Rev Respir Med* 2016; 10: 89–97.
43. Huetsch JC, Suresh K, Shimoda LA. Regulation of Smooth Muscle Cell Proliferation by NADPH Oxidases in Pulmonary Hypertension. *Antioxidants (Basel)* 2019; 8. doi:10.3390/antiox8030056.
44. Fulton DJR, Li X, Bordan Z, Haigh S, Bentley A, Chen F, et al. Reactive Oxygen and Nitrogen Species in the Development of Pulmonary Hypertension. *Antioxidants (Basel)* 2017; 6. doi:10.3390/antiox6030054.
45. Otoupalova E, Smith S, Cheng G, Thannickal VJ. Oxidative Stress in Pulmonary Fibrosis. *Compr Physiol* 2020; 10: 509–547.
46. Teker HT, Ceylani T, Keskin S, Samgane G, Baba B, Acikgoz E, et al. Reduced liver damage and fibrosis with combined SCD Probiotics and intermittent fasting in aged rat. *J Cell Mol Med* 2023; 1–11.

Research Article

DETECTION OF *Staphylococcus aureus* VIA APTAMER-GATED MCM-41 NANOPARTICLES

 Samet UÇAK*

Department of Medical Biology, Medical Faculty, Istanbul Aydin University, Istanbul, Turkiye

*Correspondence: sametucak@aydin.edu.tr

ABSTRACT

Objective: Aptamer-gated nanoparticles are a possible way to find *Staphylococcus aureus* because they are very specific, sensitive, and quick to detect.

Materials and Methods: MCM-41 nanoparticles were characterized via DLS, SEM, and FTIR techniques. Reference strains *S. aureus*, *S. epidermidis*, and *Escherichia coli* were used. After the synthesis of the fluorescence-loaded silica-coated MCM-41 nanoparticles, fluorescence release experiments were performed via a dialysis membrane.

Results: The particle size of the MCM-41 nanoparticles was determined to be 192 ± 1.782 nm. BET analysis revealed that each MCM-41 particle had a specific surface area of 1019.37 m²/g, pores that were 2.42 nm wide, and the ability to hold 0.99 cm³/g of material. The MCM-41 nanoparticles were nanosized, had a narrow size distribution, and were smooth, amorphous and spherical in shape. Amino group-functionalized MCM-41 nanoparticles via the APTES reaction. FT-IR analysis was performed to determine the correct conjugation. After the addition of amino acids, typical bands at 690 and 1460 nm appeared. These bands correspond to N-H bending vibrations and N-H asymmetric bending vibrations, respectively. The fluorescein-loaded silica particles conjugated with the aptamer and the target bacterium *S. aureus* had the maximum release. Furthermore, approximately 70% fluorescein release occurred within 6 hours. It was possible to quickly and accurately find *S. aureus* at detection limits as low as 164 CFU/mL in PBS.

Conclusion: The proposed biosensor has many benefits, such as quick response times, high sensitivity, and specificity for *S. aureus* detection. Future studies will likely concentrate on increasing the sensitivity of these technologies, decreasing detection times, and broadening their range of applications.

Keywords: Aptamer, Biosensor, MCM-41 nanoparticle, *S. aureus*, Specific detection.

Received: 26 November 2025

Revised: 27 February 2025

Accepted: 03 March 2025

Published: 20 March 2025



Copyright: © 2025 by the authors. Published by Aydın Adnan Menderes University, Faculty of Medicine and Faculty of Dentistry. This article is openly accessible under the Creative Commons Attribution-NonCommercial 4.0 International (CC BY-NC 4.0) License.

INTRODUCTION

In recent years, the rapid and sensitive detection of bacterial pathogens has become increasingly important in various disciplines, including health care, food safety, and environmental monitoring. *Staphylococcus aureus* (*S. aureus*) is a notable pathogen because of its capacity to induce various infections, ranging from superficial skin conditions to severe, life-threatening illnesses (1). One of the most clinically significant species is the *S. aureus* bacterium. *S. aureus*, which has a gram-positive coccus morphology, is highly adaptable in terms of its ability to acquire resistance to antibiotics. When faced with novel obstacles, *S. aureus* adapts quickly, which aids in its survival and clonal growth (2, 3). Information reported in 2019 by the U.S. Centers for Disease Control and Prevention (CDC), on the basis of 2017 data, revealed that *S. aureus* infections in the U.S. infected 119,000 people and caused the deaths of approximately 20,000 people, highlighting it as a major problem (4). To address the need for efficient detection methods, biosensors have emerged as promising tools for the rapid and specific detection of bacterial pathogens (5).

MCM-41 is a type of mesoporous silica material with a hexagonal array of uniform pores. Recent studies have highlighted the versatility of MCM-41 in various applications, particularly in catalysis and drug delivery. For example, its high surface area and tunable pore size make it an excellent candidate for supporting catalysts in chemical reactions, leading to enhanced reaction rates and selectivity (6, 7). MCM-41 is also biocompatible and can encapsulate a wide range of drugs. This makes it a promising material in the field of nanomedicine for targeted drug delivery systems that improve the effectiveness and controlled release of therapeutics (8).

The active targeting of nanoparticulate systems frequently involves the use of aptamers (9). Aptamers are single-stranded nucleic acids that are synthetically produced under in vitro conditions. These synthetic oligonucleotides can bind to a wide variety of target molecules (proteins, metal ions, monosaccharides, peptides, microorganisms, cells, and tissues) with high selectivity and affinity. DNA or RNA can be composed of aptamers. Their specific binding to target molecules occurs due to their three-dimensional structures. Aptamers can be easily modified to target specific molecules (10-12). Owing to their low molecular weight, ease of repeated synthesis, nontoxic nature as targeting ligands, and ability to regain their active conformation, aptamers have advantages in active targeting. In addition to their use as biosensors, active

targeting systems utilize aptamers for diagnosis, treatment, and drug delivery (13).

This paper introduces a biosensor utilizing aptamer-functionalized MCM-41 for the quick and highly sensitive detection of *S. aureus*.

MATERIALS AND METHODS

All additional compounds, including 3-(triethoxysilyl)propylamine (APTES) and MCM-41, were acquired from Sigma-Aldrich. The *S. aureus* oligonucleotide was synthesized by Sentegen (Ankara, Türkiye). In accordance with the sequence published by Cao and colleagues (14), the *S. aureus* binding aptamer was synthesized as follows: 5' amino-labeled aptamer sequence (5'-GCG CCC TCT CAC GTG GCA CTC AGA GTG CCG GAA GTT CTG CGT TAT-3'). The reference strains *S. aureus* (ATCC 29213), *S. epidermidis* (ATCC 12228), and *Escherichia coli* (ATCC 25922) were obtained recently from the American Type Culture Collection (ATCC). Figure 1 is a schematic depiction of strategy as used in this study.

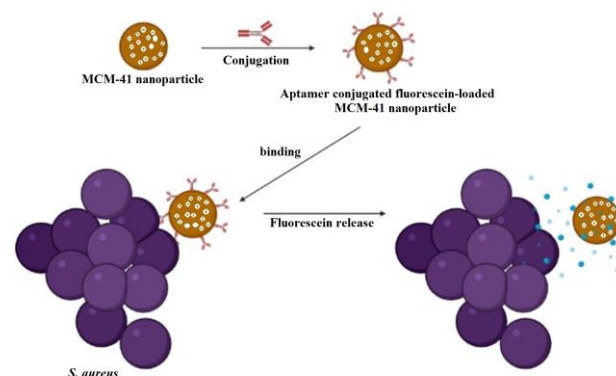


Figure 1. The general scheme of aptamer-gated specific fluorescein release profile approach.

Characterization of MCM-41 Nanoparticles

The particle sizes were measured with a Zetasizer ZEN 3600 Nano-ZS (Malvern Instruments, Worcestershire, UK). One milligram of MCM-41 particles was suspended in PBS and sonicated for 20 minutes in phosphate buffer (50 mM, pH 7.0) at room temperature to plot the intensity vs. diameter size.

The morphological evaluation of the particles was performed via Brunauer–Emmett–Teller (BET) (Quantachrome BET analyzer, Anton–Paar) and scanning electron microscopy (SEM; Zeiss EVO LS 10) at Yıldız Technical University's MERKLAB, Türkiye.

To determine whether amine groups were present on the surfaces of the MCM-41 nanoparticles, Fourier transform

infrared (FTIR) spectroscopy (Perkin Elmer Inc., Norwalk, CT, USA) fitted with a Universal ATR attachment was used. The one-bounce ATR mode was utilized to capture the ATR-FTIR spectra of the silica-coated magnetic nanoparticles. The spectral wavelengths ranged from 650 cm^{-1} to 4000 cm^{-1} when one milliliter of MCM-41 nanoparticle sample in PBS was used.

Aptamer-functionalized magnetic-silica particle preparation

The surface free amine groups of hybrid magnetic-silica particles were covalently linked with amino-modified aptamers after being initially activated with glutaraldehyde (15). Two hundred fifty milligrams of amino-functionalized hybrid magnetic-silica particles were introduced into a reactor containing 2% glutaraldehyde in 0.1 M phosphate buffer at pH 7.0. After the coupling reaction was conducted for 3h at 35°C, the mixture was subsequently rinsed with 0.1 M acetic acid, followed by 0.1 M phosphate buffer. Two hours after being placed in phosphate buffer at a concentration of 50 mM and a pH of 8.5, fifty milligrams of hybrid silica nanoparticles that were already functionalized with amino groups were transferred to phosphate buffer containing *S. aureus* binding aptamer at concentrations of 100 μL and 200 μM . An aptamer that was tagged with 5' amino acids was attached to magnetic beads at a temperature of 25°C for a period of 18h while the reaction mixture was continually mixed. Finally, the noncovalently attached aptamer molecules were extracted from the magnetic beads by using a buffer consisting of PBS. A UV-vis spectrophotometer (Agilent 8000, USA) was used to quantify the quantity of bound aptamer via the UV-absorption method at 265 nm.

Synthesis of silica coated MCM-41 nanoparticles

A previously presented approach (16) was employed to synthesize amino-functionalized SiO_2 nanoparticles. One milliliter of 95% ethanol, including 5% 1 mM acetic acid, was agitated with 50 mg of MCM-41 for 1h at room temperature. After adding the APTES solution at a molar ratio of MCM41/APTES (1/5) and mixing, the mixture was incubated overnight. The solution was rinsed three times with 1 \times PBS during centrifugation (14000 rpm, 5 min). Following the dissolution of 10 μl of amino-modified nanoparticles in 190 μl of 1 \times PBS, 100 μM fluorescein sodium salt was added. While the solution was stirred, it was incubated overnight. Finally, the fluorescein-loaded silica nanoparticles present in the PBS solution were conjugated with a 1 μM *S. aureus* 5' amino-labeled aptamer sequence. The solution was stirred while it was incubated overnight. By comparing the spectra of the initial and final

concentrations (Ex: 460 nm, Em: 520 nm), the levels of fluorescein (FL) were quantified.

Bacterial cultures

S. aureus, *S. epidermidis*, and *E. coli* were grown overnight in tryptone soy broth (TSB) from frozen stocks at 37°C. To attain the desired concentrations, the cultures were serially diluted in PBS buffer. The individual colony-forming units (CFUs) were enumerated following the surface plating of samples on TSB agar plates, which were incubated 37°C overnight.

Fluorescence assay

The samples spiked with the specific bacteria were culture-plated for colony counting, and fluorescence was assayed after the addition of one milligram of aptamer-nanoparticles. Eluted cells were serially diluted on TSB agar plates and cultivated overnight at 37°C. The number of viable colonies was counted and reported as CFU/ml.

Fluorescence release experiments

A fluorescence spectrophotometer (Fluoromax 4, Horiba) with Ex. 460 nm and Em. 520 nm was used to measure the release of fluorescein molecules from pores. The coated mesoporous silica particles were placed in a cell holder. The particles were confined within a compartment formed by a dialysis membrane (molecular cutoff of 12,000 Da) at the top of the spectroscopic cuvette, thereby preventing their mixing, as previously documented (17). Throughout the readings, the mixture was constantly swirled to make it uniform. The samples were measured at different points in time. The cumulative fluorescein release as a percentage of total molecules was plotted.

RESULTS

The particle size of the MCM-41 nanoparticles was determined to be 192 ± 1.782 nm on the basis of the findings of three separate particle size analyses as determined by dynamic light scattering (DLS), the results of which are shown in Figure 2. The size distribution of the MCM-41 nanoparticles was found to be within a narrow range, on the basis of the size distribution study results shown in Figure 2. According to BET analysis, the MCM-41 particles had a specific surface area of 1019.37 m^2/g , a pore size of 2.42 nm, and a pore volume of 0.99 cm^3/g .

SEM analysis was used to examine the morphological structure of MCM-41. The SEM characterization results shown in Figure 3 revealed that the MCM-41 nanoparticles were nanosized, had a narrow size distribution, and were smooth, amorphous and spherical in shape. Additionally, SEM analysis, revealed that the images of the MCM-41

nanoparticles (Figure 3-A) and APTES-coated MCM-41 nanoparticles (Figure 3-B) were similar.

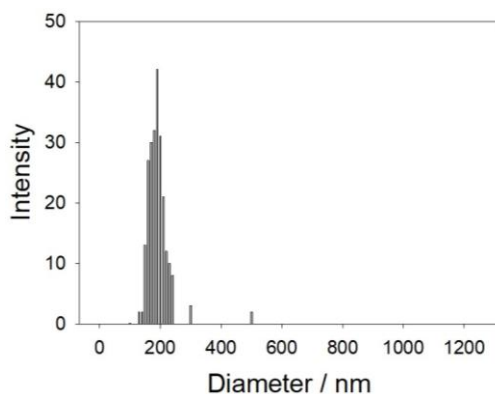


Figure 2. DLS particle size analysis of the MCM-41 nanoparticles

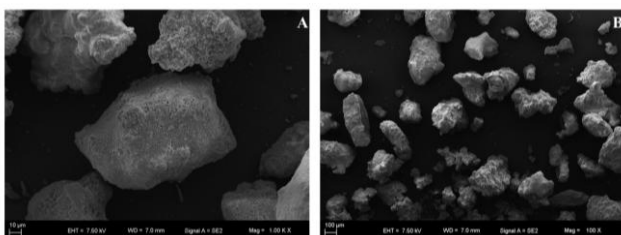


Figure 3. SEM images for morphological analysis of the MCM-41 nanoparticles (A), and APTES-coated MCM-41 nanoparticles (B).

Through an APTES reaction, MCM-41 nanoparticles (shown in Figure 4-A) were functionalized with amino groups (shown in Figure 4-B). FT-IR analysis was performed to determine the correct conjugation. The FT-IR study was performed in ATR mode with 3 replicates. Typical bands at 690 and 1460 nm, which correspond to N-H bending vibrations and N-H asymmetric bending vibrations, respectively, emerged following amino grafting, as shown in Figure 4-B.

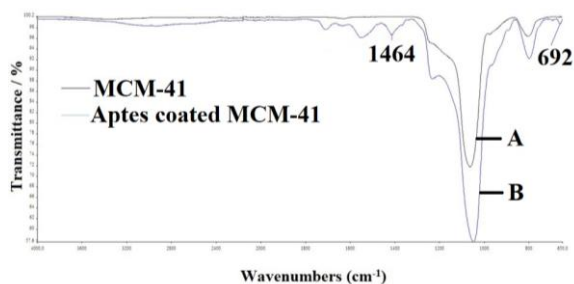


Figure 4. FTIR spectra of the MCM-41 nanoparticles (A), and APTES-coated MCM-41 nanoparticles (B).

The use of aptamer-functionalized silica magnetic nanoparticles for prepurification in a homogeneous test for the detection of *S. aureus* in PBS samples allowed for

the elimination of interference from PBS. At detection limits as low as 164 CFU/mL in PBS, rapid and sensitive detection of *S. aureus* was obtained. Adsorption by electrostatic attraction between negatively charged oligonucleotides and the positively charged silica surface was used to achieve DNA capping.

In Figure 5, the green line shows fluorescein-loaded silica particles without aptamer and any target bacteria. The blue line shows fluorescein-loaded silica particles conjugated with the aptamer and the target bacterium *S. aureus*. The gray line shows fluorescein-loaded silica particles conjugated with the aptamer and the target bacteria *S. epidermidis*. The red line shows fluorescein-loaded silica particles conjugated with the aptamer without any target bacteria. The yellow line shows fluorescein-loaded silica particles conjugated with the aptamer and the target bacteria *E. coli*. The release of fluorescein was measured at various intervals. The standard deviation of experiments conducted in triplicate is shown by error bars.

The *S. aureus* aptamer blocked the silica nanoparticles after they were loaded with reporter fluorescein molecules. In the release experiments (Figure 5), minimal release of fluorescein was observed in the fluorescein-loaded silica particles conjugated with the aptamer without any target bacteria and in the fluorescein-loaded silica particles conjugated with the aptamer and the target bacteria *E. coli*. Fluorescein-loaded silica particles conjugated with aptamer and the target bacterium *S. epidermidis* also resulted in minimal release. The maximum release profile of fluorescein-loaded silica particles conjugated with the aptamer and the target bacterium *S. aureus* was similar to that of the positive control (fluorescein-loaded silica particles without the aptamer and any target bacteria). In addition, approximately 70% fluorescein release occurred within 6h.

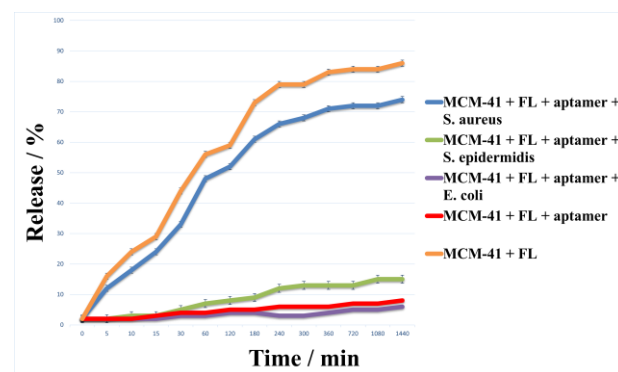


Figure 5. Fluorescein release profile from aptamer conjugated MCM-41 nanoparticles.

DISCUSSION

Numerous infections are caused by the important human pathogen *S. aureus*. For treatment and control to be effective, quick and precise detection techniques are essential. Recently, researchers have investigated how to use aptamer-gated nanoparticles to find *S. aureus*. This is possible because aptamers are very sensitive and specific (18).

The size range of MCM-41 nanoparticles is usually between 40 and 200 nm, and their size distribution is narrow, which makes them uniform (19, 20). Transmission electron microscopy and X-ray diffraction revealed that the nanoparticles had a smooth surface and a structure made of amorphous silica. The display of these characteristics of the nanoparticles (21) supports this finding. SEM, revealed that the majority of the nanoparticles that make up MCM-41 have a spherical shape (21, 22).

The band at 690 nm represents the N–H bending vibrations. This is a typical feature of hydrogen-bonded amino group infrared spectra, where anharmonic interactions couple the bending and stretching vibrations together. N–H asymmetric bending vibrations are linked to the band at 1460 nm. This band is made up of complex vibrational interactions inside the amino group, especially those involving asymmetric stretching and bending modes (23). In line with this study, Ercan and colleagues (24) reported that the bands that appeared in the FTIR analysis at approximately 690 and 1460 after amine functionalization are responsible for N–H bending vibrations and N–H asymmetric bending vibrations. The existence of these two bands was often regarded as proof of the presence of amino groups on the silica surfaces.

Using fluorescein-loaded silica particles linked with aptamers has been shown to be a successful way to target *S. aureus*. This strategy ensures sensitive and targeted detection and release, depending on the strong affinity of the aptamer for *S. aureus*. This study achieved rapid and sensitive detection of *S. aureus*, with detection limits as low as 164 CFU/mL in PBS. This study was similar to that of Shangguan et al., who used click chemistry to attach chloropropyl-functionalized fluorescent silica nanoparticles (FSiNPs) to aptamers that bind strongly to *S. aureus*. In microfluidic channels, this bioconjugate (Apt(*S.aureus*)/FNPs) enabled sensitive and rapid detection of *S. aureus*, with detection limits of 270 cfu/mL in spiked water samples and 93 cfu/mL in deionized water (25). Another study used a dual-color flow cytometry assay with aptamer/FSiNPs to show that *S. aureus* could be

easily identified and fluorescently labeled, with limits of detection of 150 cells/mL in buffer and 760 cells/mL in spiked milk (26). They reported that *S. aureus* could be easily identified and fluorescently labeled, with limits of detection of 150 cells/mL in buffer and 760 cells/mL in spiked milk (26). Zhu and colleagues reported that signal molecules (4-aminothiophenol, 4-ATP) were placed on mesoporous silica nanoparticles (MSNs). Raman spectroscopy was used to detect the signal molecules after the aptamer gates opened upon binding to *S. aureus*. This method revealed a straight-line connection between the amount of *S. aureus* and the signal strength, with a detection limit of 17 cfu/mL (27).

Using aptamer-gated nanocapsules, Kavruk et al. reported that mesoporous silica nanoparticles could be used to target *S. aureus* for antibiotic delivery, which led to a specific decrease in the minimum inhibitory concentration (MIC) of vancomycin (28). Borsa and colleagues published a homogeneous test for *S. aureus* identification that uses aptamer-functionalized silica magnetic nanoparticles to prepurify blood samples. This method eliminates interference from blood components. This technique detected as few as 682 CFU of *S. aureus* in whole blood (29). Chen and colleagues reported that the fiber sensor they made can find *S. aureus* in PBS with a response time of less than 30 minutes and a limit of detection of 3.1 CFU/mL (30). He and colleagues reported that they used aptamer recognition and fluorescent silica nanoparticles to develop a sensitive and specific way to find *S. aureus*. This method can find as few as 1.5×10^2 cells/mL in buffer and spiked milk, which is much lower than Aptamer/FITC-based flow cytometry (31). In their study, Qiao and colleagues developed a new aptamer-based fluorometric assay that can quickly and accurately find methicillin-resistant *S. aureus* in clinical samples. Within two hours, methicillin-resistant *S. aureus* can be detected in clinical samples. It can find as few as 2.63×10^3 CFU/mL in PBS and 1.38×10^3 CFU/mL in spiked nasal swabs (32).

CONCLUSION

The proposed biosensor offers several advantages, including rapid response times, high sensitivity, and specificity for *S. aureus* detection. It can also work with different sample matrices and can be added to portable and automated platforms, which makes it a useful tool for onsite detection in a range of situations. This platform's unique properties make it an ideal candidate for many applications in healthcare and biotechnology.

Acknowledgments

The author expresses his gratitude to Prof. Dr. Veli Cengiz Özalp for his valuable insights and support.

Authorship contributions

S.U. was the designer of the study and contributed to every section of the article. The author reviewed and approved the final draft of the text.

Data availability statement

Data will be made available on request.

Declaration of competing interest

The author declares that he has no conflict of interest.

Ethics

This study does not require ethical committee approval.

Funding

This research did not receive any specific grant from funding agencies in the public, commercial, or not-for-profit sectors.

REFERENCES

1. Liu A, Garrett S, Hong W, Zhang J. Staphylococcus aureus Infections and Human Intestinal Microbiota. *Pathogens* 2024; 13(4): 276.
2. Idrees M, Sawant S, Karodia N, Rahman A. Staphylococcus aureus biofilm: Morphology, genetics, pathogenesis and treatment strategies. *Int J Environ Res Public Health* 2021; 18(14): 7602.
3. Alves J, Vrieling M, Ring N, Yebra G, Pickering A, Prajsnar TK, Renshaw SA, Fitzgerald JR. Experimental evolution of Staphylococcus aureus in macrophages: dissection of a conditional adaptive trait promoting intracellular survival. *mBio* 2024; 15(6): e0034624.
4. Kavanagh KT. Control of MSSA and MRSA in the United States: protocols, policies, risk adjustment and excuses. *Antimicrob Resist Infect Control* 2019; 8: 103.
5. Qiu M, Zheng M, Zhang J, Yang X, Zhang Y, Zhang W, Man C, Zhao Q, Jiang Y. Recent advances on emerging biosensing technologies and on-site analytical devices for detection of drug-resistant foodborne pathogens. *Trends Anal Chem* 2023; 167: 117258.
6. García-Uriostegui L, Meléndez-Ortiz HI, Mata-Padilla JM, Toriz G. Fast fabrication of mesostructured MCM-41-type nanoparticles by microwave-induced synthesis. *Ceram Int* 2023; 49: 28693-28701.
7. Wei Y, Yang W, Yang Z. An excellent universal catalyst support-mesoporous silica: Preparation, modification and applications in energy-related reactions. *Int J Hydrogen Energy* 2022; 47(16): 9537-9565
8. Trzeciak K, Chotera-Ouda A, Bak-Sypien II, Potrzebowski MJ. Mesoporous silica particles as drug delivery systems-the state of the art in loading methods and the recent progress in analytical techniques for monitoring these processes. *Pharmaceutics* 2021; 13(7): 950.
9. Fu Z, Xiang J. Aptamer-functionalized nanoparticles in targeted delivery and cancer therapy. *Int J Mol Sci* 2020; 21(23): 9123.
10. Stoltenburg R, Reinemann C, Strehlitz B. Selex—a (r) evolutionary method to generate high-affinity nucleic acid ligands. *Biomol Eng* 2007; 24(4): 381-403.
11. Mairal T, Özalp VC, Sánchez PL, Mir M, Katakis I, O'Sullivan CK. Aptamers: Molecular tools for analytical applications. *Anal Bioanal Chem* 2008; 390: 989-1007.
12. Zhou H, Li Y, Wu W. Aptamers: Promising Reagents in Biomedicine Application. *Adv Biol* 2024; 8(6): 2300584.
13. Anarjan FS. Active targeting drug delivery nanocarriers: Ligands. *Nano-Struct Nano-Objects* 2019; 19: 100370.
14. Cao X, Li S, Chen L, Ding H, Xu H, Huang Y, Li J, Liu N, Cao W, Zhu Y, Shen B, Shao N. Combining use of a panel of ssDNA aptamers in the detection of staphylococcus aureus. *Nucl Acids Res* 2009; 37(14): 4621-4628.
15. Borsa BA, Tuna BG, Hernandez FJ, Hernandez LI, Bayramoglu G, Arica MY, Ozalp VC. Staphylococcus aureus detection in blood samples by silica nanoparticle-oligonucleotides conjugates. *Biosens Bioelectron* 2016; 86: 27-32.
16. Ozalp VC, Eyidogan F, Oktem HA. Aptamer-gated nanoparticles for smart drug delivery. *Pharmaceutics* 2011; 4(8): 1137-1157.

17. Ozalp VC, Schäfer T. Aptamer - based switchable nanovalves for stimuli - responsive drug delivery. *Chem Eur J* 2011; 17(36): 9893-9896.
18. Chen W, Lai Q, Zhang Y, Liu Z. Recent advances in aptasensors for rapid and sensitive detection of *Staphylococcus aureus*. *Front Bioeng Biotechnol* 2022; 10: 889431.
19. Castillo RR, de la Torre L, García-Ochoa F, Ladero M, Vallet-Regí M. Production of MCM-41 nanoparticles with control of particle size and structural properties: optimizing operational conditions during scale-up. *Int J Mol Sci* 2020; 21(21): 7899.
20. Jomekian A, Mansoori SAA, Monirimanesh N. Synthesis and characterization of novel PEO–MCM-41/PVDC nanocomposite membrane. *Desalination*, 2011; 276(1-3): 239-245.
21. Dau TAN, Le VMH, Pham TKH, Le VH, Cho SK, Nguyen TNU TKH, Van Tran, TT. Surface functionalization of doxorubicin loaded MCM-41 mesoporous silica nanoparticles by 3-aminopropyltriethoxysilane for selective anticancer effect on A549 and A549/DOX cells. *J Electron Mater* 2021; 50: 2932-2939.
22. Khalil KMS. Cerium modified MCM-41 nanocomposite materials via a nonhydrothermal direct method at room temperature. *J Colloid Interface Sci* 2007; 315(2): 562-568.
23. Mishra S, Nguyen HQ, Huang QR, Lin CK, Kuo JL, Patwari GN. Vibrational spectroscopic signatures of hydrogen bond induced NH stretch–bend Fermi-resonance in amines: The methylamine clusters and other N–H... N hydrogen-bonded complexes. *J Chem Phys* 2020; 153(19): 194301
24. Ercan M, Ozalp VC, Tuna BG. Genotyping of single nucleotide polymorphism by probe-gated silica nanoparticles. *Anal Biochem* 2017; 537: 78-83.
25. Shangguan J, Li Y, He D, He X, Wang K, Zou Z, Shi H. A combination of positive dielectrophoresis driven on-line enrichment and aptamer-fluorescent silica nanoparticle label for rapid and sensitive detection of *Staphylococcus aureus*. *Analyst*, 2015; 140(13): 4489-4497.
26. He X, Li Y, He D, Wang K, Shangguan J, Shi H. Aptamer-fluorescent silica nanoparticles bioconjugates based dual-color flow cytometry for specific detection of *Staphylococcus aureus*. *J Biomed Nanotechnol* 2014; 10(7): 1359-1368.
27. Zhu A, Jiao T, Ali S, Xu Y, Ouyang Q, Chen Q. SERS sensors based on aptamer-gated mesoporous silica nanoparticles for quantitative detection of *Staphylococcus aureus* with signal molecular release. *Anal Chem* 2021; 93(28): 9788-9796.
28. Kavruk M, Celikbicak O, Ozalp VC, Borsa BA, Hernandez FJ, Bayramoglu G, Salih B, Arica MY. Antibiotic loaded nanocapsules functionalized with aptamer gates for targeted destruction of pathogens. *Chem comm* 2015; 51(40): 8492-8495.
29. Borsa BA, Tuna BG, Hernandez FJ, Hernandez LI, Bayramoglu G, Arica MY, Ozalp VC. *Staphylococcus aureus* detection in blood samples by silica nanoparticle-oligonucleotides conjugates. *Biosens Bioelectron* 2016; 86: 27-32.
30. Chen L, Leng YK, Liu B, Liu J, Wan SP, Wu T, Yuan J, Shao L, Gu G, Fu Y, Xu H, Xiong Y, He X, Wu Q. Ultrahigh-sensitivity label-free optical fiber biosensor based on a tapered singlemode-no core-singlemode coupler for *Staphylococcus aureus* detection. *Sens Actuators B Chem* 2020; 320: 128283.
31. He X, Li Y, He D, Wang K, Shangguan J, Shi H. Aptamer-fluorescent silica nanoparticles bioconjugates based dual-color flow cytometry for specific detection of *Staphylococcus aureus*. *J Biomed Nanotechnol* 2014; 10(7): 1359-1368.
32. Qiao J, Meng X, Sun Y, Li Q, Zhao R, Zhang Y, Wang J, Yi Z. Aptamer-based fluorometric assay for direct identification of methicillin-resistant *Staphylococcus aureus* from clinical samples. *J Microbiol Methods* 2018; 153: 92-98.

Research Article

GENE EXPRESSIONS ASSOCIATED WITH NEUROTRANSMITTER METABOLISM IN CHILDREN WITH ATTENTION DEFICIT HYPERACTIVITY DISORDER

 Hilal AKALIN ¹,  Yakut ERDEM ²,  Recep ERÖZ ³,  İzel Olcay ŞAHİN ¹,  Nuriye GÖKÇE ¹,
 Sevgi ÖZMEN ⁴,  Muhammet Ensar DOĞAN ⁵,  Munis DÜNDAR ¹,  Yusuf ÖZKUL ¹

¹ Erciyes University, Faculty of Medicine, Department of Medical Genetics, Kayseri, Türkiye

² Erciyes University, Faculty of Pharmacy, Department of Basic Sciences, Kayseri, Türkiye

³ Aksaray University Medical Faculty, Department of Medical Genetics, Aksaray, Türkiye

⁴ Erciyes University, Faculty of Medicine, Department of Child and Adolescent Psychiatry, Kayseri, Türkiye

⁵ Kayseri Training and Research Hospital, Kayseri, Türkiye

*Correspondence: hakalin@erciyes.edu.tr

ABSTRACT

Objective: To investigate the expression levels of genes (*SLC6A3*, *SLC6A4*, *SLC1A2*, *SLC18A2*, *MAOA*, *COMT*, *GLYAT*, *GRM5*, *DRD4*, *TPH1*, and *ADRA2C*) associated with attention deficit hyperactivity disorder (ADHD) by pre and post-treatment with methylphenidate to see if they may serve as biomarkers in the etiopathogenesis of diseases.

Materials and Methods: Thirty-five ADHD-diagnosed children and 38 healthy controls were included and divided three groups as control, pre-treatment and post-treatment group. Following total RNA isolation from participants' peripheral blood samples, cDNA was synthesized via reverse transcription and used for qPCR analyses.

Results: Elevated *SLC6A3* and decreased *SLC6A4*, *SLC1A2*, *SLC18A2*, *ADRA2C*, *MAOA*, *COMT*, *GLYAT*, *DRD4* and *TPH1* genes expression levels of children with ADHD were detected ($p < 0.01$). In post-treatment group, while *SLC6A3* and *COMT* expression levels decreased, the expression levels of *SLC6A4*, *SLC1A2*, *SLC18A2*, *ADRA2C*, *MAOA*, *GLYAT*, *GRM5* and *TPH1* significantly increased ($p < 0.01$). Highlighted relationships among gene expressions levels of control, pre-treatment, and post-treatment groups were detected. Additionally, cut-off values with diagnostic power for *SLC6A3*, *SLC6A4*, *SLC1A2*, *SLC18A2*, *ADRA2C*, *MAOA*, *COMT*, *GLYAT*, *DRD4*, and *TPH1* were detected.

Conclusion: The expression levels of the *SLC6A3*, *SLC6A4*, *SLC1A2*, *SLC18A2*, *ADRA2C*, *MAOA*, *COMT*, *GLYAT*, *DRD4*, and *TPH1* genes may play an important role in the formation, prognosis and etiopathogenesis of the disease, and these changes can also be used as biomarkers in the differential diagnosis and development of treatment strategies for the disease.

Keywords: ADHD, methylphenidate, gene expression, qPCR

Received: 11 December 2025

Revised: 09 February 2025

Accepted: 09 February 2025

Published: 20 March 2025



Copyright: © 2025 by the authors. Published by Aydın Adnan Menderes University, Faculty of Medicine and Faculty of Dentistry. This article is openly accessible under the Creative Commons Attribution-NonCommercial 4.0 International (CC BY-NC 4.0) License.

INTRODUCTION

Attention Deficit Hyperactivity Disorder (ADHD) is an early-onset, heterogeneous neuropsychiatric disorder whose etiology and pathogenesis are still largely unknown. It is characterized with inattention, hyperactivity, impulsivity and incompatible with age and developmental levels (1). The incidence and prevalence of ADHD were reported as 0.061% and 1.13%, respectively (2). In Turkey, ADHD prevalence and male/female ratio were found to be 13.8% and 2/1, respectively (3). ADHD is multifactorial disorder related with genetic, epigenetic and biological signatures (3). The prefrontal cortex, caudate nucleus, globus pallidus, corpus callosum, and cerebellum volumes decreased in individuals with ADHD (4). Genetic changes may affect cortical functions in the prefrontal area, dopamine (DA) level in the synaptic region, or dopaminergic receptor function. Although the pathophysiology of ADHD states that the change in dopaminergic and noradrenergic pathways is not related to attention and impulse control, studies have focused on catecholaminergic norepinephrine (NE) and DA (5). Drugs for ADHD are effective on NE and DA release in the prefrontal cortex. In the treatment of ADHD, stimulants drugs such as methylphenidate (MPH) and non-stimulants drugs such as atomoxetine are commonly used. Psychostimulants act by preventing the reuptake of NE and DA from the synapse gap to the presynaptic neuronal space and increasing the release of monoamines into the extraneuronal space (6).

In addition to disclosing the roles of genetic variants in the etiopathogenesis of diseases (7-10), the exploration of both the expression levels of the genes (11-13) and their products (8,14-16) are crucial to understand their function and role in cellular homeostasis, viability and heterogeneous neuropsychiatric disorder. Most studies based on related candidate genes, meta-analyses, genome-wide association studies (GWAS), omics data, transcriptome profiling show that dopaminergic, serotonergic, and glutamatergic signaling, neuronal transmission, neuronal migration, and cell adhesion pathways etc. play a role in the etiology of ADHD (17-22). It is important overrepresentation of candidate genes previously studied in ADHD selected from the gene list provided by the ADHD gene database (<http://adhd.psych.ac.cn/index.do>) and a comprehensive search for published reviews of ADHD genetic and pharmacogenetic studies (23). Therefore, the genes *solute carrier family 6 member 3 (SLC6A3)*, *solute carrier family 6 member 4 (SLC6A4)*, *solute carrier family 1 member 2*

(SLC1A2), *solute carrier family 18 member A2 (SLC18A2)*, *monoamine oxidase A (MAOA)*, *catechol-O-methyltransferase (COMT)*, *glycine-N-acyltransferase (GLYAT)*, *glutamate metabotropic receptor 5 (GRM5)*, *dopamine receptor D4 (DRD4)*, *tryptophan hydroxylase 1 (TPH1)* and *adrenoceptor alpha 2C (ADRA2C)* that roles in the neurotransmitter pathway were included in the current study. Thus we aim to investigate the role of the mRNA expression profiles of these genes to see if they may serve as biomarkers in the etiopathogenesis of diseases and the possible effect of stimulant drugs such as MPH on the expression of these candidate genes.

MATERIALS AND METHODS

After the study was approved by the Local Ethics Committee (Erciyes University Local Ethic Committee's approval document dated TSD-12-4112 dated 28.07.2017), informed consents were obtained from all of the patients and their parents. The 35 boys between 6-12 years old who applied to the Pre-Interview Polyclinic of Erciyes University Faculty of Medicine, Department of Child and Adolescent Mental Health and Diseases and newly diagnosed as ADHD according to DSM IV (Diagnostic and Statistical Manual of Mental Disorders, Fifth Edition) diagnostic criteria and K-SADS-PL (Schedule for Affective Disorders and Schizophrenia for School-Age Children – Present and Lifetime version) criteria by an experienced psychiatrist and drug-naïve were included as patients group. The Clinical Global Impression-Severity (CGI-S) scale was ≥ 4 . A dosage range of 0.3 - 1 mg/kg MPH was prescribed depending on the weight and age of patients, prognosis and severity of the diseases by an experienced psychiatrist. 10 ml peripheral blood samples with EDTA was taken from the patient group using MPH (0.3-1 mg/kg) both before and after treatment and from the control group.

One month after the treatment had started, blood samples were taken after the ADHD symptoms had been evaluated. Also 38 boys age matched (6-12 years) without any psychiatric or chronic medical diseases were included as a control group in the study. The blood samples of individuals in the control group were also taken for expression analysis of the targeted genes. The demonstrative example of the study protocol was given in the figure 1.

Blood collection and leukocytes isolation

Blood samples were processed within 24 h of being collected in EDTA tubes. Leukocyte isolation was performed using Erythrocyte buffer. (Qiagen,cat

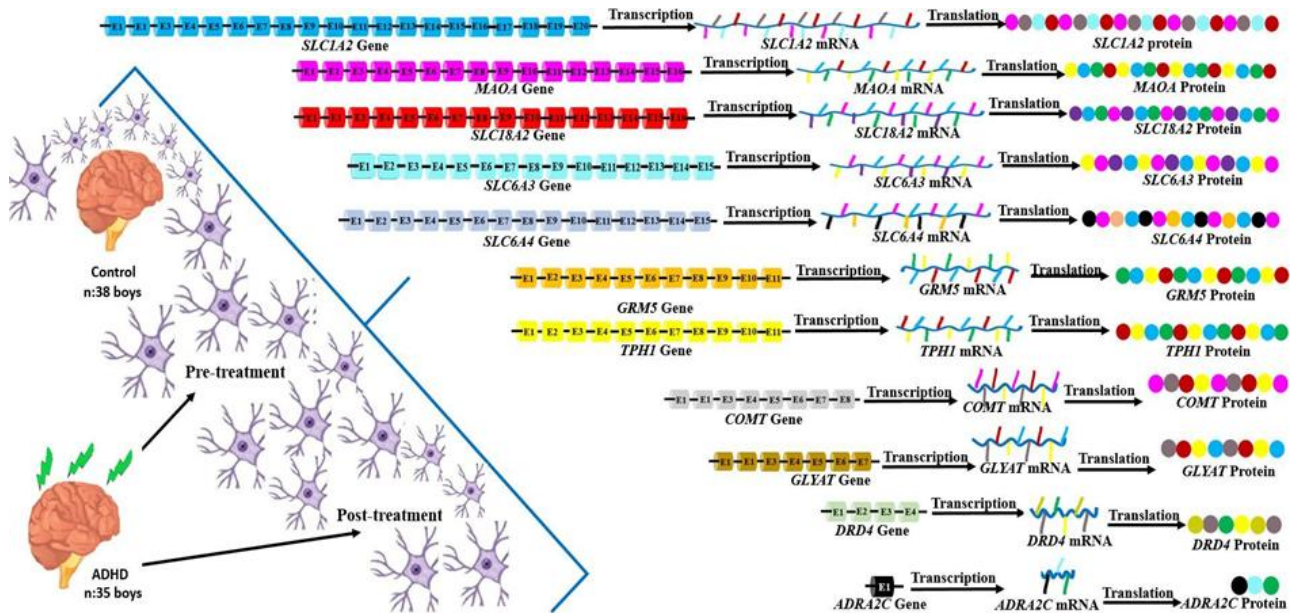


Figure 1. The demonstrative example of the study protocol

no:79217,Germany). Leukocytes were stored at -80°C in Trizol (QIAzol, cat no:79306, Germany) until RNA extraction.

Table 1. Probe sequences and assay ID used in Real-time PCR

Gene	Assay ID	Primer sequence (5'-3')
SLC6A3	143278	F;CAGACACCGTGAGCTTTC R;CAGGAGCGTGAAGACGTAGAT
SLC6A4	112029	F;AAGTTCAACAACAACACTGCTACCAA R;GAAGCTCGTCATGCAGTTCA
SLC1A2	111792	F;CCTGCCAACAGAGGACATC R;GACTGAAGTTCTCATCCTGTCCA
SLC18A2	112188	F;CGAAGTTGGAGTTGGTTTG R;CCCATGATAGGCATCATTGAC
ADRA2C	145162	F;CAGGAGCTTGGCAGAGAGAT R;GAAGGCCAAAGGGTCTCC
MAOA	113315	F;GGAGGTGGCATTTCAGGAC R;AAAACCAAAACACTAACGCCATA
COMT	112923	F;GTCTTCCTCGACCACTGGAA R;TCACGTGTGTCAGCCAGTAGC
GLYAT	118559	F;TGGCTGATTTTAATACAGTGG R;TTGGTATAGTGATCAAGGTCATCTG
GRM5	100941	F;CCTGCCAACAGAGGACATC R;GACTGAAGTTCTCATCCTGTCCA
DRD4	112907	F;CAGACTCCACCGCAGACC R;GTGATGTGCCACCACGAAGAA
TPH1	113010	F;GGACTTATAAAAGCCCTGAAAATCT R;TTCGGGACTCGATATGTAACAG
B.ACT	101125	F;GGCCAGGTATCACCATT R;GGATGCCACAGGACTCCAT

RNA isolation and cDNA synthesis

After the leukocyte isolation, RNA isolation and cDNA synthesis were performed from individuals in ADHD and control group (1xRBC LysisBuffer, Invitrogen. Leukocytes

were taken into 1000 μL of TriPure reagent (Roche Applied Science, Basel, Switzerland) for RNA isolation, and total RNA isolation was performed according to the protocol (24). The quality and quantification of RNA samples were detected with measurement of RNA concentrations and optical density at 260 and 280 nm using Nanodrop 1000 (Thermo Fisher Scientific, Germany). The cDNA was synthesized via the Transcriptor High Fidelity cDNA Synthesis Kit (Roche, Mannheim, Germany) following the manufacturer's protocol.

Relative gene expressions of the SLC6A3, SLC6A4, SLC1A2, VMAT2, MAOA, COMT, GLYAT, GRM5, DRD4, TPH1 and ADRA2C Genes by Real-Time qPCR

From the obtained cDNA samples, the mRNA expression levels of SLC6A3, SLC6A4, SLC1A2, VMAT2, MAOA, COMT, GLYAT, GRM5, DRD4, TPH1 and ADRA2C genes were determined by Real-Time qPCR method using the Roche LightCycler® 480 instrument II (Roche Diagnostics Ltd., Rotkreuz, Switzerland). Real-Time PCR mixture including 10 μL LightCycler 480 Probes Master, 1 μL RealTime ready Assays, 4 μL dH₂O was prepared. Temperatures and times set in LightCycler 480 II software were as follows; 1 cycles of preincubation is at 95°C for 10min (Temperature increase-decrease rate (oC/sec):4.4), 45 cycles of amplification at 95°C for 10sec, at 60°C for 30sec and at 72°C for 1sec {Temperature increase-decrease rate (oC/sec):4.4/2.2 and 4.4, respectively}, 1 cycles of Cooling at 40°C for 30sec {Temperature increase-decrease rate (oC/sec):2.2} in 20 μL total reaction volume. Real-Time qPCR was performed using cDNA, UPL probe,

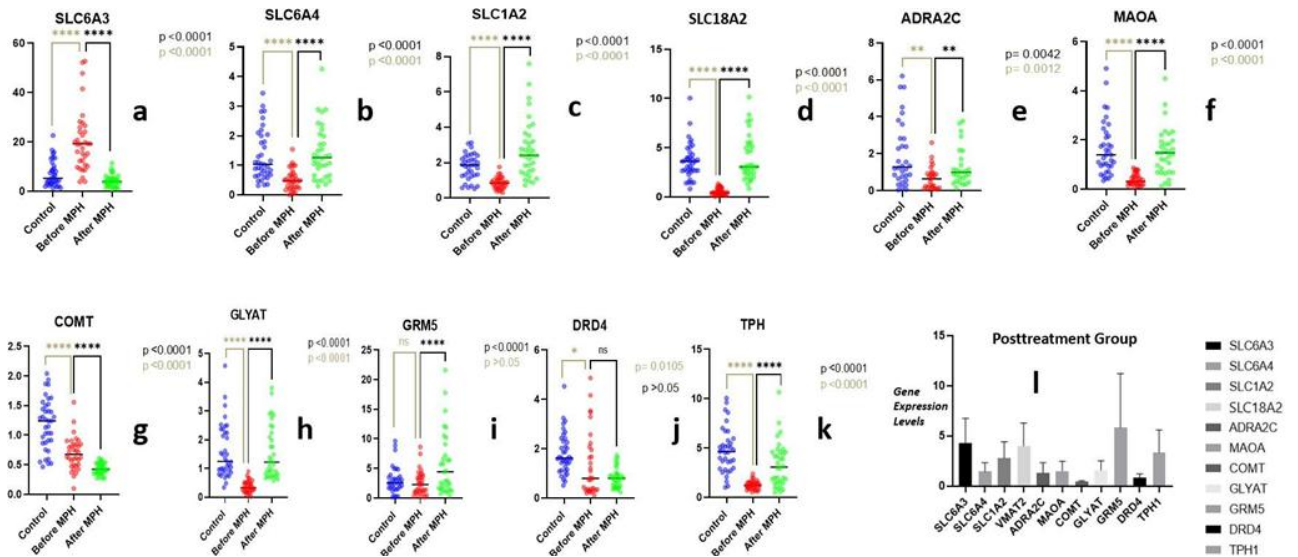


Figure 2. Comparison of groups in terms of expression levels of genes

LightCycler 480 Probes Master mix (Roche Diagnostics, Germany), hydrolysis probes and distilled water. Each sample was run in duplicate, with two negative controls and one calibrator used twice in each run. RealTime ready Catalog (Roche Diagnostic GmbH, Mannheim, Germany) primer-probe kits specific to each gene were used in the study. Analyzes were made with Light Cyler 480 Software (release 1.5.0 SP4) and $2^{-\Delta\Delta Ct}$ levels of the genes were detected.

The Beta-actin mRNA expression level was taken as a reference to normalize *SLC6A3*, *SLC6A4*, *SLC1A2*, *SLC18A2*, *MAOA*, *COMT*, *GLYAT*, *GRM5*, *DRD4*, *TPH1*, and *ADRA2C* gene expression levels. Expression levels of target genes were calculated according to the relative quantification method using the software program of the LightCycler 480 device. The Universal Probe Library (UPL) probe numbers that are specific to the cDNAs of the investigated genes are given in Table 1.

Statistical Analysis

Statistical analysis was performed using Graphpad Prism software (Graphpad Prism Inc., version 9.4.1, California, USA). Outlier values were determined by the route (Q = 1%) method, and all analyses were performed with the cleaned data. According to the distribution of the data detected by Shapiro-Wilk test, while the Wilcoxon matched-pairs signed rank test or paired t-test was used to compare dependent groups, the Mann-Whitney test or unpaired t-test was used to compare independent groups. The correlation between genes in each group was determined by Spearman's correlation coefficient. Bayesian statistics, based on receiver operating

Table 2. CGI-S, sex and comorbidities of both pre and post-treatment ADHD patients

Patient	Pre-treatment CGI-S	Post-treatment CGI-S
1	5	1
2	4	2
3	5	2
4	6	2
5	5	2
6	5	2
7	5	1
8	6	2
9	5	1
10	5	2
11	5	2
12	5	1
13	5	2
14	6	2
15	5	1
16	5	2
17	5	2
18	5	1
19	6	2
20	6	1
21	5	2
22	5	1
23	5	1
24	5	2
25	5	1
26	4	1
27	4	1
28	6	2
29	6	1
30	6	1
31	5	2
32	6	2
33	5	1
34	6	2
35	5	2

CGI-S: The Clinical Global Impression-Severity scale (1 = normal, not at all ill; 2 = borderline ill; 3 = mildly ill; 4 = moderately ill; 5 = markedly ill; 6 = severely ill; or 7 = among the most extremely ill.)

Table 3. Positive and negative correlations among SLC6A3, SLC6A4, SLC1A2, SLC18A2, MAOA, COMT, GLYAT, GRM5, DRD4, TPADRA2C genes expression levels in the groups. *p<0.05, **p<0.001

Groups	SLC6A3	SLC6A4	SLC1A2	SLC18A2	ADRA2C	MAOA	COMT	GLYAT	GRM5	DRD4
Control Group	SLC6A3	1	0.47*	0.14	0.30	0.66**	0.08	0.21	0.10	0.06
	SLC6A4	0.47*	1	0.12	0.68**	0.19	0.43*	0.21	0.46*	-0.11
	SLC1A2	0.14	0.12	1	0.02	0.07	-0.03	-	-0.14	0.07
	SLC18A2	0.30	0.68**	0.02	1	-0.06	0.28	-0.03	0.49*	-0.06
	ADRA2C	0.66**	0.19	0.07	-0.06	1	-0.10	0.08	-0.11	-0.09
	MAOA	0.08	0.043*	-0.03	0.28	-0.10	1	0.31	0.28	0.19
	COMT	0.21	0.21	-0.03	-0.03	0.08	0.31	1	0.24	0.18
	GLYAT	0.10	0.46*	-0.14	0.49*	-0.11	0.28	0.24	1	-0.26
	GRM5	0.06	-0.11	0.07	-0.06	-0.09	0.19	0.18	-0.26	1
	DRD4	0.10	0.26	0.24	0.24	-0.25	0.42*	0.17	0.16	0.23
	TPH1	0.19	0.39*	0.16	0.43*	-0.22	0.28	-0.05	0.32	0.10
Pre-treatment Group	SLC6A3	1	0.26	0.31	0.20	0.21	0.15	-0.11	0.19	-0.06
	SLC6A4	0.26	1	-0.10	0.73**	0.17	0.29	-0.10	0.44*	0.21
	SLC1A2	0.31	-0.10	1	0.24	-0.15	0.23	0.45*	0.05	0.12
	SLC18A2	0.20	0.73**	0.24	1	0.10	0.14	0.08	0.26	0.31
	ADRA2C	0.21	0.17	-0.15	0.10	1	0.14	-0.18	0.23	0.06
	MAOA	0.15	0.29	0.23	0.14	0.14	1	0.27	0.12	0.08
	COMT	-0.11	-0.10	0.45*	0.08	-0.18	0.27	1	-	0.13
	GLYAT	0.19	0.44*	0.05	0.26	0.23	0.12	-	1	0.01
	GRM5	-0.06	0.21	0.12	0.31	0.06	0.08	0.13	0.01	1
	DRD4	0.01	0.10	-0.10	0.02	-0.15	-0.04	0.24	0.17	-0.12
	TPH1	-0.02	0.05	0.31	0.35*	-0.23	0.11	0.25	0.05	0.51*
Post-treatment Group	SLC6A3	1	0.10	0.09	0.46*	0.18	0.22	0.20	0.20	0.14
	SLC6A4	0.10	1	0.52*	0.46*	0.34	0.26	-0.15	0.59**	-0.09
	SLC1A2	0.09	0.52*	1	0.30	0.18	0.17	-0.12	0.24	0.07
	SLC18A2	0.46*	0.46*	0.30	1	0.06	0.35*	-	0.43*	0.33
	ADRA2C	0.18	0.34	0.18	0.06	1	0.12	-0.08	0.33	-0.13
	MAOA	0.22	0.26	0.17	0.35*	0.12	1	-0.01	0.21	-0.14
	COMT	0.20	-0.15	-0.12	-	-0.08	-0.01	1	-0.19	0.09
	GLYAT	0.20	0.59**	0.24	0.43*	0.33	0.21	-0.19	1	-0.02
	GRM5	0.14	-0.09	0.07	0.33	-0.13	-0.14	0.09	-0.02	1
	DRD4	0.02	-0.06	-	-0.28	0.52*	0.22	0.25	0.08	-0.45*
	TPH1	0.14	0.29	0.29	0.40*	0.10	-0.08	-0.14	0.22	0.01

characteristic (ROC)-derived cutoff values was performed to determine the diagnostic power of genes in ADHD. The data were given as n, mean, Standard deviation (SD), minimum, maximum, the area under the ROC curve (AUC), Confidence Interval (CI), Cut-off specificity, sensitivity, r and p, The level of significance was set at p<0.05.

RESULTS

All of the individuals in the groups were male. None of the participants have comorbidities. Statistically significant differences were not found between the patients and control group for mean age (8.91± 0.31 vs 9.11± 0.31) and weight, (31.80 ± 1.98 vs 35.18 ± 2.19), respectively (p>0.05). The Clinical Global Impression-Severity (CGI-S) scale was ≥4. In the pre-treatment group, CGI-S of 22 participants was 5, CGI-S of 10 participants was 6 and CGI-S of 3 participants was 4. After the MPH (0.3-1 mg/kg) treatments by an experienced psychiatrist, CGI-S of 15 participants was detected as 1 and CGI-S of 20 participants was detected as 2. The CGI-S, sex and comorbidities of both

pre and post-treatment ADHD patients given in the table 2.

A comparison of the groups in terms of expression levels of genes is shown in figure 2. The only expression levels of SLC6A3 gene was statistically higher in the pre-treatment patient group than the control group (p<0.0001) (Figure 2a). The significantly decreased mRNA levels of SLC6A4 (p<0.0001) (Figure 2b), SLC1A2 (p<0.0001) (Figure 2c), SLC18A2 (p<0.0001) (Figure 2d), ADRA2C (p=0.0012) (Figure 2e), MAOA(p<0.0001) (Figure 2f), COMT (p<0.0001) (Figure 2g), GLYAT (p<0.0001) (Figure 2h), DRD4 (p<0.0105) (Figure 2j) and TPH1 (p<0.0001) (Figure 2k) were detected in the pre-treatment group compared to the control group. There is no significant differences between the pre-treatment patient and control group for GRM5 gene expression levels (p>0.05) (Figure 2i). The posttreatment correlation of the all genes were given in the figure 2l.

When the pre-and post-treatment groups were compared, significantly decreased mRNA levels of the SLC6A3

Table 4. Bayesian statistics, based on ROC derived cutoff values of the genes

Genes	AUC (95% CI)	Cut-off	p	Sensitivity%	Specificity%
<i>SLC6A3</i>	0.8723 (0.7911 to 0.9534)	10.47	<0.0001	77.14	76.47
<i>SLC6A4</i>	0.8351 (0.7451 to 0.9252)	0.675	<0.0001	76.47	76.32
<i>SLC1A2</i>	0.8571 (0.7630 to 0.9513)	1.149	<0.0001	81.82	80
<i>SLC18A2</i>	0.9934 (0.9796 to 1.000)	1.24	<0.0001	96.97	97.3
<i>ADRA2C</i>	0.7419 (0.6164 to 0.8674)	0.863	0.0015	62.96	62.5
<i>MAOA</i>	0.9363 (0.8842 to 0.9883)	0.672	<0.0001	82.35	83.33
<i>COMT</i>	0.8274 (0.7302 to 0.9246)	0.857	<0.0001	79.41	78.95
<i>GLYAT</i>	0.9705 (0.9360 to 1.000)	0.675	<0.0001	93.94	94.59
<i>GRM5</i>	0.5843 (0.4429 to 0.7257)	2.424	0.2429	56.25	57.58
<i>DRD4</i>	0.6791 (0.5383 to 0.8200)	1.44	0.0109	64.52	65.79
<i>TPH1</i>	0.9615 (0.9140 to 1.000)	1.838	<0.0001	90.91	91.89

AUC: Area under curve, CI: Confidence interval

($p < 0.0001$) (Figure 2a) and *COMT* ($p < 0.0001$) (Figure 2g) were detected in the post-treatment group. Although the *DRD4* gene expression level was lower in the post-treatment group than pre-treatment group, the difference was not significant ($p > 0.05$) (Figure 2j). Conversely, expression levels of *SLC6A4* ($p < 0.0001$) (Figure 2b), *SLC1A2* ($p < 0.0001$) (Figure 2c), *SLC18A2* ($p < 0.0001$) (Figure 2d), *ADRA2C* ($p = 0.0042$) (Figure 2e), *MAOA* ($p < 0.0001$) (Figure 2f), *GLYAT* ($p < 0.0001$) (Figure 2h), *GRM5* ($p < 0.0001$) (Figure 2i) and *TPH1* ($p < 0.0001$) (Figure 2k) genes significantly increased in the post-treatment group compared to the pre-treatment group (Figure 2). Spearman correlation analysis that shows relationship the expression levels of the related genes in the control, pre-treatment, and post-treatment groups were given in the table 3.

In the control group, significant positive correlations between the *SLC6A3* gene and both of the *SLC6A4* and *ADRA2C* genes ($r = 0.47$, $p = 0.0053$; $r = 0.66$, $p = 0.000058$, respectively), between the *SLC6A4* gene and all of the *SLC18A2*, *MAOA*, *GLYAT*, and *TPH1* genes ($r = 0.68$, $p = 0.000003$; $r = 0.43$, $p = 0.0089$; $r = 0.46$, $p = 0.0037$; $r = 0.39$, $p = 0.0189$, respectively), between the *SLC18A2* gene and both of the *GLYAT* and *TPH1* genes, respectively ($r = 0.49$, $p = 0.0023$; $r = 0.43$, $p = 0.009$, respectively), and between the *MAOA* gene and the *DRD4* gene ($r = 0.42$, $p = 0.011$) were detected. Conversely, the relation between the *COMT*, *SLC1A2*, *GRM5* genes and other genes were not significant (Table 2).

When the pre-treatment group to be taken into consideration, significant positive correlations between the *SLC6A4* and both of *SLC18A2* and *GLYAT* genes ($r = 0.73$, $p < 0.001$; $r = 0.44$, $p < 0.05$, respectively), between the

SLC1A2 gene and *COMT* gene ($r = 0.45$, $p < 0.05$), between the *SLC18A2* gene and *TPH1* gene ($r = 0.35$, $p < 0.05$), and between the *GRM5* gene and the *TPH1* gene ($r = 0.51$, $p < 0.05$) were detected. Conversely, the relation between the *SLC6A3*, *ADRA2C*, *MAOA*, *DRD4* genes and other genes were not significant (Table 2).

When the post-treatment group to be considered, significant positive correlations between the *SLC6A3* gene and *SLC18A2* genes ($r = 0.46$, $p < 0.05$), between the *SLC6A4* gene and all of the *SLC1A2*, *SLC18A2* and *GLYAT* genes ($r = 0.52$, $p < 0.05$; $r = 0.46$, $p < 0.05$; $r = 0.59$, $p < 0.001$, respectively), between the *SLC18A2* gene and all of the *MAOA*, *GLYAT* and *TPH1* genes ($r = 0.35$, $p < 0.05$; $r = 0.43$, $p < 0.05$; $r = 0.40$, $p < 0.05$, respectively), and between the *ADRA2C* gene and *DRD4* gene ($r = 0.52$, $p < 0.05$) were detected. Conversely, the relation between the *SLC1A2*, *COMT*, *GRM5* genes and other genes were not significant (Table 2).

Bayesian statistics, based on receiver operating characteristic (ROC)-derived cutoff values, which allows diagnostic power of the genes were given in tables 4 and figure 3.

DISCUSSION

As a neurodevelopmental disorder, ADHD can lead to functional impairment that primarily manifests in childhood and has effects over an individual's lifespan. Individuals with ADHD may show the different level of impairment, and inheritance patterns can be complex (25).

MPH is a drug commonly used to treat ADHD. MPH inhibits the reuptake of DA and NE, increasing the level of

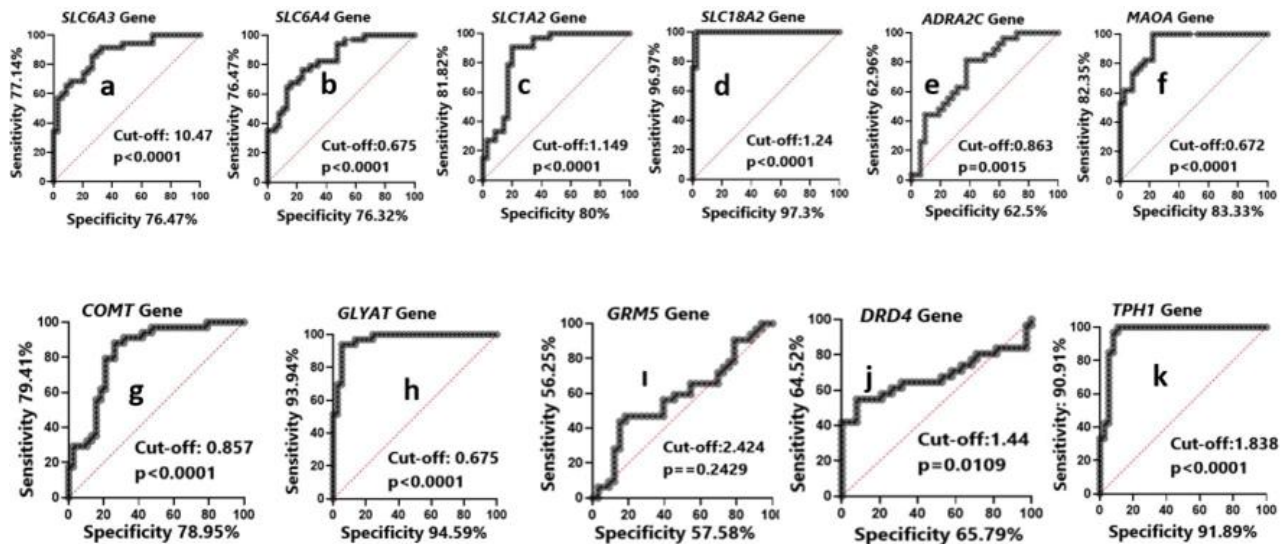


Figure 3. ROC derived cutoff values, specificity and sensitivity of the genes

these neurotransmitters in the synaptic cleft. DA is associated with reward and motivation systems, while NE plays an important role in focusing attention. MPH increases central dopamine and norepinephrine activity and may reduce distractibility and impulsivity in individuals with ADHD (5,26).

Many meta-analyses on ADHD sensitivity and MPH response do not show consistent results (Boncivini et al., 2016). Also, pharmacological studies on candidate genes indicate that *SLC6A3* as a key molecular target in drugs containing MPH and atomoxetine for ADHD (27). Grünblatt et al. showed that the expression level of the *SLC6A3* gene in patients is higher than in healthy individuals (28). Because of the high levels of *SLC6A3* in the internal globus pallidus caused a decrease in dopamine levels, it was concluded that neuronal circuits, effective in initiating behavior, are affected, and thus impulsive behaviors emerge (29). In our study, it was observed that the expression level of the *SLC6A3* gene before treatment increased almost two-fold ($p \leq 0.001$) in patients compared to the control group. But after MPH treatments, the reduced expression level of *SLC6A3* was observed ($p \leq 0.05$). This shows that this drug act by regulating the expression of this gene. When the CGI-S to be taken into consideration, CGI-S of 22 participants was 5, CGI-S of 10 participants was 6 and CGI-S of 3 participants was 4 in the pre-treatment group. After the MPH (0.3-1 mg/kg) treatments, CGI-S of 15 participants was detected as 1 and CGI-S of 20 participants was detected as 2. Thus it may be said that, the MPH act by regulating the expression levels of those genes.

The *SLC6A4* gene provides the reuptake of serotonin from the synaptic gap on the presynaptic membrane. Therefore, *SLC6A4* concentration in the membrane is one of the most

important factors determining the amount of synaptic serotonin. Also, H3 seronylation has an important role in coordinating placental transcription at the intersection of maternal physiology and offspring brain development (30). While Grünblatt et al. showed that there was no differences between the adult control and patient groups with ADHD in the *SLC6A4* gene expression levels (29). Sener et al. detected significant differences between healthy children and age matched patients group with autism spectrum disorders in terms of *SLC6A4* gene expression levels (31). The detection of lower expression in the patient group suggests a deficiency in serotonin reuptake. Allelic variants in the serotonin transporter gene (*SLC6A4*), lower transcriptional efficiency, changes in serotonin concentration in various brain regions, and differences in *SLC6A4* mRNA expression have been associated with the development of ADHD (32). In the current study, the expression level of the *SLC6A4* gene was lower the patient group than control before MPH treatment, but after MPH treatment the expression level of the *SLC6A4* gene increased three times ($p \leq 0.001$) in patient group and reached the expression level of the control group.

SLC1A2 as a brain-specific gene, encodes a glutamate transporter with high affinity in astroglial cells, is related the occurring of individuals with a high degree of brain disorder. It is known that the expression levels of *SLC1A2* changes in the glutamatergic system in the brain, especially in psychiatric disorders. The loss of *SLC1A2* expression in cases with seizures may has some possible epileptogenic role (33,34). Decreases in the expression level of this gene have been observed in many human and animal depression models (35). The dysregulation of *SLC1A2* causes amyotrophic lateral sclerosis, Alzheimer's

disease and epilepsy, as well as psychiatric disorders such as depression and autism(36). In this study, while the expression level of the *SLC1A2* gene was lower the patient goroup than control before MPH treatment ($p \leq 0.001$), Conversely after MPH treatment the expression level of the *SLC1A2* gene significantly increased ($p \leq 0.05$) in patient group.

The *SLC18A2* gene has a very important role in the storage and synaptic release of all monoamines, including serotonin. The changes in *SLC18A2* level are associated with depression, bipolar disorder, schizophrenia, Parkinson's disease (37). Tourette syndrome, alcohol addiction, ADHD symptoms in children and cognitive consequences after traumatic brain injuries in adults (38-40). In mouse models lacking *SLC18A2*, DA intake and release into vesicles were reduced by more than 80% and pathophysiologically, dopaminergic adrenergic, cellular oxidative stress, alterations in alpha-synuclein accumulation, and behaviorally decreased mobility, increased depressive mood and sleep disturbances were observed (41-44). It was reported that over-expression of *SLC18A2* resulted an increase in the uptake and relase of DA into vesicles (100%, 80%, respectively), increased mobility, anxiety and decreased depressive behaviors. High *SLC6A3* and low *SLC18A2* levels will theoretically result in cytosolic DA accumulation and minimal DA release. Also, low cytosolic DA concentration and high extracellular DA would arise from low *SLC6A3* and high *SLC18A2* levels (45). Our current study showed that the expression level of the *SLC18A2* gene was lower in the patient goroup than control before MPH treatment ($p \leq 0.001$). But after the MPH treatment, the significantly elevated expression level of the *SLC18A2* gene was detected in patient group ($p \leq 0.001$).

ADRA2C plays a role in the regulation of NE release from sympathetic nerves and drenergic neurons in the central nervous system. Noradrenergic neurons play a role in modulating wakefulness, regulation of visual attention, learning, and memory (46). Cho et al. showed a connection between the *ADRA2C* (GT) repeat polymorphism and ADHD (47). Even though Barr et al. were unable to establish a link between the same polymorphism and ADHD, they stated that other stronger SNPs in the *ADRA2C* gene are related to ADHD and should be examined (48). In the current study we detected the two fold higher *ADRA2C* expression level in control than patients group before MPH treatment ($p \leq 0.001$). After the MPH treatment, significantly elevated *ADRA2C* gene expression levels were found in patient group ($p \leq 0.05$).

MAOA roles in breaking down monoamine neurotransmitters such as DA, 5-hydroxytryptamine and NE. *MAOA* enzyme level is known to affect human behavior and characteristics (49). It has been reported that *MAOA* polymorphisms are associated with the hyperactive/impulsive ADHD type and the development of borderline personality disorder (50). Weder et al. showed a correlation between exposure to moderately traumatic conditions during childhood, low *MAOA* gene expression, and the risk of aggressive behavioral problems (51). In the current study, the six times higher expression level of the *MAOA* gene in control group than patient group was detected before MPH treatment ($p \leq 0.001$). After the MPH treatment significantly elevated *MAO* gene expression levels of patient group, which reached those of the control group were detected. ($p \leq 0.001$).

COMT plays a role in the inactivation of catecholamines, including DA (52) and has been seen as a focal point in studies including expression analyses, SNP and protein studies (53). Chen et al., was not found significant difference in *COMT* expression for age and disease parameters. Although the Val158Met and the alterations in the 3' end region are important risk factors for schizophrenia, the presence of these SNPs does not have a significant effect on mRNA expression. Researchers believe that the functional effect of *COMT* has more complex genetic bases because they cannot explain differences in protein studies and enzyme activities with mRNA expression (54). In another ADHD study, a general decrease in the surface area of the total premotor cortex was observed in males (55). Our study showed the significantly lower *COMT* expression level in patient group than control before MPH treatment ($p \leq 0.001$). But after MPH treatment, a significant increase of *COMT* gene expression level in patient group was observed ($p \leq 0.001$). Glycine-N-acyltransferase, which is responsible for metabolizing some metabolites, encoded by *GLYAT* gene in cells. Drugs are primarily metabolized to Acyl-CoA intermediates. The glycine-N-acyltransferase enzyme catalyzes the combination of mitochondrial Acyl-CoAs with glycine (56). Studies about the *GLYAT* gene on drug metabolism have been carried out, but they have not been focused on individuals with ADHD. Thus we think that the our current study has great importance. According to the our findings, the expression levels of *GLYAT* gene in patient group were lower from half of the expression leveles of the control group before the MPH treatment ($p \leq 0.02$). After the MPH treatment, the expression levels of the *GLYAT* gene significantly increased in patient group and reached the expression levels of the control grou($p \leq 0.01$).

Glutamate is the main stimulating neurotransmitter in the brain and plays a role in several ADHD-related processes, such as brain development, modulation of neuronal activity, bidirectional regulation of dopamine signaling, synaptic flexibility, memory formation and learning (57). *GRM5* appears to be critical for inhibitory learning mechanisms because impaired receptor function causes inappropriate retention of deterrent memories that can lead to anxiety disorders (58). Deletion in the CNV region of *GRM5*, one of the glutamate metabotropic receptor genes, has been associated with the presence of comorbid anxiety (59). The lower expression levels of *GRM5* gene were observed in patients with autism (60). In the current study, the expression level of *GRM5* gene was found to be lower in the patient group compared to the control group before MPH treatment, but this decrease was not statistically significant ($p > 0.05$). After the MPH treatment, significantly increased expression level of *GRM5* gene in patient group were seen compared to pretreatment ($p \leq 0.001$).

DRD4 is one of the dopaminergic system genes and DA receptors most associated with ADHD. Grünblatt et al., found the higher *DRD4* and *DRD5* gene expression levels in ADHD patients compared with controls (28). Our study compatible the literature and significantly higher expression levels of *DRD4* gene were detected in patient group compared the control group ($p < 0.05$) before MPH treatment. After MPH treatment, there was a decrease in the expression level of the *DRD4* gene in the post-treatment group compared to the pre-treatment group, but it was not statistically significant ($p > 0.05$).

TPH1 encodes a rate-limiting enzyme in the biosynthesis of the monoamine neurotransmitter serotonin. It was reported that *TPH1* and *TPH2* polymorphisms are associated with ADHD. According to a study, while no difference was found for the expression levels of *TPH1* gene between children with ADHD and healthy individuals (19), another study reported that the higher expression levels of *TPH1* gene in patient group with ADHD than the control group (28). According to the our results, significantly lower *TPH1* gene expression levels in patients were found than control group before the MPH treatment ($p \leq 0.01$). However after MPH treatment elevated expression levels of *TPH1* gene was detected in post-treatment group that reached the control group and significantly higher than pre-treatment group ($p \leq 0.01$).

Why the expression levels of the genes mentioned above differ between children with ADHD and the control group may be caused from variants in the regulatory regions of genes as well as epigenetic regulatory mechanisms such as

DNA methylation, histone modifications and micro-RNAs etc. Therefore, post-transcriptional regulators activate and inactivate the translation of mRNA in some cases. Although methylations generally has a silencing effect by suppressing the transcription of the gene, methylation of a regulatory region can sometimes lead to an increase in the gene product (61). In the current study, the expression levels of genes (*SLC6A3*, *SLC6A4*, *SLC1A2*, *SLC18A2*, *MAOA*, *COMT*, *GLYAT*, *DRD4* and *TPH1*), which are called candidate genes in the literature, differed between ADHD patients and the control group. The *SLC6A3* gene expression level was found to be higher in children with ADHD compared to controls and this elevation was reduced and reached the expression level of the control group by medical treatments with MPH ($p \leq 0.01$). Expression levels of *SLC6A4*, *SLC1A2*, *SLC18A2*, *MAOA*, *COMT*, *GLYAT*, *GRM5* and *TPH1* genes were found to be lower in children with ADHD compared to controls, and this decrease was increased with medical treatments of MPH and reached the expression level of the control group ($p \leq 0.01$). Variations and changes in the expression levels of the several common and specific genes may play an important role in the formation, prognosis and etiopathogenesis of diseases, and these changes can also be used as biomarkers in the differential diagnosis of diseases and the development of treatment strategies for them.

Bayesian statistics, ROC-derived cutoff values analysis results showed that the expression levels of genes, except the *GRM5* gene, have diagnostic power in ADHD. Especially the expression levels of *SLC18A2* (cut-off:1.24, 96.97% sensitivity and 97.3% specificity), *GLYAT* (cut-off:0.675, 93.94% sensitivity and 94.59% specificity) and *TPH1* (cut-off:1.838, 90.91% sensitivity and 91.89% specificity) genes in blood can be an important candidate diagnostic marker with higher (over 90%) specificity and sensitivity for diagnostic purpose in the etiopathogenesis of diseases.

Our study suggests a potential association between those candidate *SLC6A3*, *SLC6A4*, *SLC1A2*, *SLC18A2*, *ADRA2C*, *MAOA*, *COMT*, *GLYAT*, *DRD4*, and *TPH1* genes' expressions and ADHD. Additionally MPH, drug commonly used to treat ADHD, has possible effect on the expression of these candidate genes. It may be said that the expression levels of those genes may play an important role in the formation, prognosis and etiopathogenesis of the disease and can also be used as biomarkers in the differential diagnosis and development of treatment strategies for the disease. However, our study has certain limitations, including a small sample size, the inclusion of only male children, and the lack of control over

environmental factors. Given these limitations, validation studies with larger sample sizes and in different populations are needed to confirm our findings. To gain more definitive insights on this topic, additional studies with large cohorts should be conducted.

CONCLUSION

The findings of our study highlight the SLC6A3, SLC6A4, SLC1A2, SLC18A2, ADRA2C, MAOA, COMT, GLYAT, DRD4, and TPH1 genes affected by MPH treatment and the differences in the expression levels of these genes contribute to a better understanding of the molecular mechanisms in ADHD. In this context, the genes in question can be considered as potential biomarkers that may affect clinical outcomes with the support of further research.

Acknowledgments

This research was carried out as part of the TSD-12-4112 project at Erciyes University for a PhD thesis. The study received support from the TSD-12-4112 project of Erciyes University.

Authorship contributions

HA and YE developed the theory and concept of the study. YO and MD designed the study. MD, NG, SO, and MED investigated and supervised the findings of this work. HA wrote the manuscript with support from IOS, NG, SO, MED, YO, and MD. RE, IOS and NG performed the statistical analysis. MD, HA and SO verified the analytical methods. HA, RE, IOS, NG, and YE made literature searches. MED, SO and HA performed clinical studies. SO analyzed and interpreted the patient data. All authors discussed the results and contributed to the final manuscript. All authors read and approved the final manuscript.

Data availability statement

The data and material can be available from the corresponding author.

Declaration of competing interest

No conflict of interest was declared by the authors.

Ethics

The study received approval from the Local Ethics Committee of Erciyes University, as outlined in the approval document dated 05.06.2012, with reference number 2012/366.

Funding

The study was supported by Erciyes University project TSD-12-4112.

REFERENCES

1. Sonuga-Barke EJS, Becker SP, Bölte S, Castellanos FX, Franke B, Newcorn JH et al (2023) Annual Research Review: Perspectives on progress in ADHD science from characterization to cause. *J Child Psychol Psychiatry* 64(4):506-532. doi: 10.1111/jcpp.13696.
2. Cortese S, Song M, Farhat LC, Yon DK, Lee SW, Kim MS, Park S et al (2023) Incidence, prevalence, and global burden of ADHD from 1990 to 2019 across 204 countries: data, with critical re-analysis, from the Global Burden of Disease study. *Mol Psychiatry* 28(11):4823-4830. doi: 10.1038/s41380-023-02228-3.
3. Çetin FH, Isl Y (2018) Attention Deficit Hyperactivity Disorder and Genetics. *Current Approaches in Psychiatry* 10(1):19-39. doi: 10.18863/pgy.334547.
4. Castellanos FX, Giedd JN, Berquin PC, Walter JM, Sharp W, Tran T et al (2001) Quantitative brain magnetic resonance imaging in girls with attention-deficit/hyperactivity disorder. *Arch Gen Psychiatry* 58(3):289-95. doi: 10.1001/archpsyc.58.3.289.
5. Arnsten AF(2009) The Emerging Neurobiology of Attention Deficit Hyperactivity Disorder: The Key Role of the Prefrontal Association Cortex. *J Pediatr* 1;154(5):I-S43. doi: 10.1016/j.jpeds.2009.01.018.
6. Biederman J, Ball SW, Monuteaux MC, Mick E, Spencer TJ, McCreary M et al (2008) New insights into the comorbidity between ADHD and major depression in adolescent and young adult females. *J Am Acad Child Adolesc Psychiatry* 47(4):426-434. doi: 10.1097/CHI.0b013e31816429d3.
7. Türay S, Eröz R, Başak, AN (2021) A novel pathogenic variant in the 3' end of the AGTPBP1 gene gives rise to neurodegeneration without cerebellar atrophy: an expansion of the disease phenotype? *Neurogenetics* 22(2):127-132. doi: 10.1007/s10048-021-00643-8.
8. Yazıcı M, Yektaş Ç, Eröz R, Kaplan Karakaya ES, Sarıgedik E (2023) Investigation of the forkhead box protein P2 gene by the next-generation sequence analysis method in children diagnosed with specific learning disorder. *Psychiatr Genet* 33(1):8-19. doi: 10.1097/YPG.0000000000000326.

9. Cakmak Genc G, Yilmaz B, Karakas Celik S, Aydemir C, Eroz R, Dursun A (2024) Radiosensitivity in a newborn with microcephalia: A case report of Nijmegen breakage syndrome. *Birth Defects Res* 116(5):e2346. doi: 10.1002/bdr2.2346.
10. Dogan M, Terali K, Eroz R, Kılıç H, Gezdirici A, Gönüllü B (2024) Discovery of a novel homozygous SOD1 truncating variant bolsters infantile SOD1 deficiency syndrome. *Mol Biol Rep* 26;51(1):580. doi: 10.1007/s11033-024-09513-6.
11. Yildiz Gulhan P, Eroz R, Ataoglu O, İnce N, Davran F, Öztürk CE et al (2022) The evaluation of both the expression and serum protein levels of Caspase-3 gene in patients with different degrees of SARS-CoV2 infection. *J Med Virol* 94(3):897-905. doi: 10.1002/jmv.27362.
12. Tasdemir S, Eroz R, Dogan H, Erdem HB, Sahin I, Kara M et al (2016) Association between human hair loss and the expression levels of nucleolin, nucleophosmin, and UBTF genes. *Genet Test Mol Biomark* 20(4):197-202. doi: 10.1089/gtmb.2015.0246.
13. Tuşat M, Eroz R, Bölükbaş F, Özkan E, Erdal H (2024) Evaluation of the protective and therapeutic effects of extra virgin olive oil rich in phenol in experimental model of neonatal necrotizing enterocolitis by clinical disease score, inflammation, apoptosis, and oxidative stress markers. *Pediatr Surg Int* 17;40(1):80. doi: 10.1007/s00383-024-05669-1. PMID: 38493431.
14. Damar İH, Eroz R (2022) Argyrophilic nucleolar organizer regions as new biomarkers in ST-Elevation myocardial infarction. *J Cardiovasc Dev Dis* 9(2):58. doi: 10.3390/jcdd9020058.
15. Kaya M, Eroz R, Kabaklioglu M (2022) Expression of nucleolin, nucleophosmin, upstream binding transcription factor genes and propolis in wound models. *J Wound Care* 31(Sup10):S28-S40. doi: 10.1296/jowc.
16. Yesildag K, Kokulu K, Mutlu H, Eroz R, Taha-Sert E, Saritas A (2021) Argyrophilic nucleolar organizer regions as a promising biomarker for the detection of brain hypoxia levels caused by different doses of carbon monoxide poisoning. *Gac Med Mex* 157(6):610-617. doi: 10.2487/GMM.M21000625.
17. Bonvicini C, Faraone SV, Scassellati C (2016) Attention-deficit hyperactivity disorder in adults: A systematic review and meta-analysis of genetic, pharmacogenetic and biochemical studies. *Mol Psychiatry* ;21(7):872-84. doi: 10.1038/mp.2016.74.
18. Gizer IR, Ficks C, Waldman ID (2009) Candidate gene studies of ADHD: a meta-analytic review. *Hum Genet* 126(1):51-90. doi: 10.1007/s00439-009-0694-x.
19. Taurines R, Grünblatt E, Scheckmann M, Schwenck C, Albantakis L et al (2011) Altered mRNA expression of monoaminergic candidate genes in the blood of children with attention deficit hyperactivity disorder and autism spectrum disorder. *World J Biol Psychiatry* 1:104-8. doi: 10.3109/15622975.2011.600297.
20. McCaffrey TA, Laurent G, Shtokalo D, Antonets D, Vyatkin Y, Jones D et al (2020) Biomarker discovery in attention deficit hyperactivity disorder: RNA sequencing of whole blood in discordant twin and case-controlled cohorts. *BMC Med Genomics* 28;13(1):160. doi: 10.1186/s12920-020-00808-8.
21. Cabana-Domínguez J, Soler Artigas M, Arribas L, Alemany S, Vilar-Ribó L, Llonga N et al (2022) Comprehensive analysis of omics data identifies relevant gene networks for Attention-Deficit/Hyperactivity Disorder (ADHD). *Transl Psychiatry* 24;12(1):409. doi: 10.1038/s41398-022-02182-8.
22. Mortimer N, Sánchez-Mora C, Rovira P, Vilar-Ribó L, Richarte V (2020) Transcriptome profiling in adult attention-deficit hyperactivity disorder. *Eur Neuropsychopharmacol* 41:160-166. doi: 10.1016/j.euroneuro.2020.11.005.
23. Pagerols M, Richarte V, Sánchez-Mora C, Rovira P, Soler Artigas M, Garcia-Martínez I et al (2018) Integrative genomic analysis of methylphenidate response in attention-deficit/hyperactivity disorder. *Sci Rep* 30;8(1):1881. doi: 10.1038/s41598-018-20194-7.
24. Chomczynski P (1993) A reagent for the single-step simultaneous isolation of RNA, DNA and proteins from cell and tissue samples. *Biotechniques* 15(3):532-4, 536-7.
25. Cibrian FL, Lakes KD, Schuck SEB, Hayes GR (2022) The potential for emerging technologies to support self-regulation in children with ADHD: A literature review. *International Journal of Child-Computer Interaction* 31:100421. <https://doi.org/10.1016/J.IJCCI.2021.100421>
26. Volkow ND, Wang GJ, Fowler JS, Ding YS (2005) Imaging the effects of methylphenidate on brain dopamine: new model on its therapeutic actions for attention-deficit/hyperactivity disorder.

- Biol Psychiatry 1;57(11):1410-5. doi: 10.1016/j.biopsych.2004.11.006.
27. Coghill DR, Banaschewski T, Lecendreux M, Soutullo C, Zuddas A, Adeyi B et al (2014) Post hoc analyses of the impact of previous medication on the efficacy of lisdexamfetamine dimesylate in the treatment of attention-deficit/hyperactivity disorder in a randomized, controlled trial. *Neuropsychiatr Dis Treat* 29;10:2039-47. doi: 10.2147/NDT.S68273.
28. Grünblatt E, Geissler J, Jacob CP, Renner T, Müller M, Bartl J et al (2012) Pilot study: potential transcription markers for adult attention-deficit hyperactivity disorder in whole blood. *Atten Defic Hyperact Disord* 4(2):77-84. doi: 10.1007/s12402-012-0074-6.
29. Robertson KD (2005) DNA methylation and human disease. *Nat Rev Genet* 6(8):597-610. doi: 10.1038/nrg1655.
30. Chan JC, Alenina N, Cunningham AM, Ramakrishnan A, Shen L, Bader M et al (2024) Serotonin transporter-dependent histone serotonylation in placenta contributes to the neurodevelopmental transcriptome. *J Mol Biol* 22:168454. doi: 10.1016/j.jmb.2024.168454.
31. Sener EF, Korkmaz K, Öztöp DB, Zararsız G, Özkul Y (2015) Investigation of SLC6A4 gene expression in autism spectrum disorders. *J Clin Exp Invest* 6(2):165-9. <https://doi.org/10.5799/ahinjs.01.2015.02.0510>
32. Philibert RA, Sandhu H, Hollenbeck N, Gunter T, Adams W, Madan A (2008) The relationship of 5HTT (SLC6A4) methylation and genotype on mRNA expression and liability to major depression and alcohol dependence in subjects from the Iowa Adoption Studies. *Am J Med Genet B Neuropsychiatr Genet* 5;147B(5):543-9. doi: 10.1002/ajmg.b.30657.
33. Buccoliero AM, Caporalini C, Moscardi S, Cetica V, Mei D, Conti V (2024) Leat-associated seizures the possible role of EAAT2, pyruvate carboxylase and glutamine synthetase. *Epilepsy Res* 199:107258. doi: 10.1016/j.epilepsyres.2023.107258.
34. Choudary PV, Molnar M, Evans SJ, Tomita H, Li JZ, Vawter MP et al (2005) Altered cortical glutamatergic and GABAergic signal transmission with glial involvement in depression. *Proc Natl Acad Sci U S A* 25;102(43):15653-8. doi: 10.1073/pnas.0507901102.
35. Malki K, Lourdusamy A, Binder E, Payá-Cano J, Sluyter F, Craig I et al (2012) Antidepressant-dependent mRNA changes in mouse associated with hippocampal neurogenesis in a mouse model of depression. *Pharmacogenet Genomics* ;22(11):765-76. doi: 10.1097/FPC.0b013e328356fa90.
36. Fiorentino A, Sharp SI, McQuillin A (2015) Association of rare variation in the glutamate receptor gene SLC1A2 with susceptibility to bipolar disorder and schizophrenia. *Eur J Hum Gene* 23(9):1200-6. doi: 10.1038/ejhg.2014.261.
37. Huang J, Li B, Wei H, Li C, Liu C, Mi H et al (2024) Integrative analysis of gene expression profiles of substantia nigra identifies potential diagnosis biomarkers in Parkinson's disease. *Sci Rep* 25;14(1):2167. doi: 10.1038/s41598-024-52276-0.
38. Ben-Dor DH, Zimmerman S, Sever J, Roz N, Apter A, Rehavi M et al (2007) Reduced platelet vesicular monoamine transporter density in Tourette's syndrome pediatric male patients. *Eur Neuropsychopharmacol* 17(8):523-6. doi: 10.1016/j.euroneuro.2007.01.002.
39. Fehr C, Sommerlad D, Sander T, Anghelescu I, Dahmen N, Szegedi A et al (2013) Association of VMAT2 gene polymorphisms with alcohol dependence. *J Neural Transm (Vienna)* 120(8):1161-9. doi: 10.1007/s00702-013-0996-y. Epub 2013 Mar 17.
40. Toren P, Rehavi M, Luski A, Roz N, Laor N, Lask M et al (2005) Decreased platelet vesicular monoamine transporter density in children and adolescents with attention deficit/hyperactivity disorder. *Eur Neuropsychopharmacol* 15(2):159-62. doi: 10.1016/j.euroneuro.
41. Alter SP, Stout KA, Lohr KM, Taylor TN, Shepherd KR, Wang M et al (2016) Reduced vesicular monoamine transport disrupts serotonin signaling but does not cause serotonergic degeneration. *Exp Neurol* 275 Pt 1(Pt 1):17-24. doi: 10.1016/j.expneurol.2015.09.016
42. Caudle WM, Richardson JR, Wang MZ, Taylor TN, Guillot TS, McCormack AL et al (2007) Reduced vesicular storage of dopamine causes progressive nigrostriatal neurodegeneration. *J Neurosci* 25;27(30):8138-48. doi: 10.1523/JNEUROSCI.0319-07.2007.

43. Guillot TS, Shepherd KR, Richardson JR, Wang MZ, Li Y, Emson PC et al (2008) Reduced vesicular storage of dopamine exacerbates methamphetamine-induced neurodegeneration and astrogliosis. *J Neurochem* 106(5):2205-17. doi: 10.1111/j.1471-4159.2008.05568.x.
44. Taylor TN, Alter SP, Wang M, Goldstein DS, Miller GW (2014) Reduced vesicular storage of catecholamines causes progressive degeneration in the locus ceruleus. *Neuropharmacology*. 76 Pt A(0 0):97-105. doi: 10.1016/j.neuropharm.2013.08.033.
45. Lohr KM, Chen M, Hoffman CA, McDaniel MJ, Stout KA, Dunn AR et al (2016) Vesicular Monoamine Transporter 2 (VMAT2) Level Regulates MPTP Vulnerability and Clearance of Excess Dopamine in Mouse Striatal Terminals. *Toxicol Sci* 153(1):79-88. doi: 10.1093/toxsci/kfw106.
46. Brede M, Nagy G, Philipp M, Sorensen JB, Lohse MJ, Hein L (2003) Differential control of adrenal and sympathetic catecholamine release by alpha 2-adrenoceptor subtypes. *Mol Endocrinol* 17(8):1640-6. doi: 10.1210/me.2003-0035.
47. Cho SC, Kim JW, Kim BN, Hwang JW, Shin MS, Park M et al (2008) Association between the alpha-2C-adrenergic receptor gene and attention deficit hyperactivity disorder in a Korean sample. *Neurosci Lett* 3;446(2-3):108-11. doi: 10.1016/j.neulet.2008.09.058.
48. Barr CL, Wigg K, Zai G, Roberts W, Malone M, Schachar R et al (2001) Attention-deficit hyperactivity disorder and the adrenergic receptors alpha 1C and alpha 2C. *Mol Psychiatry* 6(3):334-7. doi: 10.1038/sj.mp.4000863.
49. Rodnyy AY, Kondaurova EM, Tsybko AS, Popova NK, Kudlay DA, Naumenko VS (2023) The brain serotonin system in autism. *Rev Neurosci* 10;35(1):1-20. doi: 10.1515/revneuro-2023-0055.
50. Liu L, Guan LL, Chen Y, Ji N, Li HM, Li ZH et al (2011) Association analyses of MAOA in Chinese Han subjects with attention-deficit/hyperactivity disorder: family-based association test, case-control study, and quantitative traits of impulsivity. *Am J Med Genet B Neuropsychiatr Genet* 156B(6):737-48. doi: 10.1002/ajmg.b.31217.
51. Weder N, Yang BZ, Douglas-Palumberi H, Massey J, Krystal JH, Gelernter J et al (2009) MAOA genotype, maltreatment, and aggressive behavior: the changing impact of genotype at varying levels of trauma. *Biol Psychiatry* 1;65(5):417-24. doi: 10.1016/j.biopsych.2008.09.013.
52. Matsumoto M, Weickert CS, Akil M, Lipska BK, Hyde TM, Herman MM et al (2003) Catechol O-methyltransferase mRNA expression in human and rat brain: evidence for a role in cortical neuronal function. *Neuroscience* 116(1):127-37. doi: 10.1016/s0306-4522(02)00556-0.
53. Sengupta S, Grizenko N, Schmitz N, Schwartz G, Bellingham J, Polotskaia A et al (2008) COMT Val108/158Met polymorphism and the modulation of task-oriented behavior in children with ADHD. *Neuropsychopharmacology* 33(13):3069-77. doi: 10.1038/npp.2008.85.
54. Chen J, Lipska BK, Halim N, Ma QD, Matsumoto M et al (2004) Functional analysis of genetic variation in catechol-O-methyltransferase (COMT): effects on mRNA, protein, and enzyme activity in postmortem human brain. *Am J Hum Genet* 75(5):807-21. doi: 10.1086/425589.
55. Dirlikov B, Shiels Rosch K, Crocetti D, Denckla MB, Mahone EM, Mostofsky SH (2014) Distinct frontal lobe morphology in girls and boys with ADHD. *Neuroimage Clin* 10;7:222-9. doi: 10.1016/j.nicl.2014.12.010.
56. Sluis R Van Der, Sc M (2015) Investigation and characterisation of the genetic variation in the coding region of the glycine N-acyltransferase gene. North-West University (Potchefstroom Campus) May 2015.
57. Mukherjee S, Manahan-Vaughan D (2013) Role of metabotropic glutamate receptors in persistent forms of hippocampal plasticity and learning. *Neuropharmacology*. 66:65-81. doi: 10.1016/j.neuropharm.2012.06.005.
58. Xu J, Zhu Y, Contractor A, Heinemann SF (2009) mGluR5 has a critical role in inhibitory learning. *J Neurosci* 25;29(12):3676-84. doi: 10.1523/JNEUROSCI.5716-08.2009.
59. Akutagava-Martins GC, Salatino-Oliveira A, Genro JP, Contini V, Polanczyk G, Zeni C et al (2014) Glutamatergic copy number variants and their role in attention-deficit/hyperactivity disorder. *Am J Med Genet B Neuropsychiatr Genet* 165B(6):502-9. doi: 10.1002/ajmg.b.32253.
60. Ansel A, Rosenzweig JP, Zisman PD, Melamed M, Gesundheit B (2017) Variation in Gene Expression in Autism Spectrum

Disorders: An Extensive Review of Transcriptomic Studies. *Front Neurosci* 5;10:601. doi: 10.3389/fnins.2016.00601.

61. Mostafavi-Abdolmaleky H, Glatt SJ, Tusuang MT (2011) Epigenetics in Psychiatry. In: *Epigenetic Aspects of Chronic Diseases*. 2011; pp 163–174.

Research Article

CLINICAL FEATURES, GENETIC SPECTRUM, AND OUTCOMES OF HEREDITARY TYROSINEMIA TYPE 1: A MULTICENTER STUDY FROM SOUTHEASTERN TÜRKIYE

Emine GÖKSOY^{1*}, Ayşe ERGÜL BOZACI², Berrak BİLGİNER GÜRBÜZ³

¹ Pediatric Metabolism Department, Faculty of Medicine, Adnan Menderes University, Aydın, Türkiye

² Pediatric Metabolism Department, Faculty of Medicine, Akdeniz University, Antalya, Türkiye

³ Pediatric Metabolism Department, Ankara Bilkent City Hospital, Ankara, Türkiye

*Correspondence: emine.goksoy@adu.edu.tr

ABSTRACT

Objective: Hereditary Tyrosinemia Type 1 (HT1) is a metabolic disorder due to fumarylacetoacetate hydrolase deficiency, which can lead to liver and kidney damage. This study aims to expand our knowledge of the clinical presentation, diagnosis, and outcomes of HT1 patients from southeastern Türkiye, a region with high consanguinity rates.

Materials and Methods: This retrospective multicenter study included 20 HT1 patients from three metabolic centers in southeastern Türkiye between January 2018 and March 2021. Demographic, clinical, laboratory, and genetic data were retrieved. Patients were divided into acute, subacute, and chronic forms according to the beginning of their symptoms. The statistical analyses consisted of descriptive and inferential methods.

Results: The parents of all 20 cases (9F/11M) were consanguineous. The mean diagnostic age was 10.53±12.54 months, with an average diagnostic delay of 2.96±4.42 months. The most common form was acute HT1 (55%), followed by chronic (25%) and subacute (20%) forms. Common finding was hepatomegaly (40%). Tubulopathy was frequent in chronic HT1 (80%). Increased α -fetoprotein levels were found in 60% of the cases at the diagnosis. Hepatocellular carcinoma developed in three patients. Two died of the disease. Genetic studies showed that the most common mutation was c.554-1G>T (27%).

Conclusion: The study highlights the clinical burden and the challenge in managing HT1 in Türkiye, attributed to late diagnosis resulting from absence of the newborn screening (NBS). Although studies have demonstrated that early nitisinone treatment improves outcomes, long-term follow-up for complications like hepatocellular carcinoma is imperative. NBS needs to be extended to reduce morbidity and mortality associated with HT1.

Keywords: Hereditary tyrosinemia type 1, hepatocellular carcinoma, nitisinone.

Received: 07 January 2025

Revised: 17 February 2025

Accepted: 17 February 2025

Published: 20 March 2025



Copyright: © 2025 by the authors. Published by Aydın Adnan Menderes University, Faculty of Medicine and Faculty of Dentistry. This article is openly accessible under the Creative Commons Attribution-NonCommercial 4.0 International (CC BY-NC 4.0) License.

INTRODUCTION

Hereditary Tyrosinemia type 1 (HT-1, OMIM 276700) is an autosomal recessive hereditary metabolic disorder that is caused by a deficiency of the enzyme fumarylacetoacetate hydrolase (FAH), which is responsible for the final step of the tyrosine (Tyr) catabolic pathway, leading to liver and kidney damage with the accumulation of toxic metabolites, especially succinylacetone (SUAC). It has acute, subacute, and chronic forms (1,2). The estimated prevalence of HT-1 is 1 in 100,000 to 120,000 live births worldwide (2). However, due to the founder effect in some regions, such as the province of Quebec in Canada, there is a higher incidence of 1 in 16,000 live births (1). Specific epidemiological data on HT-1 are limited, and the incidence of HT1 in Türkiye is currently unknown.

Toxic metabolites accumulated in HT-1, especially SUAC, cause oxidative damage, mitochondrial dysfunction, and apoptosis in hepatocytes and renal tubular cells (3). HT-1 typically presents as liver disease, including jaundice, hepatomegaly, and failure to thrive in infants (4). Clinical manifestations vary depending on the age of onset of symptoms. Renal involvement can cause Fanconi syndrome with aminoaciduria, glycosuria, and hypophosphatemia with rickets. On examination, hepatomegaly, and a characteristic "cabbage-like" odor can be detected (4,5). The accumulation of SUAC inhibits delta-aminolevulinic acid dehydratase (ALA-D) enzyme, disrupting porphyrin synthesis. This condition may lead to severe pain and tingling due to peripheral nerve involvement, and paralysis due to motor neuron impairment (4). Additionally, nitisinone (2-(2-nitro-4-trifluoromethylbenzoyl)-1,3-cyclohexanedione, NTBC) therapy increases plasma tyrosine levels by blocking the metabolic pathway further upstream to prevent the formation of SUAC. This leads to photophobia caused by corneal deposits, palmoplantar keratoderma, and cognitive impairment due to disrupted neurotransmitter synthesis may occur (3,4,6). Laboratory tests may show mildly elevated liver enzymes, SUAC (in urine or blood), and cardiomyopathy (1,7). Even with therapy, there is a substantial risk of cirrhosis, and the development of hepatocellular carcinoma (3). HT-1 diagnosis is based on clinical findings, as well as elevated levels of tyrosine and methionine in blood, and detection of SUAC in the urine or blood, which is a specific metabolite for HT-1 (1). The diagnosis should be confirmed by detecting a mutation in the FAH gene (NM_000137.3) for a definitive diagnosis (1). Early diagnosis through NBS is crucial for effective management and improved outcomes (1,2).

The use of NTBC, a powerful inhibitor of the 4-hydroxyphenylpyruvate dioxygenase enzyme that

prevents the formation of SUAC, which is held responsible for the main damage, has revolutionized the management of HT-1 and significantly reduced the risk of liver failure and HCC when started early. According to studies, renal involvement and neurological crises could be prevented by early initiation of NTBC (3,5,6). However, due to NTBC treatment, elevated plasma tyrosine levels result in ophthalmological and skin disorders that require lifetime dietary restrictions on tyrosine and phenylalanine (6). Liver transplantation may be considered for patients if they develop liver cancer or do not respond to medical treatment (8).

Our study aims to expand our knowledge of clinical outcomes to improve our comprehension of the disease course and to contribute to the literature on current clinical practices for HT1 in Türkiye.

MATERIALS AND METHODS

This study provides a comprehensive overview of the clinical approach and patient data collection related to HT1 at the three important metabolic centers in the Southeastern part of Türkiye. Medical records from HT1 patients followed at the Pediatric Metabolic Diseases Unit of Gaziantep Children's Hospital, Diyarbakır Children's Hospital, and Adana City Hospital between January 2018 and March 2021 (26/11/21-933).

Patients were identified based on high SUAC levels in their urine or blood, as well as FAH gene analysis (excluding P19). Three main clinical forms were categorized based on the age at symptom onset: the acute form (onset of symptoms at <6 months of age), the subacute form (onset of symptoms at 6-12 months of age), and the chronic form (onset of symptoms at >12 months of age) according to van Spronsen classification (9). Diagnostic delay was defined as the time interval (in months) between the onset of symptoms and the final diagnosis of HT1.

Demographic information (gender, consanguinity, family history, age of onset symptoms, current age), clinical information (symptoms such as irritability, jaundice, pallor, abdominal distension, tendency to bruise, fever, abdominal pain, abnormal urine odor; physical examination findings such as hepatomegaly, splenomegaly, anthropometric measurements, eye and neurological findings), laboratory findings (Serum alanine transferase-ALT, aspartate transaminase-AST, alpha-fetoprotein-AFP, total bilirubin, direct bilirubin, serum tyrosine, phenylalanine, methionine, urea, creatinine levels, urinary tubular functions, blood

Table 1. Main symptoms, clinical and laboratory findings at diagnosis by presentation type of patients with HT1.

	Acute (n:11)	Subacute (n:4)	Chronic (n:5)	Total (n:20)
Main symptoms				
Irritability	8 (72%)	1 (25%)	0	9 (45%)
Jaundice	7 (63%)	1 (25%)	0	8 (40%)
Growth retardation	1 (9%)	2 (50%)	4 (80%)	7 (35%)
Pallor	4 (45%)	3 (75%)	0	7 (35%)
Abdominal distention	2 (18%)	1 (25%)	3 (60%)	6 (30%)
Tendency to bruise	0	2 (50%)	4 (80%)	6 (30%)
Fever	5 (45%)	0	0	5 (25%)
Abdominal pain	0	0	3 (60%)	3 (15%)
Abnormal urine odor	1 (9%)	1 (25%)	0	2 (10%)
Clinical and laboratory findings				
Hepatomegaly/splenomegaly	4 (45%)	1 (25%)	3 (60%)	8 (40%)
Coagulopathy	6 (54%)	1 (25%)	2 (40%)	9 (45%)
Chronic liver disease	2 (18%)	1 (25%)	4 (80%)	7 (35%)
Jaundice	6 (54%)	0	1 (20%)	7 (35%)
Tubulopathy	1 (9%)	1 (25%)	4 (80%)	6 (30%)
Hypotonia	3 (27%)	2 (50%)	0	5 (25%)
Intellectual disability	0	0	3 (60%)	3 (15%)

SUAC/urine SUAC levels), radiological findings (abdominal ultrasonography, MRI) of patients diagnosed with HT-1 from three centers were collected using case report forms. Laboratory findings were evaluated based on the time of diagnosis. Furthermore, they were monitored throughout follow-up to assess the response to treatment. Parameters that normalized after treatment but increased during follow-up were documented. Histopathological findings from liver biopsies, if available, were also documented.

Serum AFP results were analysed according to age-specific normal values. Since AFP reference values in the neonatal period are much higher than the other periods, AFP values were evaluated as high or normal (10).

The neurodevelopmental status of patients was evaluated by using the Bayley Scales of Infant and Toddler Development, Third Edition (Bayley-III), Denver II test, and Wechsler Scale IQ test (WISC-R; Wechsler Intelligence Scale for Children for age 7–17 years), with the total score considered for assessment.

All patients were treated with a tyrosine and phenylalanine-restricted diet. Plasma tyrosine levels were targeted at < 400µmol/l. Nitisinone treatment was initiated immediately with a dose of 1–2 mg/kg/day.

Statistical analysis

Statistical analyses were performed using the SPSS software package (ver.18.0; SPSS Inc., Chicago, IL, USA). Numerical variables were expressed as mean ± standard deviation (SD) for normally distributed data and median (range) for non-normally distributed data. Descriptive statistics, categorical variables were presented as numbers and percentages. The normality of data distribution was assessed using the Shapiro-Wilk test.

RESULTS

The study included 20 patients (9F/11M) with HT1 from 18 families. All the parents of patients had consanguinity. The mean age at the onset of symptoms was 7.57± 8.33 months (min: 3 days, max: 30 months). The mean age of the patients at diagnosis was 10.53± 12.54 months (min: 6 days, max: 48 months). The mean diagnostic delay time was 2.96±4.42 months (min: 3 days, max: 18 months.). 11 patients (55%) had acute form, 4 patients (20%) had subacute form, and 5 patients (25%) had chronic form of disease. Very early-onset symptoms (<2 months of age) were seen in 5 patients (25%). The main symptoms are listed in Table 1. All our patients, although 2 of our patients had a sibling history, were diagnosed after the onset of symptoms.

Table 2. Main laboratory findings at diagnosis.

Patient	AST (IU/L)	ALT (IU/L)	INR	AFP (ng/ml)	AFP results	Tubulopathy	Serum tyrosine level (μmol/L)
P1	106	88	1.5	98	high	absent	493
P2	380	250	1.6	75000	high	absent	479
P3	50	45	0.9	5	normal	absent	352
P4	38	40	1	12	normal	absent	402
P5	65	88	1.4	200	high	absent	261
P6	79	69	0.9	75	high	absent	185
P7	77	83	1	234	high	absent	164
P8	186	103	1.7	83500	high	absent	286
P9	75	66	1	153	high	exist	289
P10	34	28	0.8	2	normal	exist	664
P11	46	43	1.2	5	normal	absent	89
P12	145	108	1.6	196000	high	absent	439
P13	77	65	1.2	2500	normal	absent	429
P14	39	34	0.9	4	normal	absent	723
P15	38	25	0.9	10	normal	absent	463
P16	65	55	3	789	high	exist	905
P17	68	55	2	425	high	exist	881
P18	38	22	0.9	4	normal	exist	458
P19	85	66	6.1	685000	high	absent	670
P20	95	78	1.9	135	high	exist	557.44

Abbreviations: AST: Aspartate transaminase; ALT: Serum alanine amino transferase; INR: International Normalized Ratio; AFP: Serum a-fetoprotein
Normal values of liver transaminase: ALT (6–50 IU/L for 0–5days, 35–140 for 1–19 years), AST: (5–45 IU/ml for 0–5days, 15–55 IU/ml for 1–19 years)

The primary clinical findings included hepatomegaly and/or splenomegaly in 8 patients (40%). Hypotonia was detected in 5 patients (25%), and intellectual disability (ID) in 3 patients (15%), based on total scores from standardized developmental tests (Table 1). Coagulopathy and jaundice were seen in 6/11 (36.3%) patients as the most common findings in the acute form. In the subacute form, there was no jaundice. In chronic type 4/5 patients had (80%) tubulopathy (Table 1).

One patient (P19) presented with hyperinsulinemic hypoglycemia at the time of diagnosis requiring continuous diazoxide treatment until death. Additionally, hepatocellular carcinoma (HCC) developed in three patients (P9, P16, and P17). Patient 17 died while waiting for transplantation after HCC, and the other one (P19) died due to acute liver failure in the newborn period. NTBC started immediately after the elevated SUAC results. It was used at a dose of 2 mg/kg/d for 4 (20%) patients and 1mg/kg/d for 16 (80%) patients.

Twelve patients (60%) (Table 2) had high AFP levels at the time of diagnosis. All patients had elevated serum tyrosine

levels and increased urinary excretion of SUAC by gas chromatography-mass spectrometry (qualitative). Patient 9 was prescribed NTBC treatment at a dose of 1g/kg/day after being diagnosed at 4 months of age. Although AFP levels normalized within six months, a subsequent increase was observed during follow-up. ALT, AST, and serum Tyr levels were documented in Table 2. None of the patients underwent liver transplantation.

The most common mutation in our study was c.554-1G>T (27%), followed by c.315-3C>G (22%) and c.1062+5G>A (16%), respectively. Other detected mutations were c.441_448del, c.554-1G>A, c.709C>T, c.698A>T, and c.520C>T (Table 3). All mutations were detected as homozygous.

DISCUSSION

This study is the first multicenter study in our country showing the course and outcomes of HT1 and reflects the results of the southeastern region of Türkiye, which has a very high rate of consanguineous marriage(11). The present study describes the relation between phenotype

Table 3. Clinical type, clinical findings, and mutations of the patients

Patient	Current age (month)	Age at diagnosis (month)	Type	Clinical Findings				Mutation*		
				HM/SM	Renal involvement	Neurologic involvement	Others	Exon	Nucleotid	Protein
1	36	6	Acute					9	c.709C>T	R237X
2	19	6 days	Acute					8	c.698A>T	D233V
3	51	12	Subacute					5	c.441_448del	
4	168	6	Acute					5	c.441_448del	
5	10	3	Acute						NA	
6	37	6	Acute	+				3	c.315-3C>G	
7	40	3	Acute					12	c.1062+5G>A	
8	84	6 days	Acute			ID		3	c.315-3C>G	
9	17	4	Acute	+		Hypotonia		6	c.554-1G>T	
10	204	18	Chronic		+	ID+epilepsy		6	c.520C>T	R174X
11	21	8	Subacute	+		Hypotonia		6	c.554-1G>T	
12	132	10 days	Acute	+				6	c.554-1G>T	
13	9	1	Acute	+		Hypotonia		6	c.554-1G>T	
14	72	18	Chronic					3	c.315-3C>G	
15	10	8	Subacute			Hypotonia		3	c.315-3C>G	
16	36	20	Chronic	+	+	ID		12	c.1062+5G>A	
17	60	48	Chronic	+	+	ID		12	c.1062+5G>A	
18	84	12	Subacute		+			6	c.554-1G>T	
19	1.5	1	Acute		+		Hyperinsulinemic Hypoglycemia		NA	
20	84	36	Chronic	+	+			6	c.554-1G>A	

NA: Not available. * All patients with available genetic data have homozygous mutations. ** Patients P9, P16, and P17 were diagnosed with HCC. *** Patients P17 and P19 died due to disease-related complications.

and genotype as well as the long-term outcome of HT1 in Türkiye. Although the exact incidence of HT1 in Türkiye remain unclear, it is expected to be high due to given the high prevalence of inborn errors of metabolism (5,12). All our patients were born from consanguineous marriages.

Diagnosis

In our study, the mean age at diagnosis was 10.53 ± 12.54 months (range: 6 days to 48 months), with a mean diagnostic delay of 2.96 ± 4.42 months (range: 3 days to 18 months). Literature from Türkiye revealed a mean diagnostic age of 15.3 months (range: 0.06 to 108 months) in extracted 43/69 patients (5). In cases identified through selective screening (2 patients via NBS and five patients screened due to affected siblings), the mean age at diagnosis was 10.5 months (range: 1 to 45 months). In Palestine, the mean age at diagnosis was 8 months (13). Conversely, in Pakistan, there was a considerable delay, with the average age of symptom onset at 8 months and diagnosis at 34.7 months, resulting in an average delay of 26.8 months (14). In Spain, despite the lack of newborn screening (NBS), the mean age at diagnosis was 4.3 ± 3.6 months, reflecting prompt clinical recognition and early initiation of nitisinone treatment (15). With the screening

of HT1 with the newborn screening program, early diagnosis and treatment have become possible, and the reduction of such serious deteriorations and mortality rates has been achieved. All our patients were diagnosed after the onset of symptoms. Therefore, in our country diagnosis depends on clinical suspicion and laboratory findings. In regions with organized newborn screening programs, the occurrence of NBS decreases the delay of diagnosis. Countries with well-organized health system, like Spain, have better opportunities for early diagnosis and treatment. However, regions like Pakistan which lacks good health facilities may experience diagnosis delays. Furthermore, high clinical suspicion and awareness of the health care provider's community is necessary for early diagnosis. Screened affected siblings of the patients as implemented in Türkiye may help to minimize the diagnostic delays for subsequent cases.

Clinical presentation with subtypes

Our study identified three main clinical forms of HT1 based on symptom onset: acute (55%), subacute (20%), and chronic (25%). This distribution contrasts with previous studies in Türkiye, where the acute form was reported in

35% (5) and 27% (16). A multicenter study in Spain reported a higher prevalence of acute form HT1, which is 67%. This may be due to the high percentage of acute liver failure in the acute form (15). Similarly, Dweikat et al. (13) reported nearly half of the cases as acute in Palestine, resembling our findings. Our study, conducted in the Southeastern Türkiye, found that this region has higher birth rates that may increase detection of the acute form, which typically presents early. The time of diagnosis may also be affected by difficulties in accessing health services. The higher prevalence of the acute form in our study may be due to differences in birth rates and demographics across the region, genetic factors, and access to health care, which are essential for understanding the population and developing appropriate screening and management systems.

In contrast to earlier research conducted in Türkiye, the primary symptoms in our study were jaundice and irritability. Many parents reported misdiagnosis with infantile colic due to irritability, and this may cause a delay in the exact diagnosis. Similarly, the largest cohort study in Türkiye, attention was drawn to patients diagnosed with infantile colic due to irritability (5). This finding emphasizes how crucial it is to include HT1 when making a differential diagnosis for children who exhibit persistent irritability, a common but generic symptom that is sometimes mistaken for benign illnesses like infantile colic.

Neurological and metabolic complications

In the present study, although hypotonia and intellectual disability (ID) were rare conditions, they were observed in 5 patients (20%) and in 3 patients (15%) at the time of diagnosis, respectively. Hypotonia has been reported in HT1 patients, particularly in severely affected infants or during porphyria-like crises, as also described in previous studies (4). Additionally, Hajji et al. reported isolated hypotonia in 2 out of 33 patients (17). Concerning intellectual disability, studies emphasized that high plasma tyrosine levels under NTBC treatment may be associated with neurocognitive impairment (6,18). Although the precise mechanism is still unknown, research using mouse models suggests that tyrosinemia, not NTBC treatment, is the cause of the cognitive deficits (19).

Neurologic crises presenting with porphyria-like symptoms and restrictive cardiomyopathy have been rarely documented; however, both conditions have shown responsiveness to nitisinone therapy (7,20,21). None of our patients exhibited neurologic crises or cardiomyopathy.

Patient 19 in our study presented with persistent hyperinsulinemic hypoglycemia requiring continuous diazoxide treatment until death, a condition infrequently reported in HT1. Baumann et al. (22) reported 3 HT-1 patients with hyperinsulinemic hypoglycemia. They stated that they controlled the condition with diazoxide and chlorothiazide and tapered it over months. Naser et al. (23) emphasized the need for higher-dose treatment in the case they presented. Sethuram et al. (24) reported that the same condition was observed in the HT-1 case along with the transient hypertyrosinemia case and attributed the hyperinsulinism to elevated insulinotropic amino acids. Our patient revealed persistent, resistant hypoglycemia, and high-dose diazoxide treatment was used. This shows that early recognition and management of hyperinsulinemic hypoglycemia in Tyrosinemia Type 1, especially in severe cases, requires personalized treatment strategies.

Laboratory findings

In our study, consistent with previous studies, the most frequent laboratory findings included impaired liver function, elevated AFP levels, and increased plasma tyrosine levels, often accompanied by abnormal liver functions (5,13,15,16,21). In patients with the acute form of HT1, laboratory results aligned with findings reported in the literature. Interestingly, however, all patients diagnosed with the subacute form exhibited normal liver enzyme levels, preserved liver synthetic function, and normal AFP values at the time of diagnosis. This situation may be due to the small number of patients, and it also suggests that liver involvement may be obscured due to the less severe subacute form. Since all these patients had high plasma tyrosine levels, it has become important to measure plasma amino acids, especially in patients with nonspecific symptoms such as growth retardation, loss of appetite, and irritability.

In our study, elevated AFP levels were observed in 81.8% of patients with the acute form of HT1, and 60% of those with the chronic form, whereas none of the patients with the subacute form exhibited elevated AFP levels. Among acute cases with normal AFP levels, the ages at diagnosis were notably early at 1 and 6 months. Similarly, Rokaite et al. (25) stated that AFP concentrations are often high in the acute form, and may be normal in the chronic form. Furthermore, a study conducted by Aktuglu-Zeybek et al. (5) in our country revealed that AFP elevations were statistically significantly higher in the acute form. Despite these arguments, the difference in AFP levels between clinical forms has limited efficacy as a definitive diagnostic marker for differentiation. However, high AFP levels are

still supportive and still an important indicator of response to treatment, especially in acute forms(4–6).

Genetic variability

A review of the literature reveals that the most common mutation identified in Turkish patients and in the Mediterranean region, consistent with our findings, is c.554-1G>T, detected in five patients (25%) in our cohort. In the analyses conducted by Dursun et al. (21), c.315-3C>G, one of the three most frequent mutations in the Turkish population, was identified as the second most common mutation in our study. Furthermore, c.1062+5G>A, a mutation reported as rare globally in the literature review by Aktuğlu-Zeybek et al. (5), was found to be the third most frequent mutation in our cohort. Similar to other studies, no genotype-phenotype correlation was identified for the frequently observed mutations in our study.

Long-term outcomes

Tubulopathy was identified in 30% of the patients, with a prevalence of 80% (4/5) in those with the chronic form, 25% (1/4) in the subacute form, and 9% (1/11) in the acute form. As all patients were initiated on NTBC therapy immediately after diagnosis, it can be hypothesized that earlier initiation of NTBC treatment may effectively prevent the development of tubulopathy (1,3,6). Aktuğlu-Zeybek et al. (5) reported tubulopathy in 85% of HT-1 patients, while Yazıcı et al. (16) reported 66%. However, the lower acute case rates in these studies (35%, and 27%, respectively) may have contributed to the higher prevalence of tubulopathy. Similarly, Gokay et al. (26) also detected tubulopathy in 71% of patients, and the rate of acute forms in their study was 42%. However, the small sample size in this study significantly limits its generalizability. Dweikat et al. (13) detected tubulopathy half of the cases in acute form.

HCC developed in patient 9, who experienced a re-elevation of AFP levels despite treatment during follow-up. It is generally accepted that secondary AFP elevation is a risk factor for the development of HCC and that patients who start treatment before the age of one have a lower risk of HCC. In our case, although treatment was started in the fourth month and AFP levels returned to normal, the development of HCC may have been due to the patient receiving a dose of 1 g/kg/day of NTBC. The inability to measure NTBC levels represents a limitation of our study.

Future perspectives

Over the years, there have been developments in treatment management, but there are still challenges in the

long-term management of HT1. Monitoring for hepatocellular carcinoma is crucial, as the risk remains even during NTBC treatment. Gene therapy research can bring a potential curative approach, as it aims to address the underlying cause of the disease (27). Newer medications and improved biodistribution are also being developed to enhance NTBC adherence and treatment outcomes.

CONCLUSION

This study has some limitations. We were not able to measure nitisinone levels, which could provide important information on treatment efficacy and management. The retrospective nature of the study did not allow us to control for suspicious values. The fact that the examinations were performed in different centers may have caused variability in test results due to differences in methodologies and reference intervals. The follow-up period was relatively short, which limited our ability to evaluate long-term outcomes and disease progression.

Tyrosinemia Type 1 is a complex metabolic condition that, if left untreated, can have serious morbidity and mortality consequences. The disease severity in HT1 changed dramatically with the emergence of NTBC, changing the picture of disease management from a lethal one to a chronic one. Further studies and effective integrative approaches are alike needed to solve the remaining issues and enhance the welfare of HT1 patients. It is crucial for the management of the condition that it is diagnosed as early as possible, that treatment is instituted without delay, and that the patient is monitored regularly.

Acknowledgments

We sincerely thank our patients' family for their cooperation and willingness to participate in this study. We also extend our gratitude to our metabolic dietitians for their valuable support in dietary adjustments. Additionally, we acknowledge the hospital administration for their help in data collection.

Authorship contributions

Contributed to conception and design EG, Surgical and Medical Practices EG, AEB, BBG, collecting data EG, AEB, BBG, analysis EG, AEB, BBG, literature search EG, AEB, writing and editing EG.

Data availability statement

The data that support the findings of this study are available upon reasonable request from the corresponding author.

Declaration of competing interest

Authors declared no conflict of interest.

Ethics

Ethical approval was obtained from Health Sciences University Gazi Yaşargil Training and Research Hospital Clinical Research Ethics Committee by decision no: 933, dated 26/11/2021.

Funding

Authors declared no financial support.

REFERENCES

1. Chinsky JM, Singh R, Ficicioglu C, van Karnebeek CDM, Grompe M, Mitchell G, et al. Diagnosis and treatment of tyrosinemia type I: a US and Canadian consensus group review and recommendations. *Genet Med*. 2017;19(12):1380–95.
2. Stinton C, Geppert J, Freeman K, Clarke A, Johnson S, Fraser H, et al. Newborn screening for Tyrosinemia type 1 using succinylacetone – a systematic review of test accuracy. *Orphanet J Rare Dis*. 2017;12(1):48.
3. Holme E, Lindstedt S. Tyrosinaemia type I and NTBC (2-(2-nitro-4-trifluoromethylbenzoyl)-1,3-cyclohexanedione). *J Inher Metab Dis*. 1998;21(5):507–17.
4. Morrow G, Tanguay RM. Biochemical and clinical aspects of hereditary tyrosinemia type 1. *Adv Exp Med Biol*. 2017;959:9–21.
5. Aktuglu-Zeybek AC, Kiykim E, Cansever MS. Hereditary tyrosinemia type 1 in Turkey. *Adv Exp Med Biol*. 2017;959:157–72.
6. van Ginkel WG, Rodenburg IL, Harding CO, Hollak CEM, Heiner-Fokkema MR, van Spronsen FJ. Long-Term Outcomes and Practical Considerations in the Pharmacological Management of Tyrosinemia Type 1. *Pediatric Drugs*. 2019;21(6):413–26.
7. Bilginer Gürbüz B, Aykan H, Çiki K, Karagöz T, Sivri S, Dursun A, et al. Cardiomyopathy in patients with type 1 tyrosinemia, and the effect of nitisinone treatment on cardiomyopathy. *Cukurova Med J*. 2021 Dec 30;46(4):1419–25.
8. van Ginkel WG, Pennings JP, van Spronsen FJ. Liver cancer in tyrosinemia type 1. *Adv Exp Med Biol*. 2017;959:101–9.
9. van Spronsen FJ, Thomasse Y, Smit GP, Leonard J V, Clayton PT, Fidler V, et al. Hereditary tyrosinemia type I: a new clinical classification with difference in prognosis on dietary treatment. *Hepatology*. 1994;20(5):1187–91.
10. Wu JT, Book L, Sudar K. Serum Alpha Fetoprotein (AFP) Levels in Normal Infants. *Pediatr Res*. 1981;15(1):50–2.
11. Hacettepe Universitesi Nufus Etutleri Enstitüsü. Türkiye Nufus ve Sağlık Arastirmasi. Hacettepe Universitesi Nufus Etutleri Enstitüsü, T.C. Cumhurbaskanligi ve TUBITAK. Türkiye: Ankara; 2018: 47-48.
12. Ozalp I, Coskun T, Tokol S, Demircin G, Monch E. Inherited Metabolic Disorders in Turkey. *J. Inher. Metab. Dis*. 1990;13
13. Dweikat I, Qawasmi N, Najeeb A, Radwan M. Phenotype, genotype, and outcome of 25 Palestinian patients with hereditary tyrosinemia type 1. *Metabol Open*. 2021;9:100-83.
14. Khan SA, Fakih M, Taufiq N, Ahmerin A, Bangash A, Iqbal Malik M. Clinical Spectrum of Hereditary Tyrosinemia Type 1 in a Cohort of Pakistani Children. *Clin Med Insights Pediatr*. 2024;18.
15. Couce ML, Dalmau J, Del Toro M, Pintos-Morell G, Aldámiz-Echevarría L. Tyrosinemia type 1 in Spain: Mutational analysis, treatment and long-term outcome. *Pediatr Int*. 2011;53(6):985–9.
16. Yazıcı H, Er E, Canda E, Habif S, Kalkan Uçar S, Çoker M. Clinical Features of 29 Patients with Hereditary Tyrosinemia I in Western Turkey. *J Pediatr Res*. 2018;21:1–6.
17. Hajji H, Imbard A, Spraul A, Taibi L, Barbier V, Habes D, et al. Initial presentation, management and follow-up data of 33 treated patients with hereditary tyrosinemia type 1 in the absence of newborn screening. *Mol Genet Metab Rep*. 2022;8;33:100933
18. Bendadi F, De Koning TJ, Visser G, Prinsen HCMT, De Sain MGM, Verhoeven-Duif N, et al. Impaired cognitive functioning in patients with tyrosinemia type 1 receiving nitisinone. *J of Pediatr*. 2014;164(2):398–401.
19. Hillgartner MA, Coker SB, Koenig AE, Moore ME, Barnby E, MacGregor GG. Tyrosinemia type I and not treatment with NTBC causes slower learning and altered behavior in mice. *J Inher Metab Dis*. 2016;6;39(5):673–82.
20. Önenli Mungan N, Yıldızdaş D, Kör D, Horoz ÖÖ, İncecik F, Öktem M, et al. Tyrosinemia type 1 and irreversible neurologic

crisis after one month discontinuation of nitisone. *Metab Brain Dis.* 2016;31(5):1181-3.

21. Dursun A, Özgül RK, Sivri S, Tokatlı A, Güzel A, Mesci L, et al. Mutation spectrum of fumarylacetoacetase gene and clinical aspects of tyrosinemia type I disease. *J Inherit Metab Dis.* 2011;1:17-21.

22. Baumann U, Preece MA, Green A, Kelly DA, Mckiernan PJ. Hyperinsulinism in tyrosinaemia type I. *J Inherit Metab Dis.* 2005;28:131-135.

23. Nasir S, Raza M, Siddiqui SI, Saleem A, Abbas A. Hereditary Tyrosinemia Compounded With Hyperinsulinemic Hypoglycemia: Challenging Diagnosis of a Rare Case. *Cureus.* 2020;12:e11541.

24. Sethuram S, Sperling MA, Gujral J, Romero CJ. Neonatal hyperinsulinism in transient and classical forms of tyrosinemia. *Orphanet J Rare Dis.* 2021;1:16(1).


25. Rokaitė R, Čibirkaitė A, Zeleckytė V, Lazdinytė G, Dženkaitis M. A Lithuanian Case of Tyrosinemia Type 1 with a Literature Review: A Rare Cause of Acute Liver Failure in Childhood. *Medicina (Lithuania).* 2024;60(1):1-9.

26. Gokay S, Ustkoyuncu PS, Kardas F, Kendirci M. The outcome of seven patients with hereditary tyrosinemia type 1. *J Pediatr Endocrinol Metab.* 2016;29(10):1151-7.

27. Ates I, Stuart C, Rathbone T, Barzi M, He G, Major AM, et al. Ex vivo gene editing and cell therapy for hereditary tyrosinemia type 1. *Hepatol Commun.* 2024;8(5):e0424

Research Article

MOUSE MODEL STUDY: EARLY LIFE CHRONIC STRESS EFFECTS ON *Sox2* AND *Bcl2* mRNA EXPRESSION IN GASTROINTESTINAL TISSUES

 Keziban Korkmaz BAYRAM^{1,2*},  Aida Nurul BAROKAH³,  Merve Hilal DÖNMEZ^{3,4},
 Tuba Dilay KÖKENEK ÜNAL⁵,  Arslan BAYRAM⁶

¹Department of Medical Genetics, Faculty of Medicine, Ankara Yıldırım Beyazıt University, Ankara, Türkiye.

²Gene Targeting and Transgenic Models Platform, Izmir Biomedicine and Genome Center (İBG), Izmir, Türkiye.

³Graduate School of Health Sciences, Department of Translational Medicine, Ankara Yıldırım Beyazıt University, Ankara, Türkiye.

⁴Faculty of Process Sciences, Institute of Biotechnology, Technical University of Berlin, Germany.

⁵Department of Pathology, Faculty of Medicine, Ankara Yıldırım Beyazıt University, Ankara, Türkiye.

⁶GENTAN, Genetic Diseases Evaluation Centre, Izmir Türkiye.

*Correspondence: k.korkmaz.bayram@aybu.edu.tr

ABSTRACT

Received: 27 November 2024
Revised: 14 January 2025
Accepted: 27 January 2025
Published: 20 March 2025



Copyright: © 2025 by the authors. Published by Aydın Adnan Menderes University, Faculty of Medicine and Faculty of Dentistry. This article is openly accessible under the Creative Commons Attribution-NonCommercial 4.0 International (CC BY-NC 4.0) License.

Objective: Chronic stress in early life can impact the gastrointestinal (GI) tract and increase cancer risk. Studies on mouse models have shown that maternal stress can cause lasting changes in the offspring's physiology and behaviour. These changes can be observed in the GI tract, where disturbances in cellular processes, such as apoptosis, can occur. This study examined mRNA expression in the GI tissues of maternally stressed mice, focusing on *Sox2* and *Bcl2* mRNA expressions.

Materials and Methods: Pregnant *Balb/c* mice were randomly divided into three groups. The litters of the control were exposed to routine conditions. In contrast, others were randomly exposed to unpredictable maternal separation (MS) for three hours every day between 1-14 postnatal days (PND). Half of the MS dams were exposed to unpredictable maternal stress (MSUS) within these three hours. Five-week-old litters were sacrificed, and total RNA was isolated from the muscle, duodenum, and stomach tissues using the Phenol-Chloroform technique. *Sox2*, *Bcl2* and *Gapdh*, mRNA expression was measured by Rotor-Gene Q. The data obtained were analysed using One-Way ANOVA tests and Kruskal-Wallis in GraphPad Prism9.

Results: Although the *Bcl2* mRNA expression in the stomach remained unchanged, it significantly increased in the duodenum of MS ($p=0.0132$). Similarly, while the *Sox2* mRNA expression in muscle did not change substantially, it increased significantly in gastric tissue of MSUS ($p=0.0030$). Furthermore, a significant positive correlation was found between the *Sox2* and *Bcl2* genes in gastric tissue ($p=0.005$).

Conclusion: Early life stress (ELS), GI dysfunction, and cancer susceptibility may be intricately linked. Understanding the molecular mechanisms involved in cancer susceptibility may have new implications for developing interventions that can reduce the risk of developing cancer. This research may also provide insights into new strategies for treating cancer in predisposed individuals.

Keywords: Maternal Deprivation; Maternal Stress; *Sox2*; *Bcl2*; cDNA Profile; Apoptosis

INTRODUCTION

Chronic stress, particularly during critical developmental periods in early life, has emerged as a significant factor influencing various aspects of health and disease susceptibility later in life (1). The GI tract is particularly vulnerable among the myriad physiological systems ELS affects. In mice and humans, this vulnerable gastric system's epithelium comprises glandular units that produce acid, hormones, mucus, and digestive enzymes (2). The glandular stomach is divided into two parts— antrum and corpus—with different cell ratios and turnover rates. SRY-box transcription factor 2 (*Sox2*) is believed to represent stem and progenitor cell compartments at the base of antral glands (3). Research has shown multipotent stem cells expressing *Sox2* in the glandular stomach (4). Our study aims to investigate how ELS affects the mRNA expression level of *Sox2* in the gastric corpus region.

The GI tract serves as a primary interface for nutrient absorption and immune surveillance and harbours a complex ecosystem of microbes crucial for maintaining overall health. Emerging evidence suggests that ELS can profoundly disrupt the delicate balance within the GI tract, predisposing individuals to a spectrum of GI disorders and potentially impacting cancer susceptibility (5).

The interplay between ELS, GI health and cancer susceptibility is fascinating and has garnered attention in recent research endeavours (5). This study uses maternally stressed mice models to gain insights into the molecular mechanisms underlying these associations.

One intriguing aspect of this research is the examination of apoptotic pathways and the expression of critical regulatory genes within the GI tract, notably *Sox2* and *Bcl2* mRNA expression. *Sox2*, a pivotal transcription factor known for its roles in embryonic development and stem cell pluripotency maintenance, has garnered interest for its potential involvement in GI homeostasis and cancer pathogenesis (6). Likewise, *Bcl2*, an anti-apoptotic protein crucial for cell survival, has been implicated in modulating apoptotic processes within the GI tract (7).

Recent investigations have begun to detect the intricate connections between cancer and apoptosis by *Sox2* and *Bcl2* mRNA expression (6). It has been observed, suggesting a potential link between ELS, altered gene expression, and GI dysfunction.

Considering these findings, understanding the impact of ELS on GI health and cancer susceptibility holds significant clinical implications. Insights gleaned from

maternally stressed mice models may offer valuable avenues for developing targeted interventions to mitigate the long-term consequences of ELS on GI tract function and reduce the risk of GI malignancies (1,5). By elucidating the molecular underpinnings of these complex interactions, we can strive towards more effective strategies for promoting GI health and combating cancer in vulnerable populations. This study aimed to investigate *Sox2* and *Bcl2* genes mRNA expression in the GI tissues of the maternally stressed mouse model.

MATERIALS AND METHODS

Animals

The study was performed with five-week-old *Balb/c* mice (n=36). These mice were housed in a temperature-controlled room with a 12/12 light/dark cycle and 55% humidity. During the study, the mice had unlimited access to food and water. This study was performed according to the ethical standards outlined in the 1964 Declaration of Helsinki and its subsequent amendments, as well as the relevant guidelines and regulations (Ethics Committee Approval No. 001, 10 January 2023).

Maternal stress mouse model

This study consisted of three distinct groups: a control group (n=12), a group subjected to unpredictable maternal separation (MS) (n=12), and a group subjected to unpredictable maternal separation combined with unpredictable maternal stress (MSUS) (n=12). From PND 1 to 14, dams and litters for MS and MSUS were subjected to three hours of proximal separation per day, chosen randomly. In addition, during this separation, MSUS dams were exposed to either 20-minute restraint or 6-minute forced swim stress during the final 20 minutes of a three-hour unpredictable separation. Dams were placed in a 50-mL Falcon tube with holes for adequate air supply to induce 20 minutes of restraint stress. Dams were subjected to a forced swimming test where they swam for five minutes in a jar of cold water at 18°C (8). After weaning, the pups were raised in social groups of 3–4 mice per cage. The animals in the control group were not disturbed except for a once-a-week cage change. Mice were sacrificed at five weeks old.

RNA isolation, cDNA synthesis and quantitative PCR (qPCR) analysis of *Sox2* and *Bcl2* genes

All wet-lab experiments were conducted at the Research and Application Center (MERLAB) of Ankara Yıldırım Beyazıt University. Fifty milligrams of the corpus region from the stomach, muscle from gastrocnemius lateralis and the start zone of the duodenum were removed and placed in 1 mL QIAzol Lysis Reagent (Qiagen, Germany)

Table 1: Primer pairs that are used for target genes.

Primer	Sequence (5'-3')	Amplicon Size
<i>Sox2</i>	Forward: AACCCCAAGATGCACAACCTC	152 bp
	Reverse: CGCGGCCGGTATTTATAATC	
<i>Bcl2</i>	Forward:CTGGGATGCCTTTGTGGAAC Reverse:TCAAACAGAGGTCGCATGCT	51 bp
<i>Gapdh</i>	Forward: CTCTCTGCTCCTCCCTGTTC	105 bp
	Reverse: TACGGCCAAATCCGTTCCACA	

solution for homogenisation (Bandelin SONOPULS ultrasonic homogeniser HD 2070, Berlin, Germany). Total RNA was extracted from the stomach using the Phenol-Chloroform technique. The RNA samples were carefully preserved at a temperature of -80°C until they were ready to be used. The quantity and quality of RNA were estimated with NanoDrop 2000c (Thermo Fisher Scientific, Massachusetts, United States of America) (8). The concentration of total RNA was found to be greater than 100 ng/μl. cDNA synthesis was performed with the First Strand cDNA Synthesis Kit for RT-PCR (Roche, Netherlands) from total RNA. The acquired cDNA samples underwent a dilution process where nuclease-free water was added in a 1:5 ratio. qPCR was performed using specific primers (Table 1) and FastStart™ Universal SYBR® Green Master (Roche, Nederland) on Rotor-Gene Q (Qiagen, Germany). The PCR cycling conditions were as follows: 10 minutes at 95°C, followed by 50 cycles of 20 seconds at 95°C and 45 seconds at 60°C. The PCR experiment was repeated two times. *Gapdh* was utilised as a housekeeping gene. Ct values were used in a delta-delta-Ct (2-ΔΔCt) analysis. The data were normalised to the same scale using the average values obtained from the control group.

Statistical analyses

The mRNA expression data in control, MS, and MSUS underwent statistical analysis using one-way ANOVA or Kruskal-Wallis test. GraphPad Prism 9.1.0 (GraphPad Software, California, United States) performed Tukey's or Dunn's multiple comparisons post hoc. Data distribution was evaluated using a histogram, q-q plot, and the Shapiro-Wilk test. Outliers were identified and removed based on David C. Hoaglin and Boris Iglewicz's approach. Repeated measure ANOVA followed by Tukey's post hoc was used to analyse the weight data. Pearson's or Spearman's correlation was used to assess the relationship between the data when appropriate. All tests were set at a significance level of $p < 0.05$.

RESULTS

Maternal stress modulates *Sox2* mRNA expression in stomach and *Bcl2* mRNA expression in duodenum of mice

This study examined the mRNA expression of the *Sox2* gene in stomach and muscle tissues and the *Bcl2* gene in the stomach and duodenal tissues of mice exposed to maternal stress. The *Sox2* mRNA expression was significantly higher in the MSUS group than in the control ($p=0.0030$) and MS group ($p=0.0030$) (Fig.1a). However, the mRNA expression of *Bcl2* in the stomach (Fig.1b) and *Sox2* in the muscle tissue (Fig.2b) did not show any significant change among the groups. However, *Bcl2* mRNA expression increased in duodenal tissue in both MS ($p=0.0132$) and MSUS ($p>0.05$) groups compared to the control group (Fig.2a). While there was a significant positive correlation between the *Sox2* and *Bcl2* genes in the stomach ($p=0.005$) (Fig.1c). No correlation was found between *Bcl2* mRNA expression in duodenal tissue and stomach ($p=0.76$) (Fig. 2c).

DISCUSSION

SOX proteins, first identified through the sex-determining region Y gene (*Sry*) are transcription factors crucial for various developmental processes (9–11). One member of this family, the SOX2 protein, is critical in maintaining cancer stem cell properties and regulating gastrointestinal development, particularly in forming the stomach and oesophagus (6,11).

In recent years, researchers have observed that different types of tumours, including lung, pancreatic, breast, colorectal, and gastric cancer, exhibit high levels of SOX2 expression (11). SOX2 expression was significantly linked with larger tumour size, high tumour histological grade, increased risk of lymph node metastasis, and the

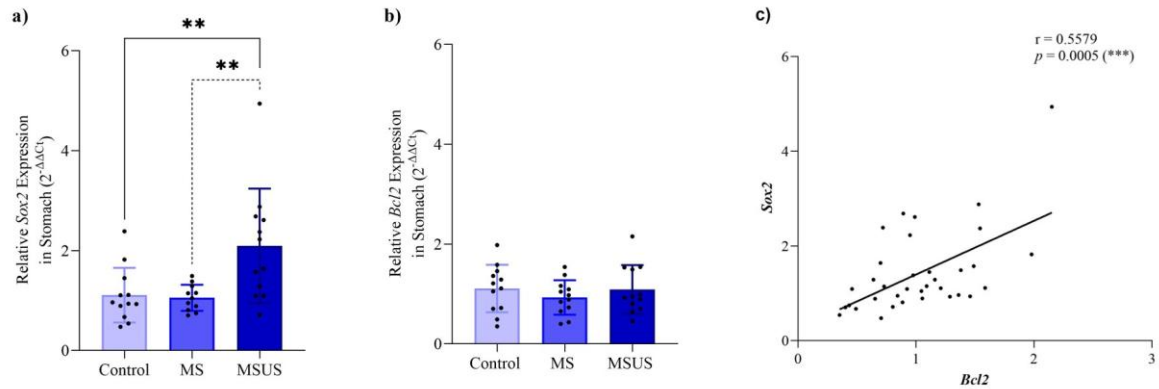


Figure 1. Comparison of *Sox2* (a) and *Bcl2* (b) mRNA expression in the stomach among the different groups. Correlation between *Sox2* and *Bcl2* mRNA profiles in the stomach (c) of the *in vivo* mouse model.

aggressive triple-negative phenotype in 1713 breast cancer patients (12). In addition, solid tumours, like hepatocellular carcinoma (HCC), may produce tumour masses due to a small group of cells known as cancer stem cells (CSC) that can increase the number of differentiated cells (6). According to the CSC hypothesis, the tumorigenicity of CSCs might be linked to the production of tumour masses due to their self-renewal and multilineage differentiation abilities (13). However, the role of SOX2 expression in gastric cancer is quite complex. Although Sarkar et al. (3) compared gastric tissues of wild-type mice with conditional *Sox2* knockout mice using tamoxifen, a selective estrogenic receptor modulator, and found no changes in gastric epithelial remodelling and

Despite its oncogenic role in most cancers, the activity of SOX2 in gastric cancer is a topic of debate, as it may function as a tumour suppressor in certain circumstances (10,14). In a meta-analysis by Li et al. (11), 32 articles covering about 4,641 patients with gastric cancer were analysed. It was found that the expression of SOX2 was significantly reduced in cancerous tissue compared to para-cancerous tissue. This decrease in the expression of SOX2 protein was associated with clinicopathological parameters such as a shorter survival time but not with prognosis. Moreover, high levels of SOX2 expression indicate a better prognosis (11). As per Otsubo et al. (15), a decrease in SOX2 expression is linked to gastric cancer development and poor prognosis. SOX2 inhibits cell

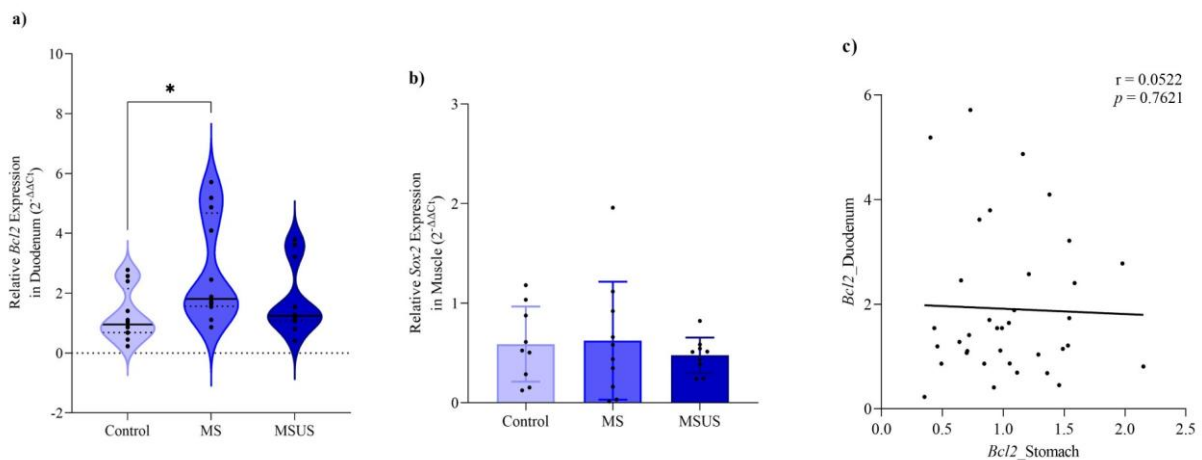


Figure 2. Comparison of *Bcl2* mRNA expression in the duodenal (a) and *Sox2* mRNA expression in the muscle tissues (b) between the groups. Correlation of *Bcl2* mRNA expression between duodenal and stomach tissue (c).

differentiation. It is known that overexpression of *Sox2* is oncogenic in many types of cancer. The exception is gastric cancer, in which SOX2 is a tumour suppressor (10,14).

growth by inducing cell cycle arrest and apoptosis (15). Following a series of studies linking low SOX2 expression with poor patient prognosis, it has been confirmed that

SOX2 inhibits proliferation, promotes apoptosis, and inhibits metastasis in vitro and in vivo (11,16). The mechanism is most likely thought to be that increased expression of interleukin 4 (IL-4) and bone morphogenetic protein-2 (BMP2) factors in gastric cancer leads to decreased SOX2 expression and increased caudal type homeobox gene 2 (CDX2) expression, causing normal gastric cells to progress towards malignant tumours (11). In this study, the mRNA expression of *Sox2* did not change in muscle tissue, but it increased in gastric tissue in litters whose dams were exposed to physical and psychological stress during early life. After exposure to chronic stress early in life, the expression of *Sox2* mRNA in the corpus region of the stomach may have increased to provide protection from stress-induced damage, adapt to stress-induced changes, or act as an early indicator of gastric cancer onset. The cells in the lining of the stomach's corpus region are unique because they contain specialised cells called gastric glands, which produce gastric acid and digestive enzymes (17). Maternal stress may initially impact the stomach, and the overexpression of the *Sox2* gene in the corpus region may be derived from multipotent stem cells. The increased expression of *Sox2* could help counteract the negative impact of chronic stress in the early stages by promoting the growth of multipotent stem cells, inhibiting proliferation, and promoting apoptosis. On the other hand, the *Sox2* protein is essential for self-renewal and repairing gastric gland cells (18). Thus, *Sox2* may have assisted in repairing damage and inflammation in the stomach caused by this chronic stress.

Apoptosis is a biological process that responds to developmental cues or cellular stress. Its impairment plays a central role in cancer development (19). The *B-cell lymphoma 2 (BCL2)*, a co-regulator of apoptosis in the endoplasmic reticulum and mitochondria, can detect various types of stress (20,21). The *Bcl2* protein family regulates pro- and anti-apoptotic activities. Maintaining the balance between these two activities is essential for healthy cells. However, if this balance is disrupted, it can lead to cell death or malignant cell growth (19,22). *Sox2* is mainly responsible for controlling gene expression to preserve stem cells' ability to differentiate into various cell types, whereas *Bcl2* prevents cell death and promotes cell survival. *Sox2* and *Bcl2* can have indirect connections or interactions in specific cellular environments. Despite their involvement in different cellular processes, there is no known direct functional relationship between *Sox2* and *Bcl2*. However, they may indirectly intersect through shared signalling pathways or regulatory networks. In a single study found in the literature, it was discovered that there is a relationship between *Sox2* and *Bcl2*. The study used qPCR to analyse mRNA expression levels of *Sox2* and

Bcl2 in paraffin-embedded tissues from patients with HCC. The findings revealed a significant increase in the mRNA expression levels of *Sox2* and *Bcl2*. A significant positive correlation was also observed between the two (6). This study was conducted using only male mice, which limits the generalizability of our findings to females. Future studies should include both sexes to investigate potential sex-specific differences. Our research has shown that the levels of *Sox2* mRNA expression in the stomach and *Bcl2* mRNA expression in the duodenum of litters exposed to chronic stress caused by early maternal separation and maternal stress have increased significantly. We also found a positive correlation between *Sox2* and *Bcl2* mRNA expression in gastric tissue. These findings support the results on HCC, the only known research in the literature that discusses the connection between *Sox2* and *Bcl2*. The positive correlation between these genes in HCC and maternal stress may result from regulating a common epigenetic mechanism, albeit in different tissues from different organisms. On the other hand, maternal stress may have similarly increased *Sox2* and *Bcl2* expression and predispose to cancer development.

Chronically stressed individuals may anticipate stress and exhibit a rapid cortisol response (23). This may increase individuals' vulnerability to oxidative stress (OXS). OXS characterized by an imbalance between the production of reactive oxygen species (ROS) and antioxidant defences, can result in ROS-induced damage to DNA, proteins, and lipids, ultimately leading to cellular damage and inflammation (24). Chronic inflammation, with its persistent activation of the immune system, contributes to cancer development (25). While the exact mechanisms linking SOX2 to oxidative stress warrant further investigation, SOX2 has been shown to contribute to an aggressive, oxidative tumour phenotype with enhanced drug resistance and metastatic potential in melanoma (27). This study observed significantly increased *Sox2* and positively correlated *Bcl2* mRNA expression levels in the stomachs of the MSUS group. These findings suggest that chronic maternal stress in early life may increase oxidative stress and inflammation, potentially predisposing individuals to diseases such as gastric cancer later in life.

Researchers have found that exposure to chronic stress during childhood or adolescence can have long-lasting effects on the body's stress response systems and immune function (28,29). Chronic stress can trigger the release of stress hormones such as cortisol, adrenaline, and inflammatory cytokines, signalling molecules in the immune response. When stress becomes chronic, these hormones and cytokines can disrupt the immune system, leading to persistent low-grade inflammation (30). Early

chronic stress may be so damaging to the stomach that *Sox2* is trying to compensate for this damage by overexpressing. Despite this compensation of *Sox2* overexpression, individuals may be more susceptible to gastric cancer. New studies can be planned by conducting more in-depth family histories about the early life of patients diagnosed with gastric cancer.

CONCLUSION

Despite technological advancements, the reasons behind the rising incidence of cancer in the population are still unclear. Some individuals may be more prone to cancer due to the chronic stress they experience early in life. The mRNA expression of *Sox2* and *Bcl2* in GI tissues such as the stomach and duodenum shows a significant positive correlation due to maternal stress exposure. Thus, we suggest that chronic maternal stress during infancy may increase oxidative stress and inflammation, potentially making individuals more susceptible to diseases such as gastric cancer later in life. In future studies, it would be essential to consider family history when exploring whether patients diagnosed with gastric cancer were exposed to chronic stress, such as maternal separation and maternal stress, during the first months of their lives, such as the breastfeeding period.

Acknowledgments

We would like to thank Ankara Yıldırım Beyazıt University (AYBU) Central Research Laboratory (AYBU MERLAB) for providing the essential facilities and resources needed to conduct the molecular laboratory studies presented in this work.

Authorship contributions

The study was a collective effort of all the authors. K.K.B. and A.B. have organized and obtained financial support. K.K.B., A.N.B., and M.H.D. performed mouse models, prepared the samples, and analysed the mRNA expression. A.N.B. prepared figures and graphs and performed statistical analysis. K.K.B., A.B., and T.D.K.U. created project hypotheses, interpreted data, reviewed the literature, and prepared the manuscript. All authors read and agreed to the published version.

Data availability statement

If all authors agree to share their data, the corresponding author should be contacted to obtain it confidentially.

Declaration of competing interest

The authors in this work declare that they have no financial or non-financial interests that could compete with the described work.

Ethics

The research activities were performed according to the ethical standards outlined in the 1964 Declaration of Helsinki and its subsequent amendments, as well as the relevant guidelines and regulations (NESA Experimental Animals Laboratory Ethics Committee Approval No. 001, 10 January 2023).

Funding

No funding was received to conduct this study.

REFERENCES

1. Dai S, Mo Y, Wang Y, Xiang B, Liao Q, Zhou M, et al. Chronic Stress Promotes Cancer Development. *Front Oncol.* 2020;10(August):1–10.
2. Mills JC, Shivdasani RA. Gastric epithelial stem cells. *Gastroenterology.* 2011;140(2):412–24.
3. Sarkar A, Huebner AJ, Sulahian R, Anselmo A, Xu X, Flattery K, et al. Sox2 Suppresses Gastric Tumorigenesis in Mice. *Cell Rep.* 2016 Aug 16;16(7):1929–41.
4. Arnold K, Sarkar A, Yram MA, Polo JM, Bronson R, Sengupta S, et al. Sox2(+) adult stem and progenitor cells are important for tissue regeneration and survival of mice. *Cell Stem Cell.* 2011 Oct 4;9(4):317–29.
5. Leigh SJ, Uhlig F, Wilmes L, Sanchez-Diaz P, Gheorghie CE, Goodson MS, et al. The impact of acute and chronic stress on gastrointestinal physiology and function: a microbiota–gut–brain axis perspective. *J Physiol.* 2023 Oct 1;601(20):4491–538.
6. Hosseini-Khah Z, Babaei MR, Tehrani M, Cucchiarini M, Madry H, Ajami A, et al. SOX2 and Bcl-2 as a Novel Prognostic Value in Hepatocellular Carcinoma Progression. *Curr Oncol.* 2021 Aug 1;28(4):3015–29.
7. Ciccocioppo R, Sabatino A Di, Gasbarrini G, Corazza G. Apoptosis and gastrointestinal tract. *Ital J Gastroenterol Hepatol.* 1999;
8. Bayram KK, Barokah AN, Dönmez MH, Işıktan ŞN, Bayram A. Unravelling the maternal stress-induced orchestrations: Fndc5 gene expression dynamics across duodenum, stomach, and whole blood in offspring. *Acta Med [Internet].* 2024 Sep 30 [cited 2024 Oct 2];55(3):153–61. Available

from:

<https://actamedica.org/index.php/actamedica/article/view/1003>

9. Gubbay J, Collignon J, Koopman P, Capel B, Economou A, Münsterberg A, et al. A gene mapping to the sex-determining region of the mouse Y chromosome is a member of a novel family of embryonically expressed genes. *Nature*. 1990;346(6281):245–50.
10. Carrasco-Garcia E, Santos JC, Garcia I, Brianti M, García-Puga M, Pedrazzoli J, et al. Paradoxical role of SOX2 in gastric cancer. *Am J Cancer Res*. 2016;6(4):701.
11. Li N, Pang Y, Sang J, Sun Y, Hou W. The controversial expression of SOX2 in gastric cancer and its correlation with *Helicobacter pylori* infection: A meta-analysis. *Medicine*. 2022 Oct 7;101(40):E30886.
12. Zheng Y, Qin B, Li F, Xu S, Wang S, Li L. Clinicopathological significance of Sox2 expression in patients with breast cancer: a meta-analysis. *Int J Clin Exp Med*. 2015 Dec 30;8(12):22382.
13. Ma S, Chan KW, Hu L, Lee TKW, Wo JYH, Ng IOL, et al. Identification and characterization of tumorigenic liver cancer stem/progenitor cells. *Gastroenterology*. 2007;132(7):2542–56.
14. Ding LN, Yu YY, Ma CJ, Lei CJ, Zhang HB. SOX2-associated signaling pathways regulate biological phenotypes of cancers. *Biomedicine & Pharmacotherapy*. 2023 Apr 1;160:114336.
15. Otsubo T, Akiyama Y, Yanagihara K, Yuasa Y. SOX2 is frequently downregulated in gastric cancers and inhibits cell growth through cell-cycle arrest and apoptosis. *British Journal of Cancer* 2008 98:4. 2008 Feb 12;98(4):824–31.
16. Wang S, Tie J, Wang R, Hu F, Gao L, Wang W, et al. SOX2, a predictor of survival in gastric cancer, inhibits cell proliferation and metastasis by regulating PTEN. *Cancer Lett*. 2015 Mar 28;358(2):210–9.
17. Engevik AC, Kaji I, Goldenring JR. The Physiology of the Gastric Parietal Cell. *Physiol Rev*. 2020 Jan 1;100(2):573–602.
18. Novak D, Hüser L, Elton JJ, Umansky V, Altevogt P, Utikal J. SOX2 in development and cancer biology. *Semin Cancer Biol*. 2020 Dec 1;67(Pt 1):74–82.
19. Qian S, Wei Z, Yang W, Huang J, Yang Y, Wang J. The role of BCL-2 family proteins in regulating apoptosis and cancer therapy. *Front Oncol*. 2022 Oct 12;12.
20. Yang B, Liu Q, Bi Y. Autophagy and apoptosis are regulated by stress on Bcl2 by AMBRA1 in the endoplasmic reticulum and mitochondria. *Theor Biol Med Model*. 2019 Oct 29;16(1):1–9.
21. Siddiqui WA, Ahad A, Ahsan H. The mystery of BCL2 family: Bcl-2 proteins and apoptosis: an update. *Arch Toxicol*. 2015 Feb 20;89(3):289–317.
22. Carneiro BA, El-Deiry WS. Targeting apoptosis in cancer therapy. *Nat Rev Clin Oncol*. 2020 Jul 1;17(7):395.
23. Aschbacher K, O'Donovan A, Wolkowitz OM, Dhabhar FS, Su Y, Epel E. Good stress, bad stress and oxidative stress: Insights from anticipatory cortisol reactivity. *Psychoneuroendocrinology*. 2013;38(9).
24. Sies H. Oxidative stress: Oxidants and antioxidants. Vol. 82, *Experimental Physiology*. 1997.
25. Bardelčíková A, Šoltys J, Mojžiš J. Oxidative Stress, Inflammation and Colorectal Cancer: An Overview. Vol. 12, *Antioxidants*. 2023.
26. Carrasco-Garcia E, Santos JC, Garcia I, Brianti M, García-Puga M, Pedrazzoli J, et al. Paradoxical role of SOX2 in gastric cancer. Vol. 6, *American Journal of Cancer Research*. 2016.
27. Andreucci E, Pietrobono S, Peppicelli S, Ruzzolini J, Bianchini F, Biagioni A, et al. SOX2 as a novel contributor of oxidative metabolism in melanoma cells. *Cell Communication and Signaling*. 2018;16(1).
28. Jawaid A, Jehle KL, Mansuy IM. Impact of Parental Exposure on Offspring Health in Humans. *Trends Genet*. 2021 Apr 1;37(4):373–88.
29. Thumfart KM, Jawaid A, Bright K, Flachsmann M, Mansuy IM. Epigenetics of childhood trauma: Long term sequelae and potential for treatment. *Neurosci Biobehav Rev*. 2022 Jan 1;132:1049–66.
30. Ravi M, Miller AH, Michopoulos V. The Immunology of Stress and the Impact of Inflammation on the Brain and Behavior. *BJPsych Adv*. 2021 May;27(Suppl 3):158–65.

Research Article

CLINICAL RESULTS OF DIAGNOSIS AND TREATMENT OF PENILE FRACTURE: OUR EXPERIENCE OF THE PAST 10 YEARS

 Tuncer BAHÇECİ^{1*},  Burak GÜLER¹,  Ozan AYDOĞAN¹

¹ Aydın Adnan Menderes University School of Medicine, Department of Urology, Aydın, Türkiye

*Correspondence: tuncerbahceci@gmail.com

ABSTRACT

Objective: The objective of our study is to evaluate the clinical characteristics, diagnostic methods, surgical outcomes, and post-operative complications of penile fractures, based on extensive clinical experience over the past decade. While penile fracture (PF) is a well-established clinical condition, the originality of this study lies in its detailed analysis of both diagnostic approaches and surgical outcomes.

Materials and Methods: A retrospective review was conducted on 33 patients who underwent surgery for penile fractures between March 2014 and March 2024. Medical records were systematically reviewed to obtain epidemiological data, patient history, clinical presentation, etiology, operative findings, and postoperative complications. Statistical analysis was performed using IBM SPSS Statistics.

Results: The mean age of patients was 41.9 ± 13.17 years. The median time from the injury to presentation at the emergency department was 5 hours (range: 1–24 hours). The most common etiology was sexual intercourse-related trauma, observed in 57.6% of cases. Hematoma was present in all patients upon physical examination. Penile ultrasound was performed in 36.4% of cases, detecting cavernosal rupture in all cases. Surgical repair was performed within 24 hours of injury for all patients, with a median hospitalization of 1 day. No early complications occurred, and none of the patients developed erectile dysfunction and penile curvature during follow-up.

Conclusion: History and physical examination are usually sufficient for diagnosis. In uncertain cases, penile ultrasound by experienced radiologists is valuable. Surgical intervention within 24 hours, including pre-hospital delay, minimizes erectile dysfunction and penile curvature, ensuring better functional outcomes.

Keywords: Circumferential subcoronal incision, Coitus, Penile Fracture, Tunical tear

Received: 15 December 2024

Revised: 13 February 2025

Accepted: 13 February 2025

Published: 20 March 2025



Copyright: © 2025 by the authors. Published by Aydın Adnan Menderes University, Faculty of Medicine and Faculty of Dentistry. This article is openly accessible under the Creative Commons Attribution-NonCommercial 4.0 International (CC BY-NC 4.0) License.

INTRODUCTION

A penile fracture (PF) occurs when the tunica albuginea, which surrounds the erectile tissues of the penis, ruptures. Its overall incidence is relatively low, accounting for 1 case per 175000 of the US male population (1).

The causes of penile fracture can vary depending on geographical regions. In Western countries, trauma during sexual intercourse is the most common cause, whereas in the Middle East, a maneuver called "Taghaandan," involving the manual bending of an erect penis, is frequently observed (2). The primary diagnostic method is clinical evaluation, though imaging can help confirm the diagnosis and assess complications such as urethral involvement. Penile Doppler ultrasound (US) and magnetic resonance imaging (MRI) can be used in this purpose (3, 4). Patients often report hearing a cracking sound at the moment of injury, which is immediately followed by a loss of erection and the appearance of a purple-colored swelling resembling an eggplant deformity (5).

The European Association of Urology Guidelines on Urological Trauma recommends early repair for PF to preserve erectile function and reduce the risk of penile curvature and painful erections (6).

The subcoronal penile degloving technique is generally favored for incision, as it provides a clear view of the urethra and corpus cavernosa (7). Due to the thickness of the tunica albuginea, durable and slowly absorbable sutures are recommended for repair (2, 8, 9).

This study aims to share our clinical experiences over the past decade and critically analyze PF in light of current literature. While the topic of PF has been explored previously, this study provides new clinical data and reinforces the importance of early intervention, the role of US in diagnosis, and the effectiveness of a standardized surgical approach, making it an original contribution to the field.

MATERIALS AND METHODS

This study followed the guidelines outlined in the Strengthening the Reporting of Observational Studies in Epidemiology (STROBE) statement (10), and ethical approval was obtained from our local Ethics Committee.

We conducted a retrospective analysis of data from 38 patients who underwent surgery with a preoperative

diagnosis of PF at our tertiary care hospital between March 2014 and March 2024. Patient medical records were systematically reviewed to collect data on demographics, clinical presentation, etiology, surgical details, and postoperative outcomes.

Inclusion criteria included patients who underwent PF repair, as documented in surgical records. Exclusion criteria comprised cases with an unclear history (1 patient), tunical tear repair due to sharp object injuries (1 patient), cavernosal repair for gunshot wounds (1 patient), missing surgical records, or incomplete anamnesis and physical examination notes (2 patient).

Surgical decisions were primarily based on patient's history and physical examination findings (Figure 1, left). Penile Doppler ultrasonography (US) was performed when the diagnosis was uncertain. Preoperative assessment included a complete blood count, electrocardiogram (ECG), and chest X-ray, following a consultation with the anesthesia team. Surgical intervention was performed within 24 hours of presentation, and all patients provided written informed consent before the procedure.

A circumferential subcoronal incision and degloving of the penis was made for accessing on tunical tear (Figure 1, middle). Hematoma evacuation was performed, and tunical tear was sutured using 2-0 polyglactin sutures with a simple interrupted technique (Figure 1, right). In cases with concomitant corpus spongiosum rupture and urethral injury, urethral tears were repaired with 4-0 polyglactin sutures using a similar method.

Prophylactic broad-spectrum antibiotics were administered 30 minutes before surgery. A foley catheter was inserted in all patients to aid in urethral identification.

To ensure repair integrity, a saline-induced erection test was performed. Postoperatively, light-pressure elastic bandages were applied. Foley catheters were removed immediately in patients with dorsal vein rupture without tunical tears, while those with isolated tunical tear repair had their catheters removed the following day. The single patient with urethral repair had the catheter left in place for five days.

Early postoperative complications, including hematoma, pain, and fever, were assessed during hospitalization. Long-term outcomes, such as erectile function and penile curvature, were evaluated at six weeks and six months post-surgery. Erectile dysfunction and penile curvature

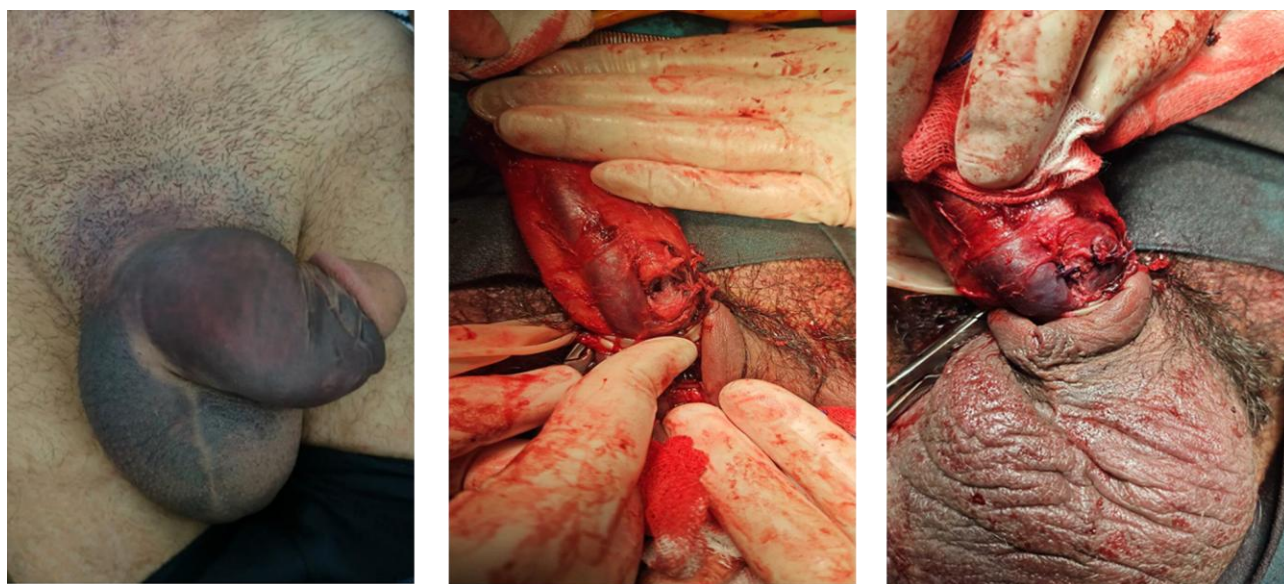


Figure 1. Clinical Presentation of Penile Fracture on Physical Examination (Left), Tunical Tear Appearance After Penile Subcoronal Incision and Degloving (Middle), Repair of Tunical Tear (Right).

were assessed through patient anamnesis and physical examination. As no patients reported complaints or showed pathological findings, erectile dysfunction questionnaires were not completed, and further evaluation was deemed unnecessary. Long-term complications were assessed during outpatient visits at six weeks postoperatively and through follow-up phone calls at six months.

Statistical analysis was performed using IBM SPSS Statistics for Windows, Version 25.0. Continuous variables were reported as mean \pm standard deviation (SD), and categorical variables were reported as frequencies and percentages.

RESULTS

This study included 33 patients who underwent surgery for PF. The patients' average age was 41.9 years, with a standard deviation of 13.17 years. Sexual intercourse was the leading cause of PF, accounting for 57.6% of cases. The median time from injury to presentation at the emergency department was 5 hours, ranging from 1 to 24 hours. Hematoma was the most common symptom, observed in all patients. Penile ultrasound (US) was performed in 36.4% of the patients in the emergency department, and cavernosal rupture was detected in all cases that underwent the procedure. Demographic data and clinical findings are presented in Table 1.

A subcoronal degloving incision was performed in all patients. Among the 33 cases, 4 had dorsal vein rupture

Table 1. The demographic and clinical data of penile fracture

Complaint	Hematoma	33 (100)
Regarding Application n, (%)	Detumesans	25 (75.8)
	Snapping sound	22 (66.7)
Etiology n, (%)	Pain	13 (39.4)
	Coitus	19 (57.6)
	Penil manipulation	5 (15.2)
	Rolling in bed	4 (12.0)
	Falling on erect penis	5 (15.2)
Side of the lesion n, (%)	No tunical defect	4 (12.1)
	Right cavernosum	20 (60.6)
	Left cavernosum	7 (21.2)
	Both corpora cavernosa	2 (6.1)
Emergency service application period n, (%)	\leq 6 hours	22 (66.7)
	>6-12 hours	3 (9.1)
	\geq 12-24 hours	8 (24.2)
Radiology n, (%)	Penil USC	12 (36.4)

without tunical tears, requiring only hematoma evacuation. The remaining 29 patients underwent tunical defect repair. The urethral catheters were promptly discontinued after surgery in patients who did not have cavernosal defects. Foley catheters were removed on the first postoperative day in 96.5% of cases. The patient with urethral repair had the catheter removed on postoperative day five. No early complications were observed during hospitalization. The median length of hospitalization was 1 day (range: 1-3 days).

Table 2. Surgical Findings and Outcomes Repair of penile fracture

Incision techniques, n (%)	Sub-coronal degloving	33 (100)
Penile fracture, n	Tunical tear	29 (87.7)
	Dorsal vein rupture	4 (12.3)
Localization of the lesion	Proximal corpus cavernosum	16 (55.2)
	Mid corpus cavernosum	12 (41.4)
	Distal corpus cavernosum	1 (3.4)
Length of rupture	<1 cm	5 (17.2)
	1-2 cm	16 (55.2)
	2-2,5 cm	8 (27.6)

During the follow-up period, 65.5% (n=19) of the patients with tunical repair attended their six-week follow-up visit. All retained erectile function without penile curvature, as confirmed by medical history and physical examination. The same cohort was re-assessed six months postoperatively, and no long-term complications were observed. Details regarding defect localization, size, side, as well as the suture types used, are shown in Table 2.

DISCUSSION

This study's purpose is to present in detail the clinical characteristics and surgical findings during the treatment process of rarely encountered PF cases in urological emergencies in the light of current literature.

When the penis is in a flaccid state, the thickness of the tunica albuginea is 2.4 mm. In an erect state, the tunica albuginea thins by 5-10 times. In an erect penis, high pressure occurs within the corpus cavernosum, which may lead to cavernosal injury in the case of trauma. The primary etiological factor for PF is trauma occurring during sexual intercourse. In a meta-analysis by Amer et al., PF was reported in 46% of patients, while a meta-analysis by Falcone et al. found that approximately 80% of patients experienced PF during sexual intercourse (2, 11). Other injury mechanisms include penile manipulation (8%- 78%) (2, 11-13), rolling in bed (18.2%, and 21.5%) (13, 14), and falling onto an erect penis (2.8%- 19.2%) (13-15). In our study, sexual intercourse was the most common etiological factor for PF, consistent with the findings of Amer et al. and Falcone et al., while other mechanisms, such as penile manipulation and rolling in bed, were less

frequently observed. These data indicate that PF mostly occurs during physical activities, and transient traumas, such as sexual intercourse, are prominent risk factors.

In anamnesis, the typical presentation involves the development of penile detumescence and sudden edematous swelling of the penis following the audible cracking sound during erection (5). In a meta-analysis by Falcone et al., the most commonly observed finding was penile hematoma, which occurred in 97.5% of cases. Other detectable findings included detumescence (79%), penile swelling (86%), a cracking sound (69%), and penile pain (79%). Additionally, urethral bleeding was identified in 14% of cases, and acute urinary retention was noted in 7% (2). A study evaluating the emergency department presentations of PF patients in our country found hematoma in 87%, detumescence in 39.1%, cracking sound in 30.4%, and pain in 10.4% (12). In the study by Barros et al., sharing their 20 years of experience, hematoma was observed in all cases (100%), while detumescence was found in 82.6%, cracking sound in 76.3%, pain in 66.3%, urethral bleeding in 12.8%, and acute urinary retention in 0.3% (7). The rate of accompanying urethral injury ranges from 3% to 38% (5). Our findings are consistent with the literature regarding the incidence of concomitant urethral injury, although no cases of acute urinary retention were observed in our study.

Although clinical diagnosis is considered the gold standard in the diagnosis of PF, radiological imaging may be required to confirm the diagnosis in some patients. In this context, penile doppler ultrasound (US) can be utilized (4, 16-18). The use of US in the literature varies between 0% and 100% (4, 16, 18, 19). In our study, the rate of US usage was found to be 36.4%. US is a useful tool for confirming the location of tears in the tunica albuginea and determining the presence of concomitant urethral injury. However, its operator dependency is a major drawback. In the study by De Luca et al., preoperative US was able to detect the exact localization of the tunica albuginea tear in all patients, while in the study by Koga et al., the success rate for detecting small tears was found to be 86% (4, 20). According to the study conducted by Küçüker et al., the success rate of US was determined to be 39.1%. (12). In our study, the 100% success rate of US in detecting the defect in all patients is consistent with the findings of De Luca et al., while differing from the lower success rates reported by Koga et al., Küçüker et al., Pavan et al., and Philips et al. This difference may be related to operator experience.

In previous years, the treatment of penile fractures, including both surgical and conservative approaches, was a subject of debate. In the study by Özorak A. et al.

published in 2014, which compared surgical and conservative treatments, no complications were observed in the early surgical group. In contrast, in the conservative group, 20% (2/10) of patients experienced erectile dysfunction, 20% (2/8) reported painful erections, and 20% (2/8) developed penile curvature (21). Today, the most common method for treating penile fractures is early surgical intervention. Additionally, the current European Association of Urology Guidelines on Urological Trauma recommend early repair of PFs (6). The definition of early repair is the performance of surgical repair within 24 hours of the patient's presentation (22). In several studies, the average time between the trauma and the patient's presentation at the hospital varied. One study reported a mean time of 13.9 ± 14.6 hours (23), and another found the mean time to be 6 ± 4 hours, with a range from 1 to 24 hours (13). In a third study, the time ranged from 2 to 504 hours, with an average of 18.5 hours (7). Kozacıoğlu et al. classified patients into three groups based on the time from initial trauma to surgery: one group for patients treated within 6 hours, a second group for those treated between 6 and 12 hours, and a third group for those treated between 12 and 24 hours. After an average follow-up of 44.9 months, no significant differences in deformity or erectile dysfunction (ED) were observed between the three groups (24). In similar studies, early surgery is recommended in the treatment of PF due to its association with better ED and a lower incidence of complications such as penile curvature and painful erection (25, 26). In the study by Hatzichristodoulou et al., data for approximately half of the patients who underwent PF repair were obtained during follow-up, and ED was detected in 53.8% of these patients (mean follow-up was 45.6 months) (3). In our study, all patients presented to the hospital within 24 hours. All patients underwent early surgical repair. No early complications were observed during hospitalization. During the follow-up period, 65.5% of the patients attended their follow-up visits within the first 6 weeks after surgery, and none of these patients reported experiencing ED, painful erections, or penile curvature in their results anamnesis. These findings align with the literature on the benefits of early surgical repair. However, longer follow-up is needed to assess long-term outcomes.

Although the postoperative hospitalization period for PF patients is generally short, the most important factors determining the length of hospital stay are early complications and severe urethral injuries. According to Bozzini, the median length of stay is 3 days (range: 1-21 days, with one patient staying 21 days due to an open wound) (27). In the study by Gedik et al., the average length of stay was 1-2 days, while in the study by El-

Bahnasawy, the average length of stay was found to be 2.3 ± 1.9 days (range: 1-12 days) (13, 25). In the 170 patients who underwent PF repair by Zargooshi et al., no significant complications occurred during or immediately after surgery, and the patients were discharged on the first day after surgery (28). In our series, patients were mostly discharged on the first postoperative day. The shorter length of stay in our study compared to many other studies in the literature is attributed to factors such as all patients being operated on within the first 24 hours, the absence of concomitant urethral injuries (except for one patient), and the lack of early postoperative complications.

Strengths of our study include providing valuable insights into the outcomes of penile fracture repair, with a detailed analysis based on patient data from a specific cohort. This focused approach enhances our understanding of the treatment and recovery process, contributing meaningful data to the existing literature. However, the limitations of our study stem from its retrospective design, which inherently limits the ability to establish causality. Additionally, the absence of patient groups who underwent delayed penile fracture repair or those managed with conservative follow-up prevents us from making comparisons between these treatment approaches, which could have further enriched the findings and conclusions of our work.

CONCLUSION

In the diagnosis of penile fracture, history and physical examination are usually sufficient. In cases with diagnostic uncertainty, penile ultrasound performed by experienced radiologists can be an effective diagnostic tool. Prompt surgical intervention, within 24 hours of injury, including the time elapsed before hospital presentation, significantly reduces the risk of erectile dysfunction and penile curvature, leading to better functional outcomes in these patients.

Acknowledgments

None

Authorship contributions

Conceptualization, TB; Methodology, TB; Data collection, BG, and OA; Analysis, BG and OA; Literature Search, TB, BG, and OA; Writing – Original Draft, BG, OA, and TB; Supervision, TB

Data availability statement

The datasets generated and/or analyzed during the current study are available from the corresponding author upon reasonable request

Declaration of competing interest

The authors declared no conflict of interest.

Ethics

Ethical approval was obtained from the Adnan Menderes University Non-Interventional Clinical Research Ethics Committee (Protocol Number: 2024/181).

Funding

This research received no funding.



REFERENCES

- 1.Koifman L, Barros R, Júnior RA, Cavalcanti AG, Favorito LA. Penile fracture: diagnosis, treatment and outcomes of 150 patients. *Urology*. 2010;76(6):1488-92. Epub 2010/08/17. doi: 10.1016/j.urology.2010.05.043. PubMed PMID: 20708223.
- 2.Falcone M, Garaffa G, Castiglione F, Ralph DJ. Current Management of Penile Fracture: An Up-to-Date Systematic Review. *Sex Med Rev*. 2018;6(2):253-60. Epub 2017/09/07. doi: 10.1016/j.sxmr.2017.07.009. PubMed PMID: 28874325.
- 3.Hatzichristodoulou G, Dorstewitz A, Gschwend JE, Herkommer K, Zantl N. Surgical management of penile fracture and long-term outcome on erectile function and voiding. *J Sex Med*. 2013;10(5):1424-30. Epub 2013/03/01. doi: 10.1111/jsm.12107. PubMed PMID: 23445526.
- 4.De Luca F, Garaffa G, Falcone M, Raheem A, Zacharakis E, Shabbir M, et al. Functional outcomes following immediate repair of penile fracture: a tertiary referral centre experience with 76 consecutive patients. *Scand J Urol*. 2017;51(2):170-5. Epub 2017/01/27. doi: 10.1080/21681805.2017.1280532. PubMed PMID: 28125311.
- 5.Muentener M, Suter S, Hauri D, Sulser T. Long-term experience with surgical and conservative treatment of penile fracture. *J Urol*. 2004;172(2):576-9. Epub 2004/07/13. doi: 10.1097/01.ju.0000131594.99785.1c. PubMed PMID: 15247735.
- 6.Serafetinidis E, Campos-Juanatey F, Hallscheidt P, Mahmud H, Mayer E, Schouten N, et al. Summary Paper of the Updated 2023 European Association of Urology Guidelines on Urological Trauma. *Eur Urol Focus*. 2024;10(3):475-85. Epub 2023/11/16. doi: 10.1016/j.euf.2023.08.011. PubMed PMID: 37968186.
- 7.Barros R, Hampl D, Cavalcanti AG, Favorito LA, Koifman L. Lessons learned after 20 years' experience with penile fracture. *Int Braz J Urol*. 2020;46(3):409-16. Epub 2020/03/14. doi: 10.1590/s1677-5538.Ibju.2019.0367. PubMed PMID: 32167705; PubMed Central PMCID: PMC7088490.
- 8.Rivas JG, Dorrego JM, Hernández MM, Portella PF, González SP, Valle JA, et al. Traumatic rupture of the corpus cavernosum: surgical management and clinical outcomes. A 30 years review. *Cent European J Urol*. 2014;67(1):88-92. Epub 2014/07/02. doi: 10.5173/ceju.2014.01.art20. PubMed PMID: 24982791; PubMed Central PMCID: PMC4074715.
- 9.El-Assmy A, El-Tholoth HS, Abou-El-Ghar ME, Mohsen T, Ibrahiem EH. Risk factors of erectile dysfunction and penile vascular changes after surgical repair of penile fracture. *Int J Impot Res*. 2012;24(1):20-5. Epub 2011/08/13. doi: 10.1038/ijir.2011.41. PubMed PMID: 21833008.
- 10.von Elm E, Altman DG, Egger M, Pocock SJ, Gøtzsche PC, Vandenbroucke JP. The Strengthening the Reporting of Observational Studies in Epidemiology (STROBE) statement: guidelines for reporting observational studies. *Lancet*. 2007;370(9596):1453-7. Epub 2007/12/08. doi: 10.1016/s0140-6736(07)61602-x. PubMed PMID: 18064739.
- 11.Amer T, Wilson R, Chlosta P, AlBuheissi S, Qazi H, Fraser M, et al. Penile Fracture: A Meta-Analysis. *Urol Int*. 2016;96(3):315-29. Epub 2016/03/10. doi: 10.1159/000444884. PubMed PMID: 26953932.
- 12.Küçüker K, Bütün S, Şimşek A. Acil Servise Başvuran Penil Fraktür Hastalarında Yaklaşım ve Yönetim. *Hipokrat Tıp Dergisi*. 2022;2(1):20-4.
- 13.Gedik A, Kayan D, Yamiş S, Yılmaz Y, Bircan K. The diagnosis and treatment of penile fracture: our 19-year experience. *Ulus Travma Acil Cerrahi Derg*. 2011;17(1):57-60. Epub 2011/02/23. doi: 10.5505/tjtes.2011.93763. PubMed PMID: 21341136.
- 14.FAYDACI UDG, TÜRK A, METİN UDM, ÇELİK O, DEMİR K, ÖZGÜL UDA. Penil Fraktür Etiyolojisi ve Erken Cerrahi Tedavinin Sonuçları: Tek Merkezde 82 Olgunun Retrospektif Değerlendirilmesi. *Journal of Reconstructive Urology*. 2012;3(1):1-4.

15. Güney S, Ergenekon E. Penil fraktürlü olgularda operasyon öncesi değerlendirme ve cerrahi deneyimlerimiz.
16. Pavan N, Tezzot G, Liguori G, Napoli R, Umari P, Rizzo M, et al. Penile fracture: retrospective analysis of our case history with long-term assessment of the erectile and sexological outcome. *Arch Ital Urol Androl.* 2014;86(4):359-70. Epub 2015/02/03. doi: 10.4081/aiua.2014.4.359. PubMed PMID: 25641472.
17. Garofalo M, Bianchi L, Gentile G, Borghesi M, Vagnoni V, Dababneh H, et al. Sex-related penile fracture with complete urethral rupture: A case report and review of the literature. *Arch Ital Urol Androl.* 2015;87(3):260-1. Epub 2015/10/03. doi: 10.4081/aiua.2015.3.260. PubMed PMID: 26428656.
18. Phillips EA, Esposito AJ, Munarriz R. Acute penile trauma and associated morbidity: 9-year experience at a tertiary care center. *Andrology.* 2015;3(3):632-6. Epub 2015/05/28. doi: 10.1111/andr.12043. PubMed PMID: 26013107.
19. Bali RS, Rashid A, Mushtaque M, Nabi S, Thakur SA, Bhat RA. Penile fracture: experience from a third world country. *Adv Urol.* 2013;2013:708362. Epub 2013/08/21. doi: 10.1155/2013/708362. PubMed PMID: 23956740; PubMed Central PMCID: PMC3730138.
20. Koga S, Saito Y, Arakaki Y, Nakamura N, Matsuoka M, Saita H, et al. Sonography in fracture of the penis. *Br J Urol.* 1993;72(2):228-9. Epub 1993/08/01. doi: 10.1111/j.1464-410x.1993.tb00693.x. PubMed PMID: 8402028.
21. Özorak A, Hoşcan MB, Oksay T, Güzel A, Koşar A. Management and outcomes of penile fracture: 10 years' experience from a tertiary care center. *Int Urol Nephrol.* 2014 Mar;46(3):519-22. doi: 10.1007/s11255-013-0531-y. Epub 2013 Sep 22. PMID: 24057767.
22. Kominsky H, Beebe S, Shah N, Jenkins LC. Surgical reconstruction for penile fracture: a systematic review. *Int J Impot Res.* 2020;32(1):75-80. Epub 2019/11/07. doi: 10.1038/s41443-019-0212-1. PubMed PMID: 31685943.
23. Swanson DE, Polackwich AS, Helfand BT, Masson P, Hwong J, Dugi DD, 3rd, et al. Penile fracture: outcomes of early surgical intervention. *Urology.* 2014;84(5):1117-21. Epub 2014/12/03. doi: 10.1016/j.urology.2014.07.034. PubMed PMID: 25443914.
24. Kozacıoğlu Z, Ceylan Y, Aydoğdu Ö, Bolat D, Günlüsoy B, Minareci S. An update of Penile Fractures: Long-term significance of the number of hours elapsed till surgical repair on long-term outcomes. *Turk J Urol.* 2017;43(1):25-9. Epub 2017/03/09. doi: 10.5152/tud.2016.39129. PubMed PMID: 28270947; PubMed Central PMCID: PMC5330264.
25. El-Bahnasawy MS, Gomha MA. Penile fractures: the successful outcome of immediate surgical intervention. *Int J Impot Res.* 2000;12(5):273-7. Epub 2001/06/27. doi: 10.1038/sj.ijir.3900571. PubMed PMID: 11424965.
26. El Atar R, Sfaxi M, Benslama MR, Amine D, Ayed M, Mouelli SB, et al. Fracture of the penis: management and long-term results of surgical treatment. Experience in 300 cases. *J Trauma.* 2008;64(1):121-5. Epub 2008/01/12. doi: 10.1097/TA.0b013e31803428b3. PubMed PMID: 18188109.
27. Bozzini G, Albersen M, Otero JR, Margreiter M, Cruz EG, Mueller A, et al. Delaying Surgical Treatment of Penile Fracture Results in Poor Functional Outcomes: Results from a Large Retrospective Multicenter European Study. *Eur Urol Focus.* 2018;4(1):106-10. Epub 2016/03/04. doi: 10.1016/j.euf.2016.02.012. PubMed PMID: 28753754.
28. Zargooshi J. Penile fracture in Kermanshah, Iran: the long-term results of surgical treatment. *BJU Int.* 2002;89(9):890-4. Epub 2002/05/16. doi: 10.1046/j.1464-410x.2002.02745.x. PubMed PMID: 12010234.

Research Article

COMPARISON OF CHROMOSOME ANALYSIS, FACTOR V LEIDEN, AND PROTHROMBIN G20210A MUTATION RESULTS ACCORDING TO THE NUMBER OF PREGNANCY LOSSES IN RECURRENT PREGNANCY LOSS

 Hande ÖZKALAYCI ^{1*},  Mehmet KOCABEY ²

¹ Bolu Abant İzzet Baysal Training and Research Hospital, Medical Genetics, Bolu, TURKIYE

² Hatay Training and Research Hospital, Medical Genetics, Hatay, TURKIYE

*Correspondence: handememis90@gmail.com

ABSTRACT

Objective: Recurrent pregnancy loss is defined as the loss of two or more pregnancies in some sources, or three or more in others, before 20-24 weeks of gestation. The causes being investigated include parental chromosomal abnormalities and hereditary thrombophilia. We aimed to reveal the frequency of parental chromosomal abnormalities, Prothrombin G20210A mutations (PGM), and Factor V Leiden (FVL) in couples presenting with recurrent pregnancy losses and to test whether there is a significant difference between two and more than two pregnancy losses.

Materials and Methods: A total of 171 couples who presented to the Medical Genetics outpatient clinics of two tertiary hospitals located in Bolu and Hatay provinces due to a history of recurrent pregnancy loss were evaluated. Demographic data, medical and family history, chromosomal analysis results of the couples, and FVL and PGM results of the women were recorded.

Results: We detected chromosomal abnormalities in 2.9% of those evaluated. Factor V Leiden frequency was found to be 11.5% and PGM frequency was 3%. No statistically significant distinction was obtained between the groups, categorized as those with two and more than two pregnancy losses, in terms of the occurrence of chromosomal abnormalities ($p=0.65$), FVL ($p=0.58$), and PGM ($p=0.65$).

Conclusion: A similar approach to requesting a test can be taken for both patient groups. Due to the limited number of patients, a meta-analysis of this result with other case series in Turkey would be beneficial.

Keywords: Thrombophilia; Recurrent pregnancy loss; Prothrombin; Factor V; Chromosome abnormalities

Received: 19 October 2024
Revised: 23 December 2024
Accepted: 27 December 2024
Published: 20 March 2025



Copyright: © 2025 by the authors. Published by Aydın Adnan Menderes University, Faculty of Medicine and Faculty of Dentistry. This article is openly accessible under the Creative Commons Attribution-NonCommercial 4.0 International (CC BY-NC 4.0) License.

INTRODUCTION

Spontaneous termination of pregnancy between conception and 20-24 weeks of gestation is considered pregnancy loss (1). While some resources define recurrent pregnancy loss (RPL) as miscarriages of two or more pregnancies (1,2), some publications include at least three consecutive pregnancy losses within the scope of this term (3,4). The frequency of this condition is about 1-2% (1,2). The cause is unknown in 50-75% of cases (5). Recurrent pregnancy loss causes increased stress and depression, especially in women (6).

In studies investigating RPL, factors such as genetics, uterine abnormalities, thrombophilia, endocrine disorders, infection, autoimmunity, sperm factors, and personal habits are considered (7). One of the causes of RPL is parental balanced chromosomal abnormalities. The frequency of this situation is 2-4% (8). European Society of Human Reproduction and Embryology (ESHRE) do not routinely recommend chromosomal analysis for parents (9). Whereas American Society for Reproductive Medicine (ASRM) recommends parental karyotyping (2). Royal College of Obstetricians and Gynaecologists (RCOG) recommends chromosomal analysis of abortion material, particularly after a third miscarriage or any miscarriage in the second trimester. Parental karyotyping is recommended if there is no sample or insufficient tissue, or if unbalanced structural chromosomal abnormalities are detected (4). Although different guidelines have contradictory recommendations regarding the indication for parental karyotyping, it is frequently performed in our country.

Another issue where genetic testing is performed regarding RPL is hereditary thrombophilia. Thrombophilia is a condition in which there is a predisposition to venous thromboembolism. It may be inherited or acquired. Inherited thrombophilic disorders encompass deficiency of Protein C, Protein S or antithrombin, FVL, and PGM. Thrombosis in the placental circulation is thought to cause placental insufficiency (10). The substitution of arginine with glutamine at position 506, known as FVL, was initially unearthed by Bertina et al.. This variant interferes with the degradation of Factor V by activated protein C (11). Factor V Leiden mutation heterozygosity enhances the advent of venous thrombosis by 5-fold, whereas homozygosity increases the risk by 50-fold (12). Factor V Leiden allele frequency was high among Europeans at 4.4% (13). The frequency of FVL in healthy Turkish population was found to be 7.9% (345/4276) (14).

Prothrombin G20210A mutation was defined by Poort et al.. This particular variant is situated in the 3' untranslated region of the F2 gene, leading to elevated levels of prothrombin (15). Carriers are 2 to 3 times more prone to the development of thromboembolism (12). The prevalence of PGM in different geographic regions was reported to be 2% (16). In a study carried out in a Turkish population, this rate was 2.3% (17). In the ESHRE guideline, testing for hereditary thrombophilia is not routinely recommended in RPL, but recommended on a research basis or if there are additional risk factors for thrombophilia (9). The RCOG guideline states that FVL and PGM in second trimester abortions can ideally be investigated on a research basis in RPL (4).

The role of PGM and FVL in RPL is controversial (18). There are studies comparing the frequencies of these mutations in individuals with two and more than two pregnancy losses. Different results were found in these studies (19,20). Some publications make comparisons in terms of chromosomal abnormality (20).

We aimed to determine the rate of chromosomal abnormalities, FVL, and PGM in patients who were evaluated for at least two pregnancy losses and to test whether there is a significant difference between two and more than two pregnancy losses.

MATERIALS AND METHODS

Patients

One hundred seventy-one couples who applied to the Medical Genetics outpatient clinics of Bolu Abant İzzet Baysal Training and Research Hospital between February 1, 2020, and July 15, 2022, as well as those who applied to the Hatay Training and Research Medical Genetics outpatient clinics between March 1, 2021, and July 15, 2022, due to experiencing at least two pregnancy losses before 20 weeks of gestation were included. Clinical and laboratory findings of the patients were examined retrospectively through the hospital registry system and files. Demographic data, medical and family history, number of pregnancies and births, total number and the gestational weeks of pregnancy losses, karyotype results of the couples, and FVL and PGM results of the women were recorded. The conduct of this study was attached to the principles of the Declaration of Helsinki, with all participants providing written informed consent. This study provided ethical approval from the Bolu Abant İzzet

Baysal Training and Research Hospital's Ethics Committee. (Date: 23.08.2022 Decision No: 2022/223).

Chromosome analysis

Peripheral blood samples were collected into sodium heparin tubes. Standard cytogenetic techniques were used in chromosome analysis. After adequate lymphocyte culture, a mitotic inhibitor (colcemid) was added. Application of hypotonic solution followed by fixation was performed. Chromosome slides were prepared, and G banding was applied. At least 20 metaphases were analyzed with a resolution of 500-700 bands. The International System for Human Cytogenetic Nomenclature (ISCN), version 2016, was utilized for reporting.

Thrombophilia mutation test

After DNA isolation was performed from EDTA-whole blood, seven different gene regions were amplified using the Thrombophilia panel kit (Seqline®, Istanbul, Turkey). A fragment analysis-based mutation detection method was employed on a capillary electrophoresis device to simultaneously detect hotspot mutations in FV (Leiden), FII (G20210A), FXIII (V34L), PAI-1 (4G/5G), MTHFR (C677T/A1298C) genes. Only the results for FVL and PGM have been evaluated due to their significance in comparison to other variants reported in the literature (1).

Statistical analysis

All collected data were analyzed with SPSS (IBM, Statistical Package for the Social Sciences) v.22 program. The Kolmogorov-Smirnov test was used to check whether the variables had a normal distribution or not. Frequencies for nominal and ordinal variables and medians with interquartile range for variables that did not follow a normal distribution were utilized. The presence or absence of chromosomal abnormality, FVL, and PGM were independent variables, and the number of pregnancy losses were dependent variables. The participants were categorized into two distinct groups based on their pregnancy history: those who experienced two pregnancy losses and those who had more than two. A comparative analysis was then conducted between these groups, examining the occurrence of chromosomal abnormalities and gene mutations using chi-square and Fisher's exact tests in cross-tables. Statistical significance was assigned by considering a p-value of less than 0.05.

RESULTS

Patients

One hundred forty-five couples were from the province of Bolu, and 26 couples were from the province of Hatay. The

median for female ages was 29 (range: 28 minimum: 18 maximum: 46), and the median for men ages was 32 (range: 31 minimum: 18 maximum: 49). The median number of pregnancy losses was 2 (range: 4 minimum: 2 maximum: 6). 57% of the couples had two pregnancy losses (n=97), 34.5% had three pregnancy losses (n=59), 4.7% had four pregnancy losses (n=8), 3.5% had five pregnancy losses (n=6), 0.6% had six pregnancy losses (n=1). 35.1% of the patients had a history of live birth, and 64.9% did not (Table 1).

Table 1. Clinical and laboratory characteristics of the patients, N=171

Age	
Female	Median 29 (Range: 28, Min: 18, Max: 46)
Male	Median 32 (Range: 31, Min: 18, Max: 49).
Number of pregnancy loss	
2	N=97 (57%)
3	N=59 (34.5%)
4	N=8 (4.7%)
5	N=6 (3.5%)
6	N=1 (0.6%)
Healthy offspring	
Yes	N=60 (35.1%)
No	N=111 (64.9%)
Chromosome abnormality	
Female	N=3 (1.75%)
Male	N=2 (1.17%)
Factor V Leiden	
Wild	N=147 (88.5%)
Heterozygous	N=19 (11.5%)
Homozygous	N=0
Prothrombin G20210A	
Wild	N=161 (97%)
Heterozygous	N=5 (3.0%)
Homozygous	N=0

Chromosome analysis

Chromosome abnormalities were detected in two women and three men out of 171 couples. There was a chromosomal abnormality in 2.9% of the couples. Chromosomal abnormalities are shown in Table 2. Reciprocal translocations were detected in four cases, and sex chromosome abnormality was detected in one case. Upon categorizing the cases into two groups based on the number of pregnancy losses, chromosomal abnormalities were detected at similar frequencies in both groups (n=2, 2.1% in two pregnancy losses; n=3, 4.1% in more than two pregnancy losses, p=0.65).

Table 2 Parental chromosome abnormalities

Chromosome Abnormality	Number of patients (n)
46,XX,t(1;7)(p36.2;p21)	1
46,XX,t(11;22)(q23;q11.2)	1
46,XX,t(12;22)(q22;q11.2)	1
46,XY,t(9;11)(q33;p15)	1
mos 47,XYY[15]/46,XY[35]	1

Factor V Leiden and Prothrombin G20210A Mutation

Mutation analyses of 166 patients were evaluated. We excluded those with abnormal chromosome results. Factor V Leiden frequency was 11.5% (19/166), and PGM frequency was 3% (5/166) (Table 1). No homozygous or double heterozygous patients were detected. When compared between the two abovementioned groups, similar rates were detected for both FVL and PGM. (FVL (p=0.58); PGM (p=0.65)) (Table 3 and 4). No significant difference was detected between mutation carriers and noncarriers in the history of live birth. Whereas the live birth history rate was 32.9% (48/146) in noncarriers, 46.2% (12/26) of the mutation carriers had a live birth history (p=0.19).

Table 3. Comparative analysis of Factor V Leiden mutation rate in cases with two pregnancy losses versus three or more pregnancy losses

Factor V G1691A	Two pregnancy losses (n=95)	Three or more pregnancy losses (n=71)
GG/Wild	83 (87.4%)	64 (90.1%)
GA/Heterozygous	12 (12.6%)	7 (9.9%)
AA/Homozygous	0	0

Chi-square; p=0.58

Table 4. Comparative analysis of Prothrombin G20210A mutation rate in cases with two pregnancy losses versus three or more pregnancy losses

Prothrombin G20210A	Two pregnancy losses (n=95)	Three or more pregnancy losses (n=71)
GG/Wild	93 (97.9%)	68 (95.8%)
GA/Heterozygous	2 (2.1%)	3 (4.2%)
AA/Homozygous	0	0

Fisher's exact test; p=0.65

DISCUSSION

Couples experiencing recurrent pregnancy loss are apprehensive about having another pregnancy loss. They want the underlying cause to be identified and the situation resolved as soon as possible. As geneticists, we carry out chromosome analysis and hereditary thrombophilia testing as part of our daily practice. When

we evaluated the test results of 171 couples, we detected a chromosomal abnormality in 2.9% (5/171) of them. While balanced reciprocal translocations were detected in four cases, sex chromosome abnormalities were detected in one. The most frequently detected chromosomal abnormality is reciprocal translocation, which is consistent with the literature. The sex chromosome abnormality we detected has rarely been reported in RPL in the literature (21). The patient may be prone to meiotic nondisjunction (22). If a parental balanced structural change is detected, preimplantation genetic testing and invasive prenatal procedures should be recommended for future pregnancies. The chances of a healthy pregnancy are influenced by the gene regions involved and the type of rearrangement (7). Genetic counseling is crucial for these couples. Detected chromosomal translocation abnormalities should also be screened for other family members. It can be helpful not only for the couple but also for the other potential carrier relatives. Additionally, chromosome analysis and microarray investigations on abort materials will be very informative in some cases. Microarray analysis does not need viable cells, so they could be preferred when it is possible.

Additionally, participants were categorized as having two or more pregnancy losses. Indistinguishable results were detected in two groups in terms of the frequency of chromosomal abnormality (n=2, 2.1% two pregnancy losses; n=3, 4.1% more than two pregnancy losses; p=1). Youssef et al. found no difference between the groups in the prevalence of chromosomal abnormalities in a study including 240 patients (23). Our result was in agreement with a meta-analysis (10 studies, OR 0.78, 95% CI 0.55–1.10). The rate of chromosomal abnormality was found to be 5.3% in two pregnancy losses, whereas it was 6.6% in more than two pregnancy losses (20). Although the number of cases is limited in our study, a similar result was found.

We evaluated hereditary thrombophilia risk factors in women. We found the frequencies of FVL and PGM in our patients to be 11.5% and 3%, respectively. Different RPL studies conducted in our country found varying rates, such as 7.9%, 9.5%, 10%, 11.2%, and 16.9% for FVL. The rates for PGM were 1.7%, 2.1%, 3.5%, 5.4% and 14.1% (24-27,19). In two studies conducted in control groups, the frequency of FVL was 7% and 11%, and the frequency of PGM was 1.6% and 5% (24,27). The effects of hereditary thrombophilia in the etiology of RPL are controversial. Although some studies reveal that FVL and PGM are associated with it (28,29,30), others do not support this argument (31,32,33). Also, two studies from our country that compare RPL and control patients did not support this

relationship (24,27). Factor V Leiden and PGM continue to be investigated in the etiology of RPL. The pregnant women detected to have thrombophilia are using anticoagulant drugs for a healthy ongoing pregnancy. These drugs have some adverse effects, like a tendency to bleed, bruising at the application site, and pain. The confusion over whether thrombophilia is a contributing factor to recurrent pregnancy loss (RPL) requires clarification. A study was recently published reporting that Low Molecular Weight Heparin (LMWH) treatment did not lead to an improvement in the live birth rate. In this study, pregnancy success in cases with FVL was found to be 70.8% (68/96) in the group using anticoagulants and 69.9% (58/83) in the group not using drugs. In prothrombin gene mutation, these rates were found to be 72.3% (26/36) and 73.2% (30/41), respectively (34). We compared the status of the healthy live birth history of the patients with thrombophilia mutation carriers and noncarriers. We did not obtain any significant difference. Whereas the live birth history rate was 32.9% (48/146) in noncarriers, 46.2% (12/26) of the mutation carriers had a live birth history ($p=0.19$). Although we do not know the patient's other risk factors for hypercoagulation, this result may also be related to the controversial effects of thrombophilia genetic factors in RPL etiology.

There are studies comparing the frequencies of these mutations in patient groups with two and more than two pregnancy losses. We detected no remarkable difference between the groups regarding thrombophilia mutations (FVL $p=0.58$; PGM $p=0.65$). In contrast to our results, one study conducted with 2660 people from Turkey found that heterozygosity for FVL and PGM was more common in three or more pregnancy losses ($p<0.01$) (19). The findings of Karadeniz et al. were comparable to ours (35). In a study including 75 cases from Turkey, Kovalak et al. detected a higher FVL mutation rate in three pregnancy loss group compared to two ($p=0.029$). They did not find any significant difference for PGM. The number of patients are very limited in that study. The chromosome results are not convenient to evaluate since some polymorphisms were evaluated as abnormalities (36). Our results were compatible with a meta-analysis (FVL (five studies, $n=1109$ OR 0.79, 95% CI 0.43-1.47) and PGM (five studies, $n=1330$ OR 1.08, 95% CI 0.44 -2.62)) (20).

In this study, the results of the chromosomal analysis revealed no significant differences between the comparison groups. In the first group, consisting of two pregnancy losses ($n=2$), the rate was 2.1%. In contrast, the second group, which experienced more than two pregnancy losses ($n=3$), showed a rate of 4.1%. No statistical significance was found ($p=1$). Furthermore, the

examination of thrombophilia mutations also showed no remarkable differences between the groups. Factor V Leiden mutations were found in 12 individuals (12.6%) in the two pregnancy loss group, and it was found in 7 individuals (9.9%) in the three pregnancy loss group. No statistically significant difference was detected ($p=0.58$). Similarly, PGM were present in 2 individuals (2.1%) in the two pregnancy loss group and 3 individuals (4.2%) in the three pregnancy loss group, with a p -value of 0.65, indicating a lack of significant difference.

While there is controversy between our thrombophilia results and several other studies from Turkey, our findings related to chromosomes and thrombophilia were consistent with a meta-analysis (20). We suggest that a similar approach of testing algorithm could be applied to both groups. However, further research is necessary to draw definitive conclusions.

This study has several limitations. First of all, it is really difficult to divide these patients into different groups because, of course, there is a possibility that some women in the first group (with two pregnancy losses) will move to the second group (with more than two pregnancy losses) in the following years. Secondly, because the mutation frequencies are low, our sample can be considered a relatively small sample. The number of patients attending the clinic due to the effects of the Covid-19 pandemic is below expectations. However, we hope the presentation of 2.5 years of patient data will contribute to the literature. Finally, in our study, we included all couples who presented to our clinic and experienced a pregnancy loss before 20 weeks gestation, with no exclusion criteria. For this reason, there may be couples in the sample whose pregnancy loss is due to non-genetic factors. However, given that the most common reason for referral to our clinic is that no other cause of pregnancy loss can be found and that genetic testing is often not requested when a known cause is present, this likelihood is not very high.

CONCLUSION

How many pregnancy losses should be considered as recurrent pregnancy loss is still a matter of debate. No statistically significant distinction was obtained between the groups, categorized as those with two and more than two pregnancy losses, in terms of the occurrence of chromosomal abnormalities, FVL, and PGM. A similar approach of testing algorithm can be applied for both groups. However, due to the limited number of patients, a meta-analysis combining our study with other case series in the Turkish population would be beneficial. In order to

gain a deeper understanding of the etiopathological connection of these genetic changes within the Turkish population, additional functional studies are needed.

Acknowledgments

We would like to thank the staff of Haseki Sultangazi Genetic Diseases Evaluation Center for their assistance in performing the genetic tests in our study.

Authorship contributions

Surgical and Medical Practices: HÖ, MK Concept: HÖ, MK Design: HÖ, MK Data collection or processing: HÖ, MK Analysis-Interpretation: HÖ, MK Literature search: HÖ Writing: HÖ

Data availability statement

The data that support the findings of this study are available from the corresponding author upon reasonable request.

Declaration of competing interest

The authors declare that they have no conflict of interest.

Ethics

This study provided ethical approval from the Bolu Abant İzzet Baysal Training and Research Hospital's Ethics Committee. (Date: 23.08.2022 Decision No: 2022/223).

Funding

The authors declare that this study has received no financial support.

REFERENCES

1. ESHRE Guideline Group on RPL, Bender Atik R, Christiansen OB, Elson J, et al. ESHRE guideline: recurrent pregnancy loss. *Hum Reprod Open*. 2018(2):hoy004.
2. Practice Committee of the American Society for Reproductive Medicine. Electronic address: asrm@asrm.org. Definitions of infertility and recurrent pregnancy loss: a committee opinion. *Fertil Steril*. 2020;113(3):533-535.
3. Jauniaux E, Farquharson RG, Christiansen OB, Exalto N. Evidence-based guidelines for the investigation and medical treatment of recurrent miscarriage. *Hum Reprod*. 2006;21(9):2216-22.

4. Regan L, Rai R, Saravelos S, Li TC; Royal College of Obstetricians and Gynaecologists. Recurrent Miscarriage Green-top Guideline No. 17. *BJOG*. 2023 Nov;130(12):e9-e39.
5. Turesheva A, Aimagambetova G, Ukybassova T, et al. Recurrent Pregnancy Loss Etiology, Risk Factors, Diagnosis, and Management. *Fresh Look into a Full Box*. *J Clin Med*. 2023;12(12):4074.
6. Hedegaard S, Landersøe SK, Olsen LR, Krog MC, Kolte AM, Nielsen HS. Stress and depression among women and men who have experienced recurrent pregnancy loss: focusing on both sexes. *Reprod Biomed Online*. 2021;42(6):1172-1180.
7. Practice Committee of the American Society for Reproductive Medicine. Evaluation and treatment of recurrent pregnancy loss: a committee opinion. *Fertil Steril*. 2012;98(5):1103-11.
8. American College of Obstetricians and Gynecologists. ACOG practice bulletin. Management of recurrent pregnancy loss. Number 24, February 2001. (Replaces Technical Bulletin Number 212, September 1995). *American College of Obstetricians and Gynecologists. Int J Gynaecol Obstet*. 2002;78(2):179-90.
9. ESHRE Guideline Group on RPL; Bender Atik R, Christiansen OB, Elson J, et al. ESHRE guideline: recurrent pregnancy loss: an update in 2022. *Hum Reprod Open*. 2023 Mar 2;2023(1):hoad002.
10. Arachchilage DRJ, Makris M. Erratum: Inherited Thrombophilia and Pregnancy Complications: Should We Test? *Semin Thromb Hemost*. 2019;45(1):e1.
11. Bertina RM, Koeleman BP, Koster T, et al. Mutation in blood coagulation factor V associated with resistance to activated protein C. *Nature*. 1994;369(6475):64-7.
12. Rosendaal FR, Reitsma PH. Genetics of venous thrombosis. *J Thromb Haemost*. 2009; 7 (Suppl. 1): 301-4.
13. Rees DC, Cox M, Clegg JB. World distribution of factor V Leiden. *Lancet*. 1995 28;346(8983):1133-4.
14. Akar N. Factor V 1691 G-A mutation distribution in a healthy Turkish population. *Turk J Hematol*. 2009; 26: 9-11
15. Poort SR, Rosendaal FR, Reitsma PH, Bertina RM. A common genetic variation in the 3'-untranslated region of the prothrombin gene is associated with elevated plasma prothrombin levels and an increase in venous thrombosis. *Blood*. 1996;88(10):3698-703.

16. Rosendaal FR, Doggen CJ, Zivelin A, et al. Geographic distribution of the 20210 G to A prothrombin variant. *Thromb Haemost.* 1998;79(4):706-8.
17. Akar N, Misirlioğlu M, Akar E, Avcu F, Yalçın A, Sözüöz A. Prothrombin gene 20210 G-A mutation in the Turkish population. *Am J Hematol.* 1998;58(3):249.
18. Hong Li Y, Marren A. Recurrent pregnancy loss: A summary of international evidence-based guidelines and practice. *Aust J Gen Pract.* 2018;47(7):432-436.
19. Barut MU, Bozkurt M, Kahraman M, et al. Thrombophilia and Recurrent Pregnancy Loss: The Enigma Continues. *Med Sci Monit.* 2018;24:4288-4294.
20. van Dijk MM, Kolte AM, Limpens J, et al. Recurrent pregnancy loss: diagnostic workup after two or three pregnancy losses? A systematic review of the literature and meta-analysis. *Hum Reprod Update.* 2020;26(3):356-367.
21. Tharapel AT, Tharapel SA, Bannerman RM. Recurrent pregnancy losses and parental chromosome abnormalities: a review. *Br J Obstet Gynaecol.* 1985;92(9):899-914.
22. Wong EC, Ferguson KA, Chow V, Ma S. Sperm aneuploidy and meiotic sex chromosome configurations in an infertile XYY male. *Hum Reprod.* 2008 Feb;23(2):374-8.
23. Youssef A, Lashley L, Dieben S, Verburg H, van der Hoorn ML. Defining recurrent pregnancy loss: associated factors and prognosis in couples with two versus three or more pregnancy losses. *Reprod Biomed Online.* 2020 Oct;41(4):679-685.
24. Altintas A, Pasa S, Akdeniz N, et al. Factor V Leiden and G20210A prothrombin mutations in patients with recurrent pregnancy loss: data from the southeast of Turkey. *Ann Hematol.* 2007;86(10):727-31.
25. Kocağa A, Kılıç H, Gülec S. Incidence and spectrum of thrombophilia in women with recurrent pregnancy loss: a retrospective study. *Eskisehir Med J.* 2023; 4(2): 116-120.
26. Doğan M, Gezdirici A, Yavaş C, Eröz R. Tekrarlayan Gebelik Kayıpları Nedeniyle Çalışılan 306 Çiftin Kromozom Analizi ve Trombofil Parametrelerinin Değerlendirilmesi: Tek Merkez Deneyimi. *SABD.* 2022;12(2):280-5.
27. Şahin Fİ, Ataç B, Yılmaz Z, Zeyneloğlu HB. Thrombophilia mutation frequencies in recurrent pregnancy losses. *Erciyes Med J.* 2009; 31(2):104-9.
28. Rey E, Kahn SR, David M, Shrier I. Thrombophilic disorders and fetal loss: a meta-analysis. *Lancet.* 2003;361(9361):901-8.
29. Kovalevsky G, Gracia CR, Berlin JA, Sammel MD, Barnhart KT. Evaluation of the association between hereditary thrombophilias and recurrent pregnancy loss: a meta-analysis. *Arch Intern Med.* 2004;164(5):558-63.
30. Liu X, Chen Y, Ye C, et al. Hereditary thrombophilia and recurrent pregnancy loss: a systematic review and meta-analysis. *Hum Reprod.* 2021;36(5):1213-1229.
31. Baumann K, Beuter-Winkler P, Hackethal A, Strowitzki T, Toth B, Bohlmann MK. Maternal factor V Leiden and prothrombin mutations do not seem to contribute to the occurrence of two or more than two consecutive miscarriages in Caucasian patients. *Am J Reprod Immunol.* 2013;70(6):518-21.
32. Vomstein K, Herzog A, Voss P, et al. Recurrent miscarriage is not associated with a higher prevalence of inherited and acquired thrombophilia. *Am J Reprod Immunol.* 2021;85(1):e13327.
33. Shehata H, Ali A, Silva-Edge M, et al. Thrombophilia screening in women with recurrent first trimester miscarriage: is it time to stop testing? - a cohort study and systematic review of the literature. *BMJ Open.* 2022;12(7):e059519.
34. Quenby S, Booth K, Hiller L, et al. ALIFE2 Block Writing Committee; ALIFE2 Investigators. Heparin for women with recurrent miscarriage and inherited thrombophilia (ALIFE2): an international open-label, randomised controlled trial. *Lancet.* 2023;402(10395):54-61.
35. Karadeniz RS, Altay MM, Ensari Altun T, Erol AO, Özdoğan S, Haberal A. There is No Relationship Between the Number of Subsequent Pregnancy Losses and Thrombophilic Factors. *Turkiye Klinikleri J Med Sci.* 2012;32(2):376-81.
36. Kovalak EE, Karabay Akgül Ö, Kurtuluş Aksoy N, Hayırhoğlu N, Kaya E. The Relationship Between the Number of Miscarriages and Diagnostic Parameters in Couples with Recurrent Pregnancy Loss: A Retrospective Cohort Study. *J Clin Obstet Gynecol.* 2023;33(3):143-150.

Research Article

COMPARISON OF RADIOFREQUENCY THERMOCOAGULATION AT HIGH TEMPERATURES WITH COMBINED RADIOFREQUENCY THERMOCOAGULATION AND PULSED RADIOFREQUENCY IN TRIGEMINAL NEURALGIA

 Esra ERTILAV ¹,  Öznur YILDIRIM ²,  Osman Nuri AYDIN ³

¹ Department of Neurology (Algology), Medical Faculty, Adnan Menderes University, Aydin, Turkey

² Department of Neurology (Algology), Medical Faculty, Adnan Menderes University, Aydin, Turkey

³ Department of Anesthesiology (Algology), Medical Faculty, Adnan Menderes University, Aydin, Turkey

*Correspondence: eertilav@gmail.com

ABSTRACT

Objective: The aim of this study was to compare the Radiofrequency Thermocoagulation (RFT) applied at high temperatures and RFT combined Pulsed Radiofrequency (PRF) to improve the efficacy in trigeminal neuralgia.

Materials and Methods: Demographic, clinical examination findings and VAS scores of the patients who underwent combined RFT + PRF and RFT for trigeminal neuralgia in the Algology clinic between May 2014 and March 2022 were recorded before the procedure and evaluated at 1 month, 12 months and 24 months after the procedure.

Results: The results of 43 patients (24 females, 19 males) were evaluated in 2 groups according to whether 20 patients underwent high-temperature RFT and 23 patients underwent PRF+ high-temperature RFT. At 1 month, 12 months and 24 months post-procedure follow-up, VAS scores were significantly lower in both groups compared to pre-procedure ($p<0.001$, $p<0.001$, respectively). The duration of pain control was 25.8 ± 4.8 months in the RFT group and 25 ± 3.4 months in the PRF+RFT group ($p=0.5$). At 24 months follow-up, recurrence was observed in 3 patients (2 patients in RFT group, 1 patient in PRF+RFT group) ($p=0.5$). Complications (masseter atony and dermatomal hypoesthesia) occurred in 10 patients in the RFT group and 5 patients in the PRF+RFT group ($p=0.052$). The mean time to resolution of complications was 75 ± 35.61 days in the RFT group and 40 ± 18.17 days in the RFT+PRF group ($p=0.04$). No irreversible complication was recorded in any patient.

Conclusion: PRF combined with RFT at high temperatures is an appropriate treatment option to prevent complications and shorten the regression time to side effects.

Keywords: Trigeminal neuralgia, radiofrequency ablation, pulse radiofrequency

Received: 22 November 2024

Revised: 15 January 2025

Accepted: 04 February 2025

Published: 20 March 2025



Copyright: © 2025 by the authors. Published by Aydın Adnan Menderes University, Faculty of Medicine and Faculty of Dentistry. This article is openly accessible under the Creative Commons Attribution-NonCommercial 4.0 International (CC BY-NC 4.0) License.

INTRODUCTION

Trigeminal neuralgia (TN) is characterized by transient, electric shock-like pain symptoms. Due to the severity of pain, patients' daily activities are significantly affected, and their quality of life is diminished. Surgical methods such as microvascular decompression and Gamma Knife radiosurgery can be applied in patients who cannot achieve adequate pain control through medical treatment or who cannot tolerate the side effects of medications. Less invasive percutaneous methods such as radiofrequency application, pulsed radiofrequency (PRF), and percutaneous balloon compression are preferred for patients who are unwilling or unsuitable for surgery (1). Gasserian ganglion RFT is a highly effective treatment for TN, with immediate pain relief achieved in 90-100% of cases (2). Comparative studies suggest that combined RFT and PRF treatment is more effective (3). In addition, some studies propose that combined RFT+PRF application reduces side effects, despite showing no difference in efficacy (4). There is no standardized protocol for temperature regulation in RFT. High-temperature RFT is often chosen to reduce the recurrence rate of TN; however, higher temperatures are associated with an increased risk of serious complications. In this study, we compared high-temperature (85°C) RFT with combined high-temperature (85°C) RFT+PRF for TN, focusing on efficacy duration, recurrence, and safety, based on 24-month follow-up results.

MATERIALS AND METHODS

The study employed a comparative retrospective design by collecting and analyzing data from patients who underwent high-temperature (85°C) RFT and combined high-temperature (85°C) RFT + PRF for TN.

Ethical approval was obtained from the Clinical Research Ethics Committee (2024/76, 527865). This study was conducted in accordance with the Declaration of Helsinki. Written informed consent was obtained from all patients. Demographic and clinical examination data, including gender, age, distribution of involved nerves, side, medications used, and VAS scores, were collected from patients who underwent combined RFT + PRF and RFT for TN in the Algology clinic between May 2014 and March 2022. Visual Analog Scale (VAS) pain scores, clinical and neurological examination results, pain control duration, recurrence, and complications were recorded 24 months post-procedure.

Primary endpoint

Patients who underwent combined PRF+ high temperature RFT with high temperature RFT in TN were evaluated for pain control time and recurrence with long-term follow-up.

Secondary endpoint

Patients who underwent combined PRF+ high temperature RFT with high temperature RFT in TN were evaluated with long-term follow-up for complications.

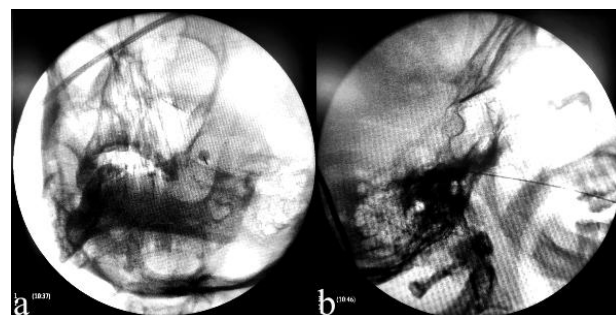


Figure 1. (a) Fluoroscopic image of cannula positioned in the foramen oval in oblique position (b) Fluoroscopic image of the cannula positioned in the foramen oval in lateral position

Interventional Procedure (RFT, RFT and PRF)

patient was taken to the operating room in the supine position. The patient was administered intravenous fentanyl (1 µg/kg), midazolam (0.05 mg/kg) as mild sedation, provided he was awake enough to respond to the test with electrical stimulation. In fluoroscopy, oblique projection was angled to approximately 15 degrees lateral to approximately 30 degrees to caudal, and foramen ovale was seen in the upper inner quadrant. The entry point was 2 to 3 cm side of the commissura labialis directed towards the pupil when viewed from the front of the face. 10 cm long 10 mm active tip radiofrequency cannula was inserted into the foramen ovale as a tunnel vision (Figure 1a), fluoroscopy was taken laterally, and the cannula entered into the bone tunnel of the foramen ovale (Figure 1b). The direction of the needle was verified in submental, lateral and Posterior-anterior view under fluoroscopy so that the tip of the cannula does not exceed 2 mm from the Clivus plane. Sensory and motor stimuli were given before radiofrequency. Paresthesia was taken in the appropriate dermatome area at 0.1- 0.5 V and 50 Hz at appropriate localization for sensorial stimulation. Masseter contraction was observed by stimulating 0.1 to 1.5 V at 2 Hz for the mandibular branch for motor stimulation.

In the combined PRF+high temperature RFT group, after the placement of the cannula in the foramen ovale and the completion of sensory and motor stimulation, PRF was first applied at 42°C for 240 seconds. After PRF, RFT was applied after the patient provided deep sedation with either midazolam, fentanyl and propofol (0.5mg/kg). RFT was performed at 85 °C for 60 seconds.

In high temperature RFT group after the placement of the cannula in the foramen ovale and the completion of sensory and motor stimulation, patient provided deep sedation with either midazolam, fentanyl and propofol (0.5mg/kg). RFT was performed at 85 °C for 60 seconds. The patient was observed for 24 hours after the procedure for side effects.

Statistical Analyses

The research data were evaluated using the SPSS 21.0 statistical program. The conformity of continuous variables to normal distribution was investigated using visual (histogram and probability graphs) and analytical methods (Kolmogorov-Smirnov/Shapiro-Wilk tests). Descriptive statistics of the study were summarized using number (n), percentage (%), mean, standard deviation

Table 1. Comparison of demographic and clinical characteristics of the groups

	RFT (n=20)	RFT+PRF (n=23)	P
Age			
Mean±SD	65.2±11.19	65.91±12.38	
Median (min-max)	65 (43-82)	65(42-86)	0.845*
Gender			
Female	8(40)	16(69.6)	0.052
Male	12(60)	7(30.4)	
Semptom Duration (year)			
Mean±SD	8.1±7.49	9.13±7.76	
Median (min-max)	6.5 (1-30)	6(1-30)	0.651**
Side			
Left	9(45)	10(43.5)	0.92
Right	11(55)	13(56.5)	
Segment			
V2	8(40)	3(13)	0.029
V3	8(40)	11(47.8)	
V1+V2	2(10)	0(0)	
V2+V3	2(10)	9(39.2)	
Drug used			
Gabapenti noid	2(10)	2(8.7)	0.959
Carbamaz epine	7(35)	9(39.1)	
Combined	11(55)	12(52.2)	

*Parametric test **Non parametric test

(SD), median, minimum and maximum. Chi-Square Test was used to show whether there was a difference between categorical variables in the study. The Student-t Test was used to compare the parametric properties of continuous variables in independent groups, the Mann Whitney U Test was used to compare the non-parametric properties of continuous variables in independent groups, and the Wilcoxon Test or Friedman Test was used to compare the non-parametric properties of continuous variables in dependent groups. For statistical significance, a p-value lower than 0.05 was set.

RESULTS

Table 2. Comparison of VAS scores of both groups before and after the procedure at 1st month, 12th month and 24th month

	RFT (n=20)	RFT+PRF (n=23)	p value
VAS (0)			
Mean±SD	7.25±1.45	7.57±0.9	0.543*
Median (min-max)	7 (3-9)	8 (6-9)	
VAS (1)			
Mean±SD	2.05±1.19	2.22±1.31	0.706*
Median (min-max)	2 (0-4)	2 (0-5)	
VAS (12)			
Mean±SD	2.2±1.15	2.09±1.38	0.516*
Median (min-max)	2(0-4)	2(0-6)	
VAS (24)			
Mean±SD	2.75±1.33	2.7±1.64	0.687*
Median (min-max)	2.5(1-6)	2(1-8)	
p value	<0.001 ^{*1,2,3}		<0.001 ^{*1,2,3}

1 There is a statistically significant difference between VAS 0-VAS 1;
2 There is a statistically significant difference between VAS 0-VAS 12;
3 There is a statistically significant difference between VAS 0-VAS 24;
*Non parametric test

The clinical and demographic characteristics of the groups were similar and are shown in the table (Table 1). The results of 43 patients (24 females, 19 males) were evaluated in 2 groups according to whether 20 patients underwent high-temperature RFT and 23 patients underwent PRF+high temperature RFT. VAS scores were significantly lower in both groups compared to the pre-procedure period at 1 month, 12 months and 24 months after the procedure (p<0.001, p<0.001, respectively)(Table 2).

Table 3. Comparison of recurrence and pain relief duration of the groups

	RFT (n=20)	RFT+PRF (n=23)	P	
Recurrence				
(-)	18(90)	22(95.7)	0.59	
(+)	2(10)	1(4.3)		
Pain relief duration	Mean±SD	25.8±4.8	25.04±3.4	0.553*

*Non parametric test

The mean duration of pain control was 25.8±4.8 months in the RFT group and 25±3.4 months in the PRF+RFT group (p=0.5)(Table 3). At 24 months follow-up, 3 patients (2 patients (10%) RFT group, 1 patient (4.3%) PRF+RFT group) recurrence was observed (p=0.5)(Table 3). Complications (masseter atony and dermatomal hypoesthesia) were observed in 10 patients in RFT group and 5 patients in PRF+RFT group. There was no significant difference between the two groups in terms of complications (p=0.052) (Table 4). The mean time to resolution of complications was 75±35.61 days in the RFT group and 40±18.17 days in the RFT+PRF group (p=0.04) (Table 4). No irreversible complication was recorded in any patient.

Table 4. Evaluation of complication development and complication regression duration of the groups

	RFT (n=20)	RFT+PRF (n=23)	P
Complication			
(-)	10(50)	18(78.3)	0.052
(+)	10(50)	5(21.7)	
Complication type			
Masseter atoni	4(40)	1(25)	0.615
Hypoesthesia	6(60)	4(75)	
Complication relief duration			
Mean±SD	75±35.61	40±18.17	0.04*
Median(min-max)	75(15-120)	37.5(15-60)	

*Parametric test

CONCLUSION

The temperature for RFT treatment varies widely (60°C to 95°C), but there is no standardized temperature. High-temperature RFT is used to enhance procedural efficacy and reduce recurrence rates. However, complications such as severe facial numbness, ptosis, keratitis, diplopia, mandibular deviation, and weakness of the masticatory muscles have been reported with high-temperature RFT ($\geq 75^\circ\text{C}$). A recent review evaluated the long-term efficacy and complications of RFT at different temperatures (5). The studies concluded that while the long-term analgesic effects of high-temperature RFT were not superior to those of relatively lower-temperature RFT, the risk of complications increased with temperature (6,7). These studies primarily assessed pain relief percentages but did not evaluate pain control duration or recurrence rates. Some studies have examined recurrence rates to evaluate the efficacy of high-temperature RFT for trigeminal neuralgia. Fraioli et al. reported a mean pain-

free period of 8.8 years after RFT at 90–95°C for 10 minutes in 129 patients with trigeminal neuralgia. The recurrence rate was 7.8%, with a follow-up period of 11.6 years (8). Kosugi et al. observed that RFT at 90°C in patients with V2 and/or V3 branch involvement resulted in 1-year and 2-year pain-free rates of 40.5–80.2% and 17.1–54.9%, respectively (9). In this study, we evaluated the efficacy of high-temperature RFT in terms of pain regression rates, pain control duration, and recurrence. The mean duration of pain palliation was 25.8 months for RFT and 25 months for combined RFT + PRF. Our findings indicate that RFT + PRF treatment demonstrated equivalent efficacy in both short- and long-term follow-ups. The mean pain control duration was 25 months, with 24-month pain-free rates of 90% and 95.7%. Unlike previous studies, our long-term pain-free rates were higher, suggesting that our high-temperature RFT application was associated with a longer duration of efficacy.

Higher temperatures are associated with increased complications, with facial numbness and masticatory weakness being the most commonly observed after RFT. Short-term facial numbness incidence after RFT treatment is reported to range from 85% to 100%, typically resolving within one month (10,11). Masticatory muscle weakness, commonly associated with the V3 branch, occurs at temperatures $\geq 65^\circ\text{C}$. Recovery time is approximately six months at $\leq 68^\circ\text{C}$ (12) but extends to over one year at 75°C (13). In our study, complications were observed in 10 patients (50%) in the RFT group and 5 patients (21.7%) in the RFT + PRF group. While high temperatures are linked to higher complication rates, we found no irreversible complications in our cohort. The regression time of complications averaged 75 days in the RFT group and 40 days in the RFT + PRF group, demonstrating significantly shorter recovery times in the combined RFT+PRF group. Zhao et al. evaluated 80 patients undergoing combined RFT (70°C and 75°C) and PRF treatment of the Gasserian ganglion under computed tomography guidance (14). They found no significant differences in pain control, but sensory loss, masticatory weakness, and decreased corneal reflex improved more rapidly in the combined group. These findings suggest that, compared to the use of RFT alone, combining PRF with RFT may benefit trigeminal neuralgia treatment by reducing complications.

In a prospective study, Yao et al. concluded that combined PRF and RFT application to the V1 branch in 56 patients reduced corneal hypoesthesia rates, shortened recovery times and decreased recurrence rates, while maintaining efficacy comparable to RFT alone (15). Elawamy et al.

analyzed 43 patients in 3 groups and concluded that combined application of PRF and RFT may reduce RFT-related complications (16). In line with these findings, our study showed that PRF treatment did not potentiate the efficacy of RFT but contributed to the regression process of side effects and side labels that may occur. We propose that the early resolution of complications associated with high-temperature RFT, applied to increase efficacy and reduce recurrence, is attributable to the adjunctive PRF application.

The limitations of our study include the small sample size and retrospective design. Prospective controlled studies will guide our current findings. Prospective, controlled studies are needed to validate our findings. Other major limitations include the absence of neuropathic pain scale records and functional outcome scores.

ACKNOWLEDGMENTS

Thanks to all contributing authors.

AUTHORSHIP CONTRIBUTIONS

Study conception and design: EE, OY, ONA; Data collection: OY; Analysis and interpretation of results: OY, EE; Draft manuscript preparation: EE, ONA ;Critical revision of the article: EE, ONA ;All authors (OY, EE, ONA) reviewed the results and approved the final version of the manuscript

DATA AVAILABILITY STATEMENT

data is available for use.

DECLARATION OF COMPETING INTEREST

Authors have no conflict of interest.

ETHICS

Clinical Research Ethics Committee approval was obtained (2024/76, 527865).

FUNDING

No funding.

REFERENCES

1. Asplund P, Blomstedt P, Bergenheim AT. Percutaneous Balloon Compression vs Percutaneous Retrogasserian Glycerol Rhizotomy for the Primary Treatment of Trigeminal Neuralgia. *Neurosurgery*. 2016

Mar;78(3):421-8; discussion 428. doi: 10.1227/NEU.0000000000001059.

2. Kanpolat Y, Savas A, Bekar A, Berk C. Percutaneous controlled radiofrequency trigeminal rhizotomy for the treatment of idiopathic trigeminal neuralgia: 25-year experience with 1,600 patients. *Neurosurgery*. 2001 Mar;48(3):524-32; discussion 532-4. doi: 10.1097/00006123-200103000-00013.

3. Ding Y, Li H, Hong T, Zhu Y, Yao P, Zhou G. Combination of Pulsed Radiofrequency with Continuous Radiofrequency Thermocoagulation at Low Temperature Improves Efficacy and Safety in V2/V3 Primary Trigeminal Neuralgia. *Pain Physician*. 2018 Sep;21(5):E545-E553.

4. Arıcı T, Kurcaloğlu M, Kılıç E, Erhan E. Radiofrequency thermocoagulation combined with pulsed radiofrequency for gasserian ganglion blockage. *Agri*. 2018 Oct;30(4):179-182. doi: 10.5505/agri.2018.88261.

5. Hong T, Ding Y, Yao P. Long-Term Efficacy and Complications of Radiofrequency Thermocoagulation at Different Temperatures for the Treatment of Trigeminal Neuralgia. *Biochem Res Int*. 2020 Mar 4;2020:3854284. doi: 10.1155/2020/3854284.

6. Tang YZ, Yang LQ, Yue JN, Wang XP, He LL, Ni JX. The optimal radiofrequency temperature in radiofrequency thermocoagulation for idiopathic trigeminal neuralgia: A cohort study. *Medicine (Baltimore)*. 2016 Jul;95(28):e4103. doi: 10.1097/MD.0000000000004103.

7. Yang JT, Lin M, Lee MH, Weng HH, Liao HH. Percutaneous trigeminal nerve radiofrequency rhizotomy guided by computerized tomography with three-dimensional image reconstruction. *Chang Gung Med J*. 2010 Nov-Dec;33(6):679-83.

8. Fraioli MF, Cristino B, Moschettoni L, Cacciotti G, Fraioli C. Validity of percutaneous controlled radiofrequency thermocoagulation in the treatment of isolated third division trigeminal neuralgia. *Surg Neurol*. 2009 Feb;71(2):180-3. doi: 10.1016/j.surneu.2007.09.024.

9. Kosugi S, Shiotani M, Otsuka Y, Suzuki T, Katori N, Hashiguchi S, Morisaki H. Long-term outcomes of percutaneous radiofrequency thermocoagulation of gasserian ganglion for 2nd- and multiple-division trigeminal neuralgia. *Pain Pract.* 2015 Mar;15(3):223-8. doi: 10.1111/papr.12163.
10. Zheng S, Wu B, Zhao Y, Wang X, Li X, Yang L, He M, Yue J, Ni J. Masticatory Muscles Dysfunction after CT-guided Percutaneous Trigeminal Radiofrequency Thermocoagulation for Trigeminal Neuralgia: A Detailed Analysis. *Pain Pract.* 2015 Nov;15(8):712-9. doi: 10.1111/papr.12247.
11. Fouad, W. Management of trigeminal neuralgia by radiofrequency thermocoagulation. *Alexandria Journal of Medicine.* 2011; 47(1), 79–86. <https://doi.org/10.1016/j.ajme.2011.02.001>
12. Koning MV, Koning NJ, Koning HM, van Kleef M. Relationship between Sensory Stimulation and Side Effects in Percutaneous Radiofrequency Treatment of the Trigeminal Ganglion. *Pain Pract.* 2014 Sep;14(7):581-7. doi: 10.1111/papr.12124.
13. Yao P, Deng YY, Hong T, Wang ZB, Ma JM, Zhu YQ, Li HX, Ding YY, Pan SN. Radiofrequency thermocoagulation for V2/V3 idiopathic trigeminal neuralgia: effect of treatment temperatures on long-term clinical outcomes: A Cohort Study. *Medicine (Baltimore).* 2016 Jun;95(26):e4019. doi: 10.1097/MD.0000000000004019.
14. Zhao WX, Wang Q, He MW, Yang LQ, Wu BS, Ni JX. Radiofrequency thermocoagulation combined with pulsed radiofrequency helps relieve postoperative complications of trigeminal neuralgia. *Genet Mol Res.* 2015 Jul 13;14(3):7616-23. doi: 10.4238/2015.July.13.5.
15. Yao P, Hong T, Zhu YQ, Li HX, Wang ZB, Ding YY, Ma JM, Pan SN. Efficacy and safety of continuous radiofrequency thermocoagulation plus pulsed radiofrequency for treatment of V1 trigeminal neuralgia: A prospective cohort study. *Medicine (Baltimore).* 2016 Nov;95(44):e5247. doi: 10.1097/MD.0000000000005247. PMID: 27858881; PMCID: PMC5591129.
16. Elawamy A, Abdalla EEM, Shehata GA. Effects of Pulsed Versus Conventional Versus Combined Radiofrequency for the Treatment of Trigeminal Neuralgia: A Prospective Study. *Pain Physician.* 2017 Sep;20(6):E873-E881. PMID: 28934792.

Research Article

FACTORS LEADING TO ELEVATED CARDIAC BIOMARKERS IN SEVERE COMMUNITY-ACQUIRED PNEUMONIA

 Betül DUMANLI ¹,  Onur YAZICI ^{2*},  Fisun KARADAĞ ²

¹Düzce Atatürk State Hospital, Department of Chest Diseases, Düzce, Turkey

²Aydın Adnan Menderes University Faculty of Medicine, Department of Chest Diseases, Aydın, Turkey

*Correspondence: dronur_yazici@hotmail.com

ABSTRACT

Objective: Community-acquired pneumonia (CAP) is a significant public health issue with high morbidity and mortality rates. This study aims to evaluate the risk factors contributing to the increase in cardiac biomarkers in patients with severe CAP.

Materials and Methods: The study has a retrospective and cross-sectional design. A total of 70 patients diagnosed with CAP and followed in the Pulmonology Department and Intensive Care Unit of Aydın Adnan Menderes University between September 2015 and February 2020 were included in the study. Demographic data, comorbidities, vital signs, laboratory results, and cardiac biomarker levels (troponin, Pro-BNP, CK-MB) were recorded in detail, and comparisons were made between subgroups.

Results: Of the patients, 68.6% were male, with a mean age of 73.05 ± 13.77 years. At least one comorbidity was present in 92.8% of the patients, with hypertension, COPD, and diabetes mellitus being the most frequently observed. CK-MB levels showed significant positive correlations with CURB-65 and Pneumonia Severity Index (PSI) scores. Troponin levels were significantly elevated in patients with impaired consciousness, Pro-BNP levels in those who developed arrhythmias, and CK-MB levels in patients with COPD. Additionally, LDH levels correlated positively with both troponin and Pro-BNP levels.

Conclusion: This study highlights the importance of evaluating cardiac biomarkers in patients with severe CAP. Elevated levels of troponin, Pro-BNP, and CK-MB are reflective of increased cardiovascular risk and infection severity. These findings underscore the need for early and thorough monitoring of these biomarkers to identify and manage potential complications effectively, thereby improving patient outcomes.

Keywords: Cardiac biomarkers, CK-MB, Community-acquired pneumonia, CURB-65, Troponin, Pro-BNP, PSI.

Received: 13 January 2025

Revised: 09 February 2025

Accepted: 10 February 2025

Published: 20 March 2025



Copyright: © 2025 by the authors. Published by Aydın Adnan Menderes University, Faculty of Medicine and Faculty of Dentistry. This article is openly accessible under the Creative Commons Attribution-NonCommercial 4.0 International (CC BY-NC 4.0) License.

INTRODUCTION

Community-acquired pneumonia (CAP) is defined as pneumonia that develops in individuals without a known immunodeficiency during their daily life (1). Despite advancements in vaccination policies and antibiotic treatments, CAP remains a significant public health concern with high morbidity and mortality rates (2,3). Scoring systems such as the Pneumonia Severity Index (PSI) and CURB-65 are widely used to assess disease severity, guide hospitalization decisions, and predict mortality in these patients (4). While PSI evaluates 20 variables related to the patient, CURB-65 is a more practical assessment tool that includes five parameters: age, blood urea nitrogen (BUN), respiratory rate, altered mental status, and systolic blood pressure (5,6). Patients with a PSI class IV or V or a CURB-65 score ≥ 2 are generally recommended for inpatient treatment. Although pneumonia-related mortality is a major concern, cardiovascular complications such as myocardial infarction, arrhythmias, and acute heart failure significantly contribute to adverse outcomes in these patients (7). Studies have shown that elevated levels of cardiac biomarkers, particularly cardiac troponins (cTn) and B-type natriuretic peptide (BNP), are associated with increased mortality in patients with CAP, independent of preexisting coronary artery disease (8–10). Elevated cardiac troponins, including high-sensitivity troponin T (cTnT) and troponin I (cTnI), have been identified as strong predictors of both short- and long-term mortality in hospitalized CAP patients, potentially reflecting acute myocardial stress or direct cardiac injury due to systemic inflammation (8,9). Similarly, BNP levels have been found to correlate with pneumonia severity, pulmonary hypertension, and cardiac dysfunction, further aiding in risk stratification (10). Given the increasing recognition of cardiovascular complications in CAP patients, understanding the factors contributing to cardiac biomarker elevation is crucial for improving risk assessment and patient management. This study aims to investigate the risk factors contributing to the elevation of cardiac biomarkers in patients with severe community-acquired pneumonia.

MATERIALS AND METHODS

This study has a retrospective and cross-sectional design. A total of 70 patients diagnosed with community-acquired pneumonia, who were followed in the Pulmonology Department or Intensive Care Unit of Aydın Adnan Menderes University between September 2015 and February 2020, were included in the study. Community-acquired pneumonia (CAP) was defined as pneumonia

acquired outside of a healthcare setting in individuals without recent hospitalization or significant immunosuppression (1). The diagnosis of CAP was based on clinical symptoms, including fever, cough, sputum production, and dyspnea, along with radiological findings such as new pulmonary infiltrates observed on chest X-ray or computed tomography, and laboratory markers indicative of infection, in accordance with established clinical guidelines (11). Immunosuppression was defined as a condition or treatment that significantly compromises immune function. This included patients with HIV infection and a CD4 count below 200/mm³, those who had undergone solid organ or hematopoietic stem cell transplantation, individuals with active malignancy receiving chemotherapy or radiotherapy, and those on long-term immunosuppressive therapy. Immunosuppressive treatments were considered to include corticosteroids at a dose of 20 mg per day or more for longer than two weeks, biologic agents, or disease-modifying antirheumatic drugs (12). Patients with a history of hospitalization or antibiotic use within the 14 days prior to admission, those with another focus of infection, and immunosuppressed patients were excluded.

The demographic characteristics of the patients (age, gender, smoking history), known comorbidities, vital signs at admission (temperature, level of consciousness, blood pressure, heart rate, respiratory rate), blood gas analyses [partial carbon dioxide pressure (pCO₂), partial oxygen pressure (pO₂), oxygen saturation (SaO₂), and pH], complete blood count parameters (hemoglobin, hematocrit, neutrophils, lymphocytes, platelets), and biochemistry results (sodium, albumin, lactate dehydrogenase, urea) were recorded in detail. Additionally, troponin-I, CK-MB, pro-BNP, CRP, procalcitonin, and D-dimer levels were also analyzed.

The cases included in the study were divided into various subgroups, and cardiac biomarker levels were compared among these groups. The subgroups were defined according to the following criteria: CURB-65 score (2, 3, and 4); Pneumonia Severity Index (PSI) class (Group IV and Group V); level of consciousness (conscious and unconscious); comorbidity status [presence or absence of chronic obstructive pulmonary disease (COPD)]; and cardiovascular complication status (patients who developed complications within the first 7 days of hospitalization and those who did not).

This study was approved by the Non-Interventional Clinical Research Ethics Committee of Aydın Adnan Menderes University Faculty of Medicine with the decision dated April 27, 2020, and numbered 18.

Statistical analysis

Statistical evaluation was performed using SPSS software (SPSS 23, IBM Corp. Released 2015. IBM SPSS Statistics for Windows, Version 23.0, Armonk, NY, USA). Categorical variables were expressed as numbers and percentages. The conformity of variables to a normal distribution was determined using the Kolmogorov-Smirnov test. For continuous variables, the Student's t-test was used to compare two groups when normal distribution was observed, and the One-Way ANOVA test was applied for comparisons involving more than two groups. For variables not following a normal distribution, the Mann-Whitney U test was used for two-group comparisons, and the Kruskal-Wallis variance analysis was applied for comparisons of more than two groups. Continuous variables not following a normal distribution were presented as medians (25th–75th percentiles), while those with a normal distribution were expressed as mean \pm standard deviation. The relationships between categorical variables were evaluated using Pearson's chi-square test and Fisher's exact test. Spearman and Pearson correlation analyses were used to analyze relationships between variables. A p-value of <0.05 was considered statistically significant.

RESULTS

A total of 70 patients diagnosed with community-acquired pneumonia, followed in the ward or intensive care unit between September 2015 and February 2020, were included in the study. Of the patients, 68.6% (n=48) were male, and 31.4% (n=22) were female. The age range varied from 40 to 97 years, with a mean age of 73.05 ± 13.77 years. Among the patients, 68.6% (n=48) were either active smokers or former smokers (ex-smokers), while 31.4% (n=22) had never smoked. At least one comorbidity was identified in 92.8% (n=65) of the patients. The most common comorbidities were hypertension (44.3%, n=31), COPD (35.7%, n=25), and diabetes mellitus (25.7%, n=18). Among patients with a history of cardiovascular disease, 44.3% (n=31) had hypertension, 24.3% (n=17) had coronary artery disease, 15.7% (n=11) had congestive heart failure, 8.6% (n=6) had arrhythmia, and 1.4% (n=1) had a history of myocardial infarction (MI). The demographic characteristics and comorbidity distribution of the patients are presented in Table 1.

According to the vital signs assessed at the time of hospitalization, the majority of the patients were conscious (91.4%). In the evaluation of body temperature, 48.6% of the patients had a normal temperature, while 27.1% were febrile ($>38^{\circ}\text{C}$). Blood pressure measurements revealed normal values in 62.9% of the patients, hypotension

($<90/60$ mmHg) in 8.6%, and hypertension ($>140/90$ mmHg) in 28.6%. Tachycardia (>100 bpm) was observed in 45.8% of the patients. Detailed vital signs of the patients are presented in Table 2.

Table 1. Demographic characteristics and comorbidities of patients

Age, Mean \pm SD	73.05 \pm 13.77
Gender n (%)	
Female	22 (31.4)
Male	48 (68.6)
Smoking status n (%)	
Smoker	48 (68.6)
Non-Smoker	22 (31)
Cardiovascular Comorbidity n (%)	
Present	45 (64.2)
Absent	25 (35.7)
Hypertension n (%)	
Present	31 (44.3)
Absent	39 (55.7)
Arrhythmia n (%)	
Present	6 (8.6)
Absent	64 (91.4)
Coronary Artery Disease n (%)	
Present	17 (24.3)
Absent	53 (75.7)
History of Myocardial Infarction n (%)	
Present	1 (1.4)
Absent	69 (98.6)
Congestive Heart Failure n (%)	
Present	11 (15.7)
Absent	59 (84.2)
Non-Cardiovascular Comorbidity n (%)	
Present	58 (82.9)
Absent	12 (17.1)

Table 2. Vital signs of patients

	n	%
Consciousness	Normal	64 91.4
	Impaired	6 8.6
Fever ($^{\circ}\text{C}$)	Normal	349 48.6
	Subfebrile (37.2°C - 38°C)	17 24.3
	Febrile (>38)	19 27.1
Blood Pressure (mmHg)	Normal	44 62.9
	Hypotensive ($<90/60$ mmHg)	6 8.6
	Hypertensive ($>140/90$ mmHg)	20 28.6
Pulse (/min)	Bradycardia (<60)	2 2.9
	Normal (60-100)	36 51.4
	Tachycardia (>100)	32 45.8
Tachypnea (/min)	Present (RR >24 /min)	5 7.1
	Absent	65 92.9

RR: Respiratory Rate, mmHg: Millimeters of Mercury, /min: Per Minute

Laboratory results showed that the median urea level was 52.5 mg/dL (25th–75th percentile: 38.0–68.0). Among inflammatory markers, the mean CRP level was 168.98 ± 91.01 mg/L, and the median procalcitonin level was 0.60 ng/mL (25th–75th percentile: 0.21–4.82). In the blood gas analysis, the median pH was 7.45 (25th–75th percentile: 7.39–7.47), and the mean oxygen saturation was 87.62 ± 5.52%. The mean PSI score, which assesses disease severity, was calculated as 116.73 ± 39.42, while the median CURB-65 score was 2.0 (25th–75th percentile: 1.0–2.0). Details of these parameters are presented in Table 3.

Table 3. Laboratory and clinical characteristics of patients

Urea, mg/dL median (25%-75%)	52.50 (38.0-68.0)
LDH, mg/dL median (25%-75%)	213.50 (186.25-300.75)
Albumin, mg/dL mean ± SD	3.10 ± 0.45
Sodium, mEq/L mean ± SD	136.54 ± 5.32
CRP, mg/L mean ± SD	168.98 ± 91.01
Procalcitonin, ng/mL median (25%-75%)	0.60 (0.21- 4.82)
D-Dimer, mg/L, mg/L median (25%-75%)	1609.0 (912.50-2620.00)
Neutrophil %, median (25%-75%)	87.00 (80.37-90.00)
Neutrophil count, 10 ³ /cells/μL (25%-75%)	12000 (7780.0-17097.50)
Lymphocyte %, median (25%-75%)	7.25 (4.150-10.925)
Lymphocyte count, cells/μL median (25%-75%)	955.0 (725.0-1420.0)
Platelet count, platelets/μL mean ± SD	265828.57 ± 1.01
pH, median (25%-75%)	7.450 (7.390-7.470)
PaO ₂ , mmHg median (25%-75%)	53.60 (49.00-60.00)
SpO ₂ , % mean ± SD	87.62 ± 5.516
PSI, mean ± SD	116.728 ± 39.424
CURB-65, median (25%-75%)	2.00 (1.00-2.00)

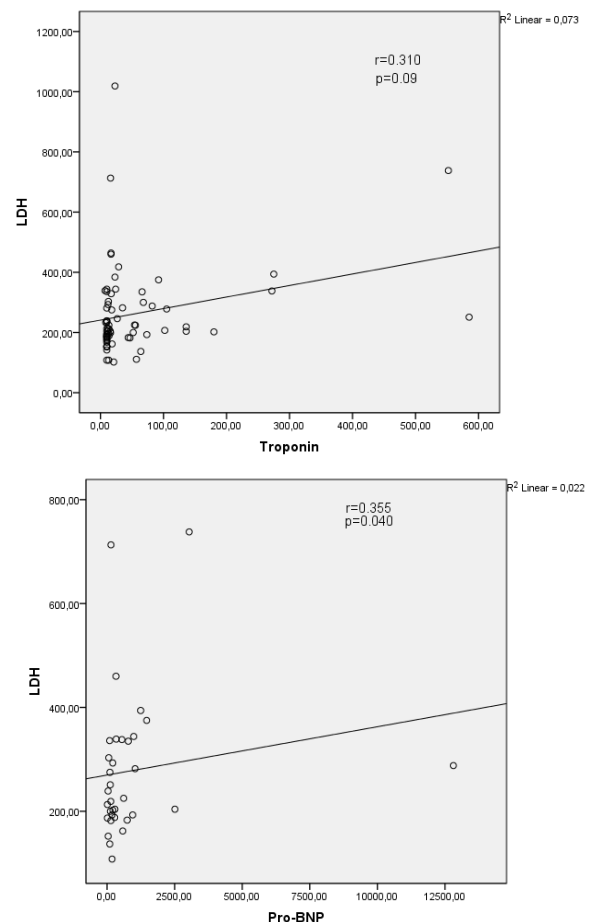
Continuous variables are presented as mean ± standard deviation or median (25th–75th percentiles), depending on their distribution. LDH: Lactate Dehydrogenase, CRP: C-Reactive Protein, PaO₂: Partial Pressure of Oxygen, SpO₂: Peripheral Capillary Oxygen Saturation, PSI: Pneumonia Severity Index, CURB-65: Confusion, Urea, Respiratory Rate, Blood Pressure, Age ≥65

Significant differences were observed in troponin, Pro-BNP, and CK-MB levels. Troponin levels were significantly higher in patients with impaired consciousness (median: 123.00 ng/L; 25th–75th percentile: 24.00–552.00) compared to those with normal consciousness (median: 13.45 ng/L; 25th–75th percentile: 10.00–45.40) ($p < 0.05$). Pro-BNP levels were significantly higher in patients who developed arrhythmias within 7 days (median: 784.00 ng/L; 25th–75th percentile: 549.00–985.00) compared to those without arrhythmias (median: 185.00 ng/L; 25th–75th percentile: 100.00–580.00) ($p = 0.011$). Similarly, CK-MB levels were significantly higher in patients with COPD (median: 2.20 ng/mL; 25th–75th

percentile: 1.05–3.95) compared to those without COPD (median: 1.05 ng/mL; 25th–75th percentile: 0.70–1.974) ($p = 0.031$). In the PSI-5 group, CK-MB levels (median: 1.80 ng/mL; 25th–75th percentile: 0.85–3.70) were significantly higher than those in the PSI-4 group (median: 1.10 ng/mL; 25th–75th percentile: 0.90–2.80) ($p = 0.038$). Details of these findings are presented in Table 4.

In our study, LDH levels were positively correlated with troponin levels ($r = 0.310$; $p = 0.09$) and Pro-BNP levels ($r = 0.355$; $p = 0.040$) (Figure 1). Additionally, CK-MB levels showed a significant negative correlation with lymphocyte count ($r = -0.303$; $p = 0.012$) and a significant positive correlation with the CURB-65 score ($r = 0.234$; $p = 0.012$) and the PSI score ($r = 0.250$; $p = 0.039$), which assess pneumonia severity (Figure 2).

Figure 1. Correlation Between LDH Levels and Troponin and Pro-BNP Levels



LDH: Lactate Dehydrogenase, Pro-BNP: Pro-Brain Natriuretic Peptide

Table 4. Comparison of Troponin, Pro-BNP, and CK-MB levels according to clinical parameters

Groups	n (%)	Troponin (ng/ml)	p	Pro-BNP (pg/mL)	p	CK-MB (IU/L)	p
COPD present	25 (35.7%)	12.00 (10.00-48.00)	0.166	234.00 (57.225-597.00)	0.234	2.20 (1.05-3.95)	0.031
COPD absent	45 (64.3%)	16.70 (10.00-65.00)		272.00 (132.500-1089.25)		1.05 (0.70-1.974)	
Conscious	64 (91.4%)	13.45 (10.00-45.40)	0.005	234.00 (73.450-581.00)	0.423	1.20 (0.80-2.30)	0.201
Unconscious	6 (8.6%)	123.00 (24.00-552.00)		272.00 (137.00-1038.00)		2.60 (1.10-4.20)	
Arrhythmia within 7 days	10 (14.3%)	30.35 (10.00-73.50)	0.347	784.00 (549.00-985.00)	0.011	1.95 (1.10-4.40)	0.133
No arrhythmia within 7 days	60 (85.7%)	13.55 (10.00-49.40)		185.00 (100.00-580.00)		1.20 (0.80-2.30)	
PSI 4	27 (38.6)	13.00 (10.00-26.60)	0.163	186.00 (100.45-891.50)	0.908	1.10 (0.90-2.80)	0.038
PSI 5	25 (35.7)	23.00 (10.00-77.75)		289.00 (119.00-784.00)		1.80 (0.85-3.70)	
CURB-65 2	34 (48.6)	16.50 (10.00%-54.75%)	0.566	313.50 (101.475%-975.675%)	0.950	1.20 (0.80%-2.425%)	0.067
CURB-65 3	11 (15.7)	12.00 (10.00%-272.00%)		211.00 (64.50%-1793.50%)		1.70 (1.075%-8.025%)	
CURB-65 4	4 (5.7)	59.00 (20.50%-151.50%)		213.00 (121.00%-784.00%)		3.45(2.175%-12.30%)	

Comparisons between groups were performed using Student's t-test or Mann-Whitney U test for two-group comparisons and One-Way ANOVA or Kruskal-Wallis test for multiple-group comparisons. COPD: Chronic Obstructive Pulmonary Disease, PSI: Pneumonia Severity Index, CURB-65: Confusion, Urea, Respiratory Rate, Blood Pressure, Age ≥ 65 . Note: Patients with a CURB-65 score of 1 and a PSI score lower than 4 or 5 were hospitalized due to hypoxemia.

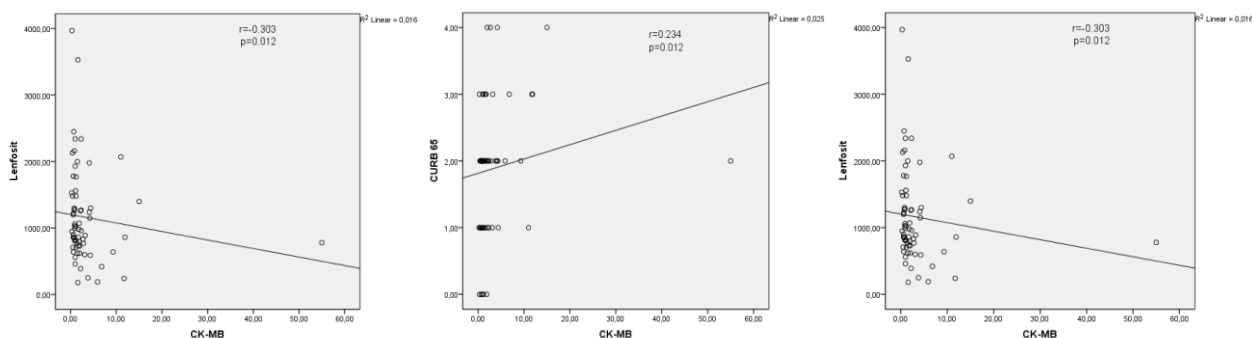


Figure 2. Correlation Between CK-MB Levels and Lymphocyte Count, CURB-65, and PSI Scores

CK-MB: Creatine Kinase-MB, CURB-65: Confusion, Urea, Respiratory Rate, Blood Pressure, Age ≥ 65 , PSI: Pneumonia Severity Index

DISCUSSION

CAP is a common infectious disease worldwide, with high morbidity and mortality rates. The incidence of cardiovascular complications is also increased in patients who develop pneumonia, and the development of cardiovascular complications during follow-up further elevates the risk of mortality (13-15). In our study, troponin levels were significantly elevated in patients with impaired consciousness and severe pneumonia. Impaired consciousness is considered a marker of severe infection and systemic inflammation and is often associated with multiple organ dysfunction (16,17). Proinflammatory cytokines released during infection can cause direct myocardial cell damage and increase stress on the heart (18). Additionally, hypoxia in patients with impaired consciousness and severe pneumonia may create an

environment where myocardial oxygen demand cannot be met, triggering subclinical myocardial ischemia (19). These patients often exhibit hemodynamic instability and increased sympathetic nervous system activity. This condition may increase the burden on the heart, contributing to elevated troponin levels (20,21). Therefore, impaired consciousness is an important indicator not only of the infection's severity but also of the risk of cardiovascular complications. Early evaluation of cardiac biomarkers in patients with impaired consciousness is critical for the prevention and management of cardiovascular complications. Our study suggests that troponin levels may serve as a marker of cardiovascular risk in this patient group and emphasizes the need for larger-scale, prospective studies to validate these findings.

In our study, baseline Pro-BNP levels were significantly elevated in patients who developed arrhythmias within 7 days after pneumonia. This finding suggests that Pro-BNP could be an important biomarker for the early prediction

of cardiovascular complications following pneumonia. Similarly, the study by Mendenez et al. demonstrated that baseline Pro-BNP levels were elevated in patients who developed cardiovascular events in the early period following pneumonia (14). This supports the prognostic value of Pro-BNP in cardiovascular risk assessment following infection. In a study conducted by Mojón-Álvarez et al. on COVID-19 patients, Pro-BNP levels were reported to be higher, particularly in those who developed myocardial damage or hemodynamic instability (22). This finding illustrates that increased systemic inflammation and hemodynamic stress during infection trigger Pro-BNP release. Our study further highlights that Pro-BNP is a valuable biomarker for detecting cardiovascular complications in the early period following infection. However, it should be noted that Pro-BNP levels vary across different patient populations and types of infections in the existing literature. Therefore, caution should be exercised in the clinical use and interpretation of Pro-BNP, and further studies are needed in diverse patient groups.

Although CK-MB is commonly used as a biomarker for myocardial damage, its sensitivity and specificity are known to be limited. The literature shows that CK-MB levels can also be elevated in conditions such as trauma, rhabdomyolysis, renal failure, and pulmonary infections (23-25). In the study by Fan et al., CK-MB levels were significantly elevated in patients with *Mycoplasma pneumoniae* pneumonia, and this was associated with the increased inflammatory response and myocardial stress during infection (26). Similarly, in Seedat et al.'s study, CK-MB levels were reported to increase due to inflammation and hypoxia in patients with severe pneumonia, and this increase was linked to cardiovascular complications (27). In our study, CK-MB levels were significantly higher in CAP patients with COPD compared to those without COPD. Additionally, a positive correlation was identified between CK-MB levels and CURB-65 and PSI scores. These findings suggest that CK-MB levels in severe pneumonia cases reflect not only myocardial damage but also the severity of the infection and the inflammatory response. The literature supports the results obtained in our study, indicating that CK-MB may be an important parameter for cardiovascular risk assessment in patients with severe pneumonia. However, it should be noted that the specificity of CK-MB is limited in clinical practice, and it should be evaluated in conjunction with other biomarkers.

LDH is an enzyme widely present in tissues and is considered a systemic marker of inflammation. In the study by Yamaguchi et al., LDH was found to represent myocardial damage and has prognostic value in acute

decompensated heart failure (28). In our study, a positive correlation was also identified between LDH and troponin and Pro-BNP levels. This finding suggests that LDH may assist in determining the risk of cardiac complications in pneumonia patients.

COPD is an independent risk factor for cardiovascular diseases, and elevated levels of Pro-BNP and troponin have been reported in these patients (29,30). In our study, CK-MB levels were found to be significantly higher in CAP patients with COPD; however, no significant differences were observed in troponin and Pro-BNP levels. This finding suggests that cardiac biomarkers should be carefully monitored in pneumonia patients with COPD and highlights the need for further studies in this patient group.

The retrospective design of our study and the limited number of patients are the primary limitations affecting the generalizability of these findings. Nevertheless, these results highlight the critical importance of carefully evaluating cardiac biomarkers in patients with severe pneumonia for the early detection and management of cardiovascular complications. It should be noted, however, that the specificity of biomarkers is limited in clinical practice, and they should be evaluated in conjunction with other clinical parameters. Validation of these findings through larger-scale, prospective studies will enhance the understanding and management of cardiovascular risks following infection.

CONCLUSION

Our study demonstrated that the increase in cardiac biomarker levels in patients with severe community-acquired pneumonia reflects both the severity of the infection and the risk of cardiovascular complications. The significantly elevated troponin levels in patients with impaired consciousness highlight the adverse cardiac effects of the systemic impacts of the infection. Furthermore, the prognostic value of Pro-BNP in predicting cardiovascular complications, such as arrhythmias, in the early stages has been emphasized. The positive correlation between CK-MB levels and both COPD patients and pneumonia severity scores (CURB-65 and PSI) suggests that CK-MB could serve as an indicator of infection severity and inflammation. The positive correlation between LDH levels and troponin and Pro-BNP underscores the need to consider LDH in understanding the cardiac effects of systemic inflammation.

Based on these findings, a structured approach for monitoring cardiac biomarkers in CAP patients may improve early risk stratification and guide clinical management.

- Patients with severe pneumonia (CURB-65 ≥ 2 , PSI class IV-V) and those with impaired consciousness or hemodynamic instability should undergo baseline troponin measurement at hospital admission.
- For patients with elevated troponin levels, follow-up measurements may be considered to assess trends and evaluate myocardial stress in collaboration with cardiology specialists.
- In patients at high risk for cardiovascular complications, Pro-BNP levels may serve as an adjunctive biomarker, particularly for predicting arrhythmias and hemodynamic instability.
- CK-MB and LDH levels, although less specific, could be considered complementary markers to further refine risk stratification.

Incorporating a biomarker-driven monitoring strategy into CAP management could facilitate early identification of high-risk patients and allow for timely cardiovascular interventions, potentially improving clinical outcomes. Future prospective studies should focus on validating this approach and assessing its impact on patient prognosis.

Acknowledgments

None.

Authorship contributions

Concept: B.D., O.Y., F.K., Design: O.Y., F.K., Data Collection or Processing: B.D., O.Y., Analysis or Interpretation: B.D., O.Y., Literature Search: B.D., O.Y., F.K., Writing: B.D., O.Y., F.K.

Data availability statement

The data that support the findings of this study are available from the corresponding author upon reasonable request.

Declaration of competing interest

The authors deny any conflicts of interest related to this study.

Ethics

The study was approved by the local Ethics Committee (approval no: 2022/18).

Funding

This work has not received any funding support.

REFERENCES

1. Acar A, Öncül O. Toplum kökenli pnömoniler. *Klinik Dergisi*. 2007;20(1):3–16.
2. Jain S, Self WH, Wunderink RG, Fakhran S, Balk R, Bramley AM, et al. Community-acquired pneumonia requiring hospitalization among US adults. *N Engl J Med*. 2015;373(5):415–27.
3. Wunderink RG, Waterer GW. Community-acquired pneumonia. *N Engl J Med*. 2014;370(6):543–51.
4. Shah BA, Ahmed W, Dhobi GN, Shah NN, Khursheed SQ, Haq I. Validity of pneumonia severity index and CURB-65 severity scoring systems in community-acquired pneumonia in an Indian setting. *Indian J Chest Dis Allied Sci*. 2010;52(1):9.
5. Aujesky D, Fine MJ. The pneumonia severity index: a decade after the initial derivation and validation. *Clin Infect Dis*. 2008;47(Suppl_3):S133–9.
6. Lim W, Van der Eerden M, Laing R, Boersma W, Karalus N, Town G, et al. Defining community-acquired pneumonia severity on presentation to hospital: an international derivation and validation study. *Thorax*. 2003;58(5):377–82.
7. Musher DM, Abers MS, Corrales-Medina VF. Pneumonia-related cardiac complications: development and impact. *Chest*. 2019;156(4):690–705. doi:10.1016/j.chest.2019.05.002.
8. Vestjens SMT, Spoorenberg SMC, Rijkers GT, Grutters JC, ten Berg JM, Noordzij PG, et al. High-sensitivity cardiac troponin T predicts mortality after hospitalization for community-acquired pneumonia. *Respirology*. 2017;22(6):1000–6. doi:10.1111/resp.12996.
9. Lee YJ, Lee H, Park J, Kim SJ, Cho YJ, Yoon HI, et al. Cardiac troponin I as a prognostic factor in critically ill pneumonia patients in the absence of acute coronary syndrome. *J Crit Care*. 2015;30(2):390–4. doi:10.1016/j.jcrr.2014.12.001.
10. Christ-Crain M, Breidthardt T, Stolz D, Zobrist K, Bingisser R, Miedinger D, et al. Use of B-type natriuretic peptide in the risk stratification of community-acquired pneumonia. *J Intern Med*. 2008;264(2):166–76. doi:10.1111/j.1365-2796.2008.01941.x.
11. Metlay JP, Waterer GW, Long AC, Anzueto A, Brozek J, Crothers K, et al. Diagnosis and treatment of adults with

- community-acquired pneumonia: an official clinical practice guideline of the American Thoracic Society and Infectious Diseases Society of America. *Am J Respir Crit Care Med.* 2019;200(7):e45-e67. doi:10.1164/rccm.201908-1581ST.
12. Cheng GS, Crothers K, Aliberti S, Bergeron A, Boeckh M, Chien JW, et al. Immunocompromised host pneumonia: definitions and diagnostic criteria: an official American Thoracic Society workshop report. *Ann Am Thorac Soc.* 2023;20(3):341-53. doi:10.1513/AnnalsATS.202212-1019ST.
13. Niederman MS, Mandell LA, Anzueto A, Bass JB, Broughton WA, Campbell GD, et al.; American Thoracic Society. Guidelines for the management of adults with community-acquired pneumonia. *Am J Respir Crit Care Med.* 2001;163(7):1730-54. doi:10.1164/ajrccm.163.7.at1010. PMID: 11401897.
14. Menéndez R, Méndez R, Aldás I, Reyes S, Gonzalez-Jimenez P, España PP, et al. Community-acquired pneumonia patients at risk for early and long-term cardiovascular events are identified by cardiac biomarkers. *Chest.* 2019;156(6):1080-91.
15. Violi F, Cangemi R, Falcone M, Taliani G, Pieralli F, Vannucchi V, et al.; SIXTUS (Thrombosis-Related Extrapulmonary Outcomes in Pneumonia) Study Group. Cardiovascular complications and short-term mortality risk in community-acquired pneumonia. *Clin Infect Dis.* 2017;64(11):1486-93. doi:10.1093/cid/cix164.
16. Peake SL, Moran JL, Leppard PI. Serum troponin concentrations in patients with sepsis: their predictive value for myocardial depression and mortality. *Crit Care Med.* 2006;34(3):962-70. doi:10.1097/01.CCM.0000201878.44810.7E.
17. Simmons LR, Patel AA, Hartman ME. Severe pneumonia, sepsis, and cardiovascular complications: an evolving paradigm. *J Intensive Care Med.* 2016;31(2):114-20. doi:10.1177/0885066615572496.
18. Ver Elst KM, Spapen HD, De Waele JJ. Myocardial dysfunction in sepsis: the role of cytokines. *Chest.* 2013;143(5):1168-75. doi:10.1378/chest.12-1980.
19. Parikh SM, Karpaliotis D. Myocardial ischemia in the critically ill patient: mechanisms and clinical management. *Crit Care Med.* 2007;35(5 Suppl):S411-7. doi:10.1097/01.CCM.0000260623.26167.BB.
20. Lyon AR, Rees PS. Mechanisms of stress-induced cardiomyopathy. *J Am Coll Cardiol.* 2008;52(24):1886-94. doi:10.1016/j.jacc.2008.08.043.
21. Jenkins WS, Vesely MR, Ottolini E. Hemodynamic changes in critically ill patients with severe sepsis. *Crit Care Clin.* 2015;31(3):541-58. doi:10.1016/j.ccc.2015.03.011.
22. Mojón-Álvarez D, Giralt T, Carreras-Mora J, Calvo-Fernández A, Izquierdo A, Soler C, et al. Baseline NT-proBNP levels as a predictor of short- and long-term prognosis in COVID-19 patients: a prospective observational study. *BMC Infect Dis.* 2024;24:58. doi:10.1186/s12879-024-08980-3.
23. Apple FS, Quist HE, Doyle PJ, Otto AP, Murakami MM. Plasma 99th percentile reference limits for cardiac troponin and creatine kinase MB mass for use with European Society of Cardiology/American College of Cardiology consensus recommendations. *Clin Chem.* 2003;49(8):1331-6. doi:10.1373/49.8.1331.
24. Melli G, Chaudhry V, Cornblath DR. Rhabdomyolysis: an evaluation of 475 hospitalized patients. *Medicine (Baltimore).* 2005;84(6):377-85. doi:10.1097/01.md.0000188565.48918.41.
25. Blanco JR, Zabalza M, Salcedo J, et al. Rhabdomyolysis of infectious and noninfectious causes. *South Med J.* 2002;95(5):542-4. doi:10.1097/00007611-200295050-00012.
26. Fan Q, Meng J, Li P, Liu Z, Sun Y, Yan P. Pathogenesis and association of *Mycoplasma pneumoniae* infection with cardiac and hepatic damage. *Microbiol Immunol.* 2015;59(7):375-80.
27. Seedat MA, Feldman C, Skoularigis J, Promnitz DA, Smith C, Zwi S. A study of acute community-acquired pneumonia, including details of cardiac changes. *Q J Med.* 1993;86:669-75. PMID: 8255965. doi:10.1093/qjmed/86.10.669.
28. Yamaguchi S, Abe M, Arakaki T, Arasaki O, Shimabukuro M. Prognostic value of lactate dehydrogenase for mid-term mortality in acute decompensated heart failure: a comparison to established biomarkers and brain natriuretic peptide. *Heart Lung Circ.* 2020;29(9):1318-27.

29. Sin DD, Man SF. Chronic obstructive pulmonary disease as a risk factor for cardiovascular morbidity and mortality. *Proc Am Thorac Soc.* 2005;2(1):8–11. doi:10.1513/pats.2306020.
30. Labaki WW, Xia M, Murray S, Curtis JL, Barr RG, Bhatt SP, et al. NT-proBNP in stable COPD and future exacerbation risk: Analysis of the SPIROMICS cohort. *Respir Med.* 2018 Jul;140:87-93. doi: 10.1016/j.rmed.2018.06.005.

Research Article

USABILITY OF SATURATION/RESPIRATORY RATE AS A PARAMETER IN PULMONARY THROMBOEMBOLISM RISK SCORING

Maşide ARI ^{1*}, Fatma YILDIRIM ², Eren USUL ³, Emrah ARI ⁴, Ömer Faruk TÜTEN ⁵,
Ali Türker ÇİFTÇİ ⁶

¹Ankara Atatürk Sanatoryum Training and Research Hospital, Department of Respiratory Disease Ankara/Türkiye

² Etlik City Hospital, Department of Respiratory Disease Ankara/Türkiye

³ Etlik City Hospital, Department of Emergency Medicine Ankara/Türkiye

⁴ Mamak Public Hospital, Department of Emergency Medicine Ankara/Türkiye

⁵ Ankara University Health Practise and Research Hospitals Ankara/ Türkiye

⁶ Niğde Ömer Halisdemir University, Biostatistics and Medical Informatics Niğde /Türkiye

*Correspondence: masidetuten@icloud.com

ABSTRACT

Objective: The first step of pulmonary thromboembolism (PTE) treatment management is the risk classification. The most commonly used scoring system for this purpose is the pulmonary embolism severity index (PESI). However, the large number of parameters it contains limits its usability. Therefore, the need for easily accessible, fast and accurate resulting parameters continues. This study was planned to evaluate the role of Saturation/Respiratory Rate (SPO₂/RR) in determining the risk group.

Materials and Methods: This study was conducted retrospectively in patients diagnosed with PTE between 01.01.2020 and 01.11.2022 in Dışkapı Yıldırım Beyazıt Training and Research Hospital Emergency Department. Sociodemographic characteristics, vitals, laboratory results and radiological images of the patients were examined through the in-hospital information management system.

Results: 188 patients were included in the study. The average age of the patients was 64.97±16.64 years. 107(56.9%) of the patients in the study were women. When patients were divided into groups according to early mortality risk, 35 patients (18.6%) were high risk; 31 patients (16.4%) intermediate-high risk; 65 patients (34.5%) were in the intermediate-low risk group and 57 patients (30.5%) were in the low-risk group. SpO₂/RR was found 3.29±0.82; 3.97±0.60; 4.50±0.92; 5.00±0.77 respectively (p<0.001). It was determined that SpO₂/RR was a guide in determining the risk group.

Conclusion: Saturation/respiratory rate can be used to determine risk groups in acute PTE and is also a guide in determining treatment management and mortality.

Keywords: Mortality, Pulmonary embolism, Saturation/respiratory rate

Received: 01 December 2024

Revised: 26 January 2025

Accepted: 17 February 2025

Published: 20 March 2025



Copyright: © 2025 by the authors. Published by Aydın Adnan Menderes University, Faculty of Medicine and Faculty of Dentistry. This article is openly accessible under the Creative Commons Attribution-NonCommercial 4.0 International (CC BY-NC 4.0) License.

INTRODUCTION

Pulmonary thromboembolism is an important cause of mortality, and its incidence increases every year (1). Therefore, PTE maintains its importance as a global burden of illness.

The presenting clinic in acute PTE is variable. It may be the cause of cardiac arrest, or it may be diagnosed incidentally in imaging taken for another reason in an asymptomatic situation. Therefore, treatment management is also variable. The first step in determining treatment is to determine the patient's mortality risk. The most used scoring system for this purpose is the pulmonary embolism severity index (PESI). PESI was designed by Aujesky D et al in 2005 and includes 11 clinical predictive variables (2). PESI is not a fast and easily applicable scoring system because it contains many parameters. Therefore, the need for easily accessible, fast and accurate resulting parameters continues.

Measurement of oxygen saturation in air (SpO₂) with pulse oximetry is one of the most important parameters to be evaluated at the time of admission. Low oxygen saturation is a poor prognostic factor in PTE (3). Respiratory rate is another clinical parameter that should be evaluated in every patient. In acute PTE, hypoxia due to occlusion in the pulmonary artery subsequently causes vasoconstriction. This may result in an increase in right heart pressure and decompensation of the patient (4). Therefore, respiratory rate and saturation are guiding parameters in critical diseases (5). In a study conducted on intensive care patients, Fuentes et al. defined the respiratory rate as a parameter that can predict weaning failure by proportioning it to the oxygen level (6). It was stated by Myers et al. that it could predict intubation in COVID-19-related respiratory failure (7). In the light of these studies, evaluation of saturation and respiratory rate may be an early warning prognostic factor in PTE. For this purpose, the role of SpO₂/RR in risk group classification and treatment management were evaluated.

MATERIALS AND METHODS

This study was designed retrospectively in patients diagnosed with PTE in the Emergency Department of Dışkapı Yıldırım Beyazıt Training and Research Hospital, as a single center. Because the study was designed retrospectively, no written informed consent form was obtained from patients. Artificial intelligence (AI) technology was not used in this study. Ethics committee approval was obtained with the decision of Ankara Etlik

City Hospital Clinical Research Ethics Committee dated 16.08.2023 and numbered AEŞH-EK1-2023-431, and it was conducted by following the ethical principles determined by the Declaration of Helsinki.

Patients under 18 years of age and over 90 years of age, pregnant women, those who previously used long-term oxygen therapy due to respiratory failure, those with decompensated congestive heart failure, those with contraindications to thrombolytic therapy, and patients with missing data were excluded from the study. In addition, patients who developed acute respiratory failure due to pulmonary thromboembolism were included in the study, but patients who had previously used NIMV and LTOT due to chronic respiratory failure were excluded from the study.

Demographic characteristics of the patients such as age and gender, additional diseases, symptoms at the time of admission, vital values, imaging tests (chest radiography, computed tomography pulmonary angiography), transthoracic echocardiography findings, laboratory values (complete blood count, biochemical tests, coagulation tests, D-dimer, Pro-BNP, troponin, blood gas values) and medical treatments were examined through HIMS and the Ministry of Health E-Pulse System. While evaluating the right ventricular dysfunction findings of the patients, right ventricular width and sPAP were examined. The sPAP values were divided into 4 separate groups as 24 and below, 25-35, 36-50 and over 50. The 30-day mortality of the patients was recorded.

PESI and sPESI (simplified PESI) indexes were used to determine risk groups by examining the comorbidities, vitals, blood tests, computed tomography images and echocardiography findings of the patients. Additionally, according to the current guideline of the European Society of Cardiology, patients were divided into risk classes as low risk, intermediate-low risk, intermediate-high risk and high risk in terms of early mortality. The saturation and respiratory rate which are the two criteria for the calculation of PESI and measured from the fingertip of these patients at the time of admission were evaluated. Patients' SpO₂/RR values, risk groups, vital signs were examined according to mortality status and treatment applied, and it was checked whether there was a statistically significant difference between the groups.

Statistical Analysis

The data were analyzed using Statistical Package for the Social Sciences (SPSS) 25.0 (IBM SPSS Statistics for Windows, Armonk, NY: IBM Corp.). The suitability of the variables to normal distribution was examined using

visual (histogram and probability graphs) and analytical methods (Shapiro-Wilk test-Kolmogorov Smirnov test), and parametric tests were used in normal distribution and non-parametric tests were used in non-normal distribution. Descriptive statistics were expressed as mean and standard deviation in normally distributed numerical data, median and minimum-maximum range in non-normally distributed data, and number and percentage in nominal data. Numerical variables that did not show normal distribution were analyzed using the "Mann Whitney U test" between two groups and the "Kruskal Wallis" between three groups. Nominal data were evaluated between the two groups using the "Pearson Chi-square test" or "Fisher's Exact test". Spearman Correlation analysis was used to examine the relationship between numerical variables. In the analysis, a p-value < 0.05 was considered statistically significant. In ROC analysis, the

area under the curve (AUC) was evaluated and the data were expressed with a 95% confidence interval.

RESULTS

188 patients were included in the study. The average age of the patients was 64.97±16.64. The demographic characteristics and the risk group of the patients are given in Table 1. Table 2 shows the patients' blood tests, vitals, transthoracic echocardiography (TTE) findings and SPO₂/RR values which are evaluated during emergency department admission.

The patients were grouped by measuring the sPAP values of the patients with echocardiography (Table 2). The sPAP values were divided into 4 separate groups as 24 and below, 25-35, 36-50 and over 50. Each of these subgroups was compared separately according to the risk groups to evaluate whether there was a significant difference.

According to the statistical analysis between the SPO₂/RR, PESI and Early Mortality Risk Classes sub-groups, each sub-group varied significantly with one other. As the risk classification progressed towards higher levels, SpO₂/RR decreased significantly (Table 3).

The correlation analysis between saturation/respiratory rate and vital signs is shown in Table 4. A positive linear relationship was detected between SpO₂/RR and systolic and diastolic blood pressure. A moderate negative linear relationship was detected between SpO₂/RR and pulse. Saturation/respiratory number was found to be lower in patients with reperfusion treatment, while higher in patients who did not need thrombolytic treatment (Table 5). There was a significant difference between the groups (p<0.001). With 80.6% sensitivity and 78.8% specificity, SpO₂/RR cut off value was determined as 3.7. SpO₂/RR was

Table 1. Distribution of patients according to socio-demographic characteristics and risk classifications

All patients 188 (100%) N(%) Mean±sd		
Age, years		64.97±16.64
Gender	Women	107 (56.9%)
	Men	81 (43.1%)
Acquired risk factor		174 (92.6%)
	Immobilization	87(46.3%)
Comorbidity		128 (68.1%)
	Hypertension	73 (38.8%)
	Diabetes Mellitus	40 (21.3%)
	COPD*	30(15.9%)
Symptoms		185 (98.4%)
	Shortness Of Breath	149 (79.3%)
	Chest Pain	101 (53.7%)
PESI classification	Low risk	67 (35.6%)
	Medium risk	44 (23.4%)
	High risk	77 (41%)
sPESI classification	Low risk	58 (30.9%)
	High risk	130 (69.1%)
Evaluation of groups according to early mortality risk	Low risk	56 (29.7%)
	Medium-low risk	64 (34.0%)
	Medium-high risk	32 (17.0%)
	High risk	36 (19.1%)

* Chronic obstructive pulmonary disease

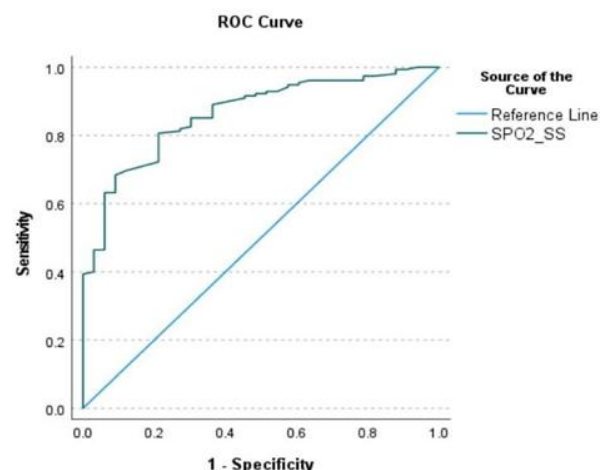


Figure 1. Roc analysis in mortality prediction of saturation/respiratory rate in pulmonary thromboembolism

Table 2. Evaluation of patients' admission vitals, laboratory tests and transthoracic echocardiography findings according to risk groups

	All patients (N=188) N(%) <i>Meant±sd</i>	High risk (N=36) N(%) <i>Meant±sd</i>	Medium-high risk (N=32) N(%) <i>Meant±sd</i>	Medium-low risk (N=64) N(%) <i>Meant±sd</i>	Low risk (N=56) N(%) <i>Meant±sd</i>	P value*
Systolic blood pressure (mmHg)	118±23	91±19	122±21	123±20	126±19	<0.001
Diastolic blood pressure (mmHg)	70±12	58±11	75±13	71±10	75±9	<0.001
Pulse (beats/min)	99±20	113±21	103±21	98±21	91±15	<0.001
Respiratory rate	21±4	25±4	22±3	20±3	19±2	<0.001
Saturation	87±8	79±10	86±6	87±6	93±3	<0.001
Saturation/ respiratory rate	4.34±1.01	3.29±0.82	3.97±0.60	4.51±0.95	5.00±0.77	<0.001
Lactate (mg/dL)	2.78±2.51	5.08±4.65	2.91±1.54	2.23±1.09	1.84±0.66	<0.001
D-Dimer (µg/mL)	7.75±6.79	10.75±7.04	10.54±6.73	7.93±6.98	4.17±4.56	<0.001
Right Spaces						
Normal	99(52.7%)	0	9	45	45	<0.001
Slightly wide	38(20.2%)	2	10	14	12	<0.001
Wide	51(27.1%)	33	12	6	0	<0.001
sPAP**						
<25 mmHg	46(24.5%)	0	0	14	31	<0.001
25-35 mmHg	60(31.9%)	3	7	31	23	<0.001
36-50 mmHg	41(21.8%)	9	13	16	3	<0.001
>50 mmHg	41(21.8%)	23	11	4	0	<0.001

* Kruskal Wallis-H Test runs applied. **sPAP: Systolic pulmonary artery pressure

treatment (AUC: 0.863, 95 %CI 0.803-0.924, $p < 0.001$). ROC analysis was given in Figure 1. 21 (11%) of the patients included in the study died within 30 days of follow-up. When the risk groups of the deceased patients were evaluated, 9 patients (25%) were in the high-risk group, 7 patients (21.8%) were in the intermediate-high risk group, and 5 patients (7.8%) were in the intermediate-low risk group. It was observed that there were no deceased patients in the low-risk group.

Table 3. Evaluation of saturation/respiratory rate according to risk groups

		Saturation/ respiratory rate (Min-Max)	p value
PESI risk classification	High risk	3.67 (1.43-6.64)	0.004*
	Medium risk	4.50 (3.33-5.81)	
	Low risk	5.06 (3.46-7)	
sPESI risk classification	High risk	4.00 (1.43-6.64)	<0.001*
	Low risk	5.08 (3.54-7)	
Classification according to early mortality risk	High risk	3.42 (1.43-5.28)	<0.001*
	Medium high risk	3.91 (2.36-5.5)	
	Medium low risk	4.50 (2.11-6.64)	
	Low risk	5.11 (3.54-7)	

* Kruskal Wallis-H Test was applied. ** Mann-Whitney U analysis was applied.

When the saturation/respiratory number was evaluated according to mortality, it was found to be lower in deceased patients. There was a significant difference between the groups ($p=0.003$) (Table 5). With 68.3% sensitivity and 71.4% specificity, SpO₂/RR cut off value was determined as 3.9. SpO₂/RR was found to be decisive in mortality estimation (AUC: 0.702, 95 %CI 0.593-0.812, $p < 0.001$). ROC analysis was given in Figure 2.

Table 4. Correlation analysis results between saturation/respiratory rate and vital signs

	Systolic blood pressure	Diastolic blood pressure	Pulse	Respiratory rate
SpO ₂ /RR*	r 0.262	r 0.177	r -0.346	r -0.954
		p<0.001	p<0.001	p<0.001

* SpO₂/RR: Saturation/respiratory rate. Spearman correlation analysis was performed.

DISCUSSION

Pulmonary thromboembolism is a cardiovascular emergency that develops as a result of varying degrees of obstruction of the pulmonary arteries. The clinical picture varies depending on the degree of obstruction in the vascular bed. It may result in sudden death, or it may be encountered incidentally during imaging taken for another reason in an asymptomatic condition. The risk of

30-day mortality should be evaluated to make the treatment approach correctly. The most commonly used scoring systems in this prognostic assessment are the PESI and sPESI. The fact that these risk classification systems contain multiple parameters restricts the use of physicians. Therefore, the need for easily accessible, fast and accurate resulting parameters continues. This study was designed to evaluate the usability of SpO₂/RR in risk classification. Acute PTE is often considered a disease of old age (8). In our study, the average age of the patients was 64.9 years. Although the clinical picture in acute PTE is variable, the most common symptoms are shortness of breath and chest pain (9). In our study, the most common symptoms were shortness of breath and chest pain.

Table 5. Evaluation of saturation/respiratory rate according to reperfusion therapy and mortality status

Treatment		SpO ₂ /RR* Median (Min-Max)	p value**
Reperfusion therapy N=33 (%17.6)		3.42 (2.80-3.75)	<0.001
	Absence of reperfusion N=155 (%82.4)	4.50 (3.91-5.28)	
Mortality Status	Ongoing survival N=167 (%89)	4.50 (3.71-5.22)	0.003
	Mortality recorded N=21 (%11)	3.73 (3.29-4.15)	

*SpO₂/RR: Saturation/respiratory rate ** Mann-Whitney U analysis was applied.

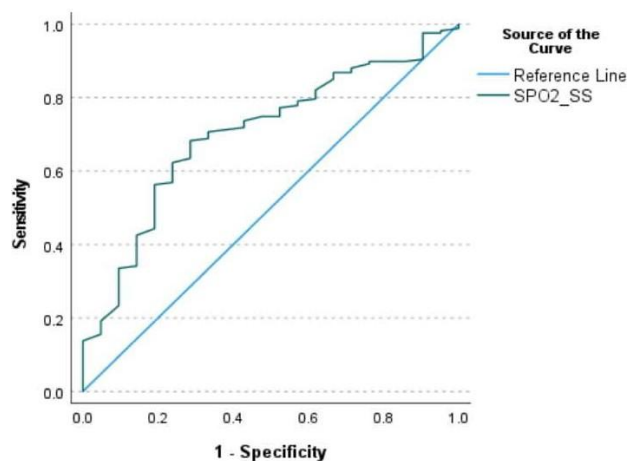


Figure 2 ROC Analysis in Mortality Prediction of Saturation/Respiratory Rate in Pulmonary Thromboembolism

The development of right ventricular dysfunction in intermediate and high-risk PTE may cause a decrease in cardiac output. This may disrupt renal perfusion and cause an increase in urea. In the study conducted by Gök et al., right ventricular dysfunction was associated with intra-hospital mortality (10). Our study also showed that high-risk patients had renal dysfunction. This condition was associated with right ventricular dysfunction.

In the meta-analysis conducted by Wang et al., it was stated that lactate level was associated with short- and long-term mortality, but it was stated that more studies were needed to evaluate it according to risk groups (11). In our study, lactate was observed to be significantly higher in the high-risk group. Hypoxia due to vascular obstruction in PTE is associated with increased lactate and may be a guide in determining the risk groups of patients.

D-dimer is one of the fibrin degradation products which is formed as a result of the endogenous fibrinolytic system breaking down the thrombus. It is frequently used in the diagnosis and exclusion of PTE along with clinical probability scores. However, it has been reported that d-dimer is higher in patients with high thrombus burden and reported to be predictive of right ventricular dysfunction (12). In our study, when patients were separated according to risk groups, it was observed that d-dimer levels were lower in low-risk PTE, where thrombus burden was less.

Brain natriuretic peptide and NT-proBNP are released as a result of increased ventricular filling pressure or in cases of myocardial ischemia. Elevated natriuretic peptide levels in acute PTE are associated with right ventricular (RV) dysfunction. Chen et al. stated that NT-proBNP is a very sensitive marker in determining RV dysfunction and mortality, and if it is detected low, mortality is significantly reduced (13). In the study conducted by Chen et al., it was stated that proBNP was higher in high-risk PTE patients and could be used in treatment management (13). In our study, NT-proBNP levels were found to be lower in the intermediate-low and low-risk groups. Because it is associated with right ventricular dysfunction, it can be used in treatment management in intermediate-high and intermediate-low risk groups.

In acute PTE, perfusion decreases because of occlusion of the vascular bed. This results in hypoxemia and reduced oxygen supply to tissues (14). Additionally, mechanical occlusion of the vascular bed by thrombus causes hypoxic vasoconstriction of the pulmonary arterial system. This results in an increase in pulmonary vascular resistance (PVD) and pulmonary artery pressure (PAP). A sudden

increase in PAP may cause dilation and dysfunction in the RV, resulting in hypotensive shock (15). Therefore, hypoxia is a poor prognostic factor in acute PTE (16). In our study, saturation was observed to be lower in the high-risk group, while it was higher in the low-risk group. Respiratory rate is the first parameter that should be evaluated in every patient presenting with shortness of breath. It is also included as a component in PESI. Tachypnea is associated with adverse outcomes in patients with PTE (2). In the study conducted by Becattini et al., it was stated that respiratory rate was a guide in grouping intermediate-risk PTE patients as intermediate-low and intermediate-high (4). In our study, it was shown that the respiratory rate was lower in low-risk patients.

In 2019, Roca et al evaluated saturation and respiratory rate in determining the need for intubation in patients with acute hypoxemic respiratory failure due to pneumonia and monitored with high-flow nasal oxygen. They defined the ratio of these two parameters as the ROX index and described it as a parameter that can be easily used at the bedside to determine the need for intubation (17). It was later defined as an important parameter that should be evaluated in critical diseases (6,7). In his study, Jolobe pointed out that respiratory rate is a guiding parameter and its accurate measurement in patients with suspected pulmonary embolism (18). In our study, when patients were divided into groups according to risk groups, the increase in SpO₂/RR was associated with low-risk disease. There was a significant difference between the groups when evaluated according to both PESI and early mortality risk. SpO₂/RR is a simple, easily applicable parameter that should be evaluated in each patient and can be used to determine risk classification.

In high-risk PTE associated with hemodynamic instability, deaths usually occur within the first hours. There is still a need for parameters that can be applied quickly and provide accurate results in the detection of these patients. In the study conducted by Vedovati et al., the ratio of oxygen saturation to respiratory rate was called respiratory index and was shown to be an independent determinant of mortality in hemodynamically stable PTE patients (19). When the patients who received reperfusion therapy were examined, it was seen that SpO₂/RR was lower. In addition, SpO₂/RR was lower in mortal patients and higher in surviving patients and was a guide for mortality evaluation.

Our study has some limitations. Although we excluded patients with previously known heart failure, previous TTE findings of the patients included in the study were mostly unknown, so it is not clear whether right

ventricular dysfunction is associated with acute pulmonary thromboembolism. In addition, due to its retrospective design, the respiratory rate was obtained by scanning the files and it was not known for how many seconds it was evaluated. An evaluation could not be made between the rate at which the respiratory rate returned to normal and mortality. The fact that it was performed in a single center is another situation that causes limitations. Supporting it with multicenter studies will increase the value of our study.

CONCLUSION

As a result, SpO₂/RR, which includes the first parameters that should be evaluated in every patient presenting with respiratory distress, can be an important early warning risk factor both in determining the risk group and management of treatment and in determining mortality in acute PTE patients. This parameter, which is easily and quickly applied with the advantage of being evaluated at the bedside, can be used in emergency departments.

Acknowledgments

None

Authorship contributions

The study was conceived by M.A., F.Y., and E.U. The design was developed by M.A., E.A., and E.U. Data collection and processing were carried out by E.A., M.A., and A.T.Ç. Analysis and interpretation were performed by A.T.Ç., E.A., and Ö.F.T. The literature review was conducted by F.Y., E.U., and A.T.Ç. The manuscript was written by M.A., F.Y., and Ö.F.T. All authors provided feedback on earlier drafts of the manuscript and approved the final version.

Data availability statement

Data available on request.

Declaration of competing interest

The authors declare that there is no conflict of interest.

Ethics

Ethics committee approval was obtained with the decision of Ankara Etlik City Hospital Clinical Research Ethics Committee dated 16.08.2023 and numbered AEŞH-EK1-2023-431.

Funding

This study was not funded by any institution or organization.




REFERENCES

1. Lehnert P, Lange T, Møller CH, Olsen PS, Carlsen J. Acute pulmonary embolism in a national Danish cohort: increasing incidence and decreasing mortality. *Thromb Haemost.* 2018;118(3):539-546.
2. Aujesky D, Obrosky DS, Stone RA, Auble TE, Perrier A, Cornuz J et al. Derivation and validation of a prognostic model for pulmonary embolism. *Am J Respir Crit Care Med.* 2005;172(8):1041-6.
3. Donadini MP, Dentali F, Castellaneta M, Gnerre P, La Regina M, Masotti L et al. Pulmonary embolism prognostic factors and length of hospital stay: a cohort study. *Thromb Res.* 2017; 156:155-9.
4. Becattini C, Vedovati MC, Pruszczyk P, Vanni S, Cotugno M, Cimmini LA et al. Oxygen saturation or respiratory rate to improve risk stratification in hemodynamically stable patients with acute pulmonary embolism. *J Thromb Haemost.* 2018;16(12):2397-402.
5. Shen Y, Zhu L, Yan J. Stability of Spo₂/Fio₂ and respiratory rate-oxygenation indexes in critical respiratory disorders. *Crit Care Med.* 2022;50(8):e694-5.
6. Fuentes YV, Carvajal K, Cardona S, Montañó GS, Ibáñez-Prada ED, Bastidas A et al. The respiratory rate-oxygenation index predicts failure of post-extubation high-flow nasal cannula therapy in intensive care unit patients: a retrospective cohort study. *Rev Bras Ter Intensiva.* 2022;34(3):360-6.
7. Myers LC, Mark D, Ley B, Guarnieri M, Hofmeister M, Paulson S et al. Validation of respiratory rate-oxygenation index in patients with COVID-19-related respiratory failure. *Crit Care Med.* 2022;50(7):e638-42.
8. Ageno W, Haas S, Weitz JI, Goldhaber SZ, Turpie AGG, Goto S et al. Characteristics and management of patients with venous thromboembolism: the GARFIELD-VTE registry. *Thromb Haemost.* 2019;119(2):319-27.
9. Ozsu S, Ozlü T, Bülbül Y. Pulmonary thromboembolism based on the Turkish national data. *Tuberk Toraks.* 2009;57(4):466-82.

10. Gök G, Karadağ M, Çınar T, Nurkalem Z, Duman D. In-hospital and short-term predictors of mortality in patients with intermediate-high risk pulmonary embolism. *J Cardiovasc Thorac Res.* 2020;12(4):321-7.
11. Wang Y, Feng Y, Yang X, Mao H. Prognostic role of elevated lactate in acute pulmonary embolism: a systematic review and meta-analysis. *Phlebology.* 2022;37(5):338-47.
12. Keller K, Beule J, Balzer JO, Dippold W. D-Dimer and thrombus burden in acute pulmonary embolism. *Am J Emerg Med.* 2018;36(9):1613-8.
13. Chen YL, Wright C, Pietropaoli AP, Elbadawi A, Delehanty J, Barrus B et al. Right ventricular dysfunction is superior and sufficient for risk stratification by a pulmonary embolism response team. *J Thromb Thrombolysis.* 2020;49(1):34-41.
14. Burrowes KS, Clark AR, Tawhai MH. Blood flow redistribution and ventilation-perfusion mismatch during embolic pulmonary arterial occlusion. *Pulm Circ.* 2011;1(3):365-76.
15. Konstantinides SV, Meyer G, Becattini C, Bueno H, Geersing GJ, Harjola VP et al. 2019 ESC guidelines for the diagnosis and management of acute pulmonary embolism developed in collaboration with the European Respiratory Society (ERS). *Eur Heart J.* 2020;41(4):543-603.
16. Jenab Y, Hosseini K, Esmaeili Z, Tofighi S, Ariannejad H, Sotoudeh H. Prediction of in-hospital adverse clinical outcomes in patients with pulmonary thromboembolism, machine learning-based models. *Front Cardiovasc Med.* 2023;10:1087702.
17. Roca O, Caralt B, Messika J, Samper M, Sztrymf B, Hernández G et al. An index combining respiratory rate and oxygenation to predict outcome of nasal high-flow therapy. *Am J Respir Crit Care Med.* 2019;199(11):1368-76.
18. Jolobe OMP. Importance of accurate respiratory rate for triage of suspected pulmonary embolism. *QJM.* 2020;113(2):143.
19. Vedovati MC, Cimini LA, Pierpaoli L, Vanni S, Cotugno M, Pruszczyk P et al. Prognostic value of respiratory index in haemodynamically stable patients with acute pulmonary embolism: the respiratory index model study. *Eur Heart J Acute Cardiovasc Care.* 2020;9(4):286-92.

Research Article

DECISION MAKING FOR OPTIMAL TREATMENT FOR PATIENTS WITH PERIODONTITIS BASED ON RECENT CLASSIFICATION CRITERIA

 Ceren KÜTÜK¹,  Hanife Merva PARLAK¹,  Ayhan PARMAKSIZ²,  Nermin TARHAN¹,
 H. Gencay KEÇELİ^{1*}

¹Department of Periodontology, Faculty of Dentistry, Hacettepe University, Ankara, Turkey

²Department of Biostatistics, Faculty of Medicine, Istanbul Health & Technology University, Istanbul, Turkey

*Correspondence: monsieur_gencay@yahoo.com

ABSTRACT

Objective: The study aimed to evaluate the accuracy and agreement of clinicians with different education levels and clinical experience in periodontitis diagnosis and treatment planning.

Materials and Methods: Depending on the stage, grade, and extent components of periodontitis, a consensus diagnosis and treatment plan document prepared by two experienced periodontists was used as a gold-standard. An anonymous survey including 10 periodontitis cases was given to 15 participants (5 periodontal experts (PE), 5 postgraduate periodontology students (PS), and 5 undergraduate dental students (DS)) and asked them to classify each case depending on the components of the disease and select their treatment plan from a multiple-choice questionnaire including 11 dental treatment options. The accuracy of the responses was detected by referring to the gold-standard and inter-examiner agreement levels were also assessed.

Results: Except grade, no significant inter-group difference was found in the periodontitis components and this difference only existed in the PE group ($p=0.012$). PE group gave more accurate treatment planning responses compared to others. The agreement levels of all examiners for stage, grade, and extent were fair ($\kappa=0.366, 0.222, \text{ and } 0.287$, respectively). Treatment planning showed low agreement ($\kappa<0.31$) except tooth extraction option ($\kappa=0.554$). Both diagnosis and treatment planning responses showed significant variations amongst groups.

Conclusion: Although education level and experience showed superiority in terms of periodontitis diagnosis and treatment planning, the results with low accuracy indicate the need for calibration to reduce the variations and enhance the accuracy.

Keywords: classification, decision making, diagnosis, periodontitis

Received: 23 September 2024

Revised: 04 December 2024

Accepted: 03 February 2025

Published: 20 March 2025



Copyright: © 2025 by the authors. Published by Aydın Adnan Menderes University, Faculty of Medicine and Faculty of Dentistry. This article is openly accessible under the Creative Commons Attribution-NonCommercial 4.0 International (CC BY-NC 4.0) License.

INTRODUCTION

According to the recent periodontitis classification system (1), periodontitis is diagnosed by using interdental clinical attachment loss (CAL) as the primary criterion, followed by radiographic bone loss (RBL) (2). Once the diagnosis is achieved, the extent, stage, and grade of the disease are also recorded (3) together with the risk and complexity factors to highlight the largeness, severity, and the progression rate of the disease. All these data are used to determine the individual aspects of periodontitis in each case and develop personalized prevention and treatment planning, accordingly (3-6).

Clinical decision-making is a complex process that is influenced by a wide variety of clinical and non-clinical factors such as clinicians' educational level, experience, personal characteristics, daily work overload, and place of initial training (7-9) that create variety in the diagnosis and treatment planning amongst the clinicians. The correct diagnosis of periodontal disease is essential for the initial step of a successful treatment, as erroneous diagnoses may result in either undertreatment, overtreatment, or unnecessary applications.

Concerning the recent periodontitis classification, previous studies reported high variations in accuracy and agreement levels for the diagnosis of periodontitis cases amongst examiners with different educational levels (10-14). Moreover, age, gender, clinical experience, education, faith, socio-economic, and guidelines may affect the decision process causing increased variations between examiners. However, the number of studies investigating the variations between examiners by considering the education level and clinical experience in the use of the recent periodontitis classification in periodontal diagnosis and treatment planning is limited (12, 13). In the light of this information, the study hypothesizes that the variations between students and experts will be high. The purpose of the present study was to evaluate the variations and agreement between final-year dental students, postgraduate periodontology students, and periodontal expert groups in the implementation of the recent classification in periodontitis diagnosis and treatment planning.

MATERIALS AND METHODS

This study was conducted at the Department of Periodontology, Hacettepe University from April to November 2021 and was approved by the Ethical Committee of Hacettepe University, (GO 21/427). All

participants were informed about the study and signed the informed consent forms.

Study design and survey

A survey consisting of 10 periodontitis cases was presented to the participants. They were asked to classify each case using stage, grade, and extent and then mark their treatment options. Fifteen participants were selected for the study and equally divided into three groups according to their education level and expertise in periodontology: (i) Periodontal experts (PE) selected amongst certified periodontists, (ii) Postgraduate periodontology students (PS) with three years of clinical experience, and (iii) Final year undergraduate dental students (DS)

Preparation of periodontitis cases

For the questionnaire, two experienced periodontists (N.T and H.G.K) who did not participate in the evaluation selected a total of 10 periodontitis cases based on the recent classification criteria and determined the correct diagnosis and treatment plan responses (gold-standard) using the S3 clinical practice guideline, published by the European Federation of Periodontology (5) (Table S1). The selected cases included various stages and grades of periodontitis excluding other forms of the disease.

Following information was included in the basic records of each case (Table S1): (i) age and gender, (ii) pertinent medical history, systemic diseases, and medication, (iii) smoking (number of cigarettes/ day), (iv) HbA1c values in diabetic patients, (v) dental history (gingival bleeding, tooth mobility, family history of periodontitis, use of interdental oral hygiene devices, parafunctional habits, previous periodontal treatment, the last dental examination and professional oral hygiene procedure (≤ 1 year, >1 year or >3 years), and the number of tooth loss attributable to periodontitis, (vi) periodontal charting including (1) full-mouth plaque and bleeding scores (FMPS and FMBS), (2) bleeding on probing (BOP; +, -), (3) probing depth (PD) and CAL (recorded at six sites per tooth of the entire dentition), (4) furcation involvement (FI)(15), and (5) mobility (16), and (vii) radiographs (periapical and/or panoramic).

Diagnosis and treatment planning of periodontitis cases

According to the recent classification and treatment guidelines, the cases presented multiple options for diagnosis and treatment plans (5). The diagnosis options for each case were as follows: a) Stage: I / II /III / IV b) Grade: A/ B/ C c) Extent: Localized/ Generalized

Table 1. Accuracy of the diagnosis responses compared to the gold-standard

	DS		PS		PE		Inter-examiner	All examiners	
	correct response	%	correct response	%	correct response	%	p-value	correct response	%
Stage	25/50a	50	33/50a	66	30/50a	60	0.296	88/150a	58.7
(I-IV)									
I	2/5	40	4/5	80	2/5	40		8/15	53
II	5/10	50	6/10	60	9/10	90		20/30	67
III	10/25	40	17/25	68	13/25	52		40/75	53
IV	8/10	80	6/10	60	6/10	60		17/30	57
Grade (A-C)	19/50b	38	27/50a,b	54	34/50a	68	0.012	80/150	53.3
A	1/5	20	2/5	40	2/5	40		8/15	53
B	5/15	33	5/15	33	6/15	40		16/45	36
C	13/30	43	20/30	67	26/30	87		59/90	66
Extent	37/50a	74	36/50a	72	44/50a	88	0.141	117/150	78

Each subscript letter denotes a subset of group categories whose column proportions do not differ significantly from each other at the .05 level. DS: dental student, PS: postgraduate periodontology students, and PE: periodontal expert

The treatment plan options for the cases were as follows:

- tooth extraction,
- mechanical supragingival plaque/calculus removal,
- subgingival instrumentation,
- repeated subgingival instrumentation,
- resective periodontal surgery for pocket elimination,
- regenerative periodontal surgery for pocket elimination,
- resective periodontal surgery for furcation involvement,
- regenerative periodontal surgery for furcation involvement,
- supportive periodontal care > 6 months,
- supportive periodontal care < 6 months,
- adjunctive therapies (host modulation, laser/ photodynamic therapy, subgingival antimicrobial, systemic antibiotics).

Statistical analysis

Qualitative data were expressed as numbers and percentages. The inter-examiner level of agreement was evaluated using the Fleiss Kappa statistics. The kappa value coefficient was interpreted according to the criteria proposed by Landis and Koch: less than 0.00 poor agreement, 0.01 to 0.20 slight agreement, 0.21 to 0.40 fair agreement, 0.41 to 0.60 moderate agreement, 0.61 to 0.80 substantial agreement, and 0.81 to 1.00 almost perfect agreement (17). The rates of correct diagnosis between groups were calculated by comparing the column percentages by applying Bonferroni correction. The significance level was set at 5%. The data were analyzed with a statistical software package (IBM SPSS Statistics version 26.0).

RESULTS

Gold-standard diagnosis and treatment plans for each case were given in Table S1. Accordingly, the distribution of periodontitis cases by stage, grade, and extent was as follows: 1 case was defined as stage I (10%), 2 as II (20%), 5 as III (50%), and 2 as IV (20%); 1 was assigned to grade A (10%), 3 to grade B (30%), and 6 to grade C (60%), and 8 were assessed as generalized (80%) and 2 as localized (20%).

Accuracy the diagnosis responses compared to the gold-standard (Table 1)

The majority of the examiners selected the correct stage (58.7%), grade (53.3%), and extent (78%) responses for the periodontitis cases. The correct response rate for the stage component was highest in the PS group (66%), but no significant inter-group difference was found ($p=0.296$). DS diagnosed the grade component less accurately (38%) than PE and PS (68% and 54%, respectively) and the difference was statistically significant ($p=0.012$). 88% of PE, 72% of PS, and 74% of DS diagnosed the extent accurately, without any significant intergroup difference.

Table 2. Accuracy of the responses of examiners in case-by-case treatment planning

	Case 1				Case 2				Case 3				Case 4				Case 5			
	DS	PS	PE	Overall	DS	PS	PE	Overall	DS	PS	PE	Overall	DS	PS	PE	Overall	DS	PS	PE	Overall
Tooth extraction	5	5	5	15/15	5	4	5	14/15	4	3	5	12/15	1	1	4	6/15	4	5	5	14/15
Mechanical supragingival plaque/calculus removal	5	5	5	15/15	5	4	5	14/15	5	5	5	15/15	5	5	5	15/15	5	5	5	15/15
SRP	5	5	4	14/15	5	4	5	14/15	3	5	5	13/15	5	5	5	15/15	5	4	4	13/15
Repeated SRP	4	1	2	7/15	2	2	2	6/15	3	2	4	9/15	3	2	2	7/15	2	1	5	8/15
Resective surgery for pocket elimination	2	2	4	8/15	4	2	5	11/15	4	5	5	14/15	4	5	5	14/15	3	4	4	12/15
Regenerative surgery for pocket elimination	1	4	3	8/15	4	5	4	13/15	2	3	3	8/15	4	0	2	6/15	1	4	5	10/15
Resective surgery for furcation involvement	4	5	5	14/15	0	0	0	0/15	2	2	0	4/15	1	3	4	8/15	4	5	5	14/15
Regenerative surgery for furcation involvement	1	5	5	11/15	5	2	4	11/15	3	0	4	7/15	4	0	3	7/15	1	5	2	8/15
Supportive periodontal care	0	1	0	1/15	0	1	0	1/15	0	3	1	4/15	0	2	0	2/15	1	1	1	7/15
Adjunctive therapies	3	3	4	10/15	4	2	1	7/15	4	3	1	8/15	1	1	2	14/15	1	4	3	8/15
	Case 6				Case 7				Case 8				Case 9				Case 10			
Tooth extraction	5	5	5	15/15	5	4	5	14/15	5	4	5	14/15	5	5	5	15/15	5	5	5	15/15
Mechanical supragingival plaque/calculus removal	5	5	5	15/15	5	5	5	15/15	5	5	5	15/15	5	5	5	15/15	5	5	5	15/15
SRP	4	5	5	14/15	5	5	5	15/15	3	4	4	11/15	5	4	5	14/15	4	4	5	13/15
Repeated SRP	3	2	4	9/15	4	2	4	10/15	4	3	2	9/15	3	2	3	8/15	2	5	0	7/15
Resective surgery for pocket elimination	2	3	4	9/15	3	4	3	10/15	4	4	4	12/15	1	4	4	9/15	4	4	5	13/15
Regenerative surgery for pocket elimination	5	4	3	12/15	4	4	5	13/15	3	1	0	4/15	2	2	3	7/15	3	5	4	12/15
Resective surgery for furcation involvement	5	5	5	15/15	5	4	5	14/15	4	4	3	11/15	1	0	0	1/15	5	5	4	14/15
Regenerative surgery for furcation involvement	1	5	5	11/15	1	5	2	8/15	2	2	4	8/15	4	0	1	5/15	3	3	3	9/15
Supportive periodontal care	0	3	2	5/15	1	2	2	5/15	0	0	0	0/15	0	1	1	2/15	3	3	2	8/15
Adjunctive therapies	3	3	2	8/15	1	3	1	15/15	3	2	3	8/15	2	0	4	6/15	5	5	4	14/15

DS: dental student, PS: postgraduate periodontology students, PE: periodontal expert, and SRP: scaling and root planning. High accuracy rates are shown in bold.

Table 3. Intra and inter-examiner agreement regarding the diagnosis and treatment plan

	DS (n= 5)		PS (n= 5)		PE (n = 5)		Overall (n=15)	
	Kappa	p-value	Kappa	p-value	Kappa	p-value	Kappa	p-value
Diagnosis								
Stage	0.290	<0.001	0.442	<0.001	0.498	<0.001	0.366	<0.001
Grade	0.108	0.089	0.159	0.017	0.4	<0.001	0.222	<0.001
Extent	0	0.5	0.542	<0.001	0.5	<0.001	0.287	<0.001
Treatment plan								
Tooth extraction	0.65	<0.001	0.397	<0.001	0.811	<0.001	0.554	<0.001
Mechanical supragingival plaque/calculus removal	.	.	-0.02	0.581	.	.	-0.007	0.586
Subgingival instrumentation (SRP)	0.053	0.298	-0.111	0.867	-0.064	0.738	-0.002	0.521
Repeated subgingival instrumentation (SRP)	-0.146	0.928	-0.114	0.873	0.064	0.261	-0.047	0.935
Resective periodontal surgery for pocket elimination	0.039	0.35	0.175	0.04	0.548	<0.001	0.255	<0.001
Regenerative periodontal surgery for pocket elimination	-0.011	0.544	0.343	<0.001	0.235	0.009	0.161	<0.001
Resective periodontal surgery for furcation involvement	0.324	0.001	0.323	0.001	0.222	0.013	0.31	<0.001
Regenerative periodontal surgery for furcation involvement	0.035	0.363	0.253	0.006	0.31	0.001	0.073	0.009
Supportive periodontal care >6 month	0.222	0.013	-0.025	0.599	0.324	0.001	0.106	<0.001
Supportive periodontal care <6 month	0.148	0.07	-0.025	0.599	0.324	0.001	0.092	0.002
Adjunctive therapies (Host modulation, Laser/ photodynamic therapy, subgingival antimicrobial, systemic antibiotics)	0.119	0.118	0.066	0.254	0.039	0.35	0.06	0.026

<0.00 poor agreement, 0.01 to 0.20 slight agreement, 0.21 to 0.40 fair agreement, 0.41 to 0.60 moderate agreement 0.61 to 0.80 substantial agreement, and 0.81 to 1.00 almost perfect agreement DS: dental student, PS: postgraduate periodontology students, PE: periodontal expert, and SRP: scaling and root planning,

Accuracy of the treatment plan responses compared to gold-standard (Table 2)

The responses regarding the treatment option of tooth extraction, mechanical supragingival, and subgingival instrumentation showed a high rate of accuracy. In contrast, the highest inaccuracy existed in the supportive periodontal care option. Surgical periodontal treatment options showed high or moderate accuracy, particularly with the highest errors in cases 2, 3, 8, and 9. The PE group chose the most accurate responses compared to others. Regarding the furcation treatment option, the highest errors were seen in cases numbers 2,3, and 9.

Agreement of diagnosis across examiners (Table 3)

The agreement levels of all examiners were fair for either stage ($\kappa=0.366$), grade ($\kappa=0.222$), or extent ($\kappa=0.287$) components, respectively. PE showed moderate agreement for stage and extent ($\kappa=0.498$ and $\kappa=0.5$) and fair agreement for grade ($\kappa=0.4$). The agreement level of PS group was moderate for stage and extent ($\kappa=0.442$ and $\kappa=0.542$), and slight for grade ($\kappa=0.159$). DS group showed fair agreement for stage and grade ($\kappa=0.29$ and $\kappa=0.108$), while showed poor agreement for extent ($\kappa=0$).

Agreement of treatment planning across examiners

All examiners showed the highest agreement for tooth extraction ($\kappa=0.554$), while there was a poor agreement for all mechanical instrumentation options. Fair levels of agreement were exhibited in resective periodontal surgery option for pocket elimination ($\kappa=0.255$) and furcation involvement ($\kappa=0.31$). All examiners had slight levels of agreement for the following options: regenerative periodontal surgery ($\kappa=0.161$ and $\kappa=0.073$), supportive periodontal care ($\kappa=0.106$ and $\kappa=0.092$), and adjunctive therapy ($\kappa=0.06$) (Table 3).

DS group mostly showed low agreement for all treatment options except tooth extraction ($\kappa=0.65$). While PS group had a poor agreement level for non-surgical treatment options (mechanical supragingival plaque/calculus removal, subgingival instrumentation, and repeated subgingival instrumentation) and supportive periodontal care and had low consistency for resective and regenerative periodontal surgeries for both pocket elimination and furcation involvement. PE group showed almost a perfect agreement level for tooth extraction ($\kappa=0.811$). PE group showed low consistency for the other treatment options

except resective periodontal surgery for pocket elimination ($\kappa=0.548$) (Table 3).

DISCUSSION

This study aimed to evaluate the impact of the education level and clinical experience, which are non-clinical factors, on diagnosis and treatment planning of periodontitis cases by referring the recent periodontitis classification. The results demonstrated that final-year dental students, postgraduate periodontology students, and periodontal experts had low to moderate accuracy in diagnosis and low agreement in treatment planning.

Considering the stage, grade, and extent components of periodontitis, the highest accuracy belonged to the extent parameter probably due to its relatively uncomplicated determination method carried out by calculating the rate of affected teeth to whole dentition whereas stage and grade determination requires detailed RBL and CAL measurements as well as the comprehensive evaluation of patient's age, risk factors, tooth loss due to periodontitis that makes their decision-process more complicated and thereby increasing the error rates. The low accuracy levels of DS and PS groups in determining grade levels also supported this phenomenon that shows consistency with the findings of Gandhi et al. (12).

In a similar study, Abou-Arraj et al. (13) gave the diagnostic options to the participants by preparing a questionnaire, not compatible with the clinical reality of the diagnostic process, including only the randomly selected cases diagnosed with various combinations of stage, grade, and extent. Instead, a case list including all response possibilities was preferred in the present study and as result, overall accuracy rates related to stage, grade, and extent were 58.7%, 53.3%, and 78%, respectively. These results were consistent with the stage and extent findings of Ravidà et al. (18) (stage: 68.9%, grade: 73.8%, and extent: 80.7%) and Abrahamian et al. (10) (stage: 68.7%, grade: 82.4%, and extent: 75.5%) and with the extent results of Marini et al. (11) (stage: 76%, grade: 71.4%, extent: 82.6%, and overall: 47.2%). The lower grade and stage scores compared to the relevant literature might be associated with the interindividual evaluation differences (8) owing to the absence of participants with higher expertise in periodontics or without an attendance to any special training prior to the study. On the other hand, the higher accuracy in the extent compared to the stage and grade components of all studies can be attributed to the errors made in the determination of CAL and bone loss that make the diagnostic process multidimensional and complex in the recent periodontitis classification.

It was seen that stage component itself did not show an influence on the accuracy of diagnosis. On the contrary, compared to grade C, a lower accuracy was detected for grades A and B probably due to the obvious characteristics of grade C cases such as high bone loss/age ratio and risk factors, and these findings were in line with Marini et al (11). On the other hand, it was observed that the participants could add the risk factors to the equation with less accuracy in the detection of grade component revealing the need to improve the knowledge and experience of the clinicians by considering the quantitative effect of these factors on the diagnosis.

The S3-level clinical practice guideline recommends that supportive periodontal care visits should be scheduled between 3- and 12-month intervals, and ought to be personalized according to the patient's risk profile and periodontal conditions after active therapy (5). In the present study, the responses regarding to supportive periodontal care showed high inaccuracy. As a possible reason, although guidelines provide advantages in reducing variations, their availability did not guarantee their use possibly due to lack of interest, lack of agreement, lack of involvement, lack of outcome expectancy, lack of time, and fear of restricted professional autonomy (19). Therefore, the importance of supportive periodontal care, which was repeatedly highlighted by guidelines in the decision-making process, should be supported by education and experience. In detail, the present findings may also associated with the relatively novel decision-making process of supportive care by including the risk factors to the determination of grade component (20). On the other hand, the responses regarding to surgical periodontal treatment option generally showed high or moderate accuracy. This may be due to the intensive preference of surgical interventions instead of preventive medicine in the country. However, the error tendency was higher in the selection of regenerative/resective periodontal surgery specifically for cases 2,3,8, and 9. This may be related to erroneous diagnosis and/or lack of knowledge in surgical treatment planning (18).

In general, the agreement on the diagnosis was fair amongst all examiners. While it was lower in dental students (DS), periodontal experts (PE) showed better within-group agreement showing the influence of different education and experience levels to the compliance and variations in diagnosis. Consistent with our findings, Marini et al. (11) reported lower accuracy and inter-rater agreement of DS compared to PE in evaluating the stage and grade components of periodontitis. Similar to diagnosis, PE had a higher agreement in treatment planning compared to other participants and except tooth extraction (moderate

agreement), a poor to fair agreement was detected for all treatment modalities amongst the participants. These findings were in line with the relevant studies (12, 21, 22) and might indicate the lack of calibration, education, experience, and up-to-date information amongst the participants showing the necessity of advancement in the training and experience of the participants.

CONCLUSION

Limitations of this study were the small number of examiners and periodontitis cases. Within these limitations, the present findings showed that except the extent component, clinicians still cannot reach a high level of accuracy in periodontitis diagnosis referring to the recent periodontitis classification. Moreover, different education levels and clinical experience that caused high variations do not affect the accuracy of the decision for stage and extent but the grade which seems much more complicated and inconsistent amongst the clinicians. In terms of treatment planning, education level and experience provide differences in making decisions about phase I therapy, tooth extraction and supportive periodontal care. However, on the whole, the results with low accuracy show that the classification could not be implemented to various clinical scenarios and the education level and clinical experience lead to variations in clinical practice. To reduce the variations and enhance the levels of accuracy in classifying and planning the treatment of periodontitis cases, encouraging the use of guidelines and supporting clinical experience with supportive training can be recommended.

Acknowledgments

This study was conducted as thesis of Ceren Kütük in Specialist in Periodontology under the supervision of H. Gencyay Keçeli.

Authorship contributions

Ceren Kütük: Data collection, literature search. Hanife Merva Parlak: Literature search, writing. Ayhan Parmaksız: Analysis. Nermin Tarhan: Concept, design, writing. H. Gencyay Keçeli: Concept, design, writing

Data availability statement

The data are available from the corresponding author.

Declaration of competing interest

The authors report no conflicts of interest related to this study.

Ethics

Permission was obtained from the Ethics Committee of Hacettepe University (GO 21/427) for the study protocol. All participants were informed about the study and signed the informed consent forms.

Funding

No funding was received for this study.

REFERENCES

1. Caton JG, Armitage G, Berglundh T, Chapple ILC, Jepsen S, Kornman KS, et al. A new classification scheme for periodontal and peri-implant diseases and conditions - Introduction and key changes from the 1999 classification. *J Clin Periodontol.* 2018;45 Suppl 20:S1-s8. Epub 2018/06/22. doi: 10.1111/jcpe.12935. PubMed PMID: 29926489.
2. Tonetti MS, Sanz M. Implementation of the new classification of periodontal diseases: Decision-making algorithms for clinical practice and education. *J Clin Periodontol.* 2019;46(4):398-405. Epub 2019/03/19. doi: 10.1111/jcpe.13104. PubMed PMID: 30883878.
3. Tonetti MS, Greenwell H, Kornman KS. Staging and grading of periodontitis: Framework and proposal of a new classification and case definition. *J Clin Periodontol.* 2018;45 Suppl 20:S149-s61. Epub 2018/06/22. doi: 10.1111/jcpe.12945. PubMed PMID: 29926495.
4. Papapanou PN, Sanz M, Buduneli N, Dietrich T, Feres M, Fine DH, et al. Periodontitis: Consensus report of workgroup 2 of the 2017 World Workshop on the Classification of Periodontal and Peri-Implant Diseases and Conditions. *J Clin Periodontol.* 2018;45 Suppl 20:S162-s70. Epub 2018/06/22. doi: 10.1111/jcpe.12946. PubMed PMID: 29926490.
5. Sanz M, Herrera D, Kebschull M, Chapple I, Jepsen S, Berglundh T, et al. Treatment of stage I-III periodontitis-The EFP S3 level clinical practice guideline. *J Clin Periodontol.* 2020;47 Suppl 22(Suppl 22):4-60. Epub 2020/05/10. doi: 10.1111/jcpe.13290. PubMed PMID: 32383274; PubMed Central PMCID: PMC7891343.
6. Herrera D, Sanz M, Kebschull M, Jepsen S, Sculean A, Berglundh T, et al. Treatment of stage IV periodontitis: The EFP S3 level clinical practice guideline. *J Clin Periodontol.* 2022;49 Suppl 24:4-71. Epub 2022/06/11. doi: 10.1111/jcpe.13639. PubMed PMID: 35688447.

7. Ghoneim A, Yu B, Lawrence H, Glogauer M, Shankardass K, Quiñonez C. What influences the clinical decision-making of dentists? A cross-sectional study. *PLoS One*. 2020;15(6):e0233652. Epub 2020/06/06. doi: 10.1371/journal.pone.0233652. PubMed PMID: 32502170; PubMed Central PMCID: PMCPCMC7274387.
8. Hajjaj FM, Salek MS, Basra MK, Finlay AY. Non-clinical influences on clinical decision-making: a major challenge to evidence-based practice. *J R Soc Med*. 2010;103(5):178-87. Epub 2010/05/04. doi: 10.1258/jrsm.2010.100104. PubMed PMID: 20436026; PubMed Central PMCID: PMCPCMC2862069.
9. Grembowski D, Fiset L, Milgrom P, Forrester K, Spadafora A. Factors influencing the appropriateness of restorative dental treatment: an epidemiologic perspective. *J Public Health Dent*. 1997;57(1):19-30. Epub 1997/01/01. doi: 10.1111/j.1752-7325.1997.tb02469.x. PubMed PMID: 9150060.
10. Abrahamian L, Pascual-LaRocca A, Barallat L, Valles C, Herrera D, Sanz M, et al. Intra- and inter-examiner reliability in classifying periodontitis according to the 2018 classification of periodontal diseases. *J Clin Periodontol*. 2022;49(8):732-9. Epub 2022/03/25. doi: 10.1111/jcpe.13618. PubMed PMID: 35322458; PubMed Central PMCID: PMCPCMC9545414.
11. Marini L, Tonetti MS, Nibali L, Rojas MA, Aimetti M, Cairo F, et al. The staging and grading system in defining periodontitis cases: consistency and accuracy amongst periodontal experts, general dentists and undergraduate students. *J Clin Periodontol*. 2021;48(2):205-15. Epub 2020/12/02. doi: 10.1111/jcpe.13406. PubMed PMID: 33260273.
12. Gandhi KK, Katwal D, Chang J, Blanchard S, Shin D, Maupome G, et al. Diagnosis and treatment planning using the 2017 classification of periodontal diseases among three dental schools. *J Dent Educ*. 2022;86(11):1521-8. Epub 2022/06/02. doi: 10.1002/jdd.12964. PubMed PMID: 35644870.
13. Abou-Arraj RV, Kaur M, Alkhoury S, Swain TA, Geurs NC, Souccar NM. The new periodontal disease classification: Level of agreement on diagnoses and treatment planning at various dental education levels. *J Dent Educ*. 2021;85(10):1627-39. Epub 2021/05/07. doi: 10.1002/jdd.12636. PubMed PMID: 33955000.
14. Jayawardena DS, Yates R, West NX, Pollard AJ. Implementing the 2017 Classification of Periodontal and Peri-Implant Diseases - how are we doing in the South West region of the UK? *Br Dent J*. 2021. Epub 2021/12/11. doi: 10.1038/s41415-021-3716-2. PubMed PMID: 34887553.
15. Hamp SE, Nyman S, Lindhe J. Periodontal treatment of multirrooted teeth. Results after 5 years. *J Clin Periodontol*. 1975;2(3):126-35. Epub 1975/08/01. doi: 10.1111/j.1600-051x.1975.tb01734.x. PubMed PMID: 1058213.
16. Miller S. *Textbook of Periodontia* Blakiston Co. Philadelphia, USA. 1950.
17. Landis JR, Koch GG. The measurement of observer agreement for categorical data. *Biometrics*. 1977;33(1):159-74. Epub 1977/03/01. PubMed PMID: 843571.
18. Ravidà A, Travan S, Saleh MHA, Greenwell H, Papapanou PN, Sanz M, et al. Agreement among international periodontal experts using the 2017 World Workshop classification of periodontitis. *J Periodontol*. 2021;92(12):1675-86. Epub 2021/09/22. doi: 10.1002/jper.20-0825. PubMed PMID: 34545953.
19. Guncu GN, Nemli SK, Carrilho E, Yamalik N, Volodina E, Melo P, et al. Clinical Guidelines and Implementation into Daily Dental Practice. *Acta Med Port*. 2018;31(1):12-21. Epub 2018/03/27. doi: 10.20344/amp.8942. PubMed PMID: 29573764.
20. Takedachi M, Shimabukuro Y, Sawada K, Koshimizu M, Shinada K, Asai H, et al. Evaluation of periodontitis-related tooth loss according to the new 2018 classification of periodontitis. *Sci Rep*. 2022;12(1):11893. Epub 2022/07/14. doi: 10.1038/s41598-022-15462-6. PubMed PMID: 35831375; PubMed Central PMCID: PMCPCMC9279363.
21. Lane BA, Luepke P, Chaves E, Maupome G, Eckert GJ, Blanchard S, et al. Assessment of the calibration of periodontal diagnosis and treatment planning among dental students at three dental schools. *J Dent Educ*. 2015;79(1):16-24. Epub 2015/01/13. PubMed PMID: 25576548.
22. John V, Lee SJ, Prakasam S, Eckert GJ, Maupome G. Consensus training: an effective tool to minimize variations in periodontal diagnosis and treatment planning among dental faculty and students. *J Dent Educ*. 2013;77(8):1022-32. Epub 2013/08/10. PubMed PMID: 23929572.

Research Article

IMPACT OF REUSE OF DENTAL IMPLANT ANALOGS ON IMPRESSION ACCURACY

 Sergen DENİZ¹,  Mustafa ZORTUK¹,  Taha Yaşar MANAV^{1*}

¹Department of Prosthodontics, Faculty of Dentistry, Mustafa Kemal University, Antakya, Hatay, Turkey

*Correspondence: tahamanav@gmail.com

ABSTRACT

Objective: This study aimed to examine the impact of repeated use of different implant impression analogs on the accuracy of the resulting impressions.

Materials and Methods: Implant bodies from three brands (Group SA: Straumann, Switzerland; Group DA: Dio Implant, South Korea; and Group MA: Mode Implant, Turkey) were used to create master models. Five reference casts were then fabricated for each brand (n=5) from these master models. Ten impressions were taken from each reference cast using the same analogs, which were sterilized between each impression. Both the reference and working casts were digitized using a three-dimensional scanner. The working casts were aligned with their respective reference casts using software (Geomagic, USA). One-way ANOVA was used to compare the groups, while repeated-measures ANOVA was used to compare the impressions within each group. Multiple comparisons were performed using the Bonferroni, Tukey's HSD, and Tamhane's T2 tests, with significance set at $p < 0.05$.

Results: The RMS value for Group SA was 0.002 mm for the first impression, while the first impression RMS values for the other two groups were 0.04 mm and 0.03 mm, respectively. By the tenth impression, the RMS value for Group SA had increased to 0.08 mm, while the tenth impression RMS values for Groups DA and MA had reached 0.14 mm. Group SA demonstrated statistically significant differences after the third impression, whereas Groups DA and MA exhibited significant differences after the first impression.

Conclusion: The results of this in vitro study demonstrated that repeated use of the same implant impression analog had a negative impact on impression accuracy.

Keywords: Dental implants, Dental prosthesis, Impression technic

Received: 27 November 2024
Revised: 19 January 2025
Accepted: 10 February 2025
Published: 20 March 2025



Copyright: © 2025 by the authors. Published by Aydın Adnan Menderes University, Faculty of Medicine and Faculty of Dentistry. This article is openly accessible under the Creative Commons Attribution-NonCommercial 4.0 International (CC BY-NC 4.0) License.

INTRODUCTION

Dental implant prosthetics represent one of the most rapidly expanding fields of dentistry with a notable impact on patient satisfaction. By expanding the range of possible treatments, these prosthetics have enabled the application of fixed implant-supported restorations in a variety of cases, thereby meeting patients' functional and aesthetic expectations more effectively (1).

When implant-supported fixed restorations are seated on abutments and do not create static loads within the prosthetic system or surrounding bone tissue, this condition is referred to as passive fit. A passive fit represents the optimal compatibility between the implant and prosthetic components. The attainment of passive fit is contingent on the implementation of a meticulous impression procedure (2).

Impressions in implant prosthetics can be obtained using a variety of techniques, which are broadly classified as conventional or digital. Impressions of conventional implants may be performed using either open-tray or closed-tray techniques. Impressions from implants differ from those from natural teeth in that they involve the use of impression copings and analogs, which vary depending on the chosen method and are screwed onto the implants. Impression copings, analogs, and screws connecting these components are critical elements that must be used with precision as they are essential for ensuring the accuracy of conventional implant impressions. The analog serves to replicate the implant embedded within the alveolar bone within the working cast, and remains a constituent part of the cast throughout the prosthetic fabrication process (3). A multitude of variables can affect impression accuracy. In conventional techniques, several factors can influence the accuracy of the impression, including the selected method of impression, modifications to the impression copings, manner of connection of the copings to the analogs, dimensional stability of the gypsum used for cast fabrication, number of implants, angulation of the implants, and depth of the implants (4,5).

Manufacturers recommend that impression copings and analogs be used only once (6). However, owing to concerns regarding the cost and environmental impacts, these components are frequently reused. In light of these considerations, it is imperative to establish evidence-based guidelines for the reuse of impression components rather than relying on clinician preference.

The existing literature contains several studies on the reuse of implant components (7,8). Although studies have

been conducted on the impact of reusing impression copings on impression accuracy, research on the effect of reusing impression analogs remains limited (8,9). The primary aim of this study was to evaluate the effect of the repeated use of impression analogs from three different implant brands on impression accuracy and surface changes, both within and between brands. The null hypothesis of this study was that the repeated use of impression analogs has no effect on impression accuracy.

MATERIALS AND METHODS

The objective of this study was to assess the influence of the repeated use of implant analogs on the accuracy of impressions. The present study was approved by the Hatay Mustafa Kemal University Non-Interventional Clinical Research Ethics Committee (Approval date: April 14, 2022; decision number: 34).

Three master models were prepared for the three different implant brands to simulate an intraoral scenario with a missing maxillary first molar (tooth #16). To this end, tooth #16 regions were removed from the maxillary models (Frasaco Study Model ANA 4; Frasco GmbH, Germany). Implant bodies from three different brands (Straumann 4.1 mm Bone Level, Dio UFII 4.5 mm Bone Level, Mode 4.5 mm Bone Level) were placed in the respective models with the aid of a parallelometer to ensure accurate positioning (Table 1). The implants were positioned within the sockets of tooth #16 until the implant neck was reached and then stabilized with cold acrylic resin (Integra, United Dental Group, Turkey). This process resulted in the creation of three maxillary models, which were divided into three groups. The resulting groups were designated as Group SA, Group DA, and Group MA.

Table 1. Details of dental implant analogs

Groups	Product	Reference Number	Material	Brand
Group SA	RC Bone Level Implant Analog	025.4101	Titanium Alloy (Ti-6Al-7Nb)	Straumann, Straumann Group
Group DA	UFII Fixture Analog Regular	SSFA4012	Titanium	Dio Implant, Dio Implant Co.
Group MA	Analog RP	08.00.00.35	Stainless steel-Cobalt alloy	Mode Implant, Mode Medikal

For each group, five reference casts were produced using a conventional impression technique with A-type silicone material (Zhermack Hydrorise, Italy). The reference casts

were digitized using an intraoral digital scanner (YouJoy Pioneering Park C, China) and saved in STL format for subsequent analysis.

Subsequently, repeated impressions were obtained from each reference cast until 10 working casts were obtained for each reference cast. Similarly, impressions were obtained using an A-type silicone material (Zhermack Hydrorise, Italy). To ensure accurate implant analog connections, a gingival simulator (Gingifast Rigid; Zhermack, Italy) was applied to the implant-level impressions to create a precise replica of the gingival margin. Subsequently, the impressions were poured with Type 4 gypsum (Elite Rock, Zhermack, Italy) to fabricate the working casts, which were then digitized and exported in the STL format.

For reuse, the implant analogs were meticulously extracted from the gypsum casts using a mechanical breaking device (GERATECH Landmaschinen GmbH, Thuringia, Germany). The analogs were manually cleaned for a period of two minutes using a soft nylon brush. Subsequently, the implant analogs were sterilized in an autoclave (Sumer Inc., Turkey) at 134°C for ten minutes, followed by a fifteen-minute drying process. The same implant analogs were utilized for subsequent impressions, although new impression copings and screws were used. This procedure was repeated ten times for each reference cast, resulting in a total of 50 working casts per group.

Digital working and reference casts were analyzed using Geomagic Control X software (Geomagic, USA). Prior to undertaking three-dimensional analyses, the reference casts for each group were aligned with their corresponding working casts using the "best fit alignment" feature of the software. The color-mapping feature of the software was employed to visualize the deviations between the aligned casts, with variations represented by a defined scale. Green areas indicated minimal deviations, while blue and red areas represented positive and negative deviations, respectively. Positive deviations (blue areas) indicated that the working cast was larger than the reference cast, whereas negative deviations (red areas) indicated narrower regions. These deviations were comparable to the expansion and shrinkage observed in conventional impressions.

Deviation thresholds were defined in accordance with the standards set forth by the American Dental Association (ADA) for elastomeric impression materials (Standard No. 19) (10). Green areas were regarded as acceptable, with deviations of $\pm 20 \mu\text{m}$, whereas blue and red areas were classified as deviations of $\pm 100 \mu\text{m}$. The software

automatically calculated the three-dimensional displacements between scanned points using the Root Mean Square (RMS) value, which represents the square root of the mean squared deviation (Figure 1).

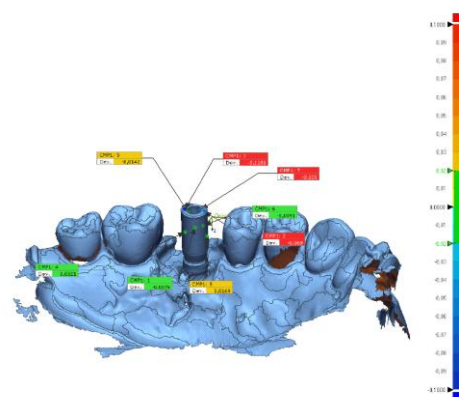


Figure 1. Calculation of RMS value by comparing 3D discrepancies between analogs in two casts by using software.

Statistical analyses were conducted using SPSS software (SPSS v23, IBM, USA). Comparison of RMS values based on impression order was performed using repeated-measures analysis of variance (ANOVA), while one-way analysis of variance (ANOVA) was used for comparisons of RMS values between groups. Post-hoc comparisons were performed using Bonferroni, Tukey's HSD, and Tamhane's T2 tests. Statistical significance was set at $p < 0.05$.

RESULTS

In each group, five root mean square (RMS) values were obtained for each impression order. The mean RMS values in millimeters for each group are presented in Table 2. Statistical analysis was conducted to examine the differences in RMS values across impression orders and between the groups. Comparisons between impression orders are presented in Table 2, and comparisons between groups are presented in Table 3. Additionally, the calculated RMS values are visually represented in Figure 2.

For Group SA, there was a statistically significant difference in the mean root-mean-square (RMS) values across impression order ($p < 0.001$). The first three impressions showed significant differences when compared with the 8th, 9th, and 10th impressions.

For Group DA, the mean RMS values showed a significant difference across impression order ($p < 0.001$). In particular, the first impression showed a statistically significant difference from all subsequent impressions, and a similar pattern was observed for the second impression. The third impression exhibited similarities to the fifth impression only. Moreover, while the fourth impression exhibited similarities to the fifth impression, it demonstrated significant differences from all other impressions.

Table 2. Comparison of calculated mean RMS (mm) values according to the impression order.

Imp Order	Group SA	Group DA	Group MA
Imp1	0.002±0.001 ^{cd}	0.043±0.016 ^e	0.033±0.017 ^f
Imp2	0.003±0.001 ^{cd}	0.054±0.015 ^f	0.055±0.017 ^e
Imp3	0.008±0.002 ^{cd}	0.064±0.015 ^e	0.065±0.016 ^d
Imp4	0.033±0.016 ^d	0.076±0.017 ^d	0.074±0.016 ^c
Imp5	0.045±0.016 ^c	0.088±0.023 ^{cde}	0.082±0.015 ^c
Imp6	0.044±0.016 ^c	0.105±0.015 ^c	0.104±0.035 ^{abcdef}
Imp7	0.055±0.017 ^{bc}	0.115±0.016 ^{bc}	0.106±0.046 ^{abcdef}
Imp8	0.064±0.015 ^b	0.124±0.016 ^b	0.124±0.016 ^b
Imp9	0.074±0.017 ^a	0.134±0.013 ^{ab}	0.133±0.015 ^b
Imp10	0.084±0.015 ^a	0.141±0.015 ^a	0.145±0.014 ^a
Test	81.646	519.591	3.155
Statistics*			
p	<0.001	<0.001	0.007

Imp: Impression; a-f: No statistical difference between measurements with the same letter within each group; *Repeated Measures ANOVA

For Group MA, the mean root-mean-square (RMS) values showed significant differences across impression order ($p < 0.001$). However, no significant differences were observed between the fourth and fifth impressions, sixth and seventh impressions, or eighth and ninth impressions.

A comparison of the groups showed that Group SA consistently exhibited more accurate results, with lower deviations than the other two groups for all repeated impressions, except for the sixth impression. No statistically significant differences were observed between the Groups DA and MA.

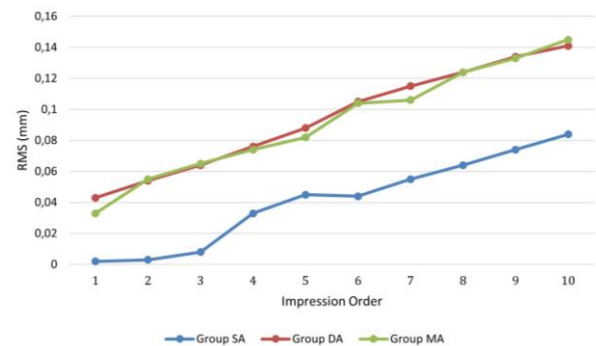
Upon examination of the data regarding the repeated use of analogs, Group SA demonstrated no statistically significant differences in the root-mean-square (RMS) values during the initial three impressions. However, a notable increase in RMS values was observed from the fourth impression onwards, and this increase was statistically significant. In contrast, both Groups DA and MA exhibited a significant increase in RMS values from the first impression, with this increase remaining statistically significant throughout the impression order.

Table 3. Calculated mean RMS (mm) values comparison between groups.

Imp Order	Group SA	Group DA	Group MA	Test Statistics*	P
Imp1	0.002 ±0.001 ^a	0.043 ±0.016 ^b	0.033 ±0.017 ^b	12.380	0.001
Imp2	0.003 ±0.001 ^a	0.054 ±0.015 ^b	0.055 ±0.017 ^b	24.107	<0.001
Imp3	0.008 ±0.002 ^a	0.064 ±0.015 ^b	0.065 ±0.016 ^b	52.427	<0.001
Imp4	0.033 ±0.016 ^a	0.076 ±0.017 ^b	0.074 ±0.016 ^b	10.238	0.003
Imp5	0.045 ±0.016 ^a	0.088 ±0.023 ^b	0.082 ±0.015 ^b	8.168	0.006
Imp6	0.044 ±0.016 ^a	0.105 ±0.015 ^b	0.104 ±0.035 ^b	10.359	0.002
Imp7	0.055 ±0.017 ^a	0.115 ±0.016 ^a	0.106 ±0.046 ^a	3.194	0.077
Imp8	0.064 ±0.015 ^a	0.124 ±0.016 ^b	0.124 ±0.016 ^b	22.586	<0.001
Imp9	0.074 ±0.017 ^a	0.134 ±0.013 ^b	0.133 ±0.015 ^b	24.622	<0.001
Imp10	0.084 ±0.015 ^a	0.141 ±0.015 ^b	0.145 ±0.014 ^b	26.632	<0.001

Imp: Impression; a-b: No statistical difference between measurements with the same letter. *One-way ANOVA

Figure 2. Graphical representation of mean RMS values



DISCUSSION

The findings revealed statistically significant differences among repeated impressions for all three groups ($p < 0.05$). These findings indicate that repeated use of implant analogs affects impression accuracy and therefore leads to rejection of the null hypothesis.

Coordinate measuring machines (CMMs) are among the most used methods in the literature for mechanical evaluation; however, they have certain disadvantages. These include challenges associated with calibration and difficulties in consistently measuring the same point

across repeated evaluations (10,11). Accordingly, research indicates that virtual measurements may offer greater reliability than their mechanical counterparts (10,11). In this study, digital measurement methods were employed to obtain more precise and repeatable results. Additionally, studies employing digital measurement methods can be found in the literature (12).

The results revealed significant differences in RMS values for Group SA after the third impression, whereas significant differences were observed starting from the first impression for the remaining two groups. It was found that repeated impression-taking, cast fabrication, and sterilization procedures affect the accuracy of implant impressions. Cleaning and sterilization processes have the potential to induce thermal and chemical stress on materials, which may result in changes in their surface morphology (13). Several studies have examined the impact of sterilization on reusable medical devices, with some indicating that morphological changes resulting from sterilization processes may affect clinical outcomes (14,15). For example, Yang et al. (15) determined that intra-aortic balloons could not be reused because of structural surface changes resulting from cleaning and sterilization processes. Furthermore, the reuse of balloon catheters has been linked to a decline in their mechanical properties (14). Conversely, other studies indicated that sterilization does not affect the clinical performance of specific medical devices. Gorokhovskiy et al. (16) discovered that sterilization had no adverse effects on the clinical efficacy of stainless steel curettes. Similarly, Pernier et al. (17) reported that although autoclave sterilization caused a slight increase in surface roughness of orthodontic wires, it did not compromise their mechanical properties or clinical performance. Moreover, a study examining the influence of sterilization on the accuracy of impression copings and analogs revealed that sterilization did not affect impression accuracy (18). However, the findings of our study are not consistent with this conclusion, as it was determined that repeated impression-taking and sterilization stages exerted an influence on impression accuracy. The factors that may be responsible for this include damage incurred during the removal of the analog from the gypsum cast or deformation caused by repeated loosening and tightening of the screws.

It is possible that the screws used to secure impression copings to the analogs may have contributed to the observed deviations. It is possible that the increased deviations observed in this study may be attributed to deformation in the threads of the analog's screw receptacle, potentially resulting from repeated tightening. In a related study, Laskar et al. (19) examined the threads of implant

analog screws made from different materials after repeated use and found significant wear, particularly in the screw threads. Yalavarthy et al. (7) advised that titanium implant analog screws should not be reused more than six times. In this study, new impression copings and screws were used for each impression. Nevertheless, analogous deformation may have occurred in the screw threads within the analogs. The occurrence of wear and damage at connection points represents a significant challenge for the accuracy of conventional impression techniques.

Another potential cause of analog non-reusability is damage incurred during the removal of the analog from the gypsum cast. When the connection region between the impression coping and the analog is damaged, it becomes impossible to accurately transfer the implant position to the impression. To ensure consistency, an industrial breaking device was employed in this study to remove the analogs, and all procedures were conducted by a single operator. Notwithstanding the implementation of standardization procedures and the utilization of automated devices, deviations were still discernible in the impressions. Given that in routine clinical workflows, the manual removal of analogs is standard practice and standardization is not maintained, the possibility of analog deformation increases.

Implant analogs are manufactured from various metal alloys, including stainless steel, aluminum, and titanium, depending on the implant system. The resistance of these alloys to changes during sterilization and reuse varies (20). In this study, Group SA analogs were composed of a titanium alloy (Ti-6Al-7Nb, TAN), Group DA analogs were made of titanium, and Group MA analogs were composed of a stainless steel-cobalt alloy. The discrepancies in accuracy observed among the groups may be attributed to variations in material composition. The TAN alloy exhibited superior corrosion resistance compared with grade 5 titanium and stainless steel (21). Additionally, the TAN alloy exhibited the lowest corrosion behavior among the titanium alloys and was therefore considered the most suitable for biomedical applications among the materials compared (22). This superior resistance may have resulted in less wear during the sterilization and removal processes, thereby explaining the higher accuracy and reduced deviations in repeated use observed for Group SA.

The literature contains an ongoing debate regarding the acceptability of deviations in impressions. Ma et al. (23) introduced the concept of "machining tolerance," which refers to the inherent inconsistency in implant impressions

due to the spatial relationships between metal components. The tolerances for these impressions ranged from 22 μm to 100 μm . Discrepancies in implant components may be attributed to the manufacturing process. Nevertheless, Assunção et al. (24) proposed that deviations of up to 50 μm along any axis might be acceptable for well-made impressions. Some studies have utilized this threshold for the interpretation of their findings (25). In a review of 41 studies on impression accuracy, Lee et al.(5) reported that clinically acceptable deviations ranged from 0.6 to 136 μm . Consequently, there is no consensus in the literature regarding the definition of a clinically acceptable level of deviation. Even when the upper limit of 136 μm was used as a reference, only Group SA permitted up to 10 repeated impressions with the same analog. Given the limited literature on the reuse of analogs, further research is required.

A limitation of this study is the reliance on root-mean-square (RMS) values to evaluate the accuracy of impressions. While RMS provides a measure of overall three-dimensional accuracy, it does not offer detailed data on coronal, angular, or rotational deviations. Additionally, this study was conducted in vitro, and therefore factors such as the effects of saliva, temperature, and soft tissue on impression materials, as well as conditions specific to the oral cavity, were not simulated.

CONCLUSION

Considering the limitations of this study, the following conclusions were drawn:

Statistically, Group SA analogs can be reused up to three times, whereas analogs from the other groups should ideally be used only once.

Given the lack of consensus in the literature on clinically acceptable deviation thresholds and the fact that the analogs were removed by breaking the casts, the reuse of impression analogs carries inherent risk.

Acknowledgments

None

Authorship contributions

Sergen Deniz contributed to the concept, design, data collection, analysis, literature search, and writing. Mustafa Zortuk contributed to the concept, design, and writing. Taha Yasar Manav contributed to the literature search and writing.

Data availability statement

The datasets analyzed during the current study are available from the corresponding author on reasonable request.

Declaration of competing interest

The authors declare no conflict of interest related to this study.

Ethics

This study was approved by the Hatay Mustafa Kemal University Non-Interventional Clinical Research Ethics Committee with the decision dated 14.04.2022 and numbered 04/34.

Funding

This research was not funded by any organization.

REFERENCES

1. Wang Y, Bäumer D, Ozga AK, Körner G, Bäumer A. Patient satisfaction and oral health-related quality of life 10 years after implant placement. *BMC Oral Health*. 2021 Dec;21(1):30.
2. Katsoulis J, Takeichi T, Sol Gaviria A, Peter L, Katsoulis K. Misfit of implant prostheses and its impact on clinical outcomes. Definition, assessment and a systematic review of the literature. *Eur J Oral Implant*. 2017;10(Suppl 1):121–38.
3. Moreira AHJ, Rodrigues NF, Pinho ACM, Fonseca JC, Vilaça JL. Accuracy Comparison of Implant Impression Techniques: A Systematic Review. *Clin Implant Dent Relat Res* [Internet]. 2015 Oct [cited 2024 Oct 31];17(S2). Available from: <https://onlinelibrary.wiley.com/doi/10.1111/cid.12310>
4. Wee AG. Comparison of impression materials for direct multi-implant impressions. *J Prosthet Dent*. 2000;83(3):323–31.
5. Lee H, So JS, Hochstedler JL, Ercoli C. The accuracy of implant impressions: a systematic review. *J Prosthet Dent*. 2008;100(4):285–91.
6. Straumann. Instructions for Use: Straumann Impression Components [Internet]. 2024 [cited 2024 Oct 31]. Available from: <https://ifu.straumann.com/STMN/GB/STMNPortfolio?keycode=7630031746719>
7. Yalavarthy R, Alla J, Kalluri S, Mahadevan S, Kumar S, Ronanki S. Effect of multiple reuse of commonly used implant

- analog on the changes in the distance between internal threads: An in vitro study. *J Indian Prosthodont Soc.* 2022;22(1):48.
8. Hashemi AM, Hasanzadeh M, Payaminia L, Alikhasi M. Effect of Repeated Use of Different Types of Scan Bodies on Transfer Accuracy of Implant Position. *J Dent.* 2023 Dec 1;24(4):410–6.
 9. Sawyers J, Baig M, ElMasoud B. Effect of Multiple Use of Impression Copings and Scanbodies on Implant Cast Accuracy. *Int J Oral Maxillofac Implants.* 2019 Jul;34(4):891–8.
 10. Mangano FG, Veronesi G, Hauschild U, Mijiritsky E, Mangano C. Trueness and precision of four intraoral scanners in oral implantology: a comparative in vitro study. *PLoS One.* 2016;11(9):e0163107.
 11. Jemt T, Hjalmarsson L. In Vitro Measurements of Precision of Fit of Implant - Supported Frameworks. A Comparison between “Virtual” and “Physical” Assessments of Fit Using Two Different Techniques of Measurements. *Clin Implant Dent Relat Res [Internet].* 2012 May [cited 2024 Oct 19];14(s1). Available from: <https://onlinelibrary.wiley.com/doi/10.1111/j.1708-8208.2011.00416.x>
 12. Amin S, Weber HP, Finkelman M, El Rafie K, Kudara Y, Paspaspyridakos P. Digital vs. conventional full - arch implant impressions: a comparative study. *Clin Oral Implants Res.* 2017 Nov;28(11):1360–7.
 13. Younis O. The effects of sterilization techniques on the properties of intracanal instruments. *Oral Surg Oral Med Oral Pathol.* 1977;43(1):130–4.
 14. Unverdorben M, Quaden R, Werner C, Bloss P, Degenhardt R, Ackermann H, et al. Change of the mechanical properties of two different balloon catheters with increasing numbers of cycles of reesterilization. *Catheter Cardiovasc Interv.* 2003 Jan;58(1):29–33.
 15. Yang M, Deng X, Zhang Z, Julien M, Pelletier F, Desaulniers D, et al. Are intraaortic balloons suitable for reuse? A survey study of 112 used intraaortic balloons. *Artif Organs.* 1997;21(2):121–30.
 16. Gorokhovskiy V, Heckerman B, Watson P, Bekesch N. The effect of multilayer filtered arc coatings on mechanical properties, corrosion resistance and performance of periodontal dental instruments. *Surf Coat Technol.* 2006;200(18–19):5614–30.
 17. Pernier C, Grosgeat B, Ponsonnet L, Benay G, Lissac M. Influence of autoclave sterilization on the surface parameters and mechanical properties of six orthodontic wires. *Eur J Orthod.* 2005;27(1):72–81.
 18. Aldosari AAM. Does Steam Autoclaving Affect the Accuracy of Implant Impression Systems? *J Biomater Tissue Eng.* 2014 Jul 1;4(7):550–4.
 19. Laskar P, Mansuri AH, Patel S, Kewalramani C, Sutradhar W, Karpathak S, et al. Alterations in internal threads of implant analog of different materials after multiple reuse. *Bioinformatics.* 2024 Jun 30;20(6):695–9.
 20. Junker B. Corrosion in bioprocessing applications. *Bioprocess Biosyst Eng.* 2009;32:1–29.
 21. Tamilselvi S, Raman V, Rajendran N. Corrosion behaviour of Ti–6Al–7Nb and Ti–6Al–4V ELI alloys in the simulated body fluid solution by electrochemical impedance spectroscopy. *Electrochimica Acta.* 2006 Nov 12;52(3):839–46.
 22. López MF, Jiménez JA, Gutiérrez A. Corrosion study of surface-modified vanadium-free titanium alloys. *Electrochimica Acta.* 2003 Apr;48(10):1395–401.
 23. Ma T, Nicholls JI, Rubenstein JE. Tolerance measurements of various implant components. *Int J Oral Maxillofac Implants.* 1997;12(3).
 24. Assuncao WG, Gennari Filho H, Zaniquelli O. Evaluation of transfer impressions for osseointegrated implants at various angulations. *Implant Dent.* 2004;13(4):358–66.
 25. Richi MW, Kurtulmus-Yilmaz S, Ozan O. Comparison of the accuracy of different impression procedures in case of multiple and angulated implants: Accuracy of impressions in multiple and angulated implants. *Head Face Med.* 2020 Dec;16(1):9.

Research Article

FACTORS AFFECTING ARTERIAL STIFFNESS LEVEL IN CANCER PATIENTS RECEIVING IMMUNOTHERAPY

 Emine Esra Güner Yıldırım ¹,  Merve Bıyıklı Alemdar ²,  Bilgin Demir ²,  Merve Turan ²,
 Esin Oktay ^{2*}

¹Department of Internal Medicine, Ataturk State Hospital, Aydın, Turkey

²Department of Medical Oncology, Adnan Menderes University Faculty of Medicine, Aydın, Turkey

*Correspondence: esinct@gmail.com

ABSTRACT

Objective: This study aimed to investigate the factors affecting arterial stiffness in cancer patients receiving immunotherapy.

Materials and Methods: The height, weight, body mass index (BMI), age, sex, type of cancer, previous cancer treatment, agents used in the treatment, current immunotherapy agents, comorbid conditions, smoking history of 42 patients diagnosed with renal cell carcinoma (RCC), lung cancer, malignant melanoma and receiving immunotherapy treatment were recorded at the time of their first application and their arterial stiffness levels were measured. Following the first measurement, the patients were observed again in the third and sixth therapy cycles and their measurements were repeated and recorded. Factors affecting the arterial stiffness level of the patients were evaluated.

Results: Pulse wave velocity (PWV) increased with increased age ($p<0.01$). No significant difference was found between cancer type and PWV; however, patients with lung cancer had higher pulse pressure at the first measurement than other patients. No significant difference was found between immunotherapy agents and PWV. The PWV was found to be significantly higher in patients those with concomitant diseases ($p<0.005$). Pulse pressure was found to be higher in smokers than in non-smokers ($p<0.007$).

Conclusion: Smoking, sex and cancer type were effective in changing of pulse pressure in cancer patients receiving immunotherapy, and there was no significant difference in other factors; PWV increased with age; and that PWV was higher in those with additional diseases.

Keywords: Arterial stiffness, immunotherapy, cancer.

Received: 01 December 2024

Revised: 08 January 2025

Accepted: 15 January 2025

Published: 20 March 2025



Copyright: © 2025 by the authors. Published by Aydın Adnan Menderes University, Faculty of Medicine and Faculty of Dentistry. This article is openly accessible under the Creative Commons Attribution-NonCommercial 4.0 International (CC BY-NC 4.0) License.

INTRODUCTION

Immunotherapy has become the standard treatment for cancer in recent years. Immunotherapies aim to prevent tumor cells from escaping the immune system by activating inhibitory signals at the immune control points of tumor cells (1). Especially renal cell carcinoma (RCC), malignant melanoma, head and neck cancers and lung cancer are cancers that benefit the most from immunotherapy treatment (2).

Cardiovascular disease (CVD) is a cause of mortality and morbidity in humans. Since cardiovascular events are significantly seen in people without risk factors, studies have been conducted to find various factors that can detect the development of atherosclerosis at an early stage, independent of known risk factors. Thus, has the concept of arterial stiffness emerged to assess the integrity of the arterial structure (3).

The patient's age, hypertension (HT), smoking, dyslipidemia, diabetes mellitus (DM), obesity and systemic inflammation are risk factors for atherosclerosis and increased vascular stiffness. Arterial stiffness, which occurs as a result of thickening of the arterial wall and loss of elasticity, has become an indicator of atherosclerosis (4). In hypertensive patients with renal failure and patients with coronary artery disease (CAD), arterial stiffness is a marker of morbidity (infarction, fatal stroke) and cardiovascular mortality. Cardiovascular toxicity is a cause of early morbidity and mortality after treatment with chemotherapeutic agents in cancer patients. Arterial stiffness can be used as a marker to predict subclinical cardiovascular damage (5).

The aim of our study is to investigate the factors affecting the level of arterial stiffness in cancer patients receiving immunotherapy in our clinic. There are no publications in the literature regarding the investigation of factors affecting arterial stiffness levels in patients who have previously received immunotherapy.

MATERIALS AND METHODS

This study was conducted prospectively by obtaining informed voluntary consent forms from 42 patients aged between 18-80 years who were diagnosed with malignant melanoma, lung cancer, RCC and received immunotherapy treatment and who applied to Adnan Menderes University Faculty of Medicine Medical Oncology Clinic between 01.06.2021 and 01.06.2022.

At the time of the first application, weight, height, age, BMI, sex, type of cancer, previous treatment received for cancer, agents used in the treatment received, current immunotherapy agents used, comorbid conditions, smoking history of the patients receiving immunotherapy were recorded and arterial stiffness levels were measured.

The effects of these factors on arterial stiffness were evaluated. BMI was calculated for the patients whose height and weight were measured using the weight (kg) / height² (m²) formula. The patients' smoking status was evaluated as "smoker-nonsmoker" and their comorbidity status was evaluated as "additional disease-no additional disease" and recorded. This disease was also recorded in those with additional diseases.

Following the first measurement, the patients were seen again in the third and sixth cycles, and their measurements were repeated and recorded. The measured data of the patients including pulse wave velocity (PWV), augmentation index (AIx), diastolic blood pressure (mmHg), systolic blood pressure (mmHg), mean arterial pressure (mmHg), heart rate (minute), pulse pressure (mmHg), stroke volume (ml), cardiac output (l/min), peripheral resistance (s*mmHg/ml), cardiac index (l/min*1/m²), reflection magnitude (%), augmentation pressure (mmHg), were recorded using the brachial cuff based oscillometric device Mobil-OGraph (IEM, Stolberg, Germany) and HMS CS (Hypertension Management System Client Server) software system.

Statistical analysis

The IBM-SPSS Statistics 23 program was used for statistical analysis. Descriptive statistics were presented as numbers and percentages for categorical variables and as mean, standard deviation, median, minimum and maximum for numerical variables. For numerical variables, ANOVA Test was used in multiple independent group comparisons when the normal distribution assumption was met; T Test was used in pairwise independent group comparisons when the normal distribution assumption was met. Pearson test was used for correlations where normal distribution was achieved in the association between numerical data. General Linear Model Test was used to reveal the effect of the independent variable on the dependent variable. The statistical significance was set at p value less than 0.05.

RESULTS

Demographics of the subjects are summarized in Table 1; age, height, weight, BMI values are summarized in Table

Table 1. Demographics of the subjects

		N (%)
Age	65 years old>	22 (52.3)
	65 years old≤	20 (47.7)
Sex	Male	35 (83.3)
	Female	7 (16.7)
Smoking	Smoker	30 (71.4)
	Non-smoker	12 (28.6)
BMI	<30	37 (88.1)
	≥30	5 (11.9)
Cancer type	RCC	6 (14.3)
	Malignant melanoma	9 (21.4)
	Lung cancer	27 (64.3)
Immunotherapeutic agent	Nivolumab	41 (97.6)
	Pembrolizumab	1 (2.4)
Additional disease	No	18 (42.9)
	Yes	24 (66.1)
CT (Cancer treatment)	Received	30 (71.4)
	Not received	12 (28.6)
Tyrosine kinase inhibitor	Received	8 (19.0)
	Not received	34 (81.0)

2. Comparative evaluation of patient data is shown in Table 3. For each given parameter, the 1st measurement value, 2nd measurement value, and 3rd measurement value of the patients were recorded and no significant difference was found between the measurements.

Table 2: Age, height, weight, BMI values of the subjects

	Mean	Median	SD	Minimum	Maximum
Age	63.79	66.00	9.37	35.00	80.00
Height (cm)	168.81	168.50	9.20	145.00	185.00
Weight (kg)	72.33	70.00	15.27	52.00	110.00
BMI (kg/m²)	25.43	24.95	5.44	16.40	45.20

Table 4 summarizes the changes in pulse pressure measurements according to sex, smoking status and cancer type. When the pulse pressure of women was examined, it was found to be higher than that of men in the first measurement ($p= 0.009$). When the pulse pressures of smokers and non-smokers were compared, it was seen that the pulse pressure of smokers was higher

($p=0.007$). While no significant difference was found when PWV measurements were compared according to cancer type in the study, a significant difference was found when pulse pressures were examined according to cancer type ($p=0.026$). At the first measurement, the pulse pressure of patients with lung cancer was higher than that of patients with malignant melanoma and RCC. No correlation was found between the patients' BMI and PWV measurements (Table 5). However, when looking at age, it was seen that there was an increase in PWV as age increased (1st Measurement $r:0.900$, 2nd Measurement $r:0.909$ 3rd Measurement $r:0,907$; all measurements $p<0.01$). As seen in Table 6, PWH of those with and without additional diseases were compared. PWV was higher in patients with additional diseases. However, when PWV was examined among patients with HT, DM, or CAD, no significant difference was found in PWV between the diseases.

DISCUSSION

In our study, we investigated the factors affecting the level of arterial stiffness in cancer patients who received immunotherapy as oncological treatment in our clinic. There are no publications in the literature regarding the investigation of factors affecting arterial stiffness in patients who have previously received immunotherapy.

Table 3: Comparative evaluation of patient data

n:42	1st measurement (mean±SD)	2nd measurement (mean±SD)	3rd measurement (mean±SD)	p
Systole (mmHg)	119.10±19.55	114.98±15.95	115.95±17.71	0.568
Diastole (mmHg)	77.98±13.36	75.17±12.91	75.64±75.64	0.990
MAP (Mean arterial pressure) (mmHg)	91.83±23.03	93.81±12.78	94.14±14.08	0.994
Pulse pressure (mmHg)	41.12±12.25	39.10±10.13	40.31±10.90	0.323
Pulse (1/min.)	76.86±14.50	75.24±14.57	75.02±15.35	0.848
Stroke volume (ml)	63.31±14.57	63.85±14.12	64.14±13.35	0.298
Cardiac output (L/min)	4.70±0.63	4.68±0.82	4.67±0.77	0.135
Environmental resistance	1.24±0.20	1.23±0.20	1.23±0.19	0.308
Cardiac index	2.59±0.46	2.58±0.59	2.60±0.57	0.198
PWV	9.01±1.54	8.94±1.39	8.91±1.43	0.636
Augmentation pressure	8.37±5.88	7.83±4.79	11.52±9.52	0.073
Reflection magnitude	59.30±11.33	60.16±8.56	62.50±11.04	0.104
Alx	23.11±12.33	22.00±11.37	22.92±12.45	0.117

Table 4: Change in pulse pressure measurement according to sex, smoking status and cancer type

	1st measurement (mean±SD)	3rd measurement (mean±SD)	p
SEX			
Male (n:35)	40.94±13.16	40.40±11.01	0.009
Female (n:7)	42.00±6.60	39.86±11.15	
SMOKING			
Smoker (n:30)	42.27±13.81	41.03±11.40	0.007
Non-smoker (n:12)	38.25±6.67	38.50±9.77	
CANCER TYPE			
Malignant melanoma (n:9)	39.00±7.29	41.11±10.37	0.026
RCC (n:6)	40.00±9.35	38.67±8.80	
Lung cancer (n:27)	42.07±14.17	40.41±11.77	

Table 5: Correlation between age, BMI and PWV measurements

	1st PWV	2nd PWV	3rd PWV
AGE			
r	0.900	0.909	0.907
p	<0.01	<0.01	<0.01
BMI			
r	0.032	0.088	-0.013
p	0.839	0.978	0.935

Table 6: PWV measurement of those with and without additional diseases

	1st measurement (mean±SD)	2nd measurement (mean±SD)	3rd measurement (mean±SD)
ADDITIONAL DISEASE			
With additional disease (n:24)	9.50±1.26	9.45±1.13	9.38±1.15
Without additional disease (n:18)	8.36±1.67	8.26±1.43	8.27±1.56
p	0.016	0.004	0.011

breast cancer patients and control group patients, it was found that the mean pulse wave velocity was higher in breast cancer patients. Pulse wave velocity was significantly higher in patients taking aromatase inhibitors (5).

In the study conducted by Visvikis et al., in which 70 colorectal cancer patients receiving adjuvant FOLFOX/XELOX treatment were included, cardiovascular evaluation was performed at the beginning and end of chemotherapy. Carotid-radial PWV, carotid-femoral PWV and AIx were found to be significantly higher in patients after chemotherapy ($p < 0.001$). These results were found to be significant when examined separately in each treatment subgroup. (6).

In our study, PWV was measured in patient with RCC, malignant melanoma and lung cancer patients receiving immunotherapy. No difference was found in terms of PWV among cancer types. No significant difference was found between the immunotherapy agent used and PWV. In the study conducted by Novo et al. to evaluate the subclinical vascular effects of anthracyclines and trastuzumab (TRZ), it was observed that in patients treated with anthracycline-containing chemotherapy, arterial stiffness indices increased significantly at 3 months, but not at 6 or 12 months, when anthracycline treatment was discontinued and patients were under treatment with taxanes and TRZ. There was no significant change in blood pressure values during follow-up. Changes in arterial stiffness parameters in patients occur immediately after initiation of anthracycline therapy and are thought to be reversible when anthracycline therapy is discontinued. (7).

In our study, the patients' parameters were measured and evaluated at the beginning of the immunotherapy treatment and in the 3rd and 6th cycles. No significant difference was found between immunotherapy agents and PWV measurements. The effects of immunotherapy agents (nivolumab, pembrolizumab) on arterial stiffness have not yet been demonstrated.

In a review by Smulyan et al., mean systolic blood pressure was found to be lower in women than in men. However, systolic blood pressure increased linearly and significantly with age in both men and women. Regarding diastolic blood pressure, lower values were found in women than in men, and there was a significant increase in this parameter with age. In the same study, when PWV was examined in diabetics and non-diabetics, it was significantly higher in diabetics than in non-diabetics (8).

In our study, there was no significant difference in both systolic blood pressure and diastolic blood pressure between men and women. No significant difference was found when PWV was examined between diabetic and non-diabetic patients.

In the study conducted by Demir et al. including 110 patients diagnosed with Type 2 DM without a history of coronary artery disease, PWV values were found to be higher in those receiving antihypertensive treatment. In the same study, no statistically significant difference was found between BMI and PWV (9). In the study conducted by Theilade et al., PWV was found to be statistically significantly higher in patients with a history of coronary artery disease than in patients without coronary artery disease ($p < 0.001$) (10). In the study conducted by Dahlen et al., a statistically significant positive correlation was found between PWV and BMI ($p = 0.001$; $r = 0.127$; $r = 0.175$, respectively) (11). In the study by Evans et al. examining a cohort of patients meeting the criteria for stage 3 chronic kidney disease, a statistically significant negative association was found between BMI and PWV ($p < 0.001$) (12).

In our study, PWV was higher in patients with additional diseases such as HT, DM and CAD than in those without. However, when PWV was examined among patients with any of HT, DM, or CAD, no significant difference was found between the diseases. In our study, similar to the study by Demir et al., no statistically significant difference was found between BMI and PWV.

A review by Dupont et al also found that women had greater increases in pulse pressure and wave reflection compared with men of the same age (13). In our study, when we looked at pulse pressure, pulse pressure was higher in women than in men. When PWV was examined, no significant difference was found in PWV when men and women were compared. However, an increase in PWV was also detected as age increased.

In a comparative study by Rehill et al. of AIx and PWV measured in smokers and the period after these patients quit smoking, AIx was significantly higher in smokers.

However, there was no significant difference in PWV (14). In our study, there was no significant difference in PWV measurement between smokers/nonsmokers; there was no significant difference in AIx measured in smokers/nonsmokers. In our study, pulse pressure was higher in smokers than in nonsmokers.

CONCLUSION

In conclusion, our study, it was found that smoking, sex and cancer type had an effect on pulse pressure changes in cancer patients receiving immunotherapy, that there was no significant difference in other factors; PWV increased with age; and PWV was higher in those with additional diseases.

The limitations of our study include the small number of patients and the fact that immunotherapy agents could not be compared with the same number of patients. There are no previous publications in the literature regarding the investigation of factors affecting arterial stiffness levels related to immunotherapy. The use of promising immunotherapy agents in oncological treatments is increasing and more studies are needed to determine factors affecting the level of arterial stiffness.

Acknowledgments

Adnan Menderes University Faculty of Medicine Medical Oncology Clinic staff

Authorship contributions

EEGY, MBA and EO designed the study; EEGY and MBA collected the data and carried out statistical analysis; EEGY, MBA performed the literature search; BD, MT and EO supervised the study; MBA, EEGY, and EO prepared and revised the manuscript. All authors gave the final approval of the version to be published.

Data availability statement

The data that support the findings of this study are available from the corresponding author, [E.O.], upon reasonable request.

Declaration of competing interest

The authors have no conflicts of interest to declare.

Ethics

Ethics committee approval was obtained from the Clinical Research Ethics Committee of Adnan Menderes University Faculty of Medicine (Protocol No: 2021/74 Approval Date: 14.06.2021).

Funding

This study is from Emine Esra Güner Yıldırım 's internal medicine specialization thesis, and the thesis was supported by Adnan Menderes University Scientific Research Projects (BAP) Unit with project number TPF-21035.

REFERENCES

1. Mellman I, Coukos G, Dranoff G. Cancer immunotherapy comes of age. *Nature*. 2011;480(7378):480-9.
2. Matts C, Beck A. Immunotherapy-Related Adverse Effects When Treating Cancer# 375. *Journal of Palliative Medicine*. 2019;22(6):724-5.
3. Cecelja M, Chowienczyk P. Role of arterial stiffness in cardiovascular disease. *JRSM cardiovascular disease*. 2012;1(4):1-10.
4. Vlachopoulos C, Aznaouridis K, Stefanadis C. Prediction of cardiovascular events and all-cause mortality with arterial stiffness: a systematic review and meta-analysis. *J Am Coll Cardiol*. 2010;55(13):1318-27.
5. Yersal Ö, Eryilmaz U, Akdam H, Meydan N, Barutca S. Arterial stiffness in breast cancer patients treated with anthracycline and trastuzumab-based regimens. *Cardiology Research and Practice*. 2018;2018.
6. Visvikis A, Kyvelou S, Pietri P, Georgakopoulos C, Manousou K, Tousoulis D, et al. Cardiotoxic profile and arterial stiffness of adjuvant chemotherapy for colorectal cancer. *Cancer Management and Research*. 2020;12:1175.
7. Novo G, Di Lisi D, Manganaro R, Manno G, Lazzara S, Immordino FA, et al. Arterial stiffness: effects of anticancer drugs

used for breast cancer women. *Frontiers in Physiology*. 2021;12:661464.

8. Smulyan H, Lieber A, Safar ME. Hypertension, diabetes type II, and their association: role of arterial stiffness. *American journal of hypertension*. 2016;29(1):5-13.

9. Demir B, Sezer SD, Topaloğlu Ö, TAŞKIRAN E, Burcu I, SOYALTIN U, et al. The relationship between nephropathy, retinopathy, obesity and arterial stiffness in type 2 diabetes mellitus. *İstanbul Bilim Üniversitesi Florence Nightingale Tıp Dergisi*. 2015;1(2):59-67.

10. Theilade S, Lajer M, Persson F, Joergensen C, Rossing P. Arterial stiffness is associated with cardiovascular, renal, retinal, and autonomic disease in type 1 diabetes. *Diabetes care*. 2013;36(3):715-21.

11. Dahlén EM, Tengblad A, Länne T, Clinchy B, Ernerudh J, Nystrom F, et al. Abdominal obesity and low-grade systemic inflammation as markers of subclinical organ damage in type 2 diabetes. *Diabetes & metabolism*. 2014;40(1):76-81.

12. Evans PD, McIntyre NJ, Fluck RJ, McIntyre CW, Taal MW. Anthropomorphic measurements that include central fat distribution are more closely related with key risk factors than BMI in CKD stage 3. *PLoS One*. 2012;7(4):e34699.

13. DuPont JJ, Kenney RM, Patel AR, Jaffe IZ. Sex differences in mechanisms of arterial stiffness. *British journal of pharmacology*. 2019;176(21):4208-25.

14. Rehill N, Beck CR, Yeo KR, Yeo WW. The effect of chronic tobacco smoking on arterial stiffness. *British journal of clinical pharmacology*. 2006;61(6):767-73.

Research Article

THE EFFECT OF DIFFERENT FIT-INDICATING MATERIALS AND PREPARATION DESIGNS ON THE MARGINAL AND INTERNAL FIT OF 3D-PRINTED PERMANENT ENDOCROWNS

İzım TÜRKER KADER^{1*}, Safa ÖZER², Burçin ARICAN³

¹ Bahçeşehir University School of Dental Medicine, Department of Prosthodontics, Istanbul, TURKIYE

² Bahçeşehir University Vocational School of Health Services, Dental Prosthetic Technology, Istanbul, TURKIYE

³ Bahçeşehir University School of Dental Medicine, Department of Endodontics, Istanbul, TURKIYE

*Correspondence: izim.turker@bau.edu.tr

Abstract

Objective: This study aimed to evaluate the effect of different fit-indicating materials and preparation designs on the marginal and internal fit of 3D-printed permanent endocrowns.

Materials and Methods: Maxillary right first molar typodont teeth were prepared with two designs and divided into two groups (N=80): Group 1-butt joint margin and a 4 mm pulp chamber depth, and Group 2-shoulder margin design and a 4 mm pulp chamber depth. The groups were scanned with a digital intraoral scanner, and 3D-printed master dies and permanent endocrowns were fabricated. Endocrowns were seated using vinyl polyether silicone (VPES) and polyvinyl siloxane (PVS) fit-indicating materials. Superimposition of prepared and fit-indicating material-applied master die scans was performed using 3D-analysis software. Multi-point measurements at standard points determined marginal, internal, pulp chamber and overall gap values, which were compared between the groups. Statistical analysis included Two-Way ANOVA for normally distributed data and Spearman's rho for non-normally distributed data ($\alpha=0.05$). Pairwise comparisons were conducted with post hoc Tukey tests.

Results: VPES exhibited lower marginal and internal gap values than PVS ($p<0.001$). PVS usage in the butt-joint design showed the highest marginal gap, while the lowest internal gap was observed with VPES usage in the shoulder design ($p<0.001$).

Conclusion: Using different fit-indicating materials with different preparation designs affects the fit of endocrowns. VPES provides a more accurate determination of the internal fit of a 3D-printed endocrown in the shoulder margin design and the marginal fit of the endocrown with butt-joint margin design.

Keywords: Printing, Three-Dimensional, Dental Restoration, Permanent, Fit-Checker, Dental Marginal Adaptation

Received: 05 December 2024

Revised: 03 February 2025

Accepted: 05 February 2025

Published: 20 March 2025



Copyright: © 2025 by the authors. Published by Aydın Adnan Menderes University, Faculty of Medicine and Faculty of Dentistry. This article is openly accessible under the Creative Commons Attribution-NonCommercial 4.0 International (CC BY-NC 4.0) License.

INTRODUCTION

Endocrowns are popular monoblock restorations for endodontically treated teeth with substantial coronal structure loss, combining the crown and core into a single unit that covers all cusps, typically with a circular butt margin and shoulder or chamfer margin design extending to the pulpal floor (1,2). The macromechanical retention of endocrowns is achieved by anchoring them within the pulp chamber and adapting them to cavity margins, with varying depths and configurations of the chamber and the margin design, which plays a critical role in their mechanical performance (3).

The marginal and internal adaptation of a restoration is key in determining its longterm clinical performance (4). Marginal and internal adaptation of restoration was commonly evaluated using two-dimensional (2D) methods, which limit the number of cross-sections and measurement points used to describe overall adaptation (5). In contrast, digital techniques—especially three-dimensional (3D) analysis combined with intraoral scanners—offer a more comprehensive assessment, allowing unlimited measurements of the gap between the restoration and abutment tooth and enabling evaluation of both adaptation and cement gap volume (4). This 3D analysis digitally aligns the scans of the tooth preparation and fit-indicating material over the preparation and allows the gap measurement.

Fit-indicating materials are elastomeric materials used in the fit assessment of restorations and clearly reveal gaps between the restoration and abutment tooth, facilitating precise adjustments (6,7). The light-body consistency form of polyvinylsiloxane (PVS) is a commonly used fit-indicating material in studies (8,9). Vinyl polyether silicone (VPES), marketed as Fit Checker, is an alternative impression material specifically designed to evaluate the marginal and internal fit of restorations (6,7). During the silicone disclosing procedure, they contact the restoration's internal surface and the prepared tooth (10,11).

Innovations in 3D-printing technology have provided alternative material options by offering several advantages, such as high accuracy and reduced material waste (12). Recently, 3D-printed ceramic-filled hybrid materials have emerged with application areas of single-tooth restorations, inlays, onlays, tabletops, veneers, and three-unit bridges in posterior areas. The manufacturer claims this material has high dimensional stability,

flexural strength, and modulus and can be used as a permanent restorative material (Bego; VarseoSmile Triniq technical product information data sheet. n.d.).

To the best of the authors' knowledge, there are studies in the literature evaluating the marginal and internal fit of endocrowns with different preparation designs using different fit-indicating materials. However, no study has evaluated the fit of 3D-printed ceramic-filled permanent endocrowns with different preparation designs by comparing them with different fit-indicating materials through 3D analysis. Therefore, the present study aims to evaluate the effect of different fit-indicating materials and preparation designs on the marginal and internal fit of 3D-printed permanent endocrowns. The null hypotheses for this study were as follows; there would be no effect of different fit-indicating materials on the marginal and internal fit of endocrowns, there would be no effect of different preparation designs on the marginal and internal fit of endocrowns

MATERIALS AND METHODS

The sample size calculation was performed using a statistical software program (G*Power v3.1.9.2) using data from another study by Seo et al. (13) the minimum sample size of 20 specimens for each group achieved 95% power to detect differences, with a significance level of 0.05, to test the null hypotheses.

A pilot study was performed with four samples for each group before the present study. During the pilot study, one operator experienced performing the final preparations after multiple preparation trials under a dental operation microscope and scanning them with a digital intraoral scanner. Master dies were designed and fabricated as single and in sets of four. An attempt was made to produce all prepared samples as single master dies. Because it provided ease of measurement. The endocrowns were adhered to the master dies using different fit-indicating materials and were applied with a standard 50 N force on each master die three times. When attempting to apply this force using finger pressure, gradual increases and decreases in pressure were observed. Therefore, it was decided to use an electric motor-driven machine to ensure the application of a constant force. To enable easy separation of the endocrowns from the master die, water, petroleum jelly (Vaseline), and hand lotion (Geistlich Pharma AG, Bahnhofstrasse, Wolhusen) were tested. The best and most controlled results were achieved with Vaseline. Multiple

3D analysis attempts were made by another operator. Based on these findings, the main study proceeded as outlined below.

Tooth preparations were performed by one operator according to different preparation designs on typodont maxillary first molars (AG-3 ZE, Frasco GmbH, Tettang, Germany) using a dental operation microscope (Zumax OMS 2000, Zumax, China) at x18.4 magnification. The groups were as follows:

- Group 1: Butt-joint margin and a 4 mm pulp chamber depth
- Group 2: Shoulder (1 mm) margin and a 4 mm pulp chamber depth

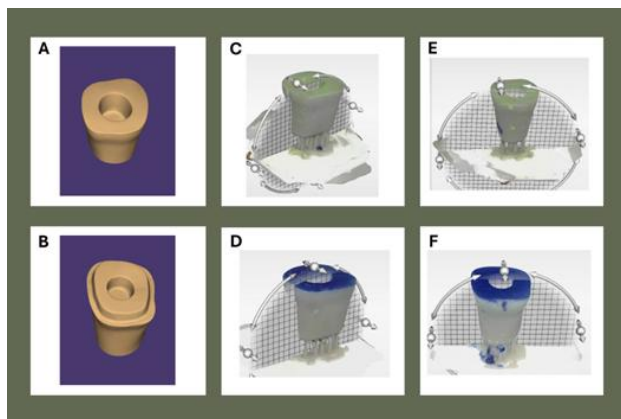


Figure 1. (A) The preparation scan of Group 1, (B) The preparation scan of Group 2, (C&D) Buccolingual section images taken via STL data superimposition in Orachek 3D analysis software, (E&F) Mesiodistal section images taken via STL data superimposition in Orach

A 2 mm occlusal reduction was performed on each group using a green belt occlusal-reduction diamond bur (Frank Dental GmbH D.828.017.G.FGA, Gmund, Germany) as the first step in the preparation process. In Group 1, a 2 mm wide circumferential butt-joint margin is prepared using a green belt wheel diamond bur (Meisinger 909G-031-FG Coarse 5/Pk, Neuss, Germany). The pulp chamber is subsequently prepared using a red belt conical diamond bur (Frank Dental GmbH D.845KR.016.G.FGA, Gmund, Germany) with an internal taper of 8° axial walls (14). Additionally, the internal line angle was rounded down, irregularities were eliminated, and a flat, polished surface was created using a red belt medium round-end tapered diamond bur (Frank Dental GmbH D.850.016.FG, Gmund, Germany). The preparation design of Group 1 is shown in **Fig.1A**. The identical burs used in Group 1 were utilized throughout the whole preparation process in Group 2. The primary difference was that in contrast to Group 1, a red belt modified shoulder fine W diamond bur (Meisinger 848WF-018-FG, Gmund, Germany) was used to prepare

the 1 mm shoulder margin following occlusal reduction with an occlusal-reduction diamond bur and pulp chamber preparation with a conical diamond bur. The preparation design of Group 2 is shown in **Fig.1B**. Following the preparations, a periodontal probe and a digital calliper (Digimatic, Mitutoyo Corporation, Japan) were utilized to confirm the measurements of pulp chamber depths, margin widths, and occlusal reductions.

A digital intraoral scanner (CEREC AC, Primescan, Dentsply Sirona, York, PA, USA) was used to scan the prepared teeth for each group, and Sirona InEos X5 software (InEos X5, Dentsply-Sirona, York, PA) to process the external CAD data. Then, Shapr 3D (Shapr 3D, Budapest, Hungary), a CAD program for generating and creating ready models, was used to import standard tessellation language (STL) files. Drawing bases beneath the prepared teeth STLs for various groups allowed for the design of the single master dies. Forty single master dies of each group were then printed with a layer thickness of 50 µm using a 3D printer (Asiga Ultra (50), ASIGA, Sydney, Australia) and 3D-printed model resin (VarseoWax Model, Bego, Bremer, Germany). Following printing, the dies were cleaned with 99% isopropanol alcohol for 3 minutes (Form Wash, Formlabs®, Somerville, USA) and post-cured twice for 20 minutes at 60° (Form Cure, Formlabs®, Somerville, USA).

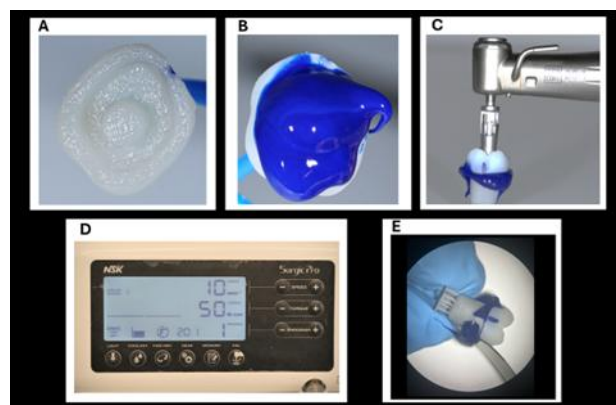


Figure 2. (A) Vaseline application to the inner surface of endocrown (B) Loading of endocrown using VPES fit-indicating (C&D) Application of 50 N force over endocrown until the setting of fit-indicating material is completed (E) Removal of excess fit-indicating material using a surgical blade under the dental microscope.

Typodont maxillary molar teeth were scanned before and after preparation for the endocrown design. The exocad DentalCAD program (exocad GmbH, Darmstadt, Germany) was utilized to process these STL data. Endocrown designs were created on the prepared tooth STLs, to reflect the tooth's initial morphology. In the

chairside CAD design, the cement space was specified at 80 μm . The endocrowns were subsequently printed with a 50 μm layer thickness using a 3D printer and 3D-printed ceramic-filled hybrid material (VarseoSmile Triniq, Bego, Bremer, Germany). Following the manufacturer's instructions, the 3D-printed endocrowns were rinsed with 99% isopropanol alcohol for a total of 5 minutes (Form Wash, Formlabs®, Somerville, USA), and post-cured twice for 20 minutes at 60° (Form Cure, Formlabs®, Somerville, USA).

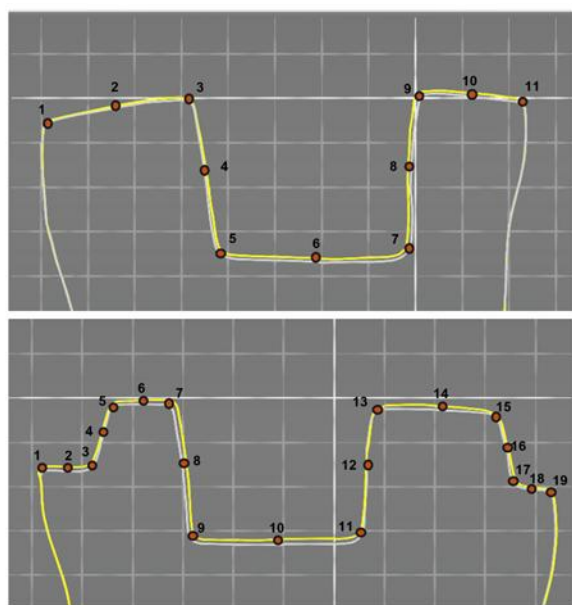


Figure 3. (A) Marginal and internal fit analysis of Group 1 from 11 points in the image taken via STL data superimposition in Oracheck 3D analysis software. (B) Marginal and internal fit analysis of Group 2 from 19 points in the image taken via STL data superimposition in Oracheck 3D analysis software. *Images represent mesiodistal (MD) sections, and each square is 1 mm².

A proprietary software (OraCheck, Cyfex AG, Zurich, Switzerland) program specifically designed for the CEREC system was used for the 3D analysis of the fit of endocrowns. Using the digital intraoral scanner, the endocrown preparation dies were initially scanned and saved as the preparation's master digital file.

The inner surface of each endocrown was gently wiped with Vaseline as a lubricant (**Fig. 2A**). Each group was divided into two subgroups according to the fit-indicating material (n=20). The VPES (Fit Checker; GC Europe, Leuven, Belgium) and PVS fit-indicating materials (Elite HD+ light-body; Zhermack SpA, Badia Polesine (RO), Italy) were used to load endocrowns before seating on master dies (**Fig.2B**). The force was standardized by applying 50 N while seating (15). For each group, after the endocrowns were seated on the master dies, 50 N was applied with an

electric motor-driven machine (Surgic Pro, NSK, IL, USA) to mimic a 5 kg weight until the setting times of the fit-indicating materials were completed (**Fig.2C&D**). The setting time was 2 min and 4 min for VPES and PVS fit-indicating material, respectively. Under the dental microscope, excess fit-indicating material was gently removed from the margins using a surgical blade (no. 12; Feather Safety Razor Co., Ltd., Osaka, Japan) (**Fig. 2E**).

The digital intraoral scanner was utilized to perform a second scan with the fit-indicating material covering the preparation die after the endocrown was removed from the preparation. For every tested group, the two recorded scans were digitally superimposed in STL files using the 3D analysis software. The distances between each surface point in the first data set and the surface points in the second data set were calculated for the subtractive analysis. Approximately 20,000 points were chosen for each surface matching by the software's best-fit algorithm (9). To assess the means of the marginal gap (MG), internal gap (IG), pulp chamber gap (PCG), and overall gaps (OG) of Group 1 and Group 2 in all three dimensions over the superimposition views, vertical sections were chosen from the core region of each superimposition in the buccolingual (**Fig.1C&D**) and mesiodistal directions (**Fig.1E&F**). The mean values for Group 1 were determined by making the MG measurement at points 1 and 11, the IG measurement at points 2 to 10, the PCG measurement at points 3 to 9, and the OG measurement at points 1 to 11 (**Fig.3A**). The means of the MG measurement points 1 and 19, the IG measurement points 2 to 18, the PCG measurement points 7 to 13, and the OG measurement points 1 to 19 were computed for Group 2 (**Fig.3B**). The PCG assessment was also included in the IG evaluation. Furthermore, both IG and MG evaluation areas are included in the OG measurements.

The data were analyzed with IBM SPSS V23 (IBM Statistics, Armonk, NY). The normality of distribution was examined with the Shapiro-Wilk and Kolmogorov-Smirnov Test. Spearman's rho Correlation Coefficient was used to examine the relationship between the parameters that were not normally distributed. A Two-Way ANOVA was used to compare the parameters that were normally distributed according to the fit-indicating material and preparation design. For pairwise comparisons, the post hoc Tukey test was applied. The results were presented as mean \pm standard deviation. The significance level was set as $p < 0.05$.

RESULTS

MG, IG, PCG, and OG measurements were compared according to the main effects of different fit-indicating materials, different preparation designs and the interaction between the two, as shown in **Table 1**. The only statistically non-significant difference was observed in the main effect of preparation design on the IG values ($p=0.317$) (**Table 1**).

Table 1. Comparison of marginal, internal, pulp chamber and overall gap values according to fit-indicating material and preparation designs

Marginal Gap Measurements (MG)			
	F	p	PES
Fit-indicating material	46.89	<0.001	0.382
Preparation design	29.43	<0.001	0.279
Fit-indicating material*Preparation design	42.66	<0.001	0.359
Internal Gap Measurements (IG)			
	F	p	PES
Fit-indicating material	57.54	<0.001	0.431
Preparation design	1.01	0.317	0.013
Fit-indicating material*Preparation design	5.31	0.024	0.065
Pulp Chamber Gap Measurements (PCG)			
	F	p	PES
Fit-indicating material	166.17	<0.001	0.686
Preparation design	50.64	<0.001	0.400
Fit-indicating material*Preparation design	59.76	<0.001	0.440
Overall Gap Measurements (OG)			
	F	p	PES
Fit-indicating material	69.42	<0.001	0.477
Preparation design	23.85	<0.001	0.239
Fit-indicating material*Preparation design	17.23	<0.001	0.185

F: Two-Way ANOVA Test Statistic; PES: Partial Eta Square. Statistically significant at $p<0.05$.

When comparing the mean values of gap measurements using different fit-indicating materials, VPES showed lower results than PVS in all groups ($p<0.001$). Lower gap values were obtained in Group 1 than in Group 2 among MG, PCG, and OG measurements in different preparation design evaluations ($p<0.001$). Regarding the interaction between different fit-indicating materials and preparation designs, VPES used in Group 1 resulted in lower MG values (0.0184 ± 0.0053 mm) than PVS and Group 1 (0.0501

± 0.0134 mm). VPES and Group 2 showed lower values (0.0736 ± 0.0055 mm) compared to PVS and Group 2 (0.1078 ± 0.0081 mm) in IG measurements. PCG

Table 3. Correlation analysis between parameters based on average marginal, internal, pulp chamber, and overall gap measurements

	1	2	3
Marginal Gap (MG) Measurements (1)			
r	1		
p	---		
Internal Gap (IG) Measurements (2)			
r	0,372	1	
p	0,001	---	
Pulp Chamber Gap (PCG) Measurements (3)			
r	0,337	0,925	1
p	0,002	<0,001	---
Overall Gap (OG) Measurements (4)			
r	0,487	0,937	0,913
p	<0,001	<0,001	<0,001

r: Spearman's rho correlation coefficient

measurements revealed a higher value in PVS and Group 2 (0.1503 ± 0.0124 mm) than VPES and Group 2 (0.0759 ± 0.0069 mm). Additionally, while PVS and Group 2 (0.1014 ± 0.0082 mm) showed a higher OG, VPES and Group 1 showed a lower value (0.0673 ± 0.0065 mm) (**Table 2**). The mean differences between groups are shown in **Figure 4**.

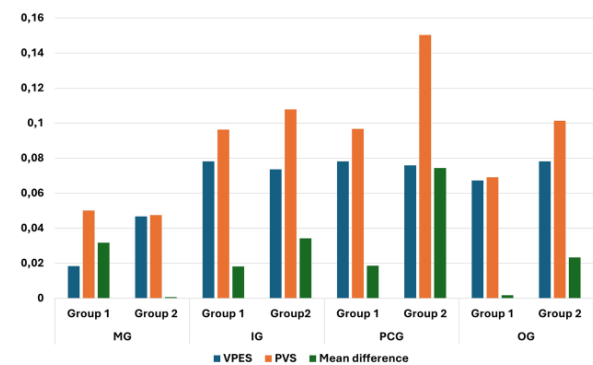


Figure 4 The column chart of mean differences of the marginal, internal, pulp chamber and overall gap values of different preparation designs using different fit-indicating materials. (VPES; Vinyl polyether silicone, PVS; Polyvinyl siloxane, Group 1; Butt joint design and 4 mm pulp chamber depth, Group 2; Shoulder design and 4 mm pulp chamber depth, MG; Marginal gap, IG; Internal gap, PCG; Pulp chamber gap, OG; Overall gap)

The results of the Spearman correlation coefficient test are presented in **Table 3**. A significant weak positive correlation was found between MG and IG measurements ($r=0.372$, $p=0.001$) as well as between MG and PCG measurements ($r=0.337$, $p=0.002$).

Table 2. The marginal, internal, pulp chamber and overall gap values (mm) of different groups

Gap Measurements	Preparation design	Fit-indicating material		Mean ± SD	p Values
		Vinylpolyether silicone (VPES)	Polyvinyl siloxane (PVS)		
Marginal Gap (MG)	Group 1	0.0184 ± 0.0053 ^B	0.0501 ± 0.0134 ^A	0.0343 ± 0.0189	< 0.001
	Group 2	0.0468 ± 0.0057 ^A	0.0475 ± 0.0145 ^A	0.0471 ± 0.0109	
	Mean ± SD	0.0326 ± 0.0154	0.0488 ± 0.0138	0.0407 ± 0.0167	
Internal Gap (IG)	Group 1	0.0781 ± 0.0074 ^B	0.0963 ± 0.0283 ^A	0.0872 ± 0.0224	0.024
	Group 2	0.0736 ± 0.0055 ^B	0.1078 ± 0.0081 ^A	0.0907 ± 0.0186	
	Mean ± SD	0.0759 ± 0.0068	0.1020 ± 0.0214	0.089 ± 0.0205	
Pulp Chamber Gap (PCG)	Group 1	0.0781 ± 0.0077 ^C	0.0967 ± 0.0279 ^B	0.0874 ± 0.0223	< 0.001
	Group 2	0.0759 ± 0.0069 ^C	0.1503 ± 0.0124 ^A	0.1131 ± 0.0389	
	Mean ± SD	0.0770 ± 0.0073	0.1235 ± 0.0345	0.1002 ± 0.0341	
Overall Gap (OG)	Group 1	0.0673 ± 0.0065 ^C	0.0781 ± 0.0200 ^B	0.0727 ± 0.0157	< 0.001
	Group 2	0.0691 ± 0.0049 ^{B/C}	0.1014 ± 0.0082 ^A	0.0853 ± 0.0177	
	Mean ± SD	0.0682 ± 0.0058	0.0897 ± 0.0192	0.0790 ± 0.0178	

Mean ± Standard Deviation (SD); No difference between values with the same letter in all directions between rows and columns of each gap measurement. Statistically significant at $p < 0.05$. Group 1; Butt joint design and a 4 mm pulp chamber depth, Group 2; Shoulder design and a 4 mm pulp chamber dep

In contrast, a moderate positive correlation was observed between MG and OG measurements ($r=0.487$, $p < 0.001$). Additionally, a very strong positive correlation was found between IG measurements and both PCG ($r=0.925$, $p < 0.001$) and OG measurements ($r=0.937$, $p < 0.001$). Similarly, PCG and OG measurements exhibited a very strong positive correlation ($r=0.913$, $p < 0.001$)

DISCUSSION

Marginal and internal fit are essential factors for the long-term success of restorations (2). While the poor marginal fit raises the likelihood of plaque accumulation, gingival inflammation, secondary caries, and cement dissolution (16), the internal fit has a major impact on the mechanical characteristics of the restoration, including retention (17). The present study evaluated the effect of different fit-indicating materials and preparation designs on the marginal and internal fit of 3D-printed permanent endocrowns. The results of this study showed that using different fit-indicating materials and preparation designs affected the determination of marginal and internal fit of 3D-printed permanent endocrowns. Thus, the null hypotheses were rejected. The 3D analysis technique used in this study requires the use of a fit-indicating material since it involves

superimposing the endocrown preparation surface with that of fit-indicating material. The properties of the fit-indicating material used may cause differences in the marginal and internal gap values of the restoration. The weight and density of the fit-indicating material, finger pressure, material flow and the base/catalyst ratio are critical factors influencing the accuracy of marginal and internal gap measurements (18). Thus, we aimed to clarify this by comparing the VPES and PVS fit-indicating materials to evaluate the marginal and internal fit of endocrowns. In the present study, the VPES material showed lower values than the PVS material in the gap measurements of endocrowns by standardizing the applied force. Habib et al. (19) stated in their study that VPES showed lower film thickness in the fit-indication performed before cementation of restorations compared to PVS material, similar to this study. The reason for this might be that the film thickness of VPES material is lower, and its fluidity is higher. Considering that the main purpose of using the material is to check the fit of restorations, this is an expected result.

The preparation design of endocrown is another influential factor in its adaptation (20). Farghal et al. (21) reported that a butt-joint design reduces marginal and internal gaps in endocrown restorations, while the 1- and

2-mm ferrule (shoulder) design offers greater retention. According to Seo et al. (13), the marginal fit is improved in endocrowns with a 1 mm shoulder margin design due to the higher surface area available for bonding. Additionally, PVS was used as fit-indicating material in both studies mentioned. In this study, consistent with the findings of Farghal et al. (21), the butt-joint margin design demonstrated a better marginal gap than the shoulder design. This difference may result from the easier removal of fit-indicating material from the two axial wall configuration of the butt-joint design compared to the four walls in the shoulder margin design. However, while the PVS and butt-joint preparation design resulted in the highest marginal gap, the VPES and butt-joint design provided the lowest gap values. This underscores the significant impact of the chosen fit-indicating material on the determination of the fit of endocrown. The flow characteristics of the VPES may have caused this result.

The internal fit plays a crucial role in the ability of restoration to provide adequate retention (17). Considering that there are studies stating that the shoulder margin design offers a larger bonding area and greater retention than the butt-joint (13,14,21), it is reasonable to expect the shoulder design to demonstrate superior fit. However, in the present study, no significant difference was found between butt-joint and shoulder margin designs regarding internal fit. Notably, the best internal fit was determined with VPES and shoulder margin designs, while the highest internal gaps were observed with PVS and shoulder design, highlighting the critical influence of fit-indicating materials on outcomes.

In the present study, pulp chamber gap measurements are incorporated into the internal gap assessment to provide a more comprehensive evaluation of the fit within the pulp chamber. Furthermore, the pulp chamber gap results in this study are similar to the internal gap results. In a study by Hajimahmoudi et al. (22), a PVS impression material was used as a fit indicator, and it was reported that the pulpal floor had the greatest gap in endocrowns with butt-joint preparation design, regardless of the ceramic materials used. However, in the present study, the shoulder design showed a higher pulp chamber gap than the butt-joint. This may be due to the technical limitations of digital intraoral scanners during scanning. In addition, the lowest pulp chamber gap values observed with the VPES and the highest gap values observed with PVS material in the fit evaluation are both seen in the shoulder margin design, which may also be influenced by the fit-indicating materials. Although there are studies that used VPES to assess the fit of crowns (23,24), there is no study using it to assess the marginal and internal fit of

endocrowns. During this study, observations showed that while the PVS material exhibited separation and tearing from the die, VPES remained stable on the surface. The setting time and flow of VPES likely contributed to better results. Given the 4 mm pulp chamber depths in the preparation designs, it is crucial to remove the fit-indicating material without tearing, especially in pulp chamber gap measurements, as this may have influenced the results.

The fit of restorations is commonly evaluated using 2D, such as the silicone replica method, which measures gaps at specific points through sectional image analysis (25). However, 2D evaluations are limited in precision and cannot easily be compared across studies as the measurements were made from artificially set reference points. This study employs 3D analysis software for more accurate assessments without data loss, allowing unlimited measurements at multiple points across all dimensions (9,10). The 3D analysis method involves scanning both the prepared tooth and fit-indicating material surface, then superimposing the scans for comprehensive marginal and internal gap evaluation. Thus, fit evaluation was conducted with better reproducibility, allowing for a greater number of measurements to be performed easily in this study.

To strengthen the validity of this study, the methodology of this study is based on the results obtained from a pilot study conducted beforehand. Despite using natural human teeth, typodont maxillary first molar teeth were chosen to standardize the measurements. All preparations were performed by one experienced operator. PVS and VPES fit-indicating materials were applied with a standard 5 kg force on each master die three times. The single master dies have been fabricated to apply fit-indicating materials within their working times. 3D analysis of the gaps was performed from two different sections after multiple trials under blinded conditions and by another operator.

The limitations of this in vitro study were that the restorations were not cemented, which may have contributed to the increase in the overall gap, the difference in setting times of fit-indicating materials, and the possibility of Vaseline remaining on the surface. Furthermore, different results can be obtained with different intraoral scanners, 3D printers, and materials. To add new insights to the literature, various materials and equipment would be beneficial to incorporate. Addressing these limitations in future in vitro research is recommended, particularly studies comparing PVS and VPES fit-indicating materials to evaluate the fit of

endocrowns on natural human teeth. Additionally, in vivo studies are essential to evaluate the findings of this study under clinical conditions.

CONCLUSION

Using different fit-indicating materials and preparation designs affects the fit values of endocrowns. Vinyl polyether silicone provides a more accurate evaluation of the fit of 3D-printed permanent endocrown restorations compared to polyvinyl siloxane. Specifically, vinyl polyether silicone enhances accuracy in assessing the internal fit of 3D-printed endocrowns with a shoulder margin and a 4 mm pulp chamber depth, yielding results comparable to the butt-joint design while also offering greater precision in evaluating the marginal fit in the latter.

Acknowledgments

The authors declare that there are no acknowledgements for this study.

Authorship contributions

Concept: BA Design: BA Data collection and processing: İTK, SÖ Analysis or interpretation: İTK Literature search: İTK, SÖ Writing: İTK

Data availability statement

The data that support the findings of this study are available from the corresponding author upon reasonable request.

Declaration of competing interest

There is no conflict of interest in this study.

Ethics

Since resources obtained from humans or animals were not used in this study, ethics committee approval was not obtained.

Funding

No financial support was received from any institution or organisation for this study.

REFERENCES

1. Biacchi GR, Mello B, Basting RT. The endocrown: an alternative approach for restoring extensively damaged molars. *J Esthet Restor Dent*. 2013;25(6):383-90.
2. El Ghoul WA, Özcan M, Ounsi H, Tohme H, Salameh Z. Effect of different CAD-CAM materials on the marginal and internal adaptation of endocrown restorations: An in vitro study. *J Prosthet Dent*. 2020;123(1):128-34.
3. Taha D, Spintzyk S, Schille C, Sabet A, Wahsh M, Salah T, Geis-Gerstorfer J. Fracture resistance and failure modes of polymer infiltrated ceramic endocrown restorations with variations in margin design and occlusal thickness. *J Prosthodont Res*. 2018;62(3):293-7.
4. Park JM, Hämmerle CHF, Benic GI. Digital technique for in vivo assessment of internal and marginal fit of fixed dental prostheses. *J Prosthet Dent*. 2017;118(4):452-4.
5. Reich S, Uhlen S, Gozdowski S, Lohbauer U. Measurement of cement thickness under lithium disilicate crowns using an impression material technique. *Clin Oral Investig*. 2011;15(4):521-6.
6. White SN, Sorensen JA, Kang SK. Improved marginal seating of cast restorations using a silicone disclosing medium. *Int J Prosthodont*. 1991;4(4):323-6.
7. Davis SH, Kelly JR, Campbell SD. Use of an elastomeric material to improve the occlusal seat and marginal seal of cast restorations. *J Prosthet Dent*. 1989;62(3):288-91.
8. Zimmermann M, Valcanaia A, Neiva G, Mehl A, Fasbinder D (2019) Three-Dimensional Digital Evaluation of the Fit of Endocrowns Fabricated from Different CAD/CAM Materials. *J Prosthodont*. 2019;28(2):e504-e509.
9. Zimmermann M, Valcanaia A, Neiva G, Mehl A, Fasbinder D. Digital evaluation of the fit of zirconia-reinforced lithium silicate crowns with a new three-dimensional approach. *Quintessence Int*. 2018;49(1):9-15.
10. Szep S, Schmid C, Weigl P, Hahn L, Heidemann D. Effect of the silicone disclosing procedure on the shear bond strength of composite cements to ceramic restorations. *J Prosthet Dent*. 2003;89(1):60-5.
11. Jampana VVSNR, Bheemalingeswar Rao D, Suresh Sajjan MC, Jitendra Babu P, Ramaraju AV, Manikyamba YJB. The effect of Fit-checking material and various subsequent cleaning methods on the wettability of the dentin surface: an in vitro study. *Int J Dent Mater*. 2021;3(1): 16-23.
12. Ahlholm P, Lappalainen R, Lappalainen J, Tarvonen PL, Sipilä K. Challenges of the direct filling technique, adoption of

- CAD/CAM techniques, and attitudes toward 3D printing for restorative treatments among Finnish dentists. *Int J Prosthodont.* 2019;32:402–10.
13. Seo D, Yi Y, Roh B. The effect of preparation designs on the marginal and internal gaps in Cerec3 partial ceramic crowns. *J Dent.* 2009;37(5):374-82.
14. Sun J, Ruan W, He J, Lin X, Ci B, Yin S, Yan W. Clinical efficacy of different marginal forms of endocrowns: study protocol for a randomized controlled trial. *Trials.* 2019;20(1):454.
15. Hezavehi M, Neshandar Asli H, Babae Hemmati Y, Falanchia M. Fracture strength and marginal and internal adaptation of lithium disilicate and hybrid ceramic endocrowns and non-retentive overlays for endodontically treated molar teeth. *BMC Oral Health.* 2024;24:1524.
16. Groten M, Axmann D, Pröbster L, Weber H. Determination of the minimum number of marginal gap measurements required for practical in-vitro testing. *J Prosthet Dent.* 2000;83(1):40-9.
17. Abduljawad DE, Rayyan MR. Marginal and internal fit of lithium disilicate endocrowns fabricated using conventional, digital, and combination techniques. *J Esthet Restor Dent.* 2022;34(4):707-14.
18. Nakamura T, Tanaka H, Kinuta S, Akao T, Okamoto K, Wakabayashi K, Yatani H. In vitro study on marginal and internal fit of CAD/CAM all-ceramic crowns. *Dent Mater J.* 2005;24(3):456-9.
19. Habib SR, Ansari AS, Bajunaid SO, Alshahrani A, Javed MQ. Evaluation of Film Thickness of Crown Disclosing Agents and Their Comparison with Cement Film Thickness after Final Cementation. *Eur J Dent.* 2020;14(2):224-32.
20. Mostafavi AS, Allahyari S, Niakan S, Atri F. Effect of Preparation Design on Marginal Integrity and Fracture Resistance of Endocrowns: A Systematic Review. *Front Dent.* 2022;19:37.
21. Farghal A, Dewedar K, AbdElaziz MH, Saker S, Hassona M, Algabri R, Alqutaibi AY. Effect of ceramic materials and tooth preparation design on computer-aided design and computer-aided manufacturing endocrown adaptation and retentive strength: An in vitro study. *Clin Exp Dent Res.* 2024;10(1):e843.
22. Hajimahmoudi M, Raseipour S, Mroue M, Ghodsi S. Evaluation of Marginal and Internal Fit of CAD/CAM Endocrowns with Different Cavity Tapers. *Int J Prosthodont.* 2023 May;36(2):189-93.
23. Zimmermann M, Valcanaia A, Neiva G, Mehl A, Fasbinder D. Influence of Different CAM Strategies on the Fit of Partial Crown Restorations: A Digital Three-dimensional Evaluation. *Oper Dent.* 2018;43(5):530-8.
24. Davis SH, Kelly JR, Campbell SD. Use of an elastomeric material to improve the occlusal seat and marginal seal of cast restorations. *J Prosthet Dent.* 1989;62(3):288-91.
25. Hasanzade M, Sahebi M, Zarrati S, Payaminia L, Alikhasi M. Comparative Evaluation of the Internal and Marginal Adaptations of CAD/CAM Endocrowns and Crowns Fabricated from Three Different Materials. *Int J Prosthodont.* 2021;34(3):341–7.

Research Article

IMPACT OF DIFFERENT SUBSTRUCTURE AND SUPERSTRUCTURE MATERIALS ON BONE STRESS DISTRIBUTION IN ALL-ON-4 PROSTHETIC RESTORATIONS

 Ege ÇOLAK^{1*},  Muharrem Erhan ÇÖMLEKOĞLU¹,  Mehmet SONUGELN¹,  Makbule Heval ŞAHAN¹

¹Department of Prosthodontics, Faculty of Dentistry, Ege University, Izmir, Turkey

*Correspondence: dt.egecolak@gmail.com

Abstract

Aim: This study aimed to examine whether different framework and superstructure materials in All-on-4 prosthetic restorations affect load distribution in peri-implant bone.

Materials and Methods: Four implants were placed according to the All-on-4 concept, with distal implants angled at 30 degrees. Framework materials (cobalt-chromium alloy, titanium, PEEK, zirconia) and superstructure materials (composite, zirconia) created eight combinations. 3D models were designed using Rhinoceros 4.0 (3670 Woodland Park Ave N, Seattle, Washington, USA) and VRMesh (VirtualGrid Inc, Bellevue City, Washington, USA), then imported into Algor Fempro (ALGOR, Inc., 150 Beta Drive, Pittsburgh, Pennsylvania, USA) for finite element analysis. A 150N force was applied perpendicular to the occlusal surfaces of the left first molar and premolar.

Results: The PEEK framework group showed the highest maximum principal stress (HMaxPS) values in the cortical bone (CB) near the applied force. The zirconia superstructure exhibited lower maximum principal stress values than the composite superstructure. Minimum principal stress (MinPS) was lower in the composite superstructure than in the zirconia superstructure. In the cantilever section, peak MinPS values in the cortical bone decreased as the elastic modulus of the frameworks increased, following the order: PEEK > titanium > Cr-Co > zirconia.

Conclusions: The PEEK framework and composite superstructure generated higher tensile forces in the cortical bone surrounding the implants. The highest compression values were observed in the PEEK framework, followed by titanium, Cr-Co, and zirconia. Greater stress accumulation occurred in the cortical bone with the composite superstructure compared to the zirconia superstructure.

Keywords: All-on-4, Framework, Finite Element Analysis

Received: 26 December 2024
Revised: 12 February 2025
Accepted: 23 February 2025
Published: 20 March 2025



Copyright: © 2025 by the authors. Published by Aydın Adnan Menderes University, Faculty of Medicine and Faculty of Dentistry. This article is openly accessible under the Creative Commons Attribution-NonCommercial 4.0 International (CC BY-NC 4.0) License.

INTRODUCTION

When planning dental implant placement in the edentulous mandible, reduced residual alveolar bone height due to bone resorption or anatomical limitations such as the mandibular canal can pose challenges, particularly in the posterior region. Long-term clinical data has demonstrated that fixed prostheses supported by four implants in the mandible exhibit similar prosthesis and implant survival rates as those supported by a greater number of implants (1). Increasing the number of implants is essential to reduce stress on implants and prosthetic components and ensure even load distribution on the underlying bone. However, in patients with severe alveolar bone loss, the area available for implant placement is limited. In some completely edentulous patients, implant-supported prostheses are almost impossible to fabricate without complex procedures such as nerve transposition, grafting in the posterior maxilla and mandible (2).

The All-on-4 concept has been introduced as an alternative to bone augmentation procedures. The All-on-4 concept, developed by Malo, is one of the most widely used methods for treating complete mandibular edentulism with angled implants. The All-on-4 concept involves placing four implants in the interforaminal region of the completely edentulous mandible followed by the use of a fixed prosthesis (1). The posterior implants are angled at 30 degrees to reduce cantilever length. The angulation of the posterior implants should not exceed 45 degrees (2). Distal angulation of the implants provides advantages such as the use of longer implants and better cortical support (3).

In full-mouth restorations, long spans can lead to more complications with the prosthetic substructure compared to short spans. A prosthesis spanning the entire arch may be subject to more deformation and bending. Therefore, cases with long spans may experience more stress. In cases with long spans, especially in the presence of cantilevers, the prosthetic substructure material becomes even more important in ensuring the stability of the system (4). Titanium alloys, cobalt-chromium, zirconia, and polyetheretherketone are frequently utilized in the manufacture of implant substructures (5).

Cobalt-chromium (Co-Cr) alloys can be defined as high-strength, non-magnetic, biocompatible alloys that are resistant to heat, wear, corrosion, and tarnishing. Thanks to their high elastic modulus, they provide the necessary strength and rigidity without the need to increase the material thickness and, consequently, the weight (6).

Cobalt-chromium alloys are frequently used as prosthetic substructure materials in implant-supported prostheses due to their low cost, low density, and good mechanical properties (4).

Titanium is one of the most commonly used materials in the substructure of All-on-4 prostheses. This is due to its biocompatibility, low cost, and good mechanical properties (7). Titanium is a practical material for the production of implant-supported prosthetic substructures (8). CAD/CAM-manufactured titanium substructures have a high degree of fit in full-arch or partial-arch restorations. Titanium substructures can cause aesthetic complications due to their grayish color (9). They can cause metal allergies (10).

PEEK is a type of linear high-performance polymer due to its mechanical properties, high temperature stability, and chemical resistance. PEEK also has a tooth-like color, is lightweight, and is an alternative for patients with metal allergies (11). PEEK is an organic, thermoplastic, high-performance polymer. It is similar to human bone in terms of weight, strength, and other chemical properties (7). While the elastic modulus of metal substructures is between 100-200 GPa, that of PEEK is around 4 GPa. Despite this difference in the mechanical properties of these two materials, it is assumed that PEEK can be an alternative as a substructure material in implant-supported fixed prosthetic restorations (12).

Zirconia is the most preferred bioengineering ceramic among all ceramic products. With its excellent biocompatibility, low thermal conductivity, high flexural strength, and suitability for white aesthetics, it is an ideal material (13). The reason for its popularity in dentistry is its transformation toughening property. This property helps prevent crack propagation and increases localized fracture resistance. 3 mol% Y_2O_3 stabilized zirconia, or yttria-stabilized tetragonal zirconia polycrystal (3Y-TZP), is the most commonly preferred zirconia when a hard material is needed (13). The use of zirconia as a substructure material helps to mask the substructure color and has survival rates similar to metal (10). Zirconia can also be used as a superstructure material in All-on-4 prostheses.

Composites are among the materials used for veneering in implant-supported prostheses. Composites have advantages such as stress distribution, reduction of prosthesis weight, and reduction of treatment costs. They are a good alternative to porcelain in full-mouth implant-supported prosthetic restorations (9).

Finite element analysis (FEA) is a widely used, non-destructive computational approach for modeling and examining the mechanical behavior of systems under various conditions. By partitioning structures into discrete elements, this technique is applied in engineering and dentistry to assess both material performance and design efficacy (5). It is a useful approach because it allows for the unlimited repetition of experiments under different scenarios—experiments that cannot be exactly reproduced in clinical settings—and also makes it possible to conduct tests that cannot be performed on patients for ethical reasons, without bearing ethical responsibility. In implants, intermittent forces during oral functions lead to bone resorption by creating overload that results in high stress and strain, rather than insufficient mechanical stimulation of the bone. Since direct measurement of bone strain via strain gauge needles in patients is impractical, indirect mathematical approaches like FEA are frequently employed to calculate values such as strain, stress, and deformation.

The finite element analysis results provided valuable insights into stress distributions within the bone and implant components under various loading conditions. This information is crucial for the design and optimization of dental implants, aiming to improve their long-term performance and patient outcomes.

In our literature review, we did not encounter any study that simultaneously evaluates the relationship between substructure and superstructure in all-on-4 prostheses with a Toronto design and examines the resulting stress on the bone. Based on the results of our study, we may have a clinical prediction regarding which substructure and superstructure in all-on-4 prostheses could lead to less bone loss.

The null hypothesis of the study is that there is no difference in the effect of different substructure and superstructure materials used in All-on-4 prosthetic restorations on bone stress distribution.

MATERIALS AND METHODS

Software

This study utilized Rhinoceros 4.0 for 3D (3- dimension) modeling, VRMesh for mesh processing, and Algor Fempro for finite element analysis.

Implant and prosthetic Design

Conical implants at bone level were used in the study. Implants with a diameter of 4.1mm (millimeter) and a length of 12mm were selected. Four implants were

positioned in the mandible: the anterior implants were placed vertically, and the posterior two implants were angled distally at 30°. The anterior implants were aligned with the lateral teeth, and the screw access points of the posterior implants aligned to the second premolar tooth. Multi-unit abutments were placed on the implants. The anterior multi-unit abutments were modeled without an angle, while the posterior two multi-unit abutments were modeled at a 30° angle to compensate for the implant angle. The prosthetic solution was planned as an All-on-4 prosthesis design. A prosthetic substructure was designed, and crowns were designed on top of the framework. The prosthetic substructures were made of cobalt-chromium alloy, titanium, PEEK, and zirconia. The prosthetic superstructures were made of composite and zirconia. A total of eight different combinations were obtained by using the substructures and superstructures together: cobalt-chromium substructure with composite superstructure, PEEK substructure with composite superstructure, titanium substructure with composite superstructure, zirconia substructure with composite superstructure, cobalt-chromium substructure with zirconia superstructure, PEEK substructure with zirconia superstructure, titanium substructure with zirconia superstructure, and zirconia substructure with zirconia superstructure.

The prosthetic restoration was designed with 12 teeth. The screw access holes opening to the occlusal surface of the distal implants were modeled to exit the occlusal surface of the second premolar tooth. The modeling was done so that the distance from the exit point of the screw holes to the distal surface of the first molar tooth (cantilever length) was 9mm. The distance between the line passing through the anterior implant and the line passing through the posterior implant was 9 mm. The cantilever length/anterior-posterior implant distance (A-P distance) ratio is 1.

Load Application

Forces were applied perpendicular to the occlusal surface of the left first molar tooth and the occlusal surface of the left first premolar tooth (Fig. 1 e,f). The force magnitude was 150N (Newton)(4).

This study employed a multi-stage computational approach for the finite element analysis of mandibular implants. A 3D scan of the mandible was acquired using an Activity 880 optical scanner. The acquired data was then processed on a workstation equipped with an Intel Xeon® R CPU 3.30 gigahertz processor, 500 gigabyte hard disk, 14 gigabyte RAM, and Windows 7 Ultimate operating system.

The initial 3D models of the mandible and prosthetic components were generated in VRMesh software. These models were subsequently exported in the industry-standard STL(Standard Triangle Language) format for compatibility with Algor Fempro, a finite element analysis software. STL format ensures the preservation of crucial node coordinate information during data transfer between different software packages.

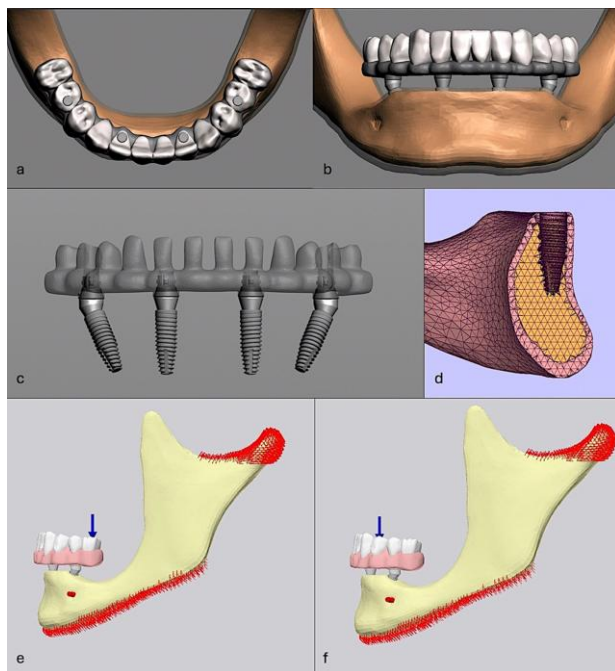


Figure 1. (a) Modeling from an occlusal view; (b) Modeling from a frontal view; (c) Model with the mandible separated and substructures faded; (d) Mesh view of implants within the mandible; (e, f) Force application to the left first molar (e) and the left first premolar (f).

Within Algor Fempro, the models were assigned appropriate material properties, including Young's Modulus and Poisson's ratio (Table 1), to accurately reflect the mechanical behavior of each component. Assuming linear elastic, homogeneous, and isotropic material behavior, the software proceeded with the meshing process.

To achieve optimal mesh quality, 8-node brick elements were predominantly used. In regions with complex geometries, elements with fewer nodes were incorporated to ensure complete mesh coverage. This approach aimed to balance mesh refinement with computational efficiency. Furthermore, sharp and narrow features within the jaw models, which can pose challenges for accurate analysis, were smoothed to improve mesh quality and stability.

Table 1. Material properties

Material	Young's Modulus (MPa)	Poisson's Ratio
Cortical Bone	13700	0.3
Spongy Bone	1370	0.3
Zirconia Substructure	210000	0.3
PEEK Substructure	4200	0.36
Titanium	110000	0.28
Composite	15000	0.24
Cr-Co Substructure	200000	0.3
Zirkonya Superstructure	213700	0.31

The number of elements within the finite element mesh was maximized within the computational constraints of the system (Table 2), considering the dimensions of the mandible model. This maximization aimed to enhance the accuracy of the subsequent stress analysis.

Table 2. Node and element numbers of substructure and superstructure combinations.

Combinations	Node Numbers	Element Numbers
Cr-Co Substructure – Composite Superstructure	470975	1932039
PEEK Substructure – Composite Superstructure	470975	1932050
Titanium Substructure – Composite Superstructure	470975	1932052
Zirconia Substructure – Composite Superstructure	470975	1932039
Cr-Co Substructure – Zirconia Superstructure	470975	1932039
PEEK Substructure – Zirconia Superstructure	470975	1932052
Titanium Substructure – Zirconia Superstructure	470975	1932050
Zirconia Substructure – Zirconia Superstructure	470975	1932052

Following the initial analysis in Algor Fempro, the models were further refined in Rhinoceros 4.0 3D Software. In this stage, prosthetic components such as screws, implants, and abutments were precisely aligned with the bone structures using Boolean operations, ensuring accurate representation of their spatial relationships.

Bone tissues were segmented based on Hounsfield units, a technique commonly used in medical imaging. The segmented regions were then rendered into a 3D model, and subsequently simplified using 3D-Doctor software to optimize model complexity and reduce computational demands. This simplified model served as a reference for

the creation of a new bone model, incorporating anatomical measurements from the Wheeler atlas.

The newly created bone model underwent dimensional and topographic adjustments in VRMesh software to achieve greater anatomical accuracy. Cancellous bone was extracted from the bone tissue using the offset method, allowing for the accurate representation of the distinct bone microstructures.

Finally, the refined models, including the mandible, prosthetic components, and bone tissues, were imported back into Algor Fempro for the final finite element analysis. Boundary conditions were applied to the model to simulate real-world constraints, such as fixation at the base of the mandible.

RESULTS

Results of maximum principal stress in cortical bone around the implant

In the Cr-Co substructure with a composite superstructure, when force was applied between the two implants, the highest MaxPS was observed in the CB of the left anterior implant region at 4.699767 N/mm², while the lowest was found in the CB of the right anterior implant region at 1.453774 N/mm² (Fig.2a) (Table 3). When force was applied to the cantilever portion of the same combination, the highest MaxPS was found in the CB of the right anterior implant region at 19.011616 N/mm², and the lowest in the CB of the right posterior implant region at 4.401233 N/mm² (Fig.2b)(Table 3).

In the PEEK substructure with a composite superstructure, when force was applied between the two implants, the highest MaxPS was observed in the CB of the left anterior implant region at 6.299223 N/mm², while the lowest was found in the CB of the right posterior implant region at 2.757486 N/mm² (Fig.2c) (Table 3). When force was applied to the cantilever portion of the same combination, the highest MaxPS was found in the CB of the left posterior implant region at 12.984744 N/mm², and the lowest in the CB of the right posterior implant region at 2.373965 N/mm² (Fig2d) (Table 3).

In the titanium substructure with a composite superstructure, when force was applied between the two implants, the highest MaxPS was observed in the CB of the left anterior implant region at 4.930487 N/mm², while the lowest was found in the CB of the right anterior implant region at 1.522162 N/mm² (Fig.2e) (Table 3). When force was applied to the cantilever portion of the same combination, the highest MaxPS was found in the CB of

the right anterior implant region at 18.022934 N/mm², and the lowest in the CB of the right posterior implant region at 4.066457 N/mm² (Fig.2f) (Table 3).

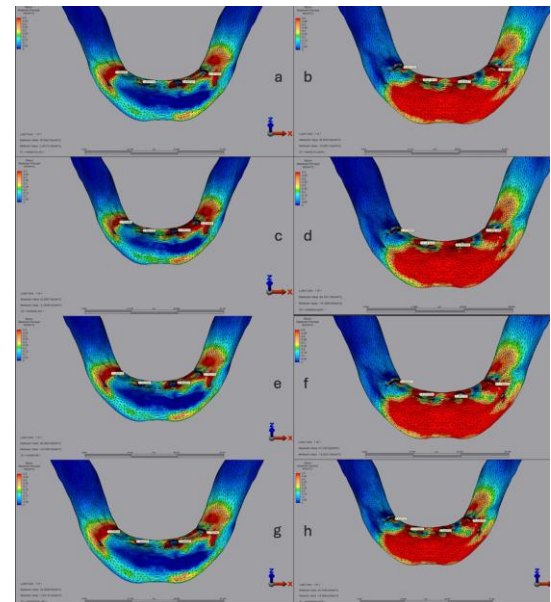


Figure 2. Composite Superstructure Maximum Principal Stress; (a, b) Cr-Co Substructure (a: anterior load, b: posterior load); (c, d) PEEK Substructure (c: anterior load, d: posterior load); (e, f) Titanium Substructure (e: anterior load, f: posterior load); (g, h) Zirconia Substructure (g: anterior load, h: posterior load).

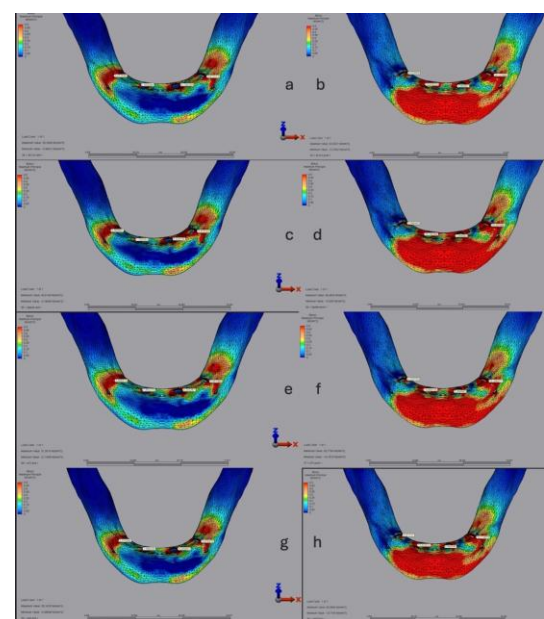


Figure 3. Zirconia Superstructure Maximum Principal Stress; (a, b) Cr-Co Substructure (a: anterior load, b: posterior load); (c, d) PEEK Substructure (c: anterior load, d: posterior load); (e, f) Titanium Substructure (e: anterior load, f: posterior load); (g, h) Zirconia Substructure (g: anterior load, h: posterior load).

Table 3. Maximum principal stress (MaxPS) values (N/mm²) in cortical bone around the implant for different substructure and superstructure combinations.

Combination	Anterior load – Right posterior implant		Anterior load – Left anterior implant		Posterior load – Right anterior implant		Posterior load – Left anterior implant	
	Right posterior implant	Left anterior implant	Right posterior implant	Left anterior implant	Right anterior implant	Left anterior implant	Right anterior implant	Left anterior implant
Cr-Co Substructure-Composite Superstructure	3.356658	1.453774	4.699767	3.791263	4.401233	19.011616	6.642647	10.954504
PEEK Substructure-Composite Superstructure	2.757486	2.984783	6.299223	4.523866	2.373965	12.141423	10.093930	12.984744
Titanium Substructure- Composite Superstructure	3.299923	1.522162	4.930487	3.752276	4.066457	18.022934	7.205133	11.136632
Zirconia Substructure-Composite Superstructure	3.359844	1.449526	4.680983	3.789548	4.424193	19.078002	6.594923	10.936705
Cr-Co Substructure -Zirconia Superstructure	3.377530	1.493344	4.106259	3.872213	4.323566	19.839220	4.880561	10.127559
PEEK Substructure-Zirconia Superstructure	3.383961	1.209262	5.028194	3.915142	3.998480	18.166266	7.359382	10.497856
Titanium Substructure-Zirconia Superstructure	3.405513	1.452275	4.242281	3.851988	4.329700	19.868105	5.304943	10.266977
Zirconia Substructure-Zirconia Superstructure	3.374380	1.496259	4.095691	3.874375	4.321727	19.824913	4.846240	10.113878

In the zirconia substructure with a composite superstructure, when force was applied between the two implants, the highest MaxPS was observed in the CB of the left anterior implant region at 4.680983 N/mm², while the lowest was found in the CB of the right anterior implant region at 1.449526 N/mm² (Fig.2g) (Table 3). When force was applied to the cantilever portion of the same combination, the highest MaxPS was found in the CB of the right anterior implant region at 19.078002 N/mm², and the lowest in the CB of the right posterior implant region at 4.424193 N/mm² (Fig2h) (Table 3).

In the Cr-Co substructure with a zirconia superstructure, when force was applied between the two implants, the highest MaxPS was observed in the CB of the left anterior implant region at 4.106259 N/mm², while the lowest was found in the CB of the right anterior implant region at 1.493344 N/mm² (Fig.3a) (Table 3). When force was applied to the cantilever portion of the same combination, the highest MaxPS was found in the CB of the right anterior implant region at 19.839220 N/mm², and the lowest in the CB of the right posterior implant region at 4.323566 N/mm² (Fig.3b) (Table 3).

In the PEEK substructure with a zirconia superstructure, when force was applied between the two implants, the highest MaxPS was observed in the CB of the left anterior implant region at 5.028194 N/mm², while the lowest was found in the CB of the right anterior implant region at 1.209262 N/mm² (Fig.3c) (Table 3). When force was applied to the cantilever portion of the same combination, the highest MaxPS was found in the CB of the right anterior implant region at 18.166266 N/mm², and the lowest in the CB of the right posterior implant region at 3.998480 N/mm² (Fig.3d) (Table 3).

In the titanium substructure with a zirconia superstructure, when force was applied between the two implants, the highest MaxPS was observed in the CB of the left anterior implant region at 4.242281 N/mm², while the lowest was found in the CB of the right anterior implant region at 1.452275 N/mm² (Fig.3e) (Table 3). When force was applied to the cantilever portion of the same combination, the highest MaxPS was found in the CB of the right anterior implant region at 19.868105 N/mm², and the lowest in the CB of the right posterior implant region at 4.329700 N/mm² (Fig.3f) (Table 3).

In the zirconia substructure with a zirconia superstructure, when force was applied between the two implants, the highest MaxPS was observed in the CB of the left anterior implant region at 4.095691 N/mm², while the lowest was found in the CB of the right anterior implant region at

1.496259 N/mm² (Fig.3g) (Table 3). When force was applied to the cantilever portion of the same combination, the highest MaxPS was found in the CB of the right anterior implant region at 19.824913 N/mm², and the lowest in the CB of the right posterior implant region at 4.321727 N/mm² (Fig.3h) (Table 3).

Results of minimum principal stress in the cortical bone around the implant

When force was applied between two implants in a Cr-Co substructure with a composite superstructure, the lowest MinPS was observed in the CB of the left posterior implant region at -10.416149 N/mm², while the highest MinPS was observed in the CB of the right posterior implant region at -1.520808 N/mm² (Fig.4a) (Table 4). When force was applied to the cantilever portion of a the same combination, the lowest MinPS was observed in the CB of the left posterior implant region at -37.027302 N/mm², and the highest MinPS was observed in the CB of the right anterior implant region at -4.175044 N/mm² (Fig.4b) (Table 4).

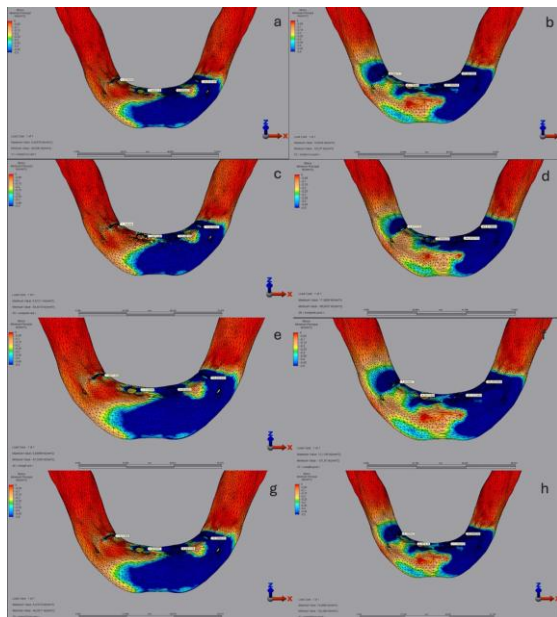


Figure 4. Composite Superstructure Minimum Principal Stress; (a, b) Cr-Co Substructure (a: anterior load, b: posterior load); (c, d) PEEK Substructure (c: anterior load, d: posterior load); (e, f) Titanium Substructure (e: anterior load, f: posterior load);(g, h) Zirconia Substructure (g: anterior load, h: posterior load).

In the PEEK substructure with a composite superstructure, when force was applied between the two implants, the lowest MinPS was observed in the CB of the left posterior implant region at -11.570927 N/mm², while the highest was found in the CB of the right anterior implant region at -1.091225 N/mm² (Fig.4c) (Table 4). When force was applied to the cantilever of the same combination, the lowest

Table 4. Minimum principal stress values (N/mm²) in the cortical bone around the implant for different substructure and superstructure combinations.

Combination	Anterior load		Anterior load		Anterior load		Anterior load		Posterior load		Posterior load		Posterior load	
	Right	posterior implant	Right	posterior implant	Left	anterior implant	Right	posterior implant	Left	anterior implant	Right	posterior implant	Left	posterior implant
Cr-Co Substructure – Composite Superstructure	-1.520808	-1.806310	-9.500462	-10.416149	-8.065777	-4.175044	-4.175044	-8.065777	-10.416149	-21.296924	-21.296924	-37.027302	-37.027302	-37.027302
PEEK Substructure – Composite Superstructure	-1.759095	-1.091225	-9.574514	-11.570927	-4.372725	-2.999020	-2.999020	-4.372725	-11.570927	-34.074733	-34.074733	-43.813800	-43.813800	-43.813800
Titanium Substructure – Composite Superstructure	-1.487134	-1.711939	-9.552552	-10.632292	-7.509867	-4.031745	-4.031745	-7.509867	-10.632292	-23.222380	-23.222380	-38.483984	-38.483984	-38.483984
Zirconia Substructure – Composite Superstructure	-1.521998	-1.814261	-9.497125	-10.398420	-8.103502	-4.181418	-4.181418	-8.103502	-10.398420	-21.142418	-21.142418	-36.904036	-36.904036	-36.904036
Cr-Co Substructure – Zirconia Superstructure	-1.416865	-2.767117	-10.126320	-10.104143	-8.417940	-4.142041	-4.142041	-8.417940	-10.104143	-17.046186	-17.046186	-33.900477	-33.900477	-33.900477
PEEK Substructure – Zirconia Superstructure	-1.523301	-1.473468	-9.349499	-10.584618	-7.417029	-3.479953	-3.479953	-7.417029	-10.584618	-24.044234	-24.044234	-37.598654	-37.598654	-37.598654
Titanium Substructure – Zirconia Superstructure	-1.432913	-2.490632	-9.975522	-10.130849	-8.463309	-4.110895	-4.110895	-8.463309	-10.130849	-18.101710	-18.101710	-34.797301	-34.797301	-34.797301
Zirconia Substructure – Zirconia Superstructure	-1.415330	-2.787156	-10.136509	-10.114685	-8.408122	-4.140722	-4.140722	-8.408122	-10.114685	-16.966652	-16.966652	-33.819820	-33.819820	-33.819820

MinPS was observed in the CB of the left posterior implant region at $-43.813800 \text{ N/mm}^2$, and the highest was found in the CB of the right anterior implant region at -2.999020 N/mm^2 (Fig.4d) (Table 4).

When force was applied between two implants in a titanium substructure with a composite superstructure, the lowest MinPS was observed in the CB of the left posterior implant region at $-10.632292 \text{ N/mm}^2$, while the highest MinPS was observed in the CB of the right posterior implant region at -1.487134 N/mm^2 (Fig.4e) (Table 4). When force was applied to the cantilever of the same combination, the lowest MinPS was observed in the CB of the left posterior implant region at $-38.483984 \text{ N/mm}^2$, and the highest MinPS was observed in the CB of the right anterior implant region at -4.031745 N/mm^2 (Fig.4f) (Table 4).

When force was applied between two implants in a zirconia substructure with a composite superstructure, the lowest MinPS was observed in the CB of the left posterior implant region at $-10.398420 \text{ N/mm}^2$, while the highest MinPS was observed in the CB of the right posterior implant region at -1.521998 N/mm^2 (Fig.4g) (Table 4). When force was applied to the cantilever of the same combination, the lowest MinPS stress was observed in the CB of the left posterior implant region at $-36.904036 \text{ N/mm}^2$, and the highest MinPS was observed in the CB of the right anterior implant region at -4.181418 N/mm^2 (Fig.4h) (Table 4).

When force was applied between two implants in a Cr-Co substructure with a zirconia superstructure, the lowest MinPS was observed in the CB of the left anterior implant region at $-10.126320 \text{ N/mm}^2$, while the highest MinPS was observed in the CB of the right posterior implant region at -1.416865 N/mm^2 (Fig.5a) (Table 4). When force was applied to the cantilever of the same combination, the lowest MinPS was observed in the CB of the left posterior implant region at $-33.900477 \text{ N/mm}^2$, and the highest MinPS was observed in the CB of the right anterior implant region at -4.142041 N/mm^2 (Fig.5b) (Table 4).

When force was applied between two implants in a PEEK substructure with a zirconia superstructure, the lowest MinPS was observed in the CB of the left posterior implant region at $-10.584618 \text{ N/mm}^2$, while the highest MinPS was observed in the CB of the right anterior implant region at -1.416865 N/mm^2 (Fig.5c) (Table 4). When force was applied to the cantilever of the same combination, the lowest MinPS was observed in the CB of the left posterior implant region at $-37.598654 \text{ N/mm}^2$, and the highest MinPS was

observed in the CB of the right anterior implant region at -3.479953 N/mm^2 (Fig.5d) (Table 4).

When force was applied between two implants in a titanium substructure with a zirconia superstructure, the lowest MinPS was observed in the CB of the left posterior implant region at $-10.130849 \text{ N/mm}^2$, while the highest MinPS was observed in the CB of the right posterior implant region at -1.432913 N/mm^2 (Fig.5e) (Table 4). When force was applied to the cantilever of the same combination, the lowest MinPS was observed in the CB of the left posterior implant region at $-34.797301 \text{ N/mm}^2$, and the highest MinPS was observed in the CB of the right anterior implant region at -4.110895 N/mm^2 (Fig.5f) (Table 4).

When force was applied between two implants in a zirconia substructure with a zirconia superstructure, the lowest MinPS was observed in the CB of the left anterior implant region at $-10.136509 \text{ N/mm}^2$, while the highest MinPS was observed in the CB of the right posterior implant region at -1.415330 N/mm^2 (Fig.5g) (Table 4). When force was applied to the cantilever of the same combination, the lowest MinPS was observed in the CB of the left posterior implant region at $-33.819820 \text{ N/mm}^2$, and the highest MinPS was observed in the CB of the right anterior implant region at -4.140722 N/mm^2 (Fig.5h) (Table 4).

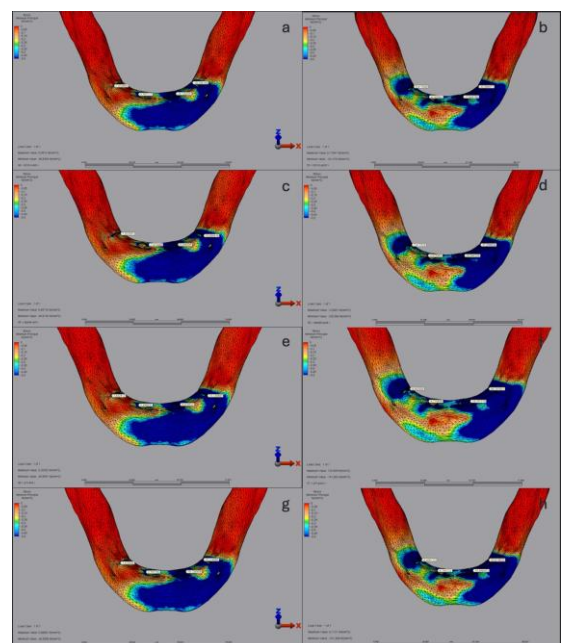


Figure 5. Zirconia Superstructure Minimum Principal Stress; (a, b) Cr-Co Substructure (a: anterior load, b: posterior load); (c, d) PEEK Substructure (c: anterior load, d: posterior load); (e, f) Titanium Substructure (e: anterior load, f: posterior load);(g, h) Zirconia Substructure (g: anterior load, h: posterior load).

DISCUSSION

The null hypothesis of the study “there is no difference in the effect of different substructure and superstructure materials used in All-on-4 prosthetic restorations on bone stress distribution” was rejected. In our study, different stress distributions in the bone were observed with different substructure and superstructure materials.

In implant-supported prostheses, the use of polymeric materials such as PEEK (polyether ether ketone), manufactured by CAD-CAM (Computer Aided Design-Computer Aided Manufacturing) milling, has been suggested as an alternative to high-elastic modulus, rigid materials like titanium, Cr-Co, and zirconia due to advantages like lower cost, light weight, and shock absorption (14,15). It is thought that PEEK substructures with an appropriate elastic modulus may be beneficial for patients with temporomandibular joint complaints (16). Some studies have shown that rigid, non-polymeric substructures with high elastic modulus do not absorb shock, thus transmitting more stress to the bone-implant interface (17). Zoidis argued that polymeric materials like PEEK, which can be milled using CAD-CAM, could be used instead of rigid substructures like Cr-Co, zirconia, or titanium (18). However, other studies have reported that using a rigid substructure provides better stress distribution and reduces stresses in the surrounding bone of the implant (19,20). There is limited information on the biomechanical behavior of polymeric and non-polymeric materials in implant-supported fixed prostheses and their effect on stress distribution in the surrounding bone (21). Oral microflora adhesion to PEEK surfaces is lower compared to zirconia, titanium, and PMMA.

There are some limitations in finite element analysis. The models used in this study are defined as linear elastic, homogeneous, and isotropic. While these assumptions are common in finite element analysis, the actual clinical behaviors cannot be fully simulated (7).

Modeling the mechanical behavior of cortical or trabecular bone is difficult because bone is highly anisotropic, heterogeneous, and depends on many parameters such as age, gender, and bone type. As a result, it is not easy to define the exact material properties of a specific bone being studied numerically. Therefore, in most finite element analyses, the mechanical properties of bone are assumed to be isotropic.

In finite element analysis studies, MaxPS is generally used to observe tensile stress, and minimum principal stress is used for compressive stress. Given the flexible and brittle

response of bone, it is appropriate to use compressive stress/strain to analyze the biomechanical behavior of the bone surrounding the implant (22).

Using the same superstructure is used in all force applications, higher MaxPS values are observed in the CB surrounding the implants in the PEEK substructure group compared to the other substructure groups, in the direction of force. Applying force between implants produces the highest MaxPS is observed in the CB of the left anterior implant region. Under these conditions, a combination of PEEK substructure and composite superstructure yields a MaxPS value of 6.299223 N/mm² in the CB surrounding the left anterior implant region. Applying force to the cantilever section results lower MaxPS values are observed in the zirconia superstructure group compared to the composite superstructure group in the same substructure combinations. In all combinations where force is applied to the cantilever section, the highest MaxPS values are observed in the CB surrounding right anterior implant. Applying force to the cantilever section with the same superstructure material results in lower MaxPS values in the CB of the implant farthest from the force in the PEEK substructure group, compared to other substructure groups. The highest MaxPS value is observed in the CB surrounding the right anterior implant in the titanium substructure and zirconia superstructure combination, which is 19.868105 N/mm². The low Young's modulus of the PEEK substructure causes it to flex, generating more tensile stress in the CB near the force application site. Rigid substructures, on the other hand, absorb the force as a whole and transmit it to the opposing arch, creating a more homogeneous stress distribution with the opposite arch stabilizing the CB.

Using the same superstructure results in the lowest minimum principal stresses in all combinations in the CB surrounding the left posterior implant in the PEEK substructure group.

Force application to the cantilever section results in MinPS values in the CB following the order from lowest to highest as: left posterior implant region, left anterior implant region, right posterior implant region, and right anterior implant region.

Force application to the cantilever section also leads to MinPS values in the CB in the direction of force (left anterior and posterior implant regions) following the order from highest to lowest as: zirconia, Cr-Co, titanium, and PEEK. These values increase as the Young's Modulus increases (Young's Modulus: PEEK 4,200 MPa, Titanium 110,000 MPa, Cr-Co 200,000 MPa, Zirconia 210,000 MPa).

In combinations where force is applied to the cantilever section and the same substructure is used, the MinPS values in the composite superstructure are lower than in the zirconia superstructure.

When force is applied between two implants and the same substructure is used, the MinPS values in the CB of the left posterior implant region are lower in the composite superstructure compared to the zirconia superstructure. The compression values in the CB are concentrated in the region closest to the force. Higher stress peak values are observed in PEEK substructure and composite superstructure materials with low elastic modulus. The low elastic modulus of the PEEK substructure and composite superstructure material allows more compression forces to be transmitted to the CB closest to the force application site.

Some authors have mentioned the cushioning effect of PEEK material in stress transmission to the peri-implant region. Wang et al. stated that the combination of PEEK substructures and PMMA crowns could show an elastic cushioning effect under chewing forces compared to metal/zirconia substructures with high elastic moduli (16). Therefore, it was noted that metal/zirconia substructures might increase stress concentration in the alveolar crest between implants. Seemann et al. reported that the combination of PEEK substructures with resin superstructures could reduce the transmission of occlusal forces (23). Zoidis suggested that combining PEEK substructures with acrylic teeth, both with low elastic moduli, might act as stress breakers and reduce occlusal stresses (18). Conserva et al. reported that rigid substructures with high elastic moduli do not absorb shock, transmitting more stress to the implant-bone interface, potentially leading to prosthetic failures, bone and implant loss (17).

Other authors recommend using relatively rigid substructure materials to prevent failure. In the study by Bacchi et al., it was reported that using more rigid materials resulted in lower stress in the bone (24). In the in-vitro study by Sirandoni et al., it was found that, despite the cushioning effect of polymeric materials, stress reduction in the substructure occurred, but there was an increase in stress in the surrounding implant bone (21). This increase was attributed to the high elasticity of the material and the lack of a rigid substructure. In the study by Jaros et al., Ni-Cr and PEEK substructure bars were compared using finite element analysis in an All-on-4 design (11). Although both systems showed similar results in stress distribution in the surrounding bone under axial force, the PEEK bar system transmitted more stress to the

implant surrounding bone under oblique forces. In the study by Kelkar et al., zirconia, titanium, and PEEK substructure materials in All-on-4 prostheses were evaluated using finite element analysis (8). In that study, the least displacement was observed with zirconia substructures, while similar values were observed for PEEK and titanium. Excessive micromovements at the implant-bone interface can have harmful effects. In the photo-elastic stress study by Çalışkan and Yöndem on All-on-4 prostheses, metal and zirconia showed lower stress values compared to PEEK (25). Based on these results, the authors suggested that an increase in the elastic modulus of the substructure material reduces the stress transmitted to the bone and implants. Our study found similar results to these conclusions. We believe that non-rigid substructures transmit more force to the implants in the region closest to the force application.

Limitations of the Study

Although we attempt to recreate intraoral structures in a computer environment using finite element analysis, intraoral conditions cannot be fully simulated, and long-term clinical studies are needed to support the data obtained from our study. The application of unidirectional and static force may not fully represent real-life conditions, and given the brittle nature of zirconia, different outcomes could be observed under cyclic loading, such as during chewing (4). The data obtained in our study should be supported by long-term clinical studies.

CONCLUSION

I. Higher tensile forces were observed in the cortical bone surrounding the implant in the direction of the applied force in the PEEK substructure and composite superstructure groups. In these groups, strain forces in the cortical bone surrounding the implant were higher in the direction of the force compared to the direction opposite to the force. Rigid substructures absorbed the strain forces as a whole and transmitted less force to the cortical bone in the direction of the applied force, while transmitting more force to the cortical bone in the opposite arch.

II. The compressive values in the cortical bone surrounding the implant were ranked by substructures from highest to lowest as follows: PEEK, titanium, Cr-Co, and zirconia. The low elastic modulus of the PEEK substructure and composite superstructure caused more compression forces to be transmitted to the cortical bone near the force application site due to their flexibility.

III. In the composite superstructure, higher stress accumulation values were observed in the cortical bone in

the direction of the applied force compared to the zirconia superstructure.

Acknowledgments

The authors declare that they have no acknowledgements to make.

Authorship contributions

EC conceived the study and wrote the manuscript. MEÇ provided guidance on structuring and editing the manuscript. MS guided the modeling and finite element analysis aspects of the study and also assisted with editing the manuscript. MHŞ assisted with editing the manuscript.

Data availability statement

The data that support the findings of this study are available from the corresponding author upon reasonable request.

Declaration of competing interest

The authors declare that they have no conflict of interest.

Ethics

This study did not involve human participants, animals, or sensitive data, and therefore did not require ethical approval.

Funding

This research did not receive any specific grant from funding agencies in the public, commercial, or not-for-profit sectors.

REFERENCES

- Horita S, Sugiura T, Yamamoto K, Murakami K, Imai Y, Kirita T. Biomechanical analysis of immediately loaded implants according to the "All-on-Four" concept. *J Prosthodont Res.* 2017 Apr;61(2):123–32.
- Taruna M. Prosthodontic Perspective to All- On-4 @ Concept for Dental Implants. *JOURNAL OF CLINICAL AND DIAGNOSTIC RESEARCH.* 2014;
- Babbush CA, Kutsko GT, Brokloff J. The All-on-Four immediate function treatment concept with nobelactive implants: A retrospective study. Vol. 37, *Journal of Oral Implantology.* 2011. p. 431–45.
- Bhering CLB, Mesquita MF, Kemmoku DT, Noritomi PY, Consani RLX, Barão VAR. Comparison between all-on-four and all-on-six treatment concepts and framework material on stress distribution in atrophic maxilla: A prototyping guided 3D-FEA study. *Mater Sci Eng C Mater Biol Appl.* 2016 Dec 1;69:715–25.
- Kupprano P, Kamonkhantikul K, Homsiang W, Takahashi H, Arksornnukit M. Finite element analysis on implant-supported bar with different geometric shapes. *BMC Oral Health.* 2024 Dec 30;24(1):1572.
- Al Jabbari YS. Physico-mechanical properties and prosthodontic applications of Co-Cr dental alloys: a review of the literature. *J Adv Prosthodont.* 2014 Apr;6(2):138–45.
- Dayan SC, Geckili O. The influence of framework material on stress distribution in maxillary complete-arch fixed prostheses supported by four dental implants: a three-dimensional finite element analysis. *Comput Methods Biomech Biomed Engin.* 2021 Nov;24(14):1606–17.
- Kelkar KC, Bhat V, Hegde C. Finite element analysis of the effect of framework materials at the bone-implant interface in the all-on-four implant system. *Dent Res J (Isfahan).* 2021;18:1.
- Jin HY, Teng MH, Wang ZJ, Li X, Liang JY, Wang WX, et al. Comparative evaluation of BioHPP and titanium as a framework veneered with composite resin for implant-supported fixed dental prostheses. *J Prosthet Dent.* 2019 Oct;122(4):383–8.
- Takaba M, Tanaka S, Ishiura Y, Baba K. Implant-supported fixed dental prostheses with CAD/CAM-fabricated porcelain crown and zirconia-based framework. *J Prosthodont.* 2013 Jul;22(5):402–7.
- Jaros OAL, De Carvalho GAP, Franco ABG, Kreve S, Lopes PAB, Dias SC. Biomechanical Behavior of an Implant System Using Polyether Ether Ketone Bar: Finite Element Analysis. *J Int Soc Prev Community Dent.* 2018;8(5):446–50.
- Tribst JPM, de Moraes DC, Alonso AA, Piva AM de OD, Borges ALS. Comparative three-dimensional finite element analysis of implant-supported fixed complete arch mandibular prostheses in two materials. *J Indian Prosthodont Soc.* 2017;17(3):255–60.
- Kohorst P, Borchers L, Stempel J, Stiesch M, Hassel T, Bach FW, et al. Low-temperature degradation of different zirconia ceramics for dental applications. *Acta Biomater.* 2012 Mar;8(3):1213–20.
- Maló P, de Araújo Nobre MA, Lopes A V, Rodrigues R. Immediate loading short implants inserted on low bone quantity for the rehabilitation of the edentulous maxilla using an All-on-4 design. *J Oral Rehabil.* 2015 Aug;42(8):615–23.
- Seemann R, Wagner F, Marincola M, Ewers R. Fixed, Fiber-Reinforced Resin Bridges on 5.0-mm Implants in Severely Atrophic Mandibles: Up to 5 Years' Follow-Up of a Prospective Cohort Study. *Journal of Oral and Maxillofacial Surgery.* 2018 May;76(5):956–62.
- Wang J, Wu P, Liu HL, Zhang L, Liu LP, Ma CF, et al. Polyetheretherketone versus titanium CAD-CAM framework for implant-supported fixed complete dentures: a retrospective study with up to 5-year follow-up. *J Prosthodont Res.* 2022 Apr 27;66(2):279–87.

17. Conserva E, Menini M, Tealdo T, Bevilacqua M, Ravera G, Pera F, et al. The use of a masticatory robot to analyze the shock absorption capacity of different restorative materials for prosthetic implants: a preliminary report. *Int J Prosthodont.* 2009;22(1):53–5.
18. Zoidis P. The all-on-4 modified polyetheretherketone treatment approach: A clinical report. *J Prosthet Dent.* 2018 Apr;119(4):516–21.
19. Zhang G, Yuan H, Chen X, Wang W, Chen J, Liang J, et al. A Three-Dimensional Finite Element Study on the Biomechanical Simulation of Various Structured Dental Implants and Their Surrounding Bone Tissues. *Int J Dent.* 2016;2016:1–9.
20. Pieri F, Aldini NN, Fini M, Corinaldesi G. Immediate Occlusal Loading of Immediately Placed Implants Supporting Fixed Restorations in Completely Edentulous Arches: A 1 - Year Prospective Pilot Study. *J Periodontol.* 2009 Mar;80(3):411 – 21.
21. Sirandoni D, Leal E, Weber B, Noritomi PY, Fuentes R, Borie E. Effect of Different Framework Materials in Implant-Supported Fixed Mandibular Prostheses: A Finite Element Analysis. *Int J Oral Maxillofac Implants.* 2019;34(6):e107–14.
22. Liu T, Mu Z, Yu T, Wang C, Huang Y. Biomechanical comparison of implant inclinations and load times with the all-on-4 treatment concept: a three-dimensional finite element analysis. *Comput Methods Biomech Biomed Engin.* 2019 May;22(6):585–94.
23. Seemann R, Marincola M, Seay D, Perisanidis C, Barger N, Ewers R. Preliminary results of fixed, fiber-reinforced resin bridges on four 4- × 5-mm ultrashort implants in compromised bony sites: a pilot study. *J Oral Maxillofac Surg.* 2015 Apr;73(4):630–40.
24. Bacchi A, Consani RLX, Mesquita MF, Dos Santos MBF. Effect of framework material and vertical misfit on stress distribution in implant-supported partial prosthesis under load application: 3-D finite element analysis. *Acta Odontol Scand.* 2013 Sep;71(5):1243–9.
25. ÇALIŞKAN A, YÖNDEM İ. Stress Analysis Of Fixed Dental Prostheses Produced With Different Materials According To The All-On-Four Concept. *Journal of Biotechnology and Strategic Health Research.* 2019 Dec 31;3(3):183–91.

Research Article

INVESTIGATION OF INFLAMMATION RATES (NEUTROPHIL/LYMPHOCYTE) AND HEMOGRAM RESULTS IN THE STAGES OF NON-ALCOHOLIC FATTY LIVER DISEASE

 Mehmet Ali GÜL ^{1*},  Duygu TOZCU YILMAZ ²,  Mustafa ÇAPRAZ ³

¹Department of Medical Biochemistry, Faculty of Medicine, Amasya University, Amasya, Türkiye

²Department of Physiology, Faculty of Medicine, Amasya University, Amasya, Türkiye

³Department of Internal Diseases, Faculty of Medicine, Amasya University, Amasya, Türkiye

*Correspondence: mehmetali.gul@amasya.edu.tr

ABSTRACT

Objective: Non-alcoholic fatty liver disease (NAFLD) is a chronic condition characterized by excessive fat accumulation in the liver accompanied by inflammation. This study aims to know the diagnostic value of NLR (neutrophil to lymphocyte ratio) in stages of NAFLD.

Materials and Methods: A retrospective case-control study was performed, including 49 NAFLD patients with NAFLD Grade 1, 48 with NAFLD Grade 2, 52 with NAFLD Grade 3, and 103 healthy control (HC) individuals. Neutrophil/Lymphocyte ratios as well as RBC, HGB, HCT, MCHC, MPV, WBC, NEUT#, RDW-CV, BASO%, MCH, LYMPH%, PDW, PCT, NLR, EO%, RDW-SD, MONO%, PLT, MCV values were examined.

Results: As the disease stages progressed (G3), a significant decrease ($p=0.005^*$) in MPV values and a significant increase ($p<0.05^{\#}$) in NLR values were observed. No statistically significant difference was found between the groups in RBC ($p=0.061$), HCT ($p=0.097$), MCHC ($p=0.747$), MCV ($p>0.05$), MCH ($p>0.05$), PDW ($p>0.05$), PCT ($p>0.05$), MONO ($p>0.05$) and EO ($p>0.05$) parameters.

Conclusion: MPV and NLR may be considered as effective biomarkers for monitoring the progression of NAFLD and evaluating the inflammatory status of patients.

Keywords: Non-Alcoholic Fatty Liver Disease, Neutrophil/Lymphocyte, Mean platelet volume

Received: 08 January 2025

Revised: 02 February 2025

Accepted: 07 February 2025

Published: 20 March 2025



Copyright: © 2025 by the authors. Published by Aydın Adnan Menderes University, Faculty of Medicine and Faculty of Dentistry. This article is openly accessible under the Creative Commons Attribution-NonCommercial 4.0 International (CC BY-NC 4.0) License.

INTRODUCTION

Non-alcoholic fatty liver disease (NAFLD) is recognized as the most prevalent form of chronic liver disease worldwide and defined as the accumulation of fat above 5% of hepatocytes or liver weight that is not caused by alcohol intake or secondary causes (1). The incidence of NAFLD is increasing due to the increase in obesity and diabetes and the lack of effective treatment methods. Global NAFLD incidence was reported at approximately 4.600/100.000 person years, with higher rates observed in men, individuals who are overweight or obese, and a more than threefold increase in incidence from 2000 to 2015 (2, 3). Although the development of non-alcoholic ateohepatitis (NASH) is a multifaceted process that remains incompletely understood, in the pathogenesis of the disease; the 'two-hit' theory, which includes several stress factors, has been replaced by the 'multiple hit' model, which includes many factors such as lipotoxicity, innate immune system activation and microbiome (4). Type 2 diabetes mellitus, obesity and dyslipidaemia are among the risk factors for NAFLD (5). NAFLD progresses in four main grading: Simple Fatty Liver (Steatosis), NASH, Fibrosis, and Cirrhosis (4). Liver biopsy is used as the gold standard for identification of NAFLD by evaluation of the degree of fibrosis and inflammation. However, this method may have serious risks such as bleeding and bile leakage. Although various inflammatory biomarkers have been used as both prognostic and predictive biomarkers in NAFLD, they have limitations (6).

Although some associations have been identified between certain blood cells and NAFLD, the exact role of blood cells in NAFLD has not been fully elucidated (7). Inflammation causes a stress response in hepatocytes, may lead to lipid accumulation and therefore may lead to steatosis. Studies have highlighted the significant presence of inflammatory factors in NAFLD, this study aimed to investigate the inflammatory indicators neutrophil to lymphocyte ratio (NLR) and Platelet/Lymphocyte ratios in the grades of NAFLD (8).

NLR is an easily accessible and low-cost indicator. The use of NLR in the prognosis of diseases such as chronic kidney disease and some cancers has increased over time (9). The NLR is considered an indicator of systemic inflammation. In NAFLD, fatty liver and inflammation may affect the immune response. An increase in this ratio may indicate increased inflammation and disease progression. However, there are few studies on whether this ratio differs between NAFLD stages. his study aims to analyze and compare the NLR, which has the potential to provide important information in terms of diagnosis and

management of the disease, in NAFLD stages and to examine its status in healthy subjects.

MATERIALS AND METHODS

The study was planned as a retrospective study and was conducted by accessing the clinical files of individuals who applied to Amasya University Sabuncuoğlu Şerefeddin Training and Research Hospital between 2020-2024 and met the inclusion criteria for our study and evaluating the data from the hospital archive. According to the diagnoses in the patient file information, staging information of NAFLD was obtained. Separate groups were created for each staging. (Grade 1, Grade 2, Grade 3, Grade 4). A control group consisting of healthy individuals was created. Routine hematology and other information of the individuals included in the groups was obtained from the hospital archive. (RBC, HGB, MCV, MCH, HCT, MCHC, MPV, PLT, NLR, RDW-CV, BASO%, WBC, PCT, EO%, RDW-SD, LYMPH%, NEUT#, PDW, MONO%) Individuals with a history of alcohol consumption (those who consume more than 20 grams of alcohol per day). Individuals with anemia, leukemia or other hematological diseases, under age 18 and those receiving anti-inflammatory, immunosuppressive or hormone therapy were not included in the study. Amasya University Non-Interventional Clinical Research Ethics Committee approval was received for the study (2024/144).

Statistical analyses

Statistical analyses were conducted using SPSS software version 25 (SPSS Inc., Chicago, IL, USA). The normality of continuous variables was assessed visually (histograms and Q-Q plots) and analytically (Kolmogorov-Smirnov/Shapiro-Wilk tests).

Variables showing normal distribution according to the Shapiro-Wilk test were analyzed using one-way ANOVA, and homogeneity of variances was evaluated by Levene's Test. When $p > 0.05$, variances were considered homogeneous, and Tukey Post-Hoc Test was applied for pairwise comparisons. Results for normally distributed variables are presented as mean \pm standard deviation (SD). For variables that did not show normal distribution, the Kruskal-Wallis test was used, and results were reported as median and interquartile range (IQR). For pairwise comparisons in non-normally distributed data, the Mann-Whitney U test was applied.

Qualitative variables were compared using the Chi-square test, and results were expressed as n (%). A p-value < 0.05 was considered statistically significant.

Table 1: Descriptive Statistics of Hematological Parameters and Comparisons Between Groups

	HC (n=103)	G1 (n=49)	G2 (n=48)	G3 (n=52)	p-values
Age (years)	55.87 ± 7.8	55 ± 12.09	55.4 ± 12.1	52.6 ± 12.7 ^a	0.02*
Gender (n/%)	M: 49/47.6	M: 34/69.4	M: 31/64.6	M: 31/59.6	0.56 [†]
	F: 54/52.4	F: 15/30.6	F: 17/35.4	F: 21/40.4	
RBC	4.94 ± 0.5	4.70 ± 0.63	4.77 ± 0.53	4.86 ± 0.52	0.061*
HGB	14.04 ± 1.7 ^d	13.32 ± 1.55	13.44 ± 1.83	13.98 ± 1.73	0.037*
HCT	42.55 ± 4.57	41.15 ± 4.67	40.80 ± 4.7	42.29 ± 4.67	0.097*
MCHC	33.04 ± 1.27	32.86 ± 1.63	32.89 ± 1.41	33.10 ± 1.29	0.747*
MPV	10.48 ± 0.99	10.36 ± 1.2	10.16 ± 0.99	9.84 ± 1.15 ^d	0.005*
WBC	6.61 (2.35)	7.09 (2.59)	7.67 (1.89) ^{a,b}	7.47(2.40)	< 0.05 [‡]
MCV	87 (6.4)	87 (5.3)	86 (6.5)	86.7 (6.7)	>0.05 [‡]
MCH	28.9 (2.9)	28.9 (2.8)	28.4 (2.3)	29.5 (2.6)	>0.05 [‡]
PLT	235 (66)	228 (101)	254 (105) ^b	262 (89) ^b	< 0.05 [‡]
RDW-SD	40.6 (3.3)	43.2 (6) ^a	43 (5.68) ^a	41.8 (4.25) ^{a,b}	< 0.05 [‡]
RDW-CV	12.8 (1.2)	13.8 (2.39) ^a	13.7 (1.55) ^a	13.1 (1.5) ^{a,c}	< 0.05 [‡]
PDW	12.6 (3.2)	13.2 (4.2)	12.1 (4.7)	13.2 (4.9)	>0.05 [‡]
PCT	0.25 (0.1)	0.24 (0.1)	0.26 (0.08)	0.26 (0.11)	>0.05 [‡]
NEUT#	3.7 (1.67)	4.1 (1.98)	4.47 (1.58) ^a	4.2 (1.35) ^a	< 0.05 [‡]
LYMPH%	2.3 (0.7)	1.9 (1.05) ^a	2.3 (1.04) ^b	2.3 (1.24) ^b	< 0.05 [‡]
NLR	1.57 (0.78)	1.9 (1.03) ^a	1.89 (1.32) ^a	1.88 (1.2)	< 0.05 [‡]
MONO%	0.5 (0.21)	0.45 (0.25)	0.6 (0.26)	0.5 (0.21)	>0.05 [‡]
EO%	0.13 (0.1)	0.13 (0.14)	0.15 (0.13)	0.15 (0.11)	>0.05 [‡]
BASO%	0.3 (0.4)	0.3 (0.2)	0.4 (0.3) ^{a,b}	0.4 (0.3) ^{a,b}	< 0.05 [‡]

a: Compared to HC. b: compared to G1. c: compared to G2. d: compared with other groups.*One-way ANOVA, †Kruskall-Wallis, ‡Chi-square test. M: Male, F: Female, HC: healthy controls, G. grade; red blood cells (RBC), white blood cell (WBC), platelet (PLT), hemoglobin (HGB), hematocrit (HCT), neutrophil (NEUT#), mean cell hemoglobin (MCH), mean cell hemoglobin concentration (MCHC), red cell distribution width-coefficient of variation (RDW-CV), red cell distribution width-standard deviation (RDW-SD), platelet distribution width (PDW), plateletcrit (PCT), lymphocyte (LYMPH), eosinophil (EO), lymphocyte percentile (LYM%), monocyte percentile (MONO%), eosinophil percentile (EOS %), basophil percentile (BASO%), neutrophil lymphocyte ratio (NLR). MPV. mean platelet volume; NLR. neutrophil lymphocyte ratio.

RESULTS

A statistically significant difference was found between the groups in age values ($p = 0.02$). In the post-hoc analysis, a significant difference was found between HC and G3; the mean age was highest in the Grade 3 group. According to the results of the Chi-Square test, there was no significant difference in gender distribution between the groups ($p = 0.56$). The proportion of males appears to be higher in the G1 and G2 groups.

No statistically significant difference was found between the groups in RBC ($p=0.061$), HCT ($p=0.097$), MCHC ($p=0.747$), MCV ($p>0.05$), MCH ($p>0.05$), PDW ($p>0.05$), PCT ($p>0.05$), MONO ($p>0.05$) and EO ($p>0.05$) parameters. HGB (a significant difference was found between the groups ($p = 0.037$); however, no significant difference was found in post hoc analysis. Especially the HGB value of the HC group was higher than the other groups. A significant difference was found between the groups in MPV values

($p = 0.005$). The results are shown in Table 1. Especially in the G3 group, MPV value was lower than the other groups. There was a significant difference between the groups in WBC values ($p < 0.05$). In the pairwise comparison made by Mann Whitney- U test, WBC values were found to be significantly higher in the G2 group compared to the HC group and the G1 group. A significant difference was found between the groups in PLT values ($p < 0.05$). In the pairwise comparison made by Mann Whitney- U test, it was significantly higher in G2 and G3 groups compared to G1 group. A significant difference was found between the groups in NLR values ($p < 0.05$). In the pairwise comparison made with Mann Whitney- U test, NLR values were significantly higher in G1 and G2 groups compared to HC group. It is shown in the Figure 1a, b, c, d, e. A significant difference was found between the groups in BASO values ($p < 0.05$). In the pairwise comparison made with Mann Whitney- U test, especially in G2 and G3 groups, BASO value is significantly higher than HC and G1 groups

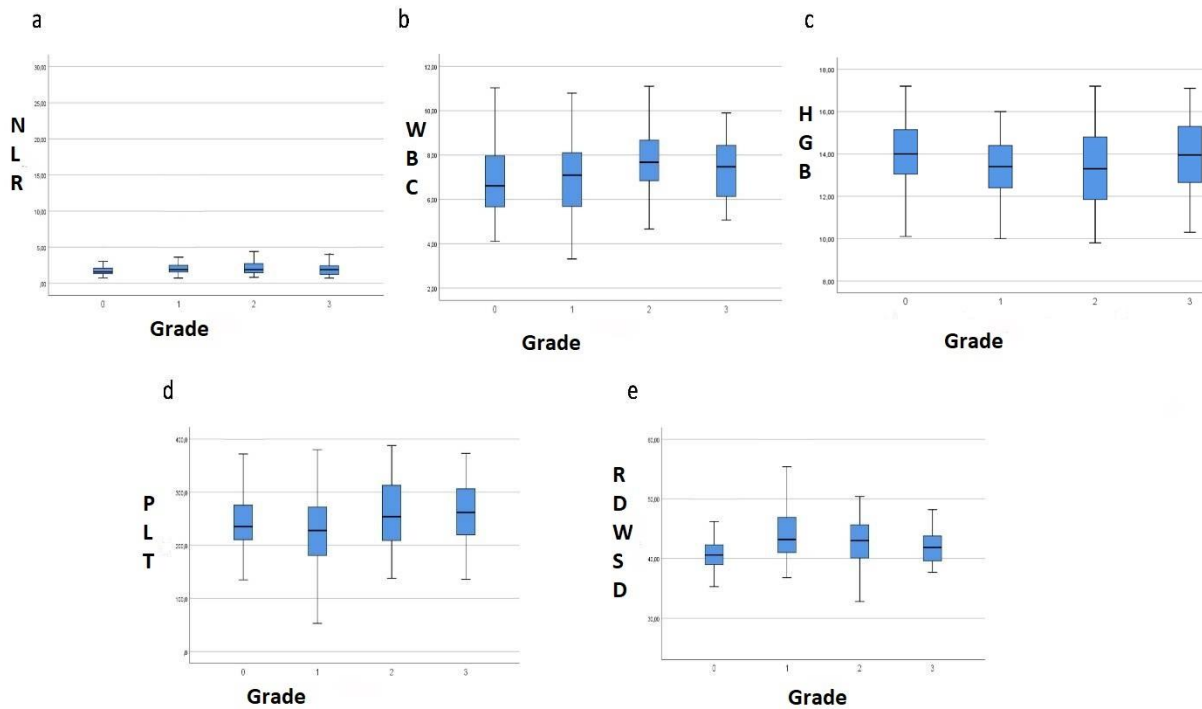


Figure 1 a: Comparison of NLR results according to NAFLD grades, b: Comparison of WBC results according to NAFLD grades, c: Comparison of HGB results according to NAFLD grades, d: Comparison of PLT results according to NAFLD grades e: Comparison of RDWSD results according to NAFLD grades, a: Compared to HC. b: compared to G1. c: compared to G2. d: compared with other groups.

DISCUSSION

Metabolic dysfunction-associated liver disease (MASLD) is a substance-independent condition with microvesicular steatosis in $\geq 5\%$ of liver cells, including several disease classes such as NASH, liver cirrhosis, non-alcoholic fatty liver and fibrosis (10). The incidence of the disease is increasing and studies on it also reveal its relationship with other diseases. While NAFLD accounts for 40% of deaths from cardiovascular disease, research shows that this disease can increase cardiovascular risk independently of typical risk factors and impacts up to 70% of diabetic patients (11). Recent studies have shown that NAFLD is higher in men and obese individuals, has increased three-fold between 2000 and 2015, treatment options are limited, and prevention of NAFLD should continue to be the focus of public health strategies (2). Additionally, this procedure is costly, prone to significant sampling error considering the ratio of the obtained sample to liver volume, has poor reproducibility, and is susceptible to post-analytical errors during interpretation (12, 13).

This study demonstrated that changes in haematological parameters become prominent in the progressive stages of NAFLD and these changes have the potential to shed light on the pathophysiology of the disease. In particular, significant increases in WBC, RDW-SD, RDW-C, NEUT and LYMP values suggest that inflammation and systemic immune response could contribute significantly to the progression of NAFLD. In our study, significant decrease in MPV values ($p= 0.005^*$) and a significant increase in NLR values ($p<0.05\#$) were observed as the disease stages progressed (G3). These two parameters indicate that platelet functions and inflammatory processes should be evaluated together in the progression of NAFLD. However, parameters such as RBC and HGB remained constant, suggesting that red blood cells and hemoglobin may be less affected by the stages of the disease. Decreased MPV may reflect changes in platelet activation and potentially microvascular dysfunction. Lower MPV values may be associated with progression of inflammation and liver fibrosis. Increased NLR indicates exacerbation of systemic inflammation and the emergence of a neutrophil-dominated immune response. This finding supports that

inflammation is a fundamental mechanism in the pathogenesis of NAFLD.

NAFLD is a major health concern and is projected to become the primary reason for liver transplantation within the next decade (14). As a result of cumulative meta analysis of NAFLD studies and a meta-analysis of changes in metabolism-related parameters, Akdas et al. showed that NAFLD patients have a high risk of metabolic dysfunction and that most of the Turkish NAFLD patients identified in previous studies may have MASLD. Also Akdas et al. showed that elevated levels of ferritin, hemoglobin, creatinine, CRP, and ESR, along with metabolism disorders related with glucose, hyperlipidemia, impaired liver function, and high blood pressure values, were observed in NAFLD patients in Türkiye (15). It has been shown how important NAFLD is and how it causes various changes in metabolism. In another metanalysis study, Shavakhi et al. showed that NLR may be suitable biomarker to help in the prediction and prevention of NASH and fibrosis in patients with NAFLD (16).

NLR ratio has the advantage of simple calculation. It is considered potential noninvasive markers for predicting advanced disease. In parallel with our work, Abdel-Razik et al. found that NLR ratio was higher in NASH group than in non-NASH patients (17). In their study, Wenyi et al. showed that there were negative correlations between high NLR levels and patients with NAFLD exhibiting severe inflammatory activity and substantial fibrosis (18). Otherwise, a large cohort study by Kara et al. revealed that NLR was not linked to the severity of NAFLD- (19). Although a large study on this condition, Kara et al.'s study had limitations: The study group mainly included mild NAFLD cases, limiting its applicability to severe cases (19).

In contrast to the literature which found a correlation between non-alcoholic steatohepatitis and NLR, Acar et al. did not find a correlation between simple fatty liver disease and NLR in their study (20). Wang et al. reported that NLR levels were positively linked to the the extent of liver fibrosis in individuals with NAFLD (21). But the initial stage of the disease or between other stages was not examined. In a case-control study conducted by Duan et al in children with NAFLD, they found that NLR showed no significant difference between the two study groups (22). Karaoğullarından et al., in contrast to our study, showed that MPV was notably higher in the NAFLD group compared to the control group. Additionally, Kocabay et al. indicated that there was no difference in MPV levels between NAFLD patients and the control group (23, 24).

In the study conducted by Alavarez et al., NAFLD patients who experienced cardiovascular events (CE) were retrospectively examined and compared with NAFLD patients who did not experience CE. It was found that the overall change in MPV level was higher in the CE group compared to the non CE group. They suggested that this finding might indicate MPV as a potential marker for elevated cardiovascular risk in NAFLD patients (25).

MPV and NLR represent different but interrelated aspects of NAFLD. MPV indicates microvascular damage and coagulopathy processes through changes in platelet activity, while NLR provides information about the severity of systemic inflammation. The combined assessment of these two parameters provides a valuable approach to understanding the critical roles played by both inflammatory and haemostatic processes in the progression of NAFLD.

CONCLUSION

In conclusion, the combined assessment of MPV and NLR can be considered as effective biomarkers to monitor the progression of NAFLD and evaluating the inflammatory status of patients. Validation of these parameters in clinical applications may provide a better understanding of both their diagnostic and prognostic value.

Acknowledgments

We would like to express our gratitude to the staff and clinicians of Amasya University Sabuncuoğlu Şerefeddin Training and Research Hospital.

Authorship contributions

GUL MA.; Concept, Design, Data Collection, Analysis and Interpretation, Literature Search, Writing-Original Draft. TOZCU D.; Concept, Design, Data Collection, Analysis, Writing-Original Draft. CAPRAZ M.; Concept, Design, Data Collection, Writing-Original Draft.

Data availability statement

The data supporting the findings of this study can be obtained from the corresponding author upon reasonable request.

Declaration of competing interest

The authors declared no conflict of interest.

Ethics

The Amasya University Non-Interventional Clinical Research Ethics Committee evaluated the study's compliance with ethical principles and obtained ethical approval (2024/144).

Funding

This work has not received any funding support.

REFERENCES

1. Idalsoaga F, Kulkarni AV, Mousa OY, Arrese M, Arab JP. Non-alcoholic Fatty Liver Disease and Alcohol-Related Liver Disease: Two Intertwined Entities. *Frontiers in medicine*. 2020;7:448. Epub 2020/09/26. doi: 10.3389/fmed.2020.00448. PubMed PMID: 32974366; PubMed Central PMCID: PMCPCMC7468507.
2. Le MH, Le DM, Baez TC, Wu Y, Ito T, Lee EY, et al. Global incidence of non-alcoholic fatty liver disease: A systematic review and meta-analysis of 63 studies and 1,201,807 persons. *J Hepatol*. 2023;79(2):287-95. Epub 2023/04/12. doi: 10.1016/j.jhep.2023.03.040. PubMed PMID: 37040843.
3. Manikat R, Ahmed A, Kim D. Up-to-date global epidemiology of nonalcoholic fatty liver disease. *Hepatobiliary Surg Nutr*. 2023;12(6):956-9. Epub 2023/12/20. doi: 10.21037/hbsn-23-548. PubMed PMID: 38115930; PubMed Central PMCID: PMCPCMC10727827.
4. Maurice J, Manousou P. Non-alcoholic fatty liver disease. *Clin Med (Lond)*. 2018;18(3):245-50. Epub 2018/06/03. doi: 10.7861/clinmedicine.18-3-245. PubMed PMID: 29858436; PubMed Central PMCID: PMCPCMC6334080.
5. European Association for the Study of the L, European Association for the Study of D, European Association for the Study of O. EASL-EASD-EASO Clinical Practice Guidelines for the management of non-alcoholic fatty liver disease. *Diabetologia*. 2016;59(6):1121-40. Epub 2016/04/08. doi: 10.1007/s00125-016-3902-y. PubMed PMID: 27053230.
6. Kopec KL, Burns D. Nonalcoholic Fatty Liver Disease: A Review of the Spectrum of Disease, Diagnosis, and Therapy. *Nutr Clin Pract*. 2011;26(5):565-76. doi: 10.1177/0884533611419668. PubMed PMID: WOS:000295222800008.
7. Zhu N, Wang X, Zhu H, Zheng Y. Blood cell parameters and risk of nonalcoholic fatty liver disease: a comprehensive Mendelian randomization study. *BMC Med Genomics*. 2024;17(1):102. Epub 2024/04/24. doi: 10.1186/s12920-024-01879-7. PubMed PMID: 38654378; PubMed Central PMCID: PMCPCMC11040836.
8. Miele L, Alberelli MA, Martini M, Liguori A, Marrone G, Cocomazzi A, et al. Nonalcoholic fatty liver disease (NAFLD) severity is associated to a nonhemostatic contribution and proinflammatory phenotype of platelets. *Transl Res*. 2021;231:24-38. Epub 2020/11/11. doi: 10.1016/j.trsl.2020.11.003. PubMed PMID: 33171266.
9. Solak Y, Yilmaz MI, Sonmez A, Saglam M, Cakir E, Unal HU, et al. Neutrophil to lymphocyte ratio independently predicts cardiovascular events in patients with chronic kidney disease. *Clin Exp Nephrol*. 2013;17(4):532-40. doi: 10.1007/s10157-012-0728-x. PubMed PMID: WOS:000323511000008.
10. Maurice J, Manousou P. Non-alcoholic fatty liver disease. *Clinical Medicine*. 2018;18(3):245-50. doi: https://doi.org/10.7861/clinmedicine.18-3-245.
11. Sinn DH, Kang D, Chang Y, Ryu S, Gu S, Kim H, et al. Non-alcoholic fatty liver disease and progression of coronary artery calcium score: a retrospective cohort study. *Gut*. 2017;66(2):323. doi: 10.1136/gutjnl-2016-311854.
12. Asil M, Dertli R. The Neutrophil-to-Lymphocyte Ratio as A Noninvasive Marker in Patients with Biopsy-Proven Non-Alcoholic Steatohepatitis. *Istanb Med J*. 2016;17(4):131-5. doi: 10.5152/imj.2016.74755. PubMed PMID: WOS:000391011900004.
13. Lesmana CRA, Kencana Y, Rinaldi I, Kurniawan J, Hasan I, Sulaiman AS, et al. Diagnostic Value of Neutrophil to Lymphocyte Ratio in Non-Alcoholic Fatty Liver Disease Evaluated Using Transient Elastography (TE) with Controlled Attenuated Parameter (CAP). *Diabet Metab Syndr Ob*. 2022;15:15-22. doi: 10.2147/Dms0.S330526. PubMed PMID: WOS:000742778300003.
14. Neuschwander-Tetri BA. Non-alcoholic fatty liver disease. *Bmc Medicine*. 2017;15. doi:10.1186/s12916-017-0806-8. PubMed PMID: WOS:000396072300001.
15. Akdas S, Yazihan N. From NAFLD to MASLD: Meta-analysis and systematic review of NAFLD patients in Turkiye in terms of metabolic profile and MASLD potential. *Hepatology forum*. 2024;5(3):126-38. Epub 2024/07/15. doi: 10.14744/hf.2023.2023.0042. PubMed PMID: 39006144; PubMed Central PMCID: PMCPCMC11237240.

16. Shavakhi M, Nourigheimasi S, Dioso E, Goutnik M, Lucke-Wold B, Khanzadeh S, et al. Prognostic Role of Neutrophil to Lymphocyte Ratio in Nonalcoholic Fatty Liver Disease: A Systematic Review and Meta-Analysis. *Canadian Journal of Gastroenterology and Hepatology*. 2022;2022(1):1554079. doi: <https://doi.org/10.1155/2022/1554079>.
17. Abdel-Razik A, Mousa N, Shabana W, Refaey M, ElMahdy Y, Elhelaly R, et al. A novel model using mean platelet volume and neutrophil to lymphocyte ratio as a marker of nonalcoholic steatohepatitis in NAFLD patients: multicentric study. *Eur J Gastroenterol Hepatol*. 2016;28(1):e1-9. Epub 2015/10/16. doi: 10.1097/meg.0000000000000486. PubMed PMID: 26469357.
18. WenYi J, Ting Q, PiaoPiao Y, JinMing W. Association Between Neutrophil-to-Lymphocyte Ratio with Inflammatory Activity and Fibrosis in Non-alcoholic Fatty Liver Disease. *The Turkish journal of gastroenterology : the official journal of Turkish Society of Gastroenterology*. 2022;33(1):53-61. Epub 2022/01/19. doi: 10.5152/tjg.2022.20715. PubMed PMID: 35040788; PubMed Central PMCID: PMC9128444.
19. Kara M, Dogru T, Genc H, Sertoglu E, Celebi G, Gurel H, et al. Neutrophil-to-lymphocyte ratio is not a predictor of liver histology in patients with nonalcoholic fatty liver disease. *Eur J Gastroenterol Hepatol*. 2015;27(10):1144-8. Epub 2015/06/11. doi: 10.1097/meg.0000000000000405. PubMed PMID: 26062078.
20. Acar, T., Adibelli, Z. H. (2017). Nötrofil/Lenfosit Oranının Abdominal Yağ Dağılımı, Karaciğer Yağlanması ve Karaciğer Hacmine Olan Etkisi. *Konuralp Tip Dergisi*, 9(2),73-77.
21. Wang Y, Guo S, He Y, Zhang Q, Zhou N, Wang D, et al. Relationship between Neutrophil-to-Lymphocyte Ratio and Liver Fibrosis in Nonalcoholic Fatty Liver Disease Among Adults in the United States: Data from the National Health and Nutrition Examination Survey 2017-2018. *The Turkish journal of gastroenterology : the official journal of Turkish Society of Gastroenterology*. 2024;35(4):335-42. Epub 2024/08/11. doi: 10.5152/tjg.2024.23231. PubMed PMID: 39128078; PubMed Central PMCID: PMC91114246.
22. Duan Y, Luo J, Pan X, Wei J, Xiao X, Li J, et al. Association between inflammatory markers and non-alcoholic fatty liver disease in obese children. *Frontiers in Public Health*. 2022;10. doi: 10.3389/fpubh.2022.991393.
23. Karaoğullarından Ü, Üsküdar O, Odabaş E, Saday M, Akkuş G, Delik A, et al. Is mean platelet volume a simple marker of non-alcoholic fatty liver disease? *Indian Journal of Gastroenterology*. 2023;42(2):219-25. doi: 10.1007/s12664-022-01330-8.
24. Kocabay G, Karabay CY, Kalayci A, Colak Y. Mean platelet volume in patients with non-alcoholic fatty liver disease: is mean platelet volume ready as a surrogate marker? *Clinical Chemistry and Laboratory Medicine (CCLM)*. 2014;52(11):e249-e52. doi:10.1515/cclm-2014-0303.
25. Alvarez L, CIPHER D, Weideman RA, Brown G. Mean platelet volumes in non-alcoholic liver disease (NAFLD): is there a relationship to cardiovascular events? *Gastroenterology & Hepatology*. 2016;5(5):325-9. doi: 10.15406/ghoa.2016.05.00157.